Analysis of 3D in vitro Models using Mesenchymal Stromal Cells

Julia Marshall

PhD

University of York

Biology

September 2015

Abstract

Mesenchymal stem cells/multipotent stromal cells (MSCs) have a variety of unique properties that have made them a popular cell type in the study of tissue engineering. Their ability to undergo osteogenic, adipogenic and chondrogenic differentiation has long been appreciated. In addition to their capacity for skeletogenic differentiation, there are suggestions that MSCs have additional roles in organising tissue vasculature through interactions with endothelial cells (ECs). However, suitable experimental models to test these unique MSC activities are lacking and the mechanisms are unclear. Here, we have developed a novel 3D *in vitro* co-culture spheroid model of MSCs and ECs.

Development and further investigations into this 3D co-culture spheroid model has resulted in many novel discoveries. Using calcium depletion from cell culture media to quantify osteogenic differentiation of MSCs in both 2D and 3D represents a complimentary assessment method that is non-destructive. Co-culture of MSCs and ECs was also found to promote osteogenic differentiation whilst having no detrimental effects on cell viability during long-term culture. Further investigations into the 3D co-culture of MSCs and ECs demonstrated spontaneous endothelial organisation. Using this model it was possible to track endothelial restructuring and identify the signalling processes involved, ultimately focusing on platelet-derived growth factor and notch signalling.

Using a combination of pre-differentiated MSCs and ECs within the 3D co-culture system, osteochondral spheroids were developed. These spheroids were analysed using a combination of novel and traditional imaging techniques; it was found that osteochondral spheroids self-organised into distinct bone and cartilage regions, similar to those observed at the osteochondral boundary and during early endochondral ossification. This *in vitro* multiple cell culture system represent a simplified tractable model of osteochondral tissue.

Table of Contents

List of Figures

List of Tables

Acknowledgements

Declaration

The work presented in this thesis was performed by the author between September 2011 and March 2015 in the Department of Biology, University of York, in the laboratory of Dr. Paul Genever. All experiments were performed by the author. Neither this thesis nor any part of it has previously been submitted for acceptance of a higher degree.

Chapter 1

Chapter 1 : Introduction

1.1 Stem Cells

Stem cells have the capacity to produce an indefinite number of cells of the same type (self-renewal) and give rise to other cell types through differentiation (Mochizuki et al., 2014). The differentiation capacity or potency of stem cells makes them unique. Stem cells can be roughly divided into four groups depending upon their potency; totipotent, pluripotent, multipotent and unipotent (Surani et al., 2008). There are two totipotent cell sources: a fertilised egg and early embryonic cells; these cells are able to produce all other cell types within the body. Pluripotent cells are able to differentiate into most cell types; specifically they are able to differentiate into cells from all three germ layers but not extra-embryonic tissues (Kerr et al., 2006). The three germ layers are: endoderm, mesoderm and ectoderm, these are the three different groups of cells that arise during the gastrulation phase of embryonic development. Multipotent cells are able to differentiate into multiple cell types, however, these cell types are from one germ layer (Pittenger, 1999). Unipotent cells are only able to differentiate into one cell type (Guettier, 2005).

Scientific publications on stem cells started in the 1960's, however, in the 1990's stem cell research became an area of intense scientific interest (Lajtha, 1967, Bradley, 1990). This interest arose due to the culture human embryonic stem cells within the laboratory. Stem cells generally have three sources; embryonic stem cells, adult stem cells and induced pluripotent stem cells (iPS cells) (Alvarez et al., 2012). Mammalian embryonic stem cells are isolated from the inner cell mass of a blastocyst and characterised as pluripotent. Adult stem cells are sourced from a wide variety of adult tissues; these are often considered to be multipotent or unipotent depending upon their source (Murphy et al., 2003). iPS cells are artificially derived from non-stem cells that have been genetically reprogrammed. The first iPS cell was created through the addition of four

transcription factors, Oct4, Sox2, KLF4 and c-Myc into mouse fibroblasts (Takahashi and Yamanaka, 2006).

1.1.1 Embryonic Stem Cells

Mammalian embryonic stem cells (ESCs) are derived from the inner cell mass of a blastocyst or developing embryo. The first ESCs were derived from mouse embryos; Evans and Kaufman were able to extract pluripotent stem cells from mice embryos. These cells were cultured and maintained *in vitro* and were shown to differentiate *in vivo* and *in vitro* (Evans and Kaufman, 1981). Mouse ESCs in vitro cell cultures were achieved through co-culture with feeder layers of mitotically inactive fibroblasts in combination with Leukaemia inhibitor factor (LIF). This co-culture promoted viability and proliferation of the cells (Martello and Smith, 2014, Onishi and Zandstra, 2015).

Human ESCs are also derived from the inner cell mass of a blastocyst; *in vitro* cell culture is maintained by co-culture with a feeder layer of mitotically inactive fibroblasts. However, human ESCs do not require LIF (Schnerch et al., 2010). This small difference highlights the importance of different species at both the molecular and cellular level. The use of human ESCs for research has great potential due to their pluripotent differentiation potential. However, due to a blastocyst being destroyed to obtain these cells they are surrounded by ethical controversy. Because of these ethical concerns, human ESC research is highly regulated; in the UK all research using human ESCs is performed under license from the human fertilisation and embryology authority (Abdalla, 2009). This does not prevent human ESC research but makes it a more complex process. This has led to an increased demand for alternative cell sources, culminating in the generation of iPS cells and the increasing trend of adult stem cells.

1.1.2 Adult Stem Cells

Adult stem cells are a multipotent or unipotent cell type that is found throughout the body post embryonic development (Vaes et al., 2015). Compared to ESCs,

adult stem cells are less potent; however, they are not ethically controversial due to being sourced from adults following informed consent (Alvarez et al., 2012). Within the body, adult stem cells are a small and unique population of cells found within tissues such as, bone, liver, teeth, cord blood and skin (Hong et al., 2014). The roles of adult stem cells are maintaining tissue homeostasis and tissue repair after injury. They are able to achieve this through their self renewal capacity and differentiation potential (Hass et al., 2011). These abilities are supported through a specialised microenvironment known as the stem cell niche (Kopp and Rafii, 2007). Adult stem cells are considered multipotent; nevertheless, a few unipotent adult stem cells exist, depending upon cell type and tissue source (Mariano et al., 2015). This multipotency is restrictive compared to the pluripotent potential of ESCs. However, controversial research has shown that under specific *in vitro* culture conditions adult stem cells are able to transdifferentiate into cell types of alternative germ layers, indicating adult stem cells may have a broader potential but further validation work is required (Fan et al., 2014).

Overall adult stem cells are considered to have a variety of advantages compared to ESCs; adult stem cells are less tumourigenic compared to ESCs, reducing the risk of tumour formation following therapeutic application (Kang et al., 2012). Due to the wide variety of adult tissue sources, autologous cell therapies have viable potential, unlike ESCs (de Munter and Wolters, 2013). However, the main advantage is the lack of ethical issues that are commonly associated with ESCs. These advantages have led to adult stem cells being used in a variety of therapies, including bone marrow transplants and coronary artery disease (Mathe, 1964, Botham et al., 2013). One of the most popular adult stem cells for these regenerative medicine therapies is mesenchymal stromal cells/mesenchymal stem cells (MSCs) (Sensebe et al., 2010).

1.2 Mesenchymal Stromal Cells

Mesenchymal stromal cells, often also referred to as mesenchymal stem cells were first isolated from bone marrow in the 1970's by Fridenstein, they were characterised as a clonogenic cell, with a fibroblast-like morphology and plastic

adherence (Friedenstein et al., 1976). In addition to this, MSCs also demonstrated the ability to differentiate into osteoblasts, adipocytes and chondrocytes (Cook and Genever, 2013). This combination of self renewal and skeletal differentiation identified MSCs as a stem cell. Unfortunately a specific cell surface marker for MSCs has not been identified. This has resulted in MSC characterisation being performed through tri-lineage differentiation potential, morphology and a panel of non-specific cell surface markers. MSCs are described as being positive for the cell surface markers CD29, CD44, CD73, CD90, CD105 and CD166. Negative for CD11a, CD13, CD19, CD34, CD45, CD79a, CD144 and CD235a (Dvorakova et al., 2008, Karp and Leng Teo, 2009). Additional markers such as Stro-1 CD146 and CD271 have also been described in the literature (Whyte et al., 2011).

1.2.1 Mesenchymal stromal cell isolation

Historically MSCs were initially sourced from adult bone marrow; subsequently this MSC source has received the most attention. Within bone marrow MSCs represent approximately 0.01-0.001% of the total cell population (Li et al., 2011). Despite the low frequency, bone marrow aspirations are able to produce enough viable cells for therapies or scientific research. In addition MSCs are easily expanded within *ex vivo* culture conditions, making this cell type popular for stem cell research and treatments. MSCs have been sourced from a wide variety of tissues such as; adipose tissue, liver, spleen, detal pulp and umbilical cord blood (Mohammadi et al., 2015, Krampera et al., 2007). Due to the wide variety of tissues from which MSCs have been sourced, it has been hypothesised that MSCs have the ability to enter the circulatory system and travel to sites of injury (Tondreau et al., 2005). This has led to MSCs being intravenously injected for therapeutic research, which has proven successful (Oh et al., 2012, Introna et al., 2014). However, several studies have failed to detect MSCs within peripheral blood diminishing this theory (Kollar et al., 2011).

MSCs sourced from different tissues all express the three main characteristics used to identify this cell type. The panel of non-specific cell surface markers

previously mentioned (Section 1.2), morphology and skeletal differentiation potential. However, the anatomical location of MSCs may affect specific characteristics; MSCs derived from synovium have demonstrated the ability to undergo chondrogenesis more readily compared to bone marrow derived MSCs (Sakaguchi et al., 2005). Adipose derived MSCs have been shown to more readily transdifferentiate into a Schwann cell-like phenotype compared to bone marrow derived MSCs (Krampera et al., 2007). This indicated that MSCs from a specific tissue might be partially programmed to enhance local tissue repair, emphasising the importance of selecting an appropriate tissue source for scientific experiments and cellular therapies.

1.2.2 Mesenchymal stromal cell differentiation

One of the main characteristics of MSCs is their ability to undergo skeletal differentiation; a schematic representation of this is shown in Figure 1.2.1. Under *ex vivo* conditions this differentiation by exposing MSCs to a cocktail of inductive stimuli has been well defined, more specifically osteogenic differentiation is induced through the addition of dexamethasone, β-glycerophosphate and ascorbic acid (Cook and Genever, 2013). Adipogenic differentiation is performed through the addition of insulin, isobutylmethylxathine, indomethacin and dexamethasone. Chondrogenic differentiation is induced through the use of dexamethasone, ascorbic acid, insulin transferring selenium, transforming growth factor-β3 (TGF-β) or TGF-β1 and proline (Vater et al., 2011, Mueller et al., 2010).

The three clearly defined cell types MSCs are able to differentiate into are all from the mesoderm. Controversially MSCs have been described as undergoing endoderm-like and ectoderm-like tissue differentiation. This transdifferentiation is possible through the addition of inductive stimuli similar to standard differentiation. MSCs have been shown to differentiate into a neuron-like cell type through the addition of β-mercaptoethanol, retinoic acid, forskolin, platelet derived growth factor, basic fibroblast growth factor and glial growth factor (Mahay et al., 2008). However, this process is limited as removal of these factors results in the loss of neuronal-like phenotype (Yi et al., 2012).
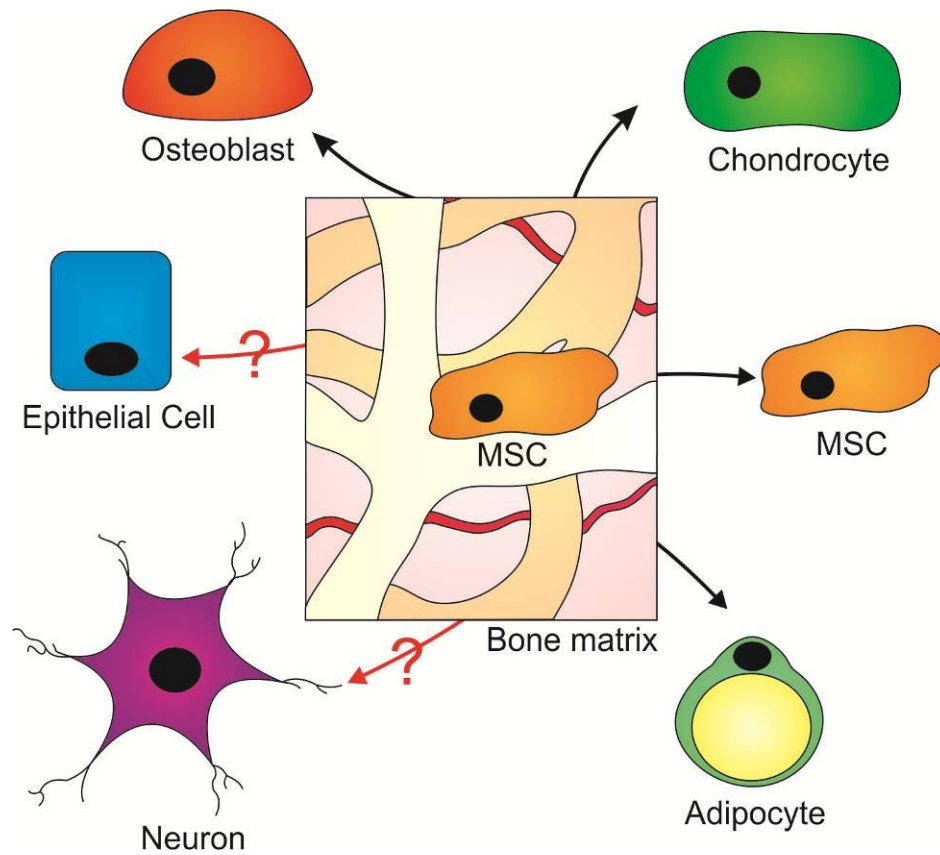
Figure 1.2.1 – Schematic representation of MSC differentiation

MSCs are able to undergo tri-lineage mesoderm differentiation into osteoblasts, chondrocytes and adipocytes. MSCs are also able to undergo self renewal to produce more MSCs. Controversially MSCs have been described as transdifferentiating into neural-like and epithelial-like cells.

1.2.3 Therapeutic potential of mesenchymal stromal cells

Since their discovery the potential of MSCs for stem cell therapies has been widely acknowledged. Indeed, MSCs were inadvertently one of the very first cell types to be used in stem cell therapy; bone marrow transplants to treat leukaemia were successfully pioneered in the 1960's (Mathe, 1964). Since this initial ground-breaking success the strategies conceived to utilise MSCs have been extensive. MSCs have a wide variety of advantageous properties for a wide range of disease therapies.

MSCs can be sourced from a wide variety of tissues, allowing autologous cell therapies, for example adipose tissue can be harvested to treat bone defects (Im et al., 2005). MSCs are a strong candidate for skeletal repair, within the native bone tissue, MSCs contributed towards the normal repair and remodelling process. MSCs differentiated into osteoblasts, the primary role of these cells is to produce the mineralised extra cellular matrix of the bone (Zanetta et al., 2009). Uniquely MSCs have been described as possessing both immunoprivileged and immunosuppressive properties, making them potentially an allogeneic cell source. MSCs do not express major histocompatible complex (MHC) class II, limiting their detection via the immune system (Liu et al., 2006, Romieu-Mourez et al., 2007). MSCs have also been shown to inhibit T-cell proliferation and natural killer cell lysis (Asari et al., 2009).

MSCs are currently being used in clinical trials for the treatment of graft versus host disease. Graft versus host disease is a common complication that occurs following allogeneic tissue transplantation. The transplanted immune cells attack the hosts own cells damaging tissues within the whole body. Intravenous infusions of MSCs from allogeneic sources have been shown to successfully treat the disease and significantly increase survival rates (Ringden et al., 2006, Introna et al., 2014). MSCs have also been used in successful clinical studies for a range of bone tissue diseases, such as osteoporosis and osteogenesis imperfecta (Antebi et al., 2014, Chan and Gotherstrom, 2014). These successes are most

likely attributed towards MSCs playing an important role in their native bone tissue. Intriguingly MSCs have also been used to successfully treat circulatory diseases, such as ischemia. Using animal models, application of MSCs in cell aggregates has been shown to improve limb ischemia, this is due to MSCs inhibiting cellular apoptosis and releasing large numbers of growth factors, such as TGF-β (Bhang et al., 2012a, Chen et al., 2013b).

Despite the success observed within clinical trials and studies, MSCs have not received FDA approval as a licensed cellular therapy; one of the major reasons for this is a lack of a specific cell surface marker (Mendicino et al., 2014). Therefore, the use of MSCs as an off the shelf allogeneic cell source within an industrial setting is not yet possible. Additionally, the efficacy of MSC engraftment and differentiation *in vivo* has also been questioned. Large quantities of MSCs have been implanted and have subsequently undergone apoptosis or virtually disappeared within the body (Noad et al., 2012). This causes safety concerns regarding tumour formation and other unwanted side effects (Volarevic et al., 2011). Consequently, studies have begun to focus on the use of MSCs as a cell source for basic research and *in vitro* models. Initially these studies focused on drug screening and toxicity, however, MSCs are starting to be utilised in cancer studies, tissue models and developmental biology (Astashkina et al., 2012). Specifically MSCs have shown promise in understanding human bone repair.

1.3 Adult bone repair

During adult bone repair, cartilage tissue initially forms at the site of injury. This cartilage tissue is then infiltrated by new blood vessels; triggering the cartilage tissue to be replaced with functional vascularised bone tissue (Tannous et al., 2013, Sisask et al., 2013). The cells that initiate this bone repair process in adult tissue have been identified as hematoma-derived cells. These hematoma-derived cells express the same cell surface markers and skeletal differentiation potential as MSCs, but have not been specifically identified as MSCs (Oe et al., 2007, Koga et al., 2013). MSCs have significant therapeutic potential for adult bone repair; they are a native cell type that plays a key role in bone tissue homeostasis, moreover, during adult bone repair hematoma-derived cells that express the same phenotype as MSCs are identified as the initiation cell source. Therefore, MSCs have close links to bone tissue homeostasis and adult bone repair.

1.3.1 Adult bone repair and mesenchymal stromal cells

Within humans the skeleton undergoes a continuous remodelling process during adulthood. This remodelling process is performed by two cell types: osteoblasts and osteoclasts. Osteoblasts are derived from MSCs and deposit the calcified bone matrix; osteoclasts are derived from haematopoietic stem cells and resorb the calcified bone matrix (Kular et al., 2012). *Ex vivo* MSCs have been shown to successfully produce bone tissue and many studies have claimed to use undifferentiated MSCs or osteogenic differentiated MSCs to successfully treat bone defects (El-Gendy et al., 2013, Granchi et al., 2012). However, few human clinical trials using MSCs have been performed and the efficacy of these treatments is disputed (Meijer et al., 2007). These poor results are mainly attributed towards a lack of vascularisation. Therefore, the use of chondrogenic MSCs could prove successful; cartilage is an avascular tissue so a lack of vascularisation is not detrimental and normal bone repair starts with the formation of cartilage tissue at the site of injury.

Alternative treatments utilising the chondrogenic differentiation potential of MSCs in bone defects have proven successful. Chondrogenic MSCs were found to have superior bone formation *in vivo* compared to osteogenic differentiated MSCs and undifferentiated MSCs (Farrell et al., 2011, Janicki et al., 2010). Indeed, the utilisation of chondrogenic adult MSCs have proven successful for bone repair. *Ex vivo* human MSCs underwent both chondrogenic differentiation and hypertrophy treatment. These hypertrophic chondrocytes were then implanted into the bone defects of mice. The cells were found to have physiologically remodelled the bone, vasculature and hematopoietic compartment. These results showed that chondrogenic MSCs were able to successfully produce a functional bone repair. These results were attributed towards an endochondral ossification-like process and this model could be used for fundamental and translational research (Scotti et al., 2013, Scotti et al., 2010).

1.3.2 Endochondral ossification

Endochondral ossification is the term used to describe the formation of long bones during embryonic development and provides a suitable environment for haematopoiesis (Chan et al., 2009). A simplified schematic version of this can be seen in Figure 1.3.1. In brief, the process of endochondral ossification starts with primitive mesenchymal cells condensing together with the centrally-located cells differentiating into chondrocytes though Sox9 expression. This a-vascular chondrocyte centre undergoes hypertrophy and begins to synthesise collagen type X and mineralise the surrounding matrix. This simultaneously triggers blood vessel recruitment through secretion of vascular endothelial growth factor (VEGF) and directs adjacent mesenchymal cells to become osteoblasts and subsequently bone matrix. The in-growth of blood vessels triggers the cartilage core to undergo resorption of the cartilage matrix and replacement with vascularised bone (Kronenberg, 2003, Maes et al., 2002). The endochondral ossification process highlights the importance of the cellular microenvironment for macro scale tissue development.
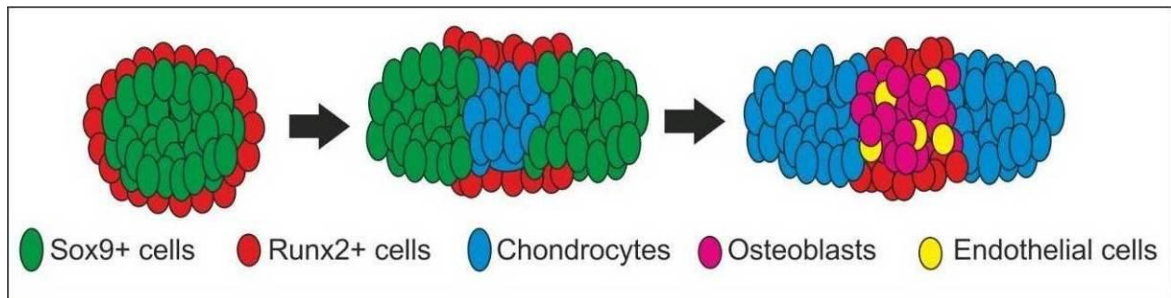
Figure 1.3.1 - Schematic representation of endochondral ossification

Endochondral ossification is the process of embryonic long bone development. Primitive mesenchymal cells condense together to form a cartilage core. The cartilage core simultaneously signals the recruitment of blood vessels and differentiation of adjacent cells into bone tissue. The in-growth of blood vessels triggers resorption of the cartilage core and replacement with vascularised bone tissue. During adult bone healing a similar process occurs, were cartilage tissue is initially produced within the damaged region before being replaced with vascularised bone tissue.

1.4 The stem cell niche

A stem cell niche is the term used to describe the microenvironment in which a stem cell resides. The concept of a stem cell niche was first conceived by Schofield in the 1970's, he hypothesised that stem cells must associate with other cells which determine behaviour. This behaviour ensures that stem cells proliferate to maintain a population but also differentiate as required (Schofield, 1978). This initial definition has since expanded and a stem cell niche refers to the specific anatomical compartment in which stem cells are located (Van Zant and Liang, 2012). This compartment is composed of different cell types alongside the microenvironment, including physical and chemical cues. More specifically biochemical signalling from neighbouring cells, soluble factors, extra-cellular matrix (ECM), sheer forces and oxygen tension all play an important role within the stem cell niche (Chen et al., 2013c). Understanding this environment is important for the *in vitro* culture of stem cells and future applications in medicine (Moore and Lemischka, 2006).

One of the most well defined stem cell niches is that of haematopoietic stem cells (HSCs). HSCs are located within the bone marrow and differentiate into all haematopoietic lineages (Greenbaum et al., 2013). The HSC niche is well defined due to clear cell surface marker profile expressed. The HSC niche is not believed to be anatomically restricted, resulting in temporary and spatial regulation (Adamo et al., 2009, Adamo and García-Cardeña, 2012). Bio-mechanical forces play a key role, fluid sheer stress on HSCs has been shown to increase expression of RUNX1 a regulator of haematopoietic development (Keung et al., 2010). Low oxygen concentration is also critical, HSC respond to hypoxic conditions to shift towards a glycolysis based metabolism that promotes survival, tracer studies have confirmed HSCs reside within poorly perfusing regions with low oxygen (Sakaguchi et al., 2005).

1.4.1 Mesenchymal stromal cell niche

Due to the lack of a specific cell surface marker in combination with the wide range of tissues in which MSC-like cells have been identified, the MSC niche has not been clearly defined. In general it is known that the MSC niche is composed of multiple cell types, ECM and an oxygen gradient (Figure 1.4.1). Nevertheless, two main types of niches within the bone marrow have been proposed; endosteal and perivascular (Balduino et al., 2012). The endosteal niche is most commonly associated with HSCs; this niche is closely associated with the endosteum region of bone, which is the interface between bone and bone marrow (Cordeiro-Spinetti et al., 2015). Within this niche stem cell specifically associate with osteoblasts, osteocytes and the bone matrix (Pazzaglia et al., 2014). The most popular theory is that MSCs reside within a perivascular niche (Jørgensen et al., 2004, Crisan et al., 2008). The perivascular niche is closely associated with the vascular structures of the tissue. Therefore, a perivascular niche is not tissue restricted, unlike an endosteal niche (Ghajar et al., 2013). This further supports the theory that MSCs reside within a perivascular niche; MSCs have been derived from a wide variety of tissues associated with the vasculature. The exception to this is MSCs sourced from cartilage which is an avascular tissue (Barbero et al., 2003). This highlights the probably important relationship between MSCs and endothelial cells due to the close association with the vasculature. Indeed, endothelial cells and the vasculature are a frequently overlooked vital component of bone tissue, bone is one of the most vascularised tissues within the body (Brandi and Collin-Osdoby, 2006).
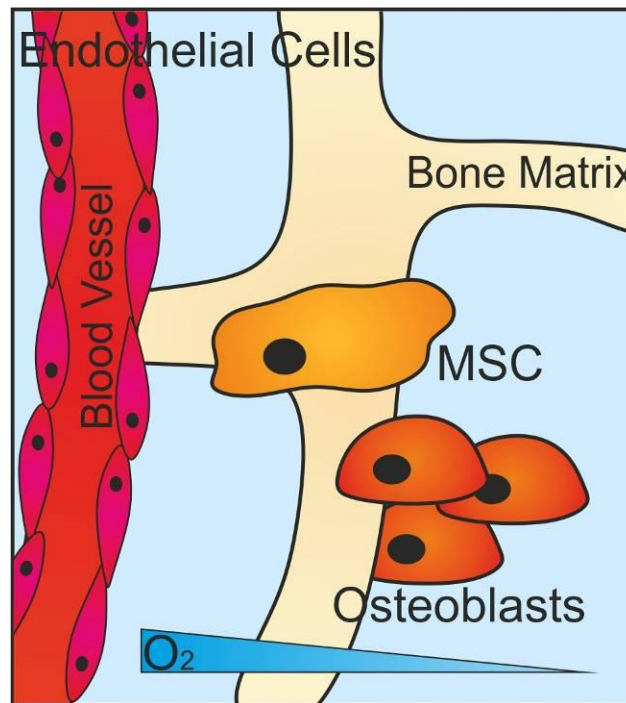
Figure 1.4.1 – Schematic representation of the perivascular MSC niche

The perivascular MSC niche is a complex microenvironment composed of multiple cell types such as: osteoblasts and endothelial cells. There are also physical cues within the niche, such as bone matrix, blood vessels and oxygen gradients.

1.5 Endothelial Cells

Endothelial cells (ECs) originate from the mesoderm and form the inner lining of blood vessels; subsequently ECs are present within the majority of the body's tissues. ECs are able to form a selectively permeable membrane that provides multiple functions; a barrier between blood and tissue, homeostasis regulation, inflammatory and immune response, angiogenesis and vasculogenesis (Bazzoni and Dejana, 2004). Homeostasis is the regulation of body temperature within mammals through blood vessel dilation or restriction. Angiogenesis is the formation of new blood vessels from a pre-existing blood vessel; this process is also referred to as vascularisation. Vasculogenesis is the formation of new blood vessels within the developing embryo (Sumpio et al., 2002). In addition to these important roles ECs are also implicated within the stem cell niche, ECs regulate the diffusion of molecules such as oxygen, growth factors and other small molecules. Specifically within the perivascular niche of MSCs, ECs are an important cell type (Colmone and Sipkins, 2008).

ECs have been sourced from a variety of tissues for *in vitro* scientific culture, sources include; human umbilical veins, aorta, coronary artery, pulmonary artery, iliac artery and dermal microvasculature (Park et al., 2006, Lloyd et al., 2013). Like MSCs, ECs vary depending upon their source. Human umbilical vein endothelial cells (HUVECs) are considered one of the most commonly used and well defined ECs. HUVECs are generally used in the study of the adult endothelium and are used to recreate normal adult blood vessels within *in vitro* conditions (Manna and Jain, 2014). Aorta, pulmonary artery and coronary artery derived ECs are sourced from large vessels and are more commonly used to study coronary artery diseases (Chang et al., 2013b). Dermal microvasculature ECs are a neonatal source that is most commonly used within tumour studies (Dong et al., 2013).

The vascularisation process is highly important for normal embryonic development, adult homeostasis and repair (Street et al., 2002). The loss of

vascularisation to any tissue results in cellular apoptosis and subsequently critical failure. One of the most common uses of ECs has been in the study of the vasculature within cancer tumours. From these cancer studies the importance of vascular endothelial growth factor (VEGF) in promoting angiogenesis within ECs has been revealed (Coultas et al., 2005, Xiong et al., 2014). Additionally transmembrane proteins such as vascular endothelial (VE)-cadherin have also been demonstrated to play an important role in the cellular arrangement of ECs (Bentley et al., 2014). Recent developments within the field of tissue engineering for regenerative medicine have found vascularisation critical for the successful implantation of the next generation of supportive devices (Novosel et al., 2011). Specifically, 3D scaffolds sympathetically designed to incorporate native vascular had improved clinical performance compared to those which did not (Xiao et al., 2015).

1.6 Three-dimensional cell culture models

The first *ex vivo* cell culture was performed in 2D on tissue culture plastic; this has subsequently developed into a variety of 3D strategies to more closely recreate the native *in vivo* environment (Haycock, 2011). Traditional 2D culture does have advantages; convenient, in-expensive, reproducible and robust for statistical analysis. However, differences in cell morphology, differentiation potential, therapeutic capacity and maintenance of phenotype have all been reported (Ivers et al., 2014, Brennan et al., 2015, Cha et al., 2015, Zeng et al., 2015). To combat this, different 3D-based cell culture strategies have been developed including; scaffolds, bioreactors and cell aggregates or spheroids (Ravi et al., 2015).

1.6.1 Scaffolds

Scaffold is the termed used to describe any material specifically developed for cells to be cultured on. Scaffolds were initially conceived as an ECM replacement on which cells would colonise and subsequently functionalise. They are

predominantly 3D in nature, however, 2D scaffolds are frequently utilised. The choice of material is fundamental in scaffold design; materials are able to adjust the physical and functional properties considerably. For example hard and soft materials can be used in various combinations to generate virtually every tissue within the body. Because of this the material and design used have significant impact on the success of the scaffold and subsequently scaffolds are designed for specific tissues. Indeed, biphasic and triphasic scaffolds are being utilised successfully to recreate both the physical and biological properties of tissues such as bone and cartilage (Marquass et al., 2010). However, the use of scaffolds has a range of advantages and disadvantages. The use of natural materials such as collagen and keratin are biocompatible, biologically functional with similar mechanical properties to the *in vivo* tissue. However, they are relatively expensive, ethically controversial due to them being sourced from healthy animals, have concerns regarding pathogen transmission and complex structural architecture is lost through synthetic production or tissue extraction (Long et al., 2014). By contrast the use of synthetic materials such as polycaprolactone and polyethylene glycol are relatively inexpensive, ethical controversy free and cannot cause pathogen transmission. However, they have poor biological compatibility, have little biological functionality and their physical properties are greatly different from those of natural tissue.

A recent development within the field of natural scaffolds, to avoid many of the disadvantages described previously is the decellularisation process. A tissue from a donor organism is harvested; the cells within the tissue are removed along with DNA and RNA, leaving a complex hierarchal organised structure. Within *in vitro* culture these decellularised scaffolds have been highly successful; however, translation into clinical use has been poor. Unfortunately, the clinical application of these decellularised tissues as heart valve replacements resulted in one study as having a 100% failure rate. Four out of four human patients who received decellularised heart valve replacements failed within a month of application. This failure was attributed to the decellularised tissue eliciting a strong inflammatory response causing rapid structural failure and degeneration of the graft (Simon,

2003). Subsequently the use of decellularised tissues for clinical applications has been conducted more conservatively with improved success rates. Overall decellularised scaffolds have a range of advantages and disadvantages. They have a complex architecture that can be easily colonised via *in vivo* or *in vitro* cell sources; they are biologically functional and have similar physical properties to the chosen material. However, they cannot be ethically produced, could cause possible pathogen transmission, have had poor success clinically and are relatively expensive (Minardi et al., 2015).

1.6.2 Bioreactors

Bioreactor is the term used to generally describe any device or system that can support biological material. Bioreactors have a wide range of sizes, from a few millilitres to thousands of litres, that are most commonly used within industry (Luh, 1995). During the 1990s one of the most numerous bioreactor systems used for cell biology research was the rotating walled vessel (NASA) bioreactor, this bioreactor was able to culture 3D cell clusters within a simulated microgravity environment (Duray et al., 1997). Since this initial development a wide range of bioreactors are now available that can exert a wide range of mechanical forces such as, stress, strain, compression and fluid forces (Rauh et al., 2011, Ji et al., 2014). The use of bioreactors is currently the only method available to exert such a wide range of forces on biological material. Additionally, they can be combined with imaging and measuring devices for combined *in situ* analysis. However, bioreactors have a variety of disadvantages such as; requiring a large number of cells, expensive, complex assembly and being prone to infections (Bilodeau and Mantovani, 2006).

1.6.3 Cell aggregates

Cell aggregates or cell spheroids are 3D structures composed entirely of cells that have aggregated together. They do not contain any scaffold material and can be frequently created without the use of specialised equipment such as a

bioreactor. There are four main methods to producing cell aggregates, rotating plate culture, hanging droplets, non-adhesive U-bottom well plates and semi-solid gel culture (Figure 1.6.1) (Hildebrandt et al., 2011). The generation of cell aggregates is relatively simple; most cell types are able to spontaneously form a 3D spheroid structure when appropriate culture methods are used. Moreover 3D spheroid aggregates have been shown to produce ECM components such as collagen in greater quantities compared to traditional 2D culture (Murphy et al., 2015). Overall cell aggregates have several advantages; they require a relatively low cell number, no materials are required due to cell-cell interactions and they are inexpensive compared to bioreactors and scaffolds. There can be variation in cell aggregate size depending upon the method used to generate them; however, using either the hanging droplet or non-adhesive U-bottom well plate method prevents this. The main disadvantage with all cell aggregates is that they require dexterous handling to prevent damage.

Within specific biological research fields the use of cell aggregates has been essential. Specifically, within cancer biology cell aggregates have been found to more closely represent the native tumour environment. In particular they have been highly important when mimicking avascular tumours due to being structurally, biologically and physically similar. Furthermore, cell aggregates have been successfully used for toxicology testing and high-throughput drug screenings with great efficacy compared to other cell culture methods (Thoma et al., 2014). From these original and highly successful single-cell aggregates the concept of more complex cell aggregates arose. The use of multiple cell types within a single cell aggregate has been used to create retinospheres. Retinospheres are composed of three different cell types from embryonic avian retina being arranged in the same layers as those of the *in vivo* retinal layers (Berchtold et al., 2011). These more advanced multi-cellular aggregates are commonly referred to as organotypic models or organoids.
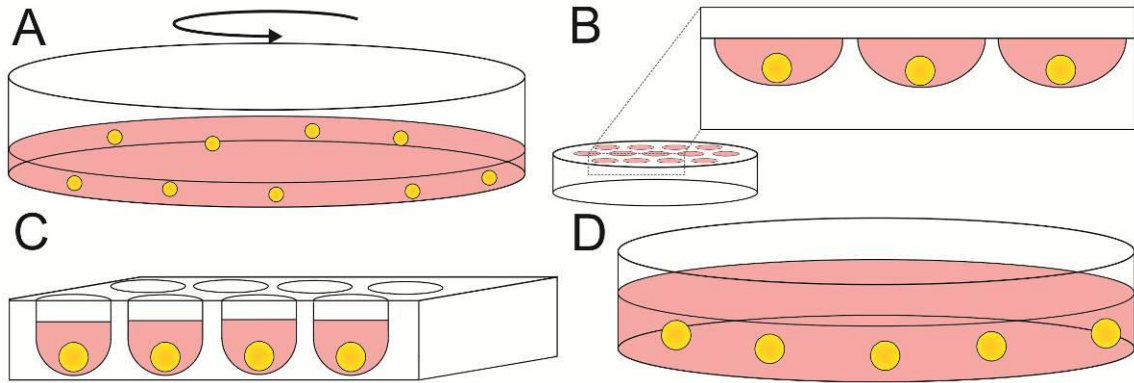
Figure 1.6.1 – Schematic representation of the different methods to produce cell aggregates

A - Rotating plate culture. B – Hanging droplet culture, a small volume of liquid is placed on the lid of a petri dish which is then inverted. C – Specialised plastic ware such as U-bottomed non-adherent plates. D – Semi-solid gel culture, this can also be combined with the technique depicted in C.

1.6.4 *Ex vivo* organotypic cell culture

The term organotypic was originally used to describe the 3D structure cells from siliceous sponges made when cultured *ex vivo*. This original organotypic model was primarily a single cell-type aggregate that formed a 3D spheroid-like structure (Wilson, 1907). Since this initial observation over 100 years ago the uses of organotypic cell culture and models have developed significantly, human tissues such as kidney and retina have been recreated. Organotypic cell culture models are unique in their ability to mimic aspects of organ function through the use of multiple cell types (Lancaster and Knoblich, 2014). Indeed, organotypic models used in combination with high-throughput imaging systems, chemical probes, biological probes and gene analysis; have made automated analysis both robust and practical (Li et al., 2015).

One of the most recent developments in organotypic models is the use of tissue slices in combination with *ex vivo* cell culture to more closely replicate the native environment. This type of model has been particularly successful in recreating dental tissue within the laboratory. Specifically, this model has been used to observe the effects of bacterial infection within dental tissue. Increased bacteria within the oral cavity are known to cause infection and subsequently abscesses. However, indentifying the specific bacteria involved has been difficult due to the lack of appropriate models. Using an organotypic model of mandible slices it was possible to identify that Streptococcus anginosus group of bacteria are an opportunistic pathogen which can causes disease within the oral cavity (Roberts et al., 2013). This model has also been further developed to include the use of MSCs for regenerative medicine purposes. Fluorescently labelled MSCs were placed into the mandible model and found to produce cells with an appropriate phenotype in the relevant regions (Colombo et al., 2015). The success of these 3D cell culture models has been attributed towards the increase in cell-adhesion molecules, such as integrin-linked kinase, compared to 2D systems (Sakai et al., 2003).

1.6.5 Integrin-linked kinase

Integrins and Integrin-linked kinase (ILK) provides a physical link between the cellular cytoskeleton and the ECM. Generation of these connections activates intracellular signals, such as Mitogen activated protein kinase (MAPK) and Phosphoinositide 3-kinase   (PI3K) that contribute towards cell proliferation, differentiation, survival and migration (Figure 1.6.2) (Hsu et al., 2015, Zheng et al., 2015, Yoon et al., 2015, Wang et al., 2014). The loss of ILK leads to a range of global cellular effects, such as a decrease in the number of cell-cell connections and decreased cadherin expression (Novak et al., 1998). However, there is limited understanding of how ILK is able to interact and be influenced by a variety of cell signalling pathways, such as Wnt (Miller and Moon, 1996).

Little is known about how ILK expression affects MSCs, however, ILK expression is down regulated during chondrogenic differentiation (Goessler et al., 2006, Goessler et al., 2009). ILK over expression was induced through adenoviral transduction *in vitro* and was found to increase MSC proliferation and reduce apoptosis. These ILK over expressing MSCs were then transplanted into a myocardial infarction porcine model and found to improve ventricular remodelling and cardiac function (Mao et al., 2014).

ILK plays an important role in the maintenance of ECs and endothelial tissues, diseases such as uraemia (urea in the blood) cause damage to the vasculature and ECs. Within a mouse model ILK knock out was induced in ECs, the cells expressed enhanced apoptosis, increased reactive oxygen species production and decreased cell proliferation when exposed to a urea toxin. Therefore, ILK plays an important role in EC protection against urea toxins through an unknown molecular mechanism (Garcia-Jerez et al., 2015). Additionally the importance of ILK in angiogenesis has been reported. Through the use of a novel inhibitor molecule, ILK transcription was suppressed. This inhibitor molecule was applied to *in vitro* and *in vivo* melanoma assays and found to suppress angiogenesis within both models. These results were attributed towards reduced EC migration

through cytoskeleton rearrangement (Lu et al., 2013, Chen et al., 2007). ILK is an important molecule that allows cells to interact with their external environment, either directly through binding with ECM or indirectly through cell-cell adhesion. Indeed, these cell-ECM and cell-cell adhesions are the force bearing structures that respond to forces from the surrounding environment of multi-cellular tissues (Collins and Nelson, 2015).
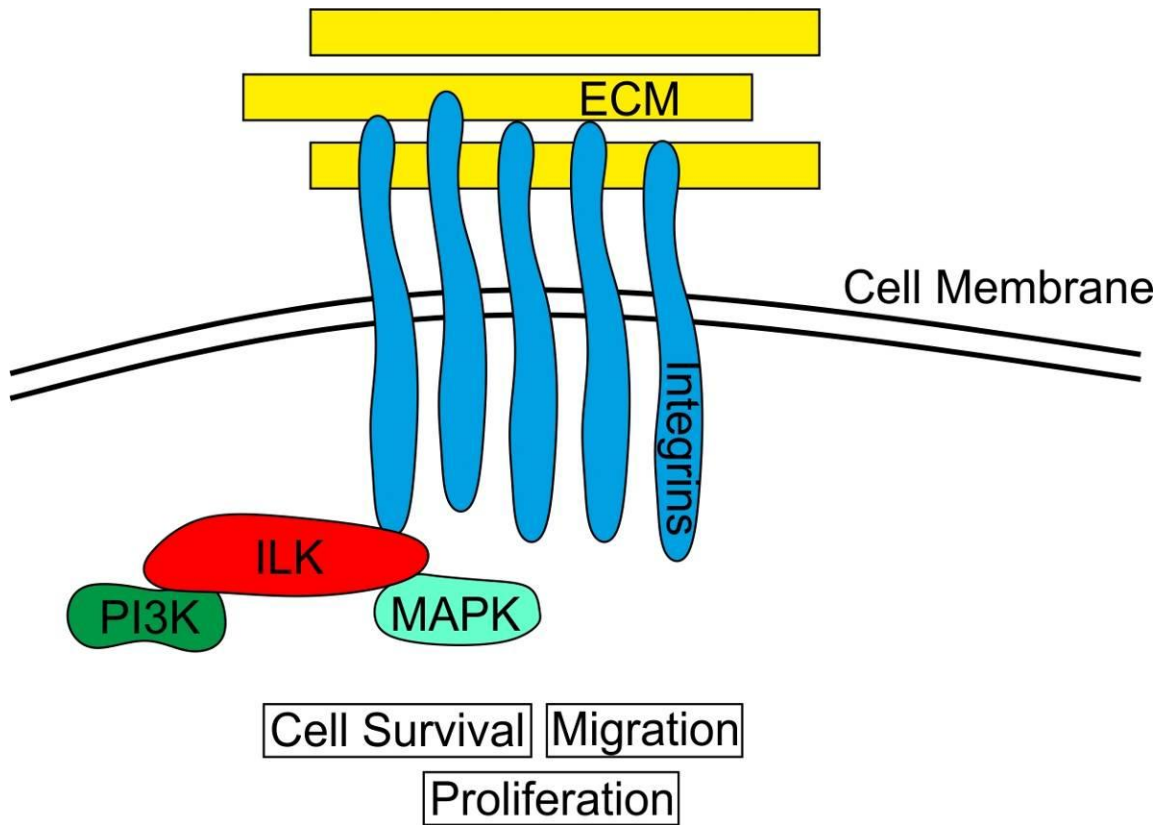
Figure 1.6.2 – Schematic representation of integrin-linked kinase

Integrins provide a link between the cytoskeleton of a cell and the extra cellular matrix (ECM), this can trigger PI3K and MAPK signalling leading to changes in cell survival, migration and proliferation.

1.6.1 Multiple cell culture

Traditional cell culture has consisted of using a single cell type; the culture of cells from an individual cell source is often used to generate a specific cell line. The continuation of these cell lines is fundamental for reproducible biological research. Therefore, culturing multiple cell types together has been shunned for fear of cross-contamination. Indeed, cross-contamination within cell lines has frequently been reported, the HeLa cell line has been reported as one of the most common contaminants (Jager et al., 2013, Kniss and Summerfield, 2014). However, the culture of a single cell type does not accurately recreate the *in vivo* environment.

Within the physiological environment, native tissues are multi-cellular systems. The interactions of these various cells is imperative for proliferation, viability, differentiation, growth factors and extra cellular matrix production (Hui and Bhatia, 2007, Nam et al., 2011, Sorrell et al., 2007, Traphagen et al., 2013). Subsequently *in vitro* co-culture of multiple cell types has been used to enhance research in a wide range of fields. Within breast cancer studies, aromatase inhibition is the main treatment method in oestrogen receptor positive breast cancer (Sasano and Harada, 1998). However, monoculture of breast cancer cell lines have below detection levels of aromatase at both mRNA and enzymatic activity level (Sanderson et al., 2001). Therefore, cell lines were developed with aromatase transfection to reduce this discrepancy (Sun et al., 1997). However, co-culture of primary breast cancer cell lines with adipose stromal cells significantly increased aromatase mRNA (Miki et al., 2007).

1.6.2 Co-culture of MSCs and ECs

MSCs are traditionally derived from bone marrow, a highly vascularised tissue. Additionally the MSC stem cell niche is most likely perivascular; therefore, within the native environment MSCs are closely associated with ECs. Indeed, a variety of studies have shown that MSCs affect ECs and vice versa (Ramasamy et al.,

2014, Kusumbe et al., 2014). MSCs are able to enhance angiogenesis through expression of VEGF (Beckermann et al., 2008, Timmers et al., 2011). ECs affect MSCs through paracrine factors; EC conditioned medium applied to MSCs was found to enhance proliferation, osteogenic differentiation and viability (Saleh et al., 2011a).

One of the first direct co-cultures of MSCs and ECs was used in the treatment of critical sized calvarial defects in immunodeficient mice. The co-culture of the two cell types resulted in a greater number of functional blood vessels compared to individual application of either ECs or MSCs (Koob et al., 2011). *Ex vivo* direct co-culture of MSCs and ECs in 3D spheroid culture had enhanced osteogenic potential and inhibited adipogenic potential. Additionally observations of cellular organisation within the spheroids revealed ECs formed a segregated network (Saleh et al., 2011b). This enhancement of osteogenic potential of MSCs in co-culture with ECs has been reported in several studies, however, the effect is attributed towards unknown paracrine cross talk (cell signalling) between MSCs and ECs that is currently undefined (Gershovich et al., 2013, Sasaki et al., 2015).

1.7 Cell Signalling

Cell signalling is a highly complex process of communication between cells. Cell signalling is important as it orchestrates development during embryogenesis, homeostasis within adult tissues and repair following injury (Jones, 2000). Cell signalling has been substantially linked with cellular organisation, both during embryonic development and tissue repair (O'Dea and King, 2013). Three signalling pathways that play an important role in these key cellular processes are: fibroblast growth factor signalling, platelet derived growth factor signalling and notch signalling, and are described in future detail below.

1.7.1 Fibroblast growth factor signalling

Fibroblast growth factor (FGF) signalling is an evolutionarily conserved signalling cascade responsible for a wide range of cellular functions such as; wound

healing, embryonic development, angiogenesis and metabolism (Katoh, 2002, Belov and Mohammadi, 2013, Dorey and Amaya, 2010, Sun et al., 1999). FGFs can have both a paracrine and autocrine effect; FGF is able to exert its cellular affects through FGF receptors (FGFR) in a complex with heparan sulphate (HS) (Yayon et al., 1991). In humans there are 22 members of the FGF family, these all share a conserved 120 amino acid sequence, however, only 18 of these members signal via interactions with FGFR (Ornitz and Itoh, 2001). There are a total of seven FGFRs that are encoded through four FGFR genes, the additional FGFRs occur due to isoforms (Johnson and Williams, 1993). Binding of FGF to FGFR results in activation of signalling cascade, four key pathways can be activated; MAPK, PI3K, Phosphoinositide phospholipase C-γ (PLC- γ) and Janus Kinase (JAK or JAK-STAT), a schematic representation of this can be seen in Figure 1.7.1 (Furdui et al., 2006). These signalling pathways are known to initiate anti-apoptotic signalling, cell growth, proliferation and enhance c-Myc expression (Gotoh, 2008). FGF signalling regulation is critical to ensure appropriate stimulation, this occurs through a negative feedback loop and receptor autoinhibition (Wang et al., 2002, Plotnikov et al., 1999).

1.7.2 Platelet derived growth factor signalling

Platelet derived growth factor (PDGF) signalling is considered to be both an autocrine and paracrine form of signalling. A wide range of cellular behaviours are known to be affected by PDGF signalling, such as: proliferation, migration, morphology and angiogenesis (Heldin and Westmark, 1999). It is able to exert its cellular effects by binding to platelet derived growth factor receptor (PDGFR). Activation of PDGFR triggers PI3K, JAK and PLC-γ signalling, this causes a range of cellular changes; some of these changes are caused by reorganisation of actin filaments within the cytoskeleton (Figure 1.7.2) (Takagi et al., 2014, Shioda et al., 2009, van Wieringen et al., 2009). Activation of PDGFR-β in fibroblasts has been known to stimulate chemotaxis on a collagen substrate (Popova et al., 2004).
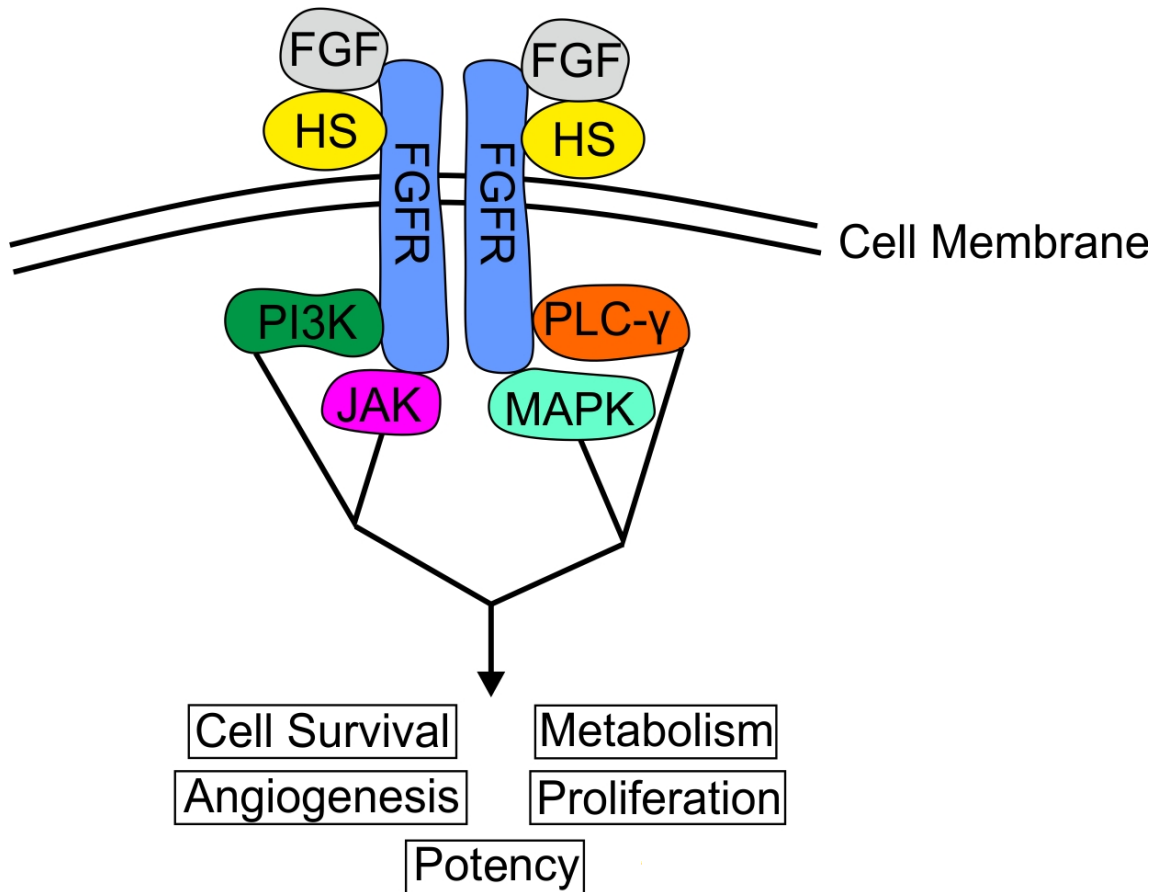
Figure 1.7.1 – Schematic representation of FGF signalling pathway

FGF binds to FGFR in a complex with heparan sulphate (HS). Binding of FGF to FGFR results in a signalling cascade of four different pathways: PI3K, JAK-STAT, MAPK and PLC-γ. This leads to changes in cell survival, metabolism, angiogenesis, proliferation and cell potency.
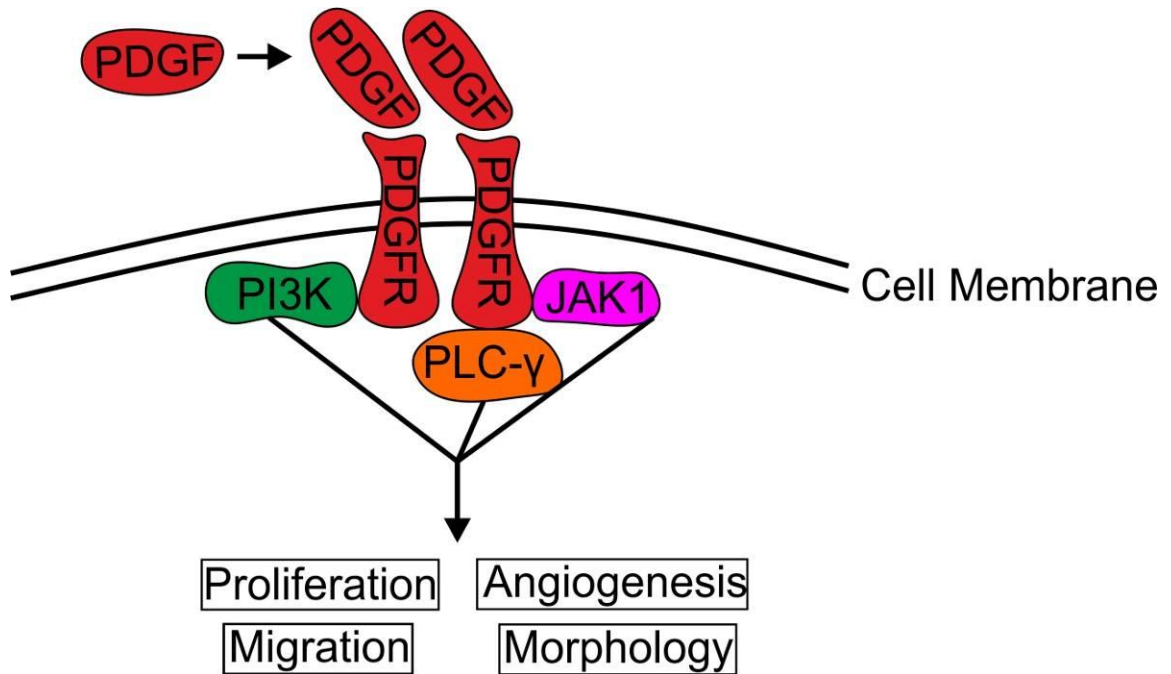
Figure 1.7.2 – Schematic representation of the PDGF signalling pathway

PDGF binds to PDGFR, this binding triggers a signalling cascade of three different pathways, PI3K, JAK-STAT and PLC-γ. This leads to changes in proliferation, angiogenesis, migration and morphology

1.7.3 Notch signalling

Nearly 100 years ago the Notch gene was initially observed in Drosophila, the phenotype of "notches" within the wings were described, resulting in the name (Morgan, 1917). Notch signalling is an evolutionary conserved juxtacrine signalling pathway (Wearing et al., 2000, Nakano et al., 2015) . Within humans there are four Notch receptors and five ligands. Activation of Notch signalling occurs through direct interaction of a receptor with the ligand of a neighbouring cell, resulting in activation of the Notch gene (Hill-Felberg et al., 2015, Wang et al., 2015). A schematic of this can be seen in Figure 1.7.3, in brief the signal-sending cell expresses Delta-like or Jagged ligand on the cell surface, Fringe is able to regulate the binding of these ligands with Notch (Moloney et al., 2000). Upon binding of Delta-like or Jagged with the signal-receiving cell, the notch intracellular domain (ICD) is released triggering changes to angiogenesis, migration, apoptosis, cell survival and proliferation (Simon et al., 2014). Abnormal Notch signalling is observed within many cancers such as; leukaemia and breast cancer. Inhibition of Notch could therefore be used as a possible cancer therapeutic (Egloff and Grandis, 2012).
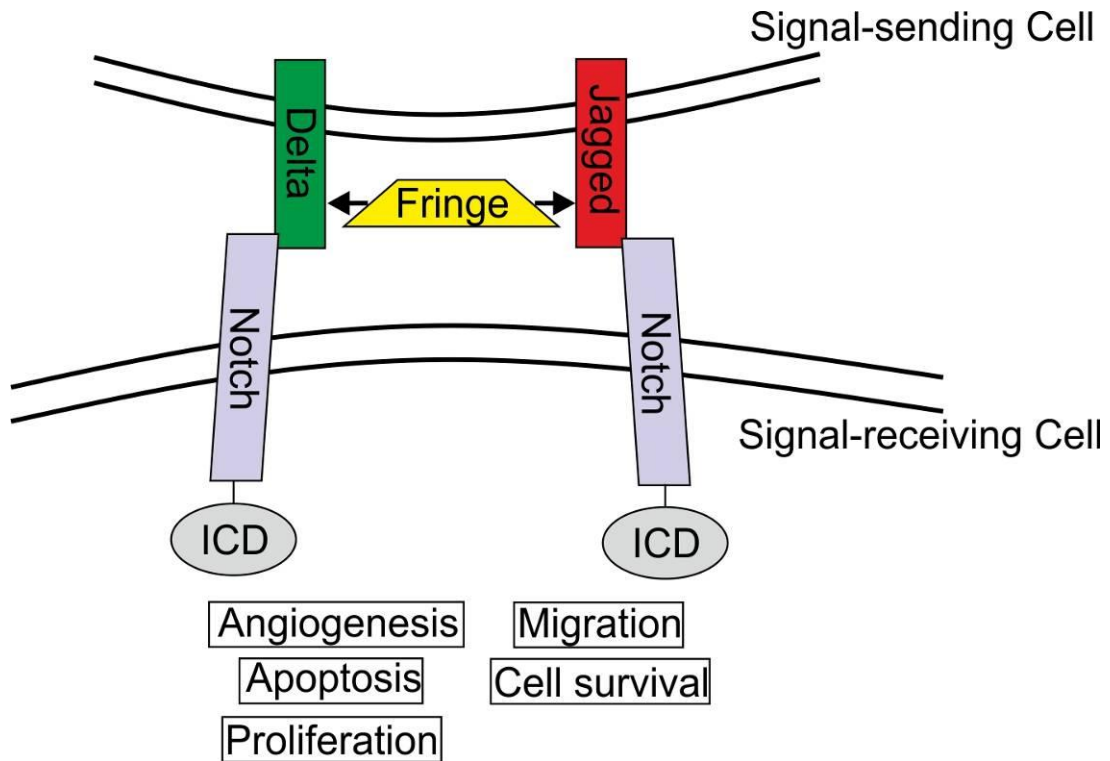
Figure 1.7.3 – Schematic representation of the Notch signalling pathway

The signal-sending cell expressed Delta-like or Jagged ligand at the cell surface, through Fringe regulation this is able to bind to Notch on the signal-receiving cell. Binding triggers release of the Notch intracellular domain (ICD) resulting in changes to angiogenesis, migration, apoptosis, cell survival and proliferation.

1.8 Project Aims

Increasing evidence has begun to highlight the importance of both three-dimensional culture and multiple cell culture systems. Traditional 2D single cell culture has frequently demonstrated poor translation compared to the native cell environment (Haycock, 2011, Miki et al., 2007). Therefore, the next generation of stem cell research requires using unconventional cell culture methods combining multiple cell types. Co-culture of MSCs with ECs has strong potential; MSCs most likely reside within a perivascular niche and subsequently interact with the ECs of the blood vessel (Crisan et al., 2008). Therefore, the aim of the project is to investigate the co-culture of MSCs and ECs in 3D spheroid culture. Initial investigations will optimise the ratio of MSCs and ECs within the spheroid model. The optimised co-culture spheroids will then be assessed during spheroid formation and long-term culture. Specifically the osteogenic differentiation potential of MSCs co-cultured with ECs will be quantified through the development of a novel assay. EC self-organisation previously described will be further characterised and investigated to establish the cell signalling pathways involved (Saleh et al., 2011b). Additionally the skeletal potential of MSCs will be investigated through partial differentiation to create osteogenic MSCs and chondrogenic MSCs, these cells will be used in combination with ECs to create *ex vivo* osteochondral models.

Chapter 2

Chapter 2 : Materials and Methods

2.1 Cell Culture Methods

Human MSCs were used with the approval of the York Local Research Ethical Committee. All experimental protocols were conducted in accordance with The University of York Department of Biology Ethics Committee guidelines and were approved by the South Humber Local Research Ethics Committee. All tissue culture flasks and plates were purchased from Corning Life Sciences (Corning, NY, USA) unless otherwise stated. Foetal bovine serum (FBS) was purchased from BioSera (Labtech International Ltd, East Sussex, UK) after batch testing. Phosphate buffer saline (PBS), trypsin-EDTA and Dulbecco's Modified Eagle Medium (DMEM) containing L-glutamine (2mM) and high glucose (Cat no. S41966-052) were all purchased from Invitrogen (Life technologies, Paisley, UK). All media contained 100 units/ml and 100 µg/ml penicillin-streptomycin (P/S) unless otherwise stated (Cat no. S15140-122, Invitrogen). Cells were incubated at 37°C, 5% CO_2, 95% air in a humidified atmosphere.

2.1.1 Extraction of Human MSCs from Femoral heads

Following informed patient consent and approval by the South Humber Local Research Ethics Committee femoral heads extracted following hip replacement surgery at Clifton NHS treatment centre were transported in honey jars (Cat no. 1LQA01, SLS, East Yorkshire, UK) containing 500 units/ml and 100 µg/ml P/S and 2.5 µg/ml Amphotericin B (Cat no. 1LXA01 Fisher Scientific, Loughborourgh, UK). The trabecular bone was removed from the femoral head and placed into a tube containing 10 ml DMEM and P/S. The trabecular bone was then minced using scissors; the supernatant was then collected and transferred to a separate tube. This process was repeated twice more, for the final stage, fresh medium was added before being vortexed for 1 minute. The supernatant was centrifuged at 450 xg for 5 minutes. The pellet was then resuspended in DMEM containing

P/S before being passed through a 70 µm cell strainer (Cat no. 11597522, Fisher Scientific). The strained supernatant was gently layered onto 12 ml Ficoll-Plaque Plus (Cat no. 1LHA02, VWR, Leicestershire, UK) and centrifuged at 350 xg for 30 minutes with low braking. The supernatant was gently removed and the white layer of mononuclear cell layer was extracted using a plastic Pasteur pipette. The mononuclear cells were then added to 10 ml of wash buffer (5mM EDTA, 0.2% Bovine Serum Albumin (BSA) in PBS) (Sigma-Aldrich, MO, USA) before being centrifuged at 450 xg for 5 minutes. The supernatant was removed and the cell pellet was resuspended in DMEM containing 15% FBS and P/S, before being seeded into a T75 cell culture flask. The cells were left for 3-4 days to allow them to settle before the media was replaced – the cells were then expanded as described below (Section 2.1.3).

2.1.2 Extraction of Human MSCs from the Tibial Plateau

Following informed patient consent and approval by the South Humber Local Research Ethics Committee, tibial plateaus were taken during knee replacement surgery at Clifton NHS treatment centre. The bone samples were dissected into small pieces approximately 1 cm^2 and placed bone marrow side down onto cell culture treated petri dishes. The petri dishes were then flooded with DMEM media containing 15% FBS and P/S. The petri dishes were incubated with the bone fragments to allow cell migration from the bone. After the one week the bone fragments were removed and the media replaced, the cells were then expanded as described below (Section 2.1.3).

2.1.3 Human MSC Culture and Expansion

Human bone marrow derived MSCs extracted via the methods described above were cultured in DMEM containing 15% FBS and P/S hereafter referred to as MSC basal medium. Upon reaching 90% confluency, the cells were passaged by incubation with 0.05% trypsin-EDTA for 5 minutes at 37°C; cell detachment was confirmed using a light microscope. The cells were then re-seeded at a 1 in 3 ratio in MSC basal medium, containing FBS to neutralise the trypsin-EDTA.

MSCs were not used in any experiments beyond passage 5. MSC basal culture medium was changed twice a week.

2.1.4 Human Umbilical Vein Endothelial Cell Culture and Expansion

Human Umbilical Vein Endothelial Cells (HUVECs) were purchased from PromoCell (PromoCell, Heidelberg, Germany) and cultured in Endothelial Cell Culture Medium (Cat no. C-22010, PromoCell) containing the accompanying supplement mix; 10% FBS and P/S. HUVECs were cultured up to 90% confluency before being passaged using trypsin-EDTA as described above and re-seeded at a 1 in 3 ratio. Endothelial culture medium was replaced twice a week and HUVECs were used for experiments between passage 4 and 6. HUVECs were used due to them being a type of endothelial cell (EC); all experiments were performed with these cells and are commonly referred to as ECs rather than HUVECs.

2.1.5 Human Dermal Fibroblast Culture and Expansion

Human dermal fibroblasts (HDF) were purchased from Cascade Biologics (Life Technologies, UK). HDFs were cultured in DMEM containing 15% FBS and P/S, medium was changed twice a week and cells were passaged at approximately 90% confluency using trypsin-EDTA and re-seeded at a 1 in 5 ratio. HDFs in all experiments were used between passage 7 and 10.

2.1.6 Mycoplasma Testing

All cells were regularly checked for mycoplasma. Mycoplasma testing was performed before every experiment on all cell types in culture. Mycoplasma testing was performed by taking a small aliquot of trypsinised cells and seeding them onto a 24-well plate. The cells were then left to adhere for at least 4 hours. Once the cells had attached, culture medium was aspirated and cells were washed with PBS twice before being fixed in 70% methanol for 5 minutes. Once the cells were fixed, methanol was removed and the cells were washed with PBS

twice, the PBS was fully removed before the cells were stained with 100 µl of 4', 6- diamidino-2-phenylindole (DAPI) at a concentration of 1 µg/ml in PBS. Once the stain was applied the cells were incubated in the dark at room temperature for 5 minutes. After the incubation the DAPI was removed and the cells were washed three times with PBS. Observations of extra nuclear DNA indicative of a mycoplasma infection were made using a DMIRB, Leica fluorescence microscope and checked by a second independent observer. If positive, mycoplasma-contaminated cells were immediately destroyed.

2.1.7 Live/Dead Cell Viability Staining

Live/Dead viability staining was performed on 3D MSC and EC co-culture spheroids to ascertain the long term viability of 3D spheroid culture (Cat no. L3224, ThermoFisher, UK). The viability assay was used to stain living cells green, whilst dead cells would be stained red, from this the percentage of dead cells within a spheroid could be calculated. The stain was able to identify living cells through the enzymatic conversion of cell-permeable Calcein AM into fluorescent Calcein which is retained within living cells (green). Dead cells were identified through EthD-1 entering cells with a damaged membrane and undergoing a 40-fold enhancement of brightness upon binding with nucleic acid (red). Cell spheroids were prepared for the Live/Dead viability assay by firstly being washed twice with PBS; spheroids were then incubated at 37°C with 50 µl of Live/Dead reagent for 45 minutes. The Live/Dead reagent contained 4 µM EthD-1 and 2 µM Calcein AM in sterile PBS.

2.1.8 3D Cell Culture

Cells were cultured in a 3D spheroid configuration; this was achieved using non-adherent U-bottomed 96-well plates (Cat no. 1LQA01, Fisher Scientific). A cell suspension totalling 30,000 cells was added into the individual wells with 100 µl of appropriate medium containing 0.25% (w/v) methyl cellulose (Sigma-Aldrich), the cells then allowed to aggregated to form a spheroid (Figure 2.1.1). Various

combinations of cells were combined to create co-culture spheroids, such as MSCs and ECs or HDFs and ECs. MSC and EC combinations were cultured in media made up of 50% DMEM, 50% Endothelial cell media, 15% FBS, P/S and 0.25% (w/v) methyl cellulose. HDF and EC were also cultured in the same media to act as a control. Media was changed twice a week via split feeding to prevent damage to the cell spheroid.
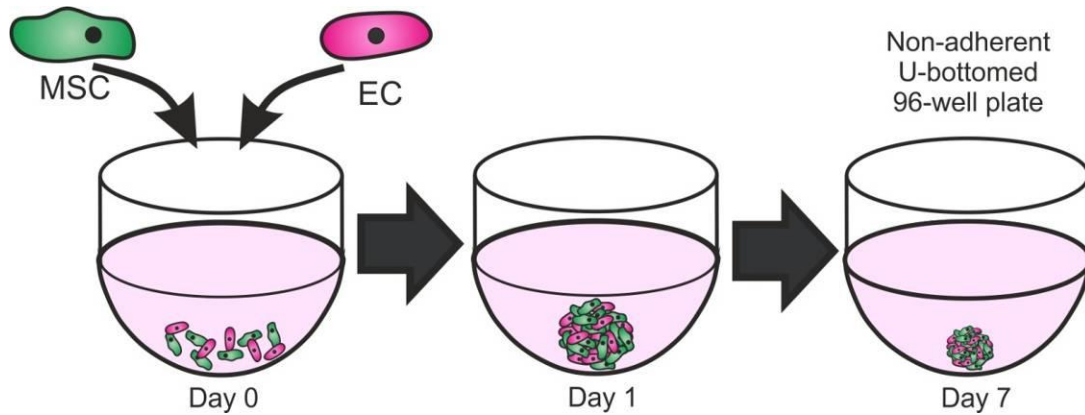
Figure 2.1.1– Formation of 3D co-culture spheroids using MSCs and ECs in non-adherent U-bottomed 96-well plates

A cell suspension totalling 30,000 cells was added into each individual well of the non-adherent U-bottomed 96-well plates. Within 24 hours the cells aggregated together to form a spheroid, this 3D structure could then be maintained and culture within this environment.

2.2 Cell Tracker™ Labelling of Cells

CellTracker™ was used to label MSCs, HUVECs and HDFs. Cells were labelled either green, red or blue using the relevant CellTracker™ described below. CellTracker™ green BIODIPY (8-chloromethyl-4,4-difluoro-1,3,5,7-tetramethyl-4-bora-3a,4a-diaza-s-indacene, Cat no. C2102, Invitrogen, UK) absorption 522 nm and emission 529 nm. CellTracker™ red CMTPX (Cat no. C34552, Invitrogen) has an absorption at 577 nm and an emission at 602 nm. CellTracker™ blue CMHC (4-chloromethyl-7-hydroxycoumarin, Cat no. C2111, Invitrogen) absorbance 372 nm and emission 470 nm.

2.2.1 Application of CellTracker™ Green, Red and Blue

Approximately $1\text{-}2\text{x}10^6$ cells were labelled using the quantity of CellTracker™ solution described below; optimisation of the CellTracker™ solution was also performed. Cells were trypsinised and counted using a haemocytometer before being centrifuged at 400 xg for 5 minutes, the supernatant was then removed and the cells washed with PBS before being centrifuged again at 400 xg for 5 minutes. The supernatant was aspirated; this was done to remove any FBS from the solution. A CellTracker™ solution was then made using DMEM (0% FBS) with a final optimised concentration of either 0.5 µM red, 2µM green or 10 µM blue CellTracker™. The appropriate cells were then incubated in 4 ml of the CellTracker™ solution for 1 hour at 37^oC, this allowed for the active uptake of the CellTracker™ into the cytoplasm of the cell were it remained for approximately 10 days. After incubation the cells were centrifuged at 400 xg for 5 minutes, the supernatant was removed and DMEM containing FBS was applied. The cells were then incubated for 30 minutes at 37^oC to ensure all extracellular CellTracker™ was neutralised, after this incubation period the cells were centrifuged at 400 xg for 5 minutes and the supernatant was removed. After this procedure the cells were fluorescently labelled in the desired colour and were seeded as required.

2.3 Histological Techniques

2.3.1 Cryosectioning of 3D Spheroids

Spheroids were carefully transferred from the U-bottomed 96-well plate into a cap of an Eppendorf tube using a cut 200 µl pipette tip. The medium was carefully removed before the cell spheroid was washed with PBS. The PBS was then gently aspirated and Tissue-Tek optimised cutting tissue (OCT) was added avoiding the incorporation of air bubbles, before being snap frozen in liquid nitrogen and stored at -80°C (Cat no. 4583, Sakura Finetek Europe, The Netherlands). The frozen spheroids were sectioned at 7 µm thickness using a Bright's cryostat (OFT5000, Bright Instruments, UK) and placed onto Superfrost positive microscope slides (Cat no. SHE2505, Thermo Scientific). The slides were stored at -20°C until required. All images shown of spheroid sections are representative of the observations made within a minimum of three sections of three different spheroids, unless otherwise stated.

2.3.2 Immuno staining

Immuno staining was performed on both spheroid sections and 2D cultured cells; however, the fixation process different slightly between them. Spheroid sections on Superfrost slides were treated with 4% paraformaldeyde (PFA) for 5 minutes at room temperature, immediately after removal from -20°C storage. 2D cultured cells were washed twice with PBS at room temperature before being fixed using 4% PFA for 5 minutes and washed twice more with PBS. After this process both samples were treated identically, non-specific binding was blocked via incubating the samples in 10% of appropriate animal serum for 30 minutes. Samples were incubated with primary antibodies (Table 2.3.1) in a PBS/0.1% BSA solution, within a humidity chamber for 1 hour at room temperature or 4°C overnight. The primary antibody was then carefully removed and the samples were washed three times with PBS before being incubated at room temperature in the dark with the appropriate conjugated secondary antibody (Table 2.3.2). Samples were then

washed a further three times with PBS to remove any excess non-specific secondary antibody. DNA staining to identify nuclei was also performed by incubating the samples for 10 minutes in 1 µg/ml DAPI. Samples were mounted using the appropriate sized coverslip and Vectashield (Vector Laboratories, Peterborough, UK) before being examined using either a Leica DMIRB fluorescent microscope or Zeiss LSM 780 multiphoton inverted microscope.

Table 2.3.1 –Primary antibodies used for immuno fluorescent labelling of cells

Primary Antibody	Isotype	Concentration Used	Supplier	Cat no.
Collagen type I	Rabbit IgG	1 in 20	AbCam	Ab292
Collagen type II	Mouse IgG	1 in 100	AbCam	Ab53047
CD31	Rabbit IgG	1 in 20	AbCam	Ab76533
Sox9	Rabbit IgG	1 in 100	AbCam	Ab36748
Hes-1	Goat IgG	1 in 100	Santa Cruz	I3002
Runx2	Rabbit IgG	1 in 100	Santa Cruz	Sc-10758
Osteocalcin	Mouse IgG	1 in 100	R&D Systems	MAB1419
Osteonectin	Mouse IgG	1 in 100	DHSB	AON-1
pERK	Rabbit IgG	1 in 100	R&D Systems	AF1018
Ki67	Rabbit IgG	1 in 100	AbCam	Ab15580
Mouse IgG	Isotype control	1 in 100	BD Pharmingen	555573
Rabbit IgG	Isotype control	1 in 100	Vector	I-1000

Table 2.3.2 – Secondary antibodies used for immuno fluorescent labelling of cells

Secondary Antibody	Species Raised In	Concentration Used	Supplier	Cat no.
Alexa Fluor anti-mouse 488	Goat	1 in 200	Invitrogen	A-11001
Alexa Fluor anti-rabbit 488	Goat	1 in 200	Invitrogen	A-11008
Alexa Fluor anti-mouse 647	Donkey	1 in 200	Bioss	Bs-0310G
Cy3 conjugated anti-goat	Rabbit	1 in 200	Millipore	AP106C
Cy3 conjugated anti-rabbit	Sheep	1 in 200	Sigma	C2306

2.4 Statistical Analysis

Data presented within graphs shows mean ± standard deviation unless otherwise stated. Experiments were performed at least in triplicate using three different biological donors unless otherwise stated (N>9). All data were analysed using PRISM software (GraphPad Software, CA, USA) one-way and two-way ANOVA was performed on appropriate data sets with Tukey post test or Bonferroni post test. P values <0.05 were considered statistically significant. * P<0.05, ** P<0.01, *** P<0.001, **** P<0.0001.

Chapter 3

Chapter 3 : Bone Formation of MSCs in 2D and 3D, With and Without ECs

3.1 Introduction

Within human bone marrow, the primary role of MSCs is to sustain tissue homeostasis (Nombela-Arrieta et al., 2011). The ability of MSCs to undergo osteogenic differentiation (bone formation) under specific *in vitro* culture conditions is often described as a method to characterise and identify this cell type (Lu et al., 2014, Siddappa et al., 2007). The majority of MSC osteogenic differentiation has been performed in 2D *in vitro* culture conditions. However, recent advances in 3D *in vitro* cell culture can be used to more accurately recreate the native environment (Laurent et al., 2013). The concept of multiple cells being cultured within the same environment has led to co-culturing MSCs and even tri-culturing MSCs with other cell types (Rinker et al., 2014, Gershovich et al., 2013, Saleh et al., 2011a). Within these studies it was found 2D and 3D co-culture of human MSCs with ECs resulted in increased osteogenesis. More specifically MSCs co-cultured with HUVECs demonstrated an increased osteogenic potential through alizarin red (calcium deposition) and alkaline phosphatise (an osteoblast marker) staining. The increased osteogenic potential within MSCs has been attributed to a soluble factor(s) released by the HUVECs. This was demonstrated by culturing MSCs in HUVEC condition medium (Saleh et al., 2011a).

These *in vitro* studies are further supported by *in vivo* evidence. Analysis of the link between angiogenesis and bone formation *in vivo* has started to suggest that MSCs play a vital role in vascular organisation and subsequent bone formation. This has been demonstrated in a variety of different ways, including implantation of MSCs to improve hind limb ischemia in mice (Bhang et al., 2012b). Again, these effects have been attributed to a soluble factor(s) which through *in vivo*

mice studies, the involvement of the Notch signalling pathway. Genetic disruption of Notch signalling within endothelial cells of mice resulted in impaired blood vessel morphology within bone marrow and reduced osteogenesis. Addition of recombinant Noggin as a Notch-controlled angiocrine regulator restored bone growth and mineralisation (Ramasamy et al., 2014).

The process of bone formation and maintenance *in vivo* is a complex 3D process involving multiple cell types, various signalling pathways and mechanical stimuli. However, most *in vitro* bone analysis has been performed in 2D environments. The use of 3D systems to more accurately represent native characteristics and behaviours has become highly compelling. Within cancer cell studies the use of 3D *in vitro* culture systems has been proven to more closely represent *in vivo* tumour behaviour. Various studies using 3D systems instead of 2D systems have shown 3D systems are more accurate when determining molecular tumour growth and facilitating drug discoveries (Laurent et al., 2013, Thoma et al., 2014). Therefore, the evolution of *in vitro* MSC bone formation from a conventional 2D to 3D system has become essential. This will require the development of novel assay strategies to quantify and assess bone formation within 3D *in vitro* environments.

Second harmonic generation (SHG) imaging can be used to visualise and quantify collagen within 2D and 3D culture. SHG is based upon a nonlinear optical effect by which photons of a specific frequency can interact with a material of the same frequency to generate new photons with twice the energy and half the wavelength. This phenomenon can be used within cell biology to visualise cells and tissue structure, without staining a material and subsequently damaging it. The use of SHG imaging for fibrillar collagen within a diverse range of tissues has been performed. Collagen type I and II are able to be SHG imaged due to their aligned fibre structure, unlike collagen type III and IV. Using this technique it is possible to assess collagen formation within diseases such as cancer and connective tissue disorders (Zipfel et al., 2003, Chen et al., 2012, Campagnola, 2011).

3.2 Aims

The general aims of the work presented within this chapter are to characterise the ability of human MSCs to undergo osteogenic differentiation within 2D and 3D environments, and to determine if the presence of human endothelial cells can affect this process.

More specifically the objectives are to:

- Determine comparative methods of quantifying osteogenic differentiation of MSCs within a 2D and 3D environment.
- Develop new methods to quantify and assess bone formation using MSCs in a 3D environment.
- Examine if co-culture of MSCs with ECs has an effect on osteogenic differentiation.
- Use second harmonic generation imaging to qualitatively and quantitatively assess collagen within a 3D *in vitro* environment.
- Determine if long term 3D culture of MSCs and ECs have detrimental effects on cell viability.

3.3 Methods

3.3.1 Analysis of MSC Markers

A panel of commonly used non-specific MSC cell surface markers were used to identify cells extracted from human hip and knee sources, using flow cytometry and approximately 50,000 MSCs were harvested per target antibody. MSCs were prepared by washing twice with PBS before being detached from the cell culture flask using wash buffer (5 mM EDTA, 0.2% BSA in PBS). Cells were centrifuged at 450 xg for 5 minutes before being resuspended in 1ml of wash buffer; this was then divided equally between 10 tubes. Primary antibodies were added to the cell suspension at the concentrations shown in Table 3.3.1 and incubated on ice for 45 minutes. After incubation the samples were centrifuged at 400 xg for 5 minutes and the supernatant was removed, fluorescently conjugated antibodies were resuspended in 500 µl wash buffer and stored on ice. Non-fluorescently conjugated antibody samples were resuspended in 100 µl of wash buffer and AlexaFlour 647 donkey anti-mouse antibody applied at a 1:200 dilution and then incubated on ice for 45 minutes. Samples were then washed with wash buffer before being centrifuged at 400 xg for 5 minutes and the supernatant removed. All samples were suspended in 1 ml of wash buffer before being analysed using CyAn™ ADP Analyzer (Beckman Coulter, CA, USA) at appropriate excitation and emission wavelengths and analysed using Summit and FlowJo software.

Table 3.3.1 MSC marker antibodies

Target	Conjugate	Host	Dilution	Cat no.	Supplier
CD45	FITC	Mouse	1:100	MRC04501	Caltag Labs
CD166	PE	Mouse	1:50	559263	BD Pharmingen
CD44	FITC	Mouse	1:10	555478	BD Pharmingen
CD34	FITC	Mouse	1:50	130-081-001	Miltenyi biotech
CD90	IgG	Mouse	1:100	14-0909-81	ebioscience
CD105	IgG	Mouse	1:100	14-1057-81	ebioscience
CD29	IgG	Mouse	1:100	36741A	BD Pharmingen
CD73	IgG	Mouse	1:100	550256	BD Pharmingen
Anti-mouse IgG	Alexaflour 647	Donkey	1:200	A-31571	Invitrogen

3.3.2 Analysis of Endothelial Cell Markers

HUVECs underwent flow cytometric analysis to determine expression of specific endothelial cell markers, specifically expression of the cell surface marker CD31 (Cat no. sc-20071, Santa Cruz). A FITC conjugated CD31 was applied to the HUVECs using the same method as previously described (Section 3.3.1).

3.3.3 Osteogenic Differentiation of 2D MSCs

Osteogenic differentiation of MSCs was induced by culturing the cells in osteogenic induction medium. Osteogenic induction medium was created by the addition of 5 mM β-glycerophosphate, 50µg/ml ascorbic acid phosphate and 10nM dexamethasone (all Sigma-Aldrich, UK) to standard 2D culture medium (DMEM, 15% FBS and P/S). The culture medium was replaced twice a week for up to 21 days.

3.3.4 3D co-culture of MSCs and endothelial cells

MSCs and ECs were co-cultured together in the 3D system described previously (Section 2.1.7). U-bottomed 96 well plates contained individual cell spheroids within each well, these where then harvested at specific times and further analysed. Medium was replaced on the cell spheroids twice a week using a pipette and split feeding.

3.3.5 Quantification of calcium within culture medium

Standard techniques to quantify osteogenesis of MSCs in 2D translate ineffectively for 3D systems. Alizarin Red S staining for example cannot be used to quantify calcium deposits within spheroids sections. Sectioning a spheroid can result in sectioned material that varies greatly in size due to where they originated from; they can also easily tear and have missing material. Calcium depletion from culture medium could be used as a non-destructive, real-time method to quantify calcium incorporation and subsequent osteogenesis within 2D and 3D systems.

To quantify the amount of calcium within culture medium, cells were first seeded for a period of 24 hours to allow them to be fully attached to tissue culture plastic (for 2D cultures) or to have formed a spheroid (for 3D). After this period the entire medium within the well was carefully removed using a pipette, and was replaced with 150 µl of appropriate medium for 96-well plate culture or 500 µl for 24-well plate culture. A schematic overview of the process within a U-bottomed 96 well plate can be seed in Figure 3.3.1. A control sample of medium was placed into an adjacent well not containing cells, an example of this within a 24-well plate format can be observed in Figure 3.3.2. To reduce any potential discrepancies due to evaporation all un-used wells were filled with PBS and the well plates were wrapped with Parafilm (Cat no. SPU5601, Fisher, UK) leaving a small 1 cm gap to allow gas exchange during culture. The samples were then incubated for precisely 96 hours at 37°C, 5% CO_2 and 95% air in a humidified environment before the medium samples were carefully removed and placed into separate Eppendorf tubes. The cell and control wells could be reused and fresh medium

was added and the process repeated for up to 24 days in culture. Individual medium samples were analysed using a QuantiChrom™ Calcium Assay Kit (Cat no. DICA-500, BioAssay Systems, CA, USA) as per the manufacturer's instructions. Briefly, calcium ion (Ca^{2+}) concentration was analysed by taking a 5 µl sample of medium and adding it to 200 µl of the Calcium Assay Kit working reagent and incubated at room temperature for 3 minutes. The working reagent was prepared by combining equal volumes of Reagent A and Reagent B. The Calcium Assay Kit allowed the concentration of calcium ions within the medium samples to be calculated through optical density readings at 570 nm using a Dynex MRX II plate reader and a calcium ion standard.
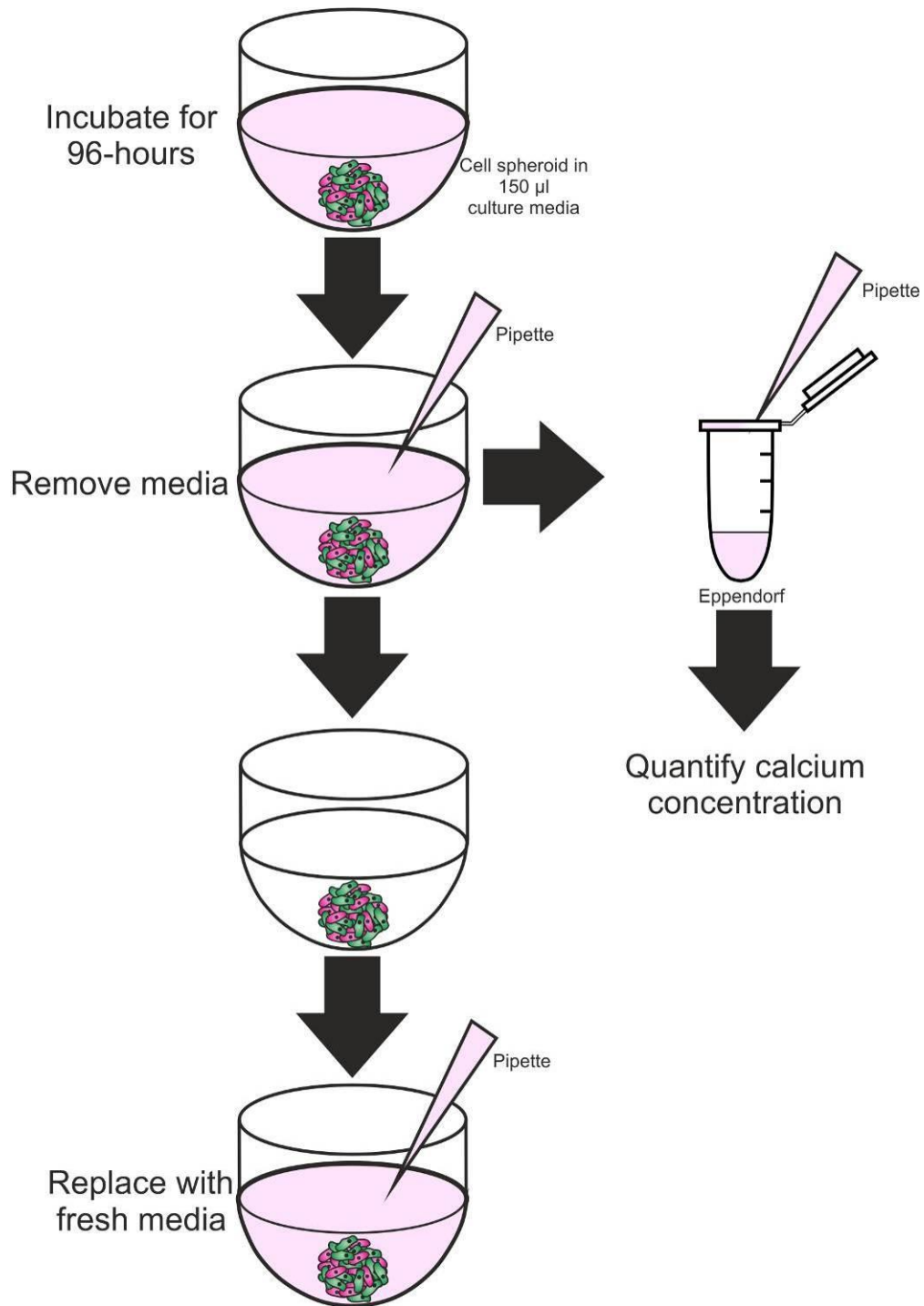
Figure 3.3.1 – Schematic representation of medium removal and replacement for 3D calcium analysis

A single well of a U-bottomed 96 well plate is filled with 150 µl of appropriate cell culture medium. After 96-hours at 37^oC, 5% CO_2 and 95% air in a humidified environment the medium is carefully removed using a pipette and replaced with fresh medium. The calcium concentration within the culture medium was then quantified and compared to a control medium sample.

Figure 3.3.2 – Schematic representation of a 24-well plate layout used to assess calcium depletion from culture medium

Unused wells are flooded with PBS to reduce evaporation. Sample and control wells contain 500 µl of the same medium, however, only sample wells contain the relevant cells or cell spheroids.

3.3.6 Histological staining

3.3.6.1 Alizarin red S

Alizarin red S staining was performed to visualise calcification within osteogenic differentiated MSCs. Samples were washed with PBS twice followed by fixation using 4% Para formaldehyde (PFA) in PBS incubated at room temperature for 5 minutes. The samples were then washed three times with PBS before being stained with a 40 mM Alizarin Red S solution pH 4.2 (Sigma-Aldrich, UK) for 20 minutes at room temperature. After the incubation, the samples were washed three more times with PBS and once with tap water to remove any non-specific staining. The samples were then imaged using a light microscope (DRB, Leica).

3.3.6.2 Alizarin red S elution and quantification

Alizarin red S staining of samples within well plates could be quantified by elution of the stain. Once the stain had dried, the Alizarin red S staining was eluted by the addition of 400 µl of 10% (w/v) cetylpyridinium chloride (CPC) (Cat no. C0732, Sigma-Aldrich), which was added into the 24-well plate and incubated for 1 hour at room temperature. After this incubation period, a 200 µl sample of the eluted stain was transferred into a 96-well plate and the absorbance of the eluted stain was measured using a Dynex MRX II plate reader at 630 nm.

3.3.6.3 Alkaline Phosphatase and von Kossa staining

To assess the osteogenic state of the MSCs, samples were stained to detect alkaline phosphatase (ALP) activity and von Kossa to identify mineralised deposits. Samples cultured in both basal and osteogenic medium conditions were examined. To stain for ALP samples were incubated in a solution of 0.2 mg/ml napthol AS-MX in 1% N,N-dimethylformamide diluted in 0.1M Tris (pH 9.2) with 1 mg/ml Fast Red TR (all Sigma Aldrich) at room temperature for 2 minutes, any positive stained regions turned a pink colour. The samples were then washed twice with PBS before being fixed using 4% PFA at room temperature for

5 minutes. After fixation von Kossa staining was performed by incubation of the samples with a 1% silver nitrate (Sigma Aldrich) solution on a light box for 60 minutes, any positive areas stained a grey/brown colour. Samples were then washed with dH_2O, incubated in 2.5% sodium thiosulphate for 5 minutes and washed again in dH_2O to remove any non-specific staining.

3.3.7 Second Harmonic Generation Imaging

Second harmonic generation imaging was used to detect collagen using a confocal multiphoton microscope. A 870 nm laser from the microscope was used to detect second harmonic generation between 400-500nm.

3.3.8 Imaging and Quantification of staining

Fluorescent and confocal microscopy was performed using a Zeiss LSM 780 multiphoton inverted microscope. This microscope was used in combination with Zen 2009 imaging software (Zeiss, Germany), Volocity software (Perkin Elmer) and Image J (MBF – McMaster Biophotonics Facility, Canada) to process and analyse images. Light microscope images were taken using a DMIRB Leica Light microscope (Leica Germany).

3.4 Results

3.4.1 MSC Characterisation

To demonstrate that MSCs sourced from either femoral head or knee extracts expressed the same cell surface markers as those typically found three randomly selected donors were subjected to characterisation using flow cytometry. All MSCs tested positive for the known markers CD29, CD44, CD73, CD90 and CD105, and negative for the haematopoietic markers CD34 and CD45. Both knee and femoral head MSCs did not show a positive shift for CD166. Examples of the flow cytometry for femoral head MSCs are shown in Figure 3.4.1 whilst knee extracted MSCs are shown in Figure 3.4.2. Due to the MSCs frequently being co-cultured with ECs, MSCs were immunofluorescently stained and analysed by flow cytometry for CD31, a common endothelial cell marker. All MSCs were negative for the CD31 (Figure 3.4.3).
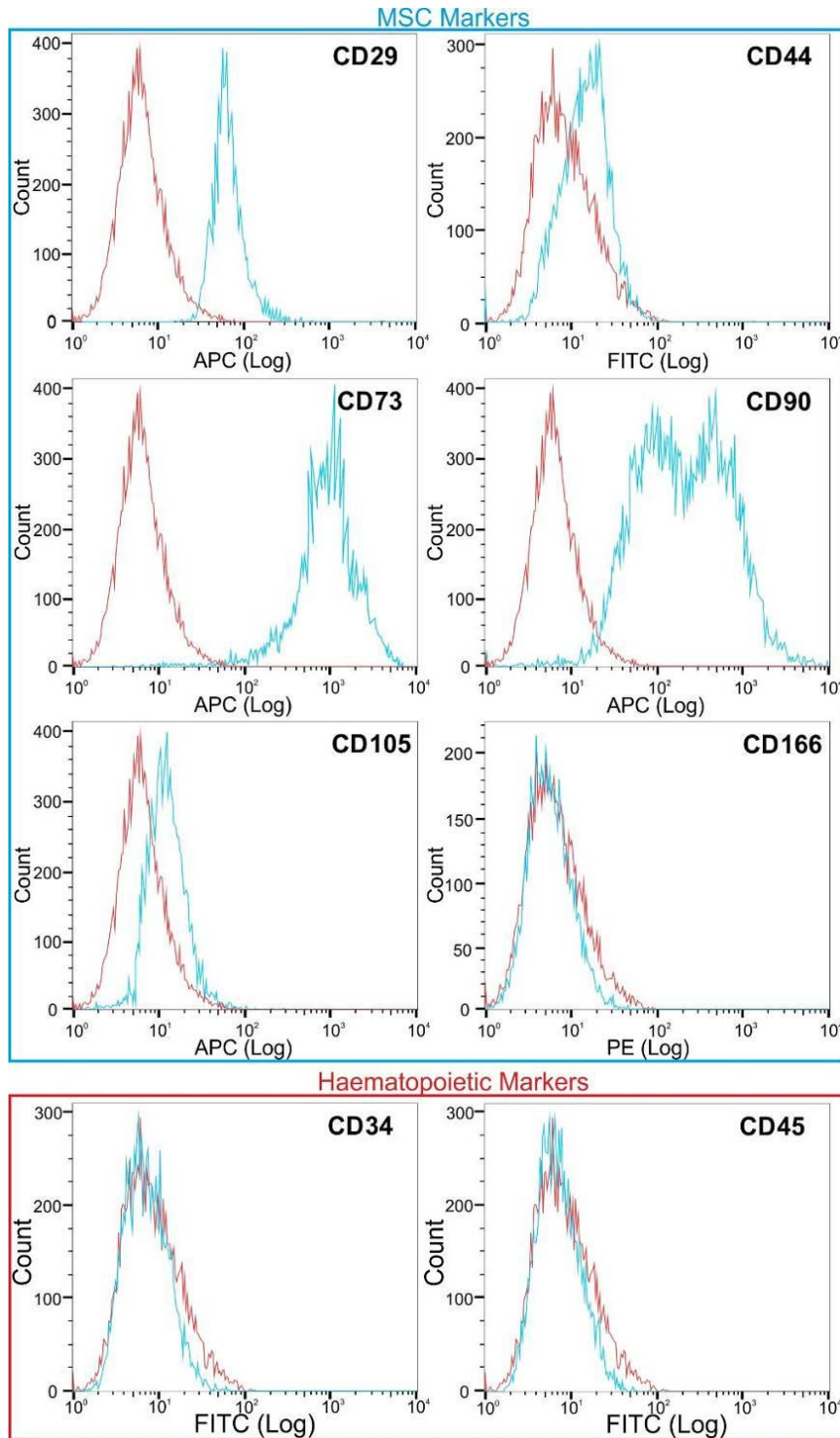
Figure 3.4.1 – Flow cytometry analysis of femoral head cell extracts

MSCs from femoral head extract and subsequent culture were antibody probed for CD29, CD34 CD44, CD45, CD73, CD90, CD105 and CD166, and analysed by flow cytometry. The histograms show marker expression (blue) relative to control (red). A positive shift in expression demonstrates antibody staining in the known MSC markers, whilst no shift was detected in the haematopoietic markers.
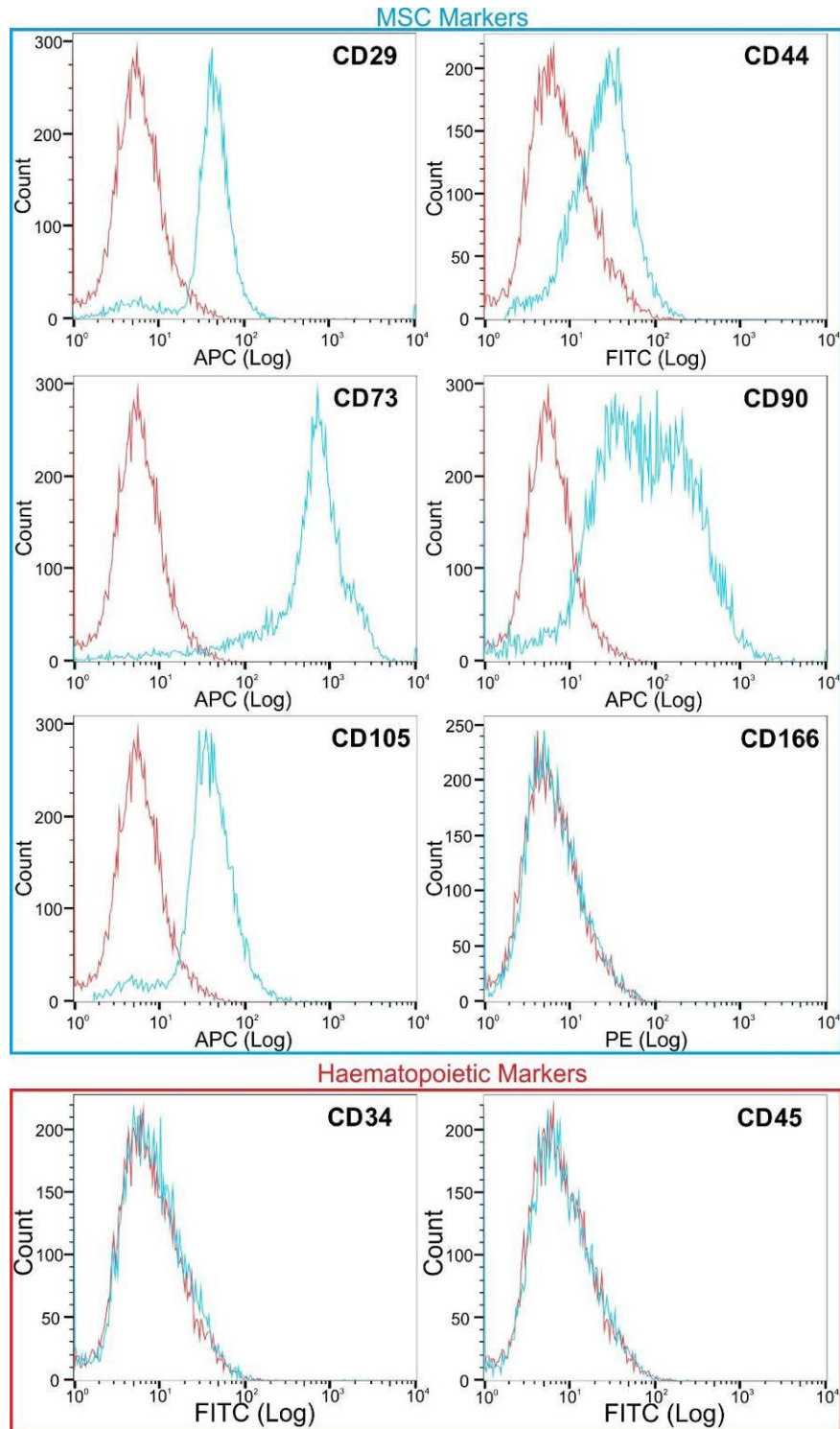
Figure 3.4.2 – Flow cytometry analysis of human knee cell extracts

MSCs from knee extract and subsequent culture were antibody probed for CD29, CD34 CD44, CD45, CD73, CD90, CD105 and CD166, and analysed by flow cytometry. The histograms show marker expression (blue) relative to control (red). A positive shift in expression demonstrates antibody staining in the known MSC markers, whilst no shift was detected in the haematopoietic markers.
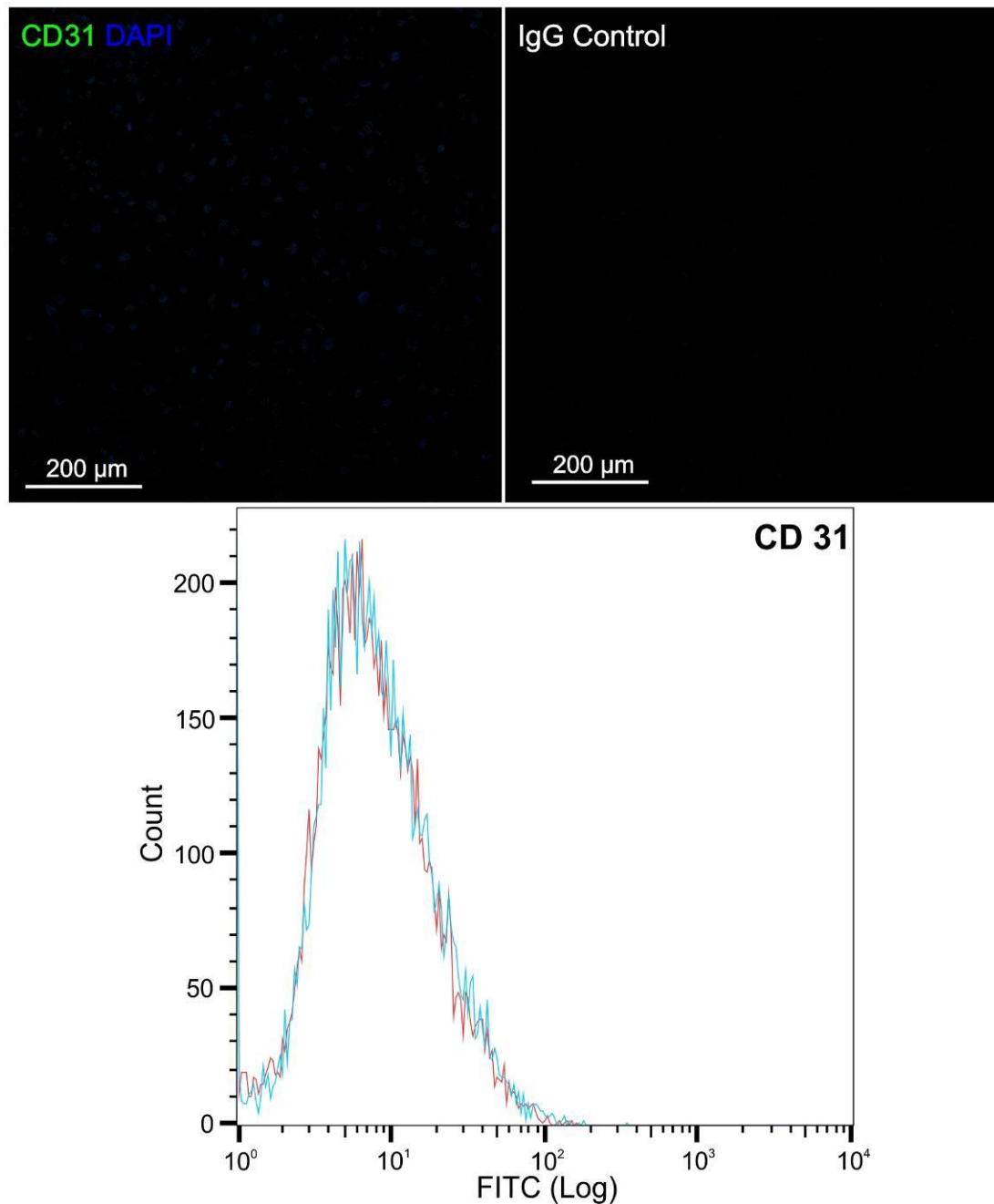
Figure 3.4.3 – Immunofluorescent and flow cytometry analysis of Mesenchymal stem cells for endothelial cell marker CD31

Representative MSC (K39) donor stained for endothelial cell marker CD31. Immunofluorescence was conducted along alongside DAPI and IgG labelling before being imaged using a fluorescence microscope. The histogram shows analysis by flow cytometry CD31 markers expression is blue relative to IgG control red. No positive CD31 expression was detected with any MSC sample.

3.4.2 Endothelial Cell Characterisation

To demonstrate that the HUVEC cells purchased from PromoCell were ECs at various passages, flow cytometric analysis of the cell surface marker CD31 was performed. All HUVECs tested positive for CD31 (Figure 3.4.4). HUVECs were also immunofluorescently labelled for CD31 and found to positively express CD31, unlike MSCs (Figure 3.4.5).
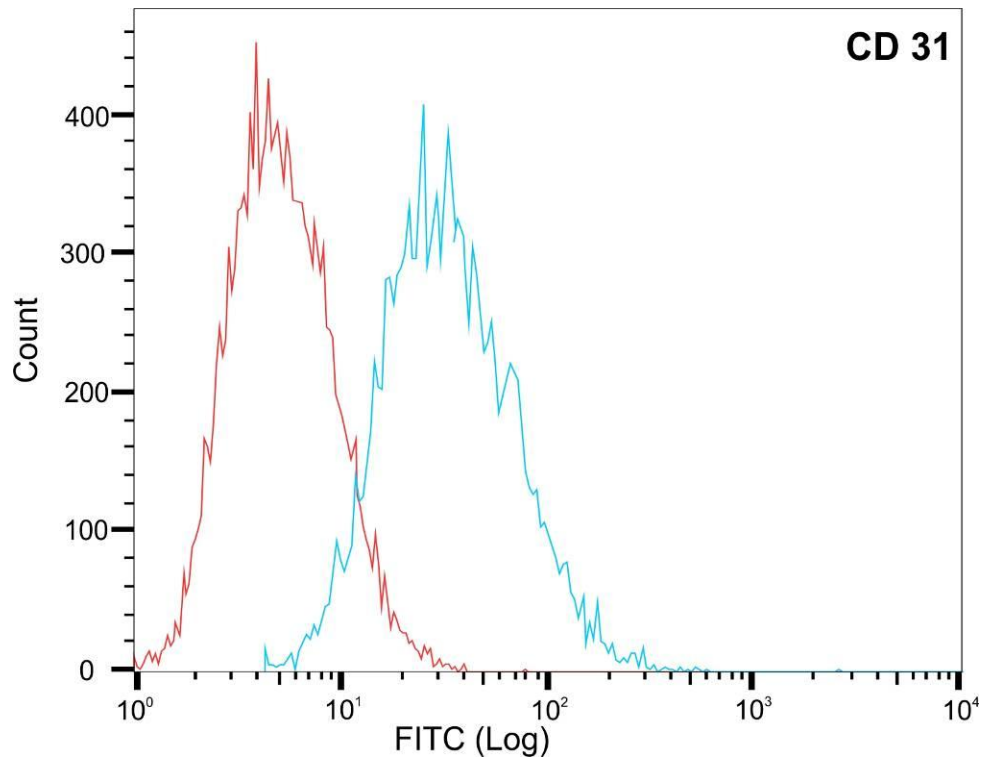
Figure 3.4.4 – Flow cytometry analysis of HUVECs for the endothelial cell marker CD31

HUVECs purchased from PromoCell were cultured and antibody probed for CD31 a common endothelial cell marker. The histogram shows CD31 expression (blue) relative to IgG control (red). A positive shift shows HUVECs are positive for the endothelial cell marker CD31.
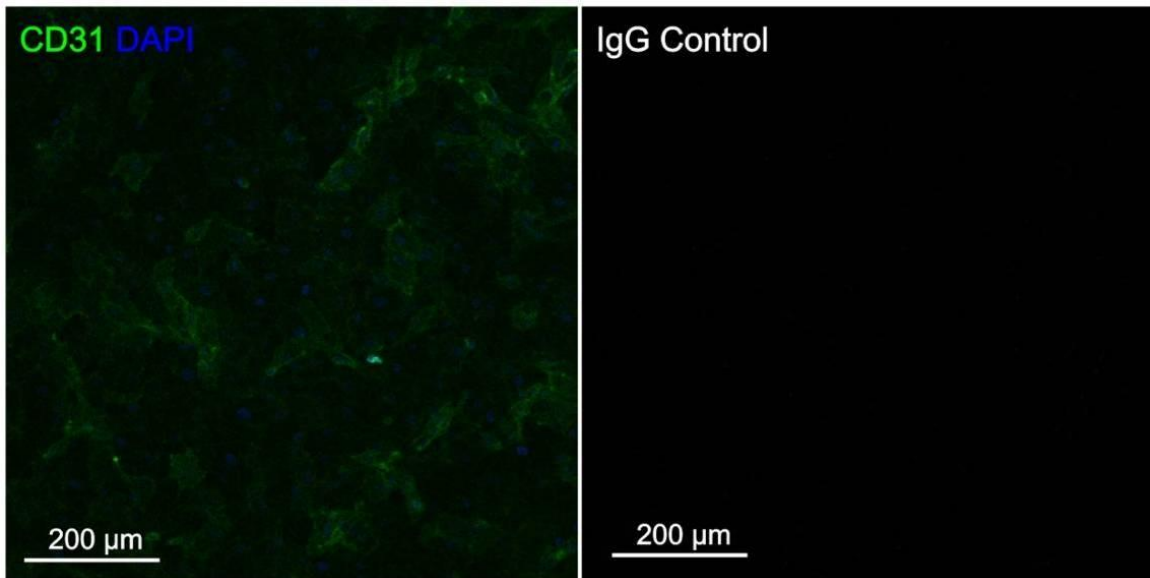
Figure 3.4.5 – Immunofluorescently labelling of HUVECs for the endothelial cell marker CD31

HUVECs were stained for endothelial cell marker CD31 and IgG control and imaged via fluorescence microscopy. Positive CD31 expression and staining is clearly observed.

3.4.3 2D Osteogenesis of MSCs

Many techniques can be used to assess osteogenic differentiation of MSCs in 2D. In this section, conventional and new methods were used to assess and quantify MSC osteogenesis in three different biological donors; Donors 1, 2 and 3 (K93, K129 and K107; K=knee sample). MSCs were cultured in basal medium or osteogenic induction medium on tissue culture plastic for up to 21 days. At various key time-points osteogenesis was assessed through ALP activity, Alizarin Red S staining for calcium deposits and von Kossa staining for phosphate deposits.

ALP and von Kossa staining was performed on the three biological Donors 1, 2 and 3 cultured in basal or osteogenic conditions (Figure 3.4.6). Pink staining indicating positive ALP activity was detected in Donors 1 and 2 following culture in osteogenic conditions after 14 and 21 days. Observations between Donor 1 and 2 were highly similar, therefore, only Donor 1 is shown in this figure. However, Donor 3 showed no positive ALP staining at any time. No positive brown/black von Kossa staining was observed in any sample.

Alizarin Red S staining was conducted and quantified via CPC elution and absorbance at 630nm (Figure 3.4.7). These results showed that Donors 1 and 2 had statistically significant Alizarin Red S staining in osteogenic conditions compared to basal at days 14 and 21. However, Donor 3 only showed statistically significant Alizarin Red S staining at day 21 compared to basal conditions.

An alternative non-destructive method to assess bone formation through the quantification of calcium within the culture medium was trialled. Using the same biological donors as previously mentioned, medium samples were collected every 96 hours for up to 20 days. The amount of calcium within the culture medium was calculated and the depletion compared to control medium was tabulated (Figure 3.4.8). Using this method it can be seen that Donors 1 and 2 had statistically significant calcium depletion in osteogenic conditions compared to basal at days

16 and 20. Donor 3 showed no significant difference in calcium depletion between osteogenic and basal culture conditions for any time point. These data indicate that Donors 1 and 2 were able to undergo osteogenic differentiation in 2D conditions whereas Donor 3 showed little evidence of osteogenic capacity.
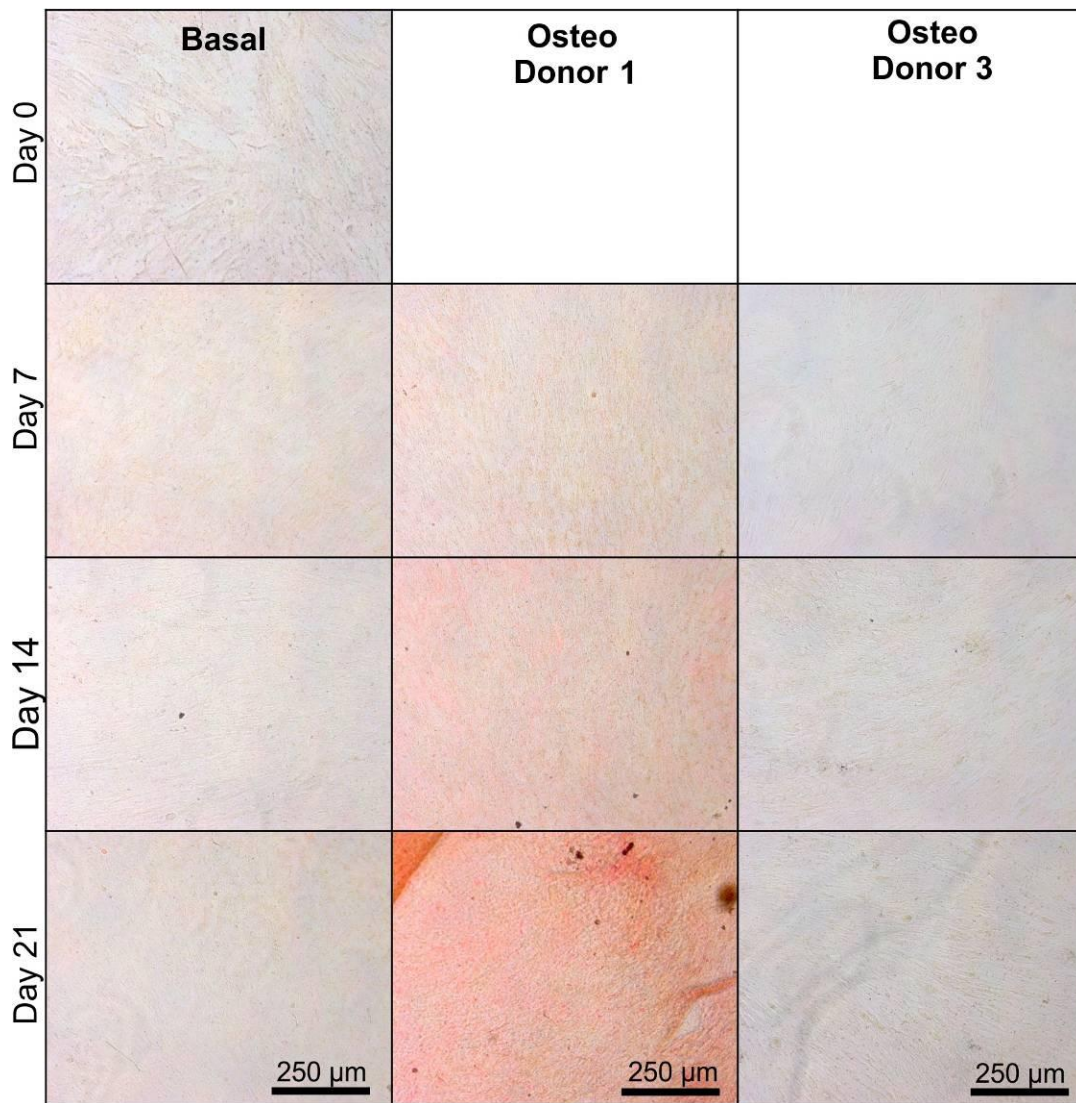
Figure 3.4.6 – ALP and von Kossa staining of 2D MSCs cultured in basal and osteogenic conditions for up to 21 days

MSC Donors 1, 2 and 3 (K93, K129, K107) were cultured in either basal or osteogenic conditions for up to 21 days. At the key time points 0, 7, 14 and 21 days they were stained with ALP and von Kossa and imaged by a bright field microscope. Both Donors 1 and 2 stained positive for ALP and von Kossa by day 21, this figure only shows Donor 1. However, Donor 3 did not have positive ALP or von Kossa staining.
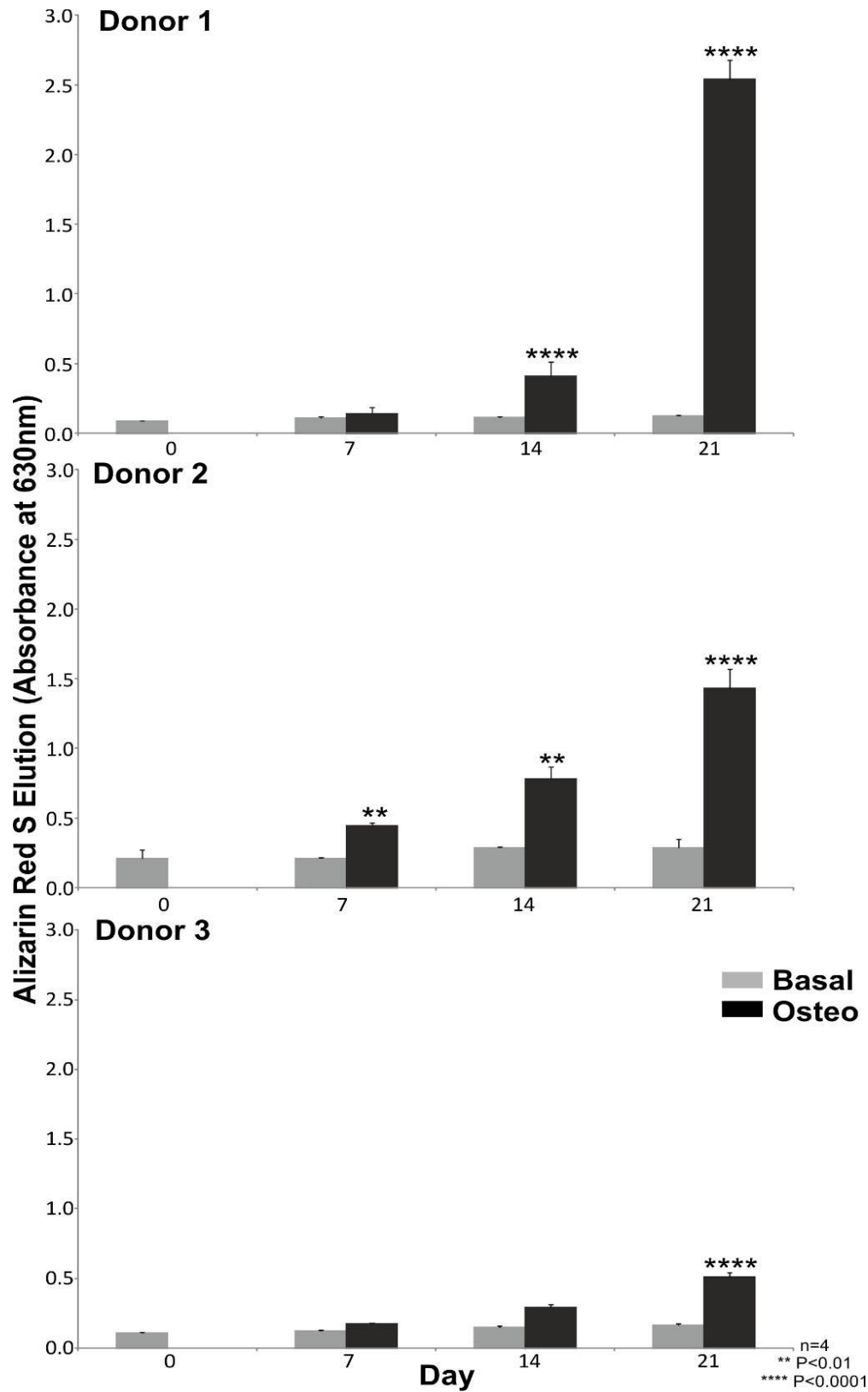
Figure 3.4.7 – 2D MSC Alizarin red S elution in both basal and osteogenic conditions in three different biological donors

MSC donors 1, 2 and 3 (K93, K129 and K107) were cultured in either basal or osteogenic conditions for up to 21 days. At key time points 0, 7, 14 and 21 days samples were fixed and stained with Alizarin red S before the dye was eluted using CPC. Using optical cytometry at 630nm comparison between basal and osteogenic conditions can be made. All three donors showed significant increases in Alizarin Red S staining after 21 days. Similarities can be seen with Donor 1 and 2 compared to calcium depletion studies. Donor 3 showed no positive ALP or von Kossa staining and minimal calcium depletion, however, a significant increase in Alizarin Red S staining can be seen at day 21. For each time point and biological donor four individual samples were tested (n=4).
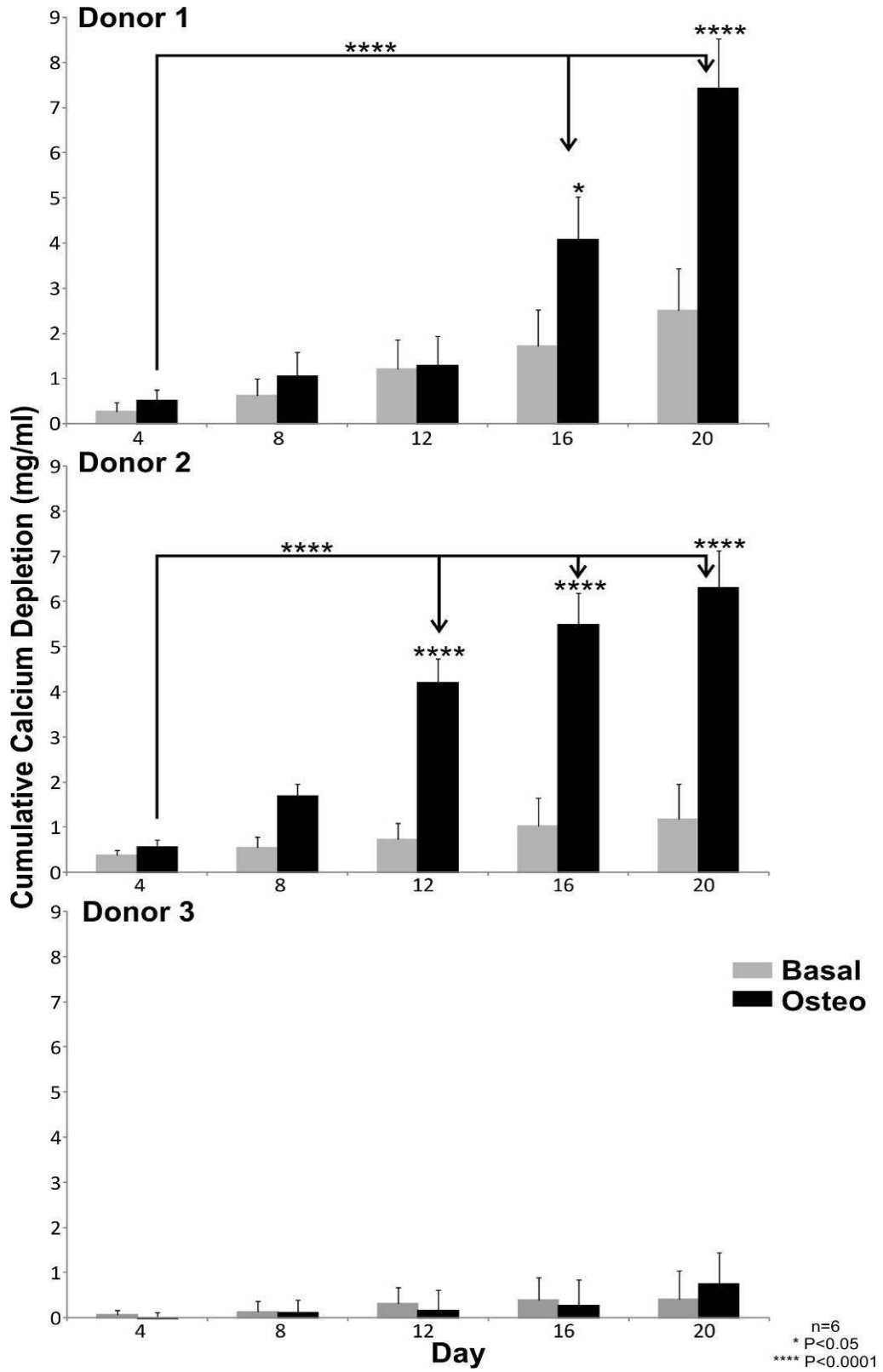
Figure 3.4.8 – 2D MSC cumulative calcium depletion from basal and osteogenic culture medium with three different biological donors

MSC donors 1, 2 and 3 (K93, K129 and K107) were cultured in either basal or osteogenic conditions for up to 20 days. Medium samples were collected every 96 hours and analysed to calculate calcium concentration compared to control medium. From this cumulative calcium depletion from the culture medium over a period of 20 days was calculated. Donors 1 showed significant calcium depletion from the culture medium compared to basal medium at days 16 and 20, these time points also show significant differences compared to day 4 osteogenic conditions. Donor 2 showed significant calcium depletion from the culture medium compared to basal at days 12, 16 and 20. Donor 3 showed no significant differences in calcium depletion, complementing previous results showing a lack of ALP and von Kossa staining (Figure 3.4.6). For each time point and biological donor six individual medium samples were tested (n=6).

3.4.4 3D Osteogenesis of Mesenchymal Stem Cells Co-cultured with Endothelial Cells

In order to quantify bone formation in 3D spheroid culture a variety of different assays were conducted. Alizarin Red S staining was performed on 3D MSC-only and MSC-EC spheroids, unlike traditional 2D culture positive staining was observed from day 1, making this stain impractical for 3D analysis (Figure 3.4.9). Para-Nitrophenylphosphate (pNPP) based ALP activity assay were also performed on 3D MSC-EC spheroids and was found to show irregular results with large error bars, rendering this analysis method inappropriate (Figure 3.4.10). ALP and von Kossa staining showed positive results for MSC-only and MSC-EC spheroid sections (Donors 1 and 2), particularly strong ALP staining was observed in MSC-EC spheroids after 21 days in osteogenic conditions. However, negligible von Kossa staining was detected (Figure 3.4.11).
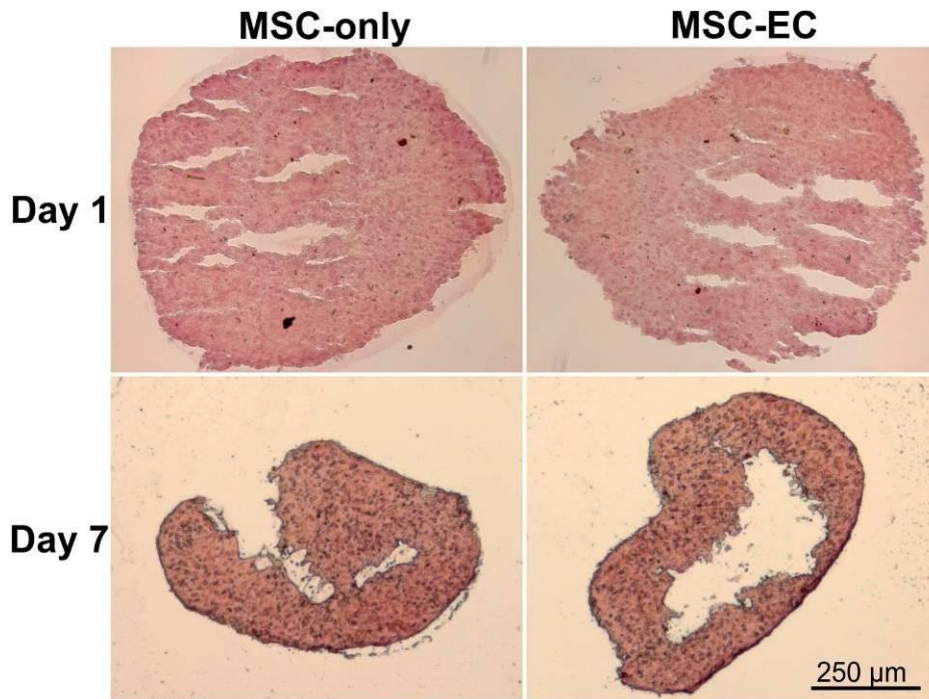
Figure 3.4.9 – 3D MSC-only and MSC-EC spheroid sections stained with Alizarin Red S at days 1 and 7

Positive Alizarin Red S staining was observed at Day 1 and at Day 7 for both MSC-only and MSC-EC spheroids, making this stain impractical for 3D spheroid sections to assess osteogenesis.
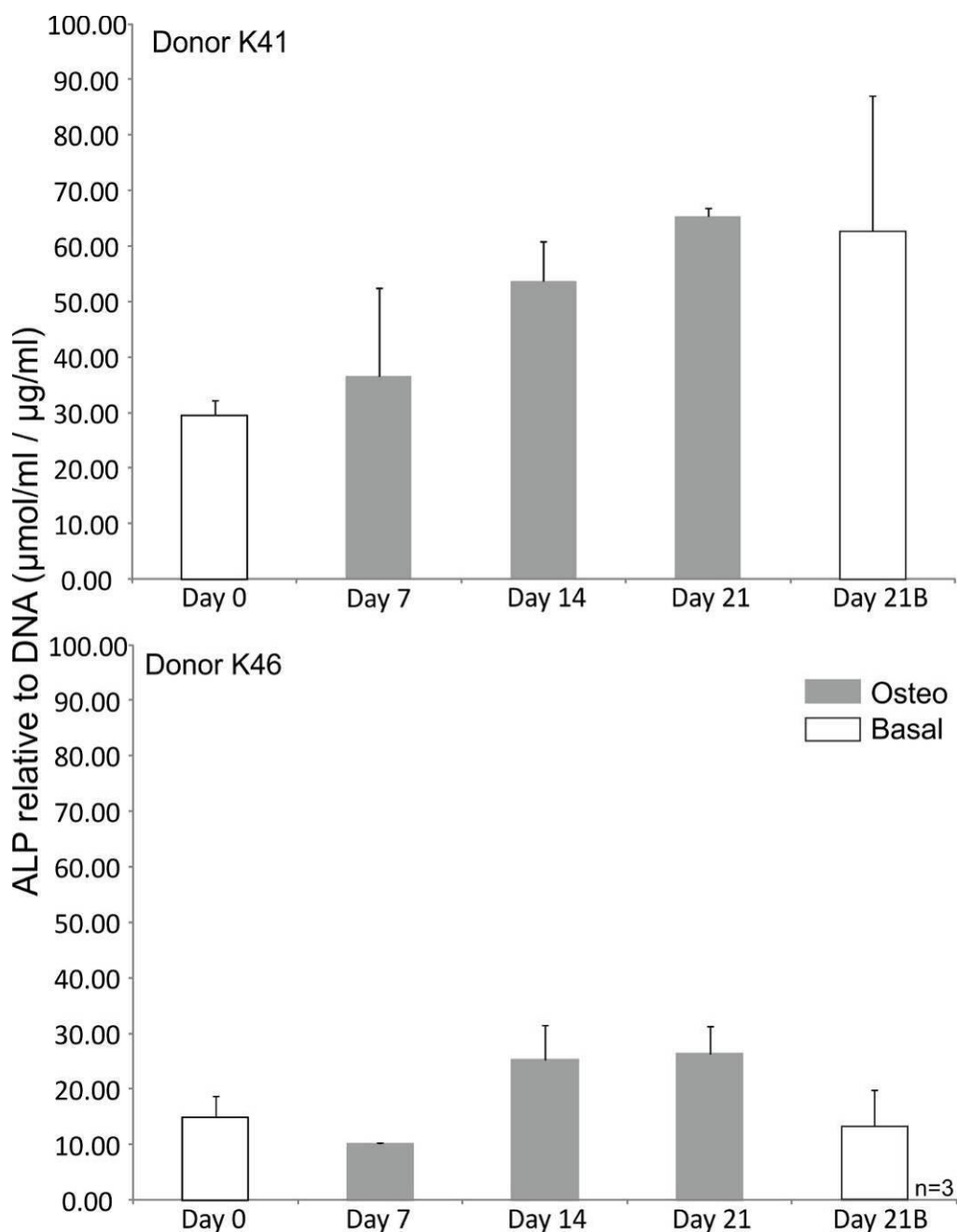
Figure 3.4.10 – pNPP analysis on MSC-EC spheroids over 21 days in osteogenic and basal conditions using two different biological donors

pNPP analysis was performed on biological donors K41 and K46 at days 0, 7, 14 and 21. For day 21 spheroids cultured in both basal and osteogenic conditions are shown. pNPP analysis was inconsistent between time points, donors and conditions. Therefore, this analysis method was not further used to quantify bone formation in 3D spheroids. For each time point and biological donor three individual samples were tested (n=3).
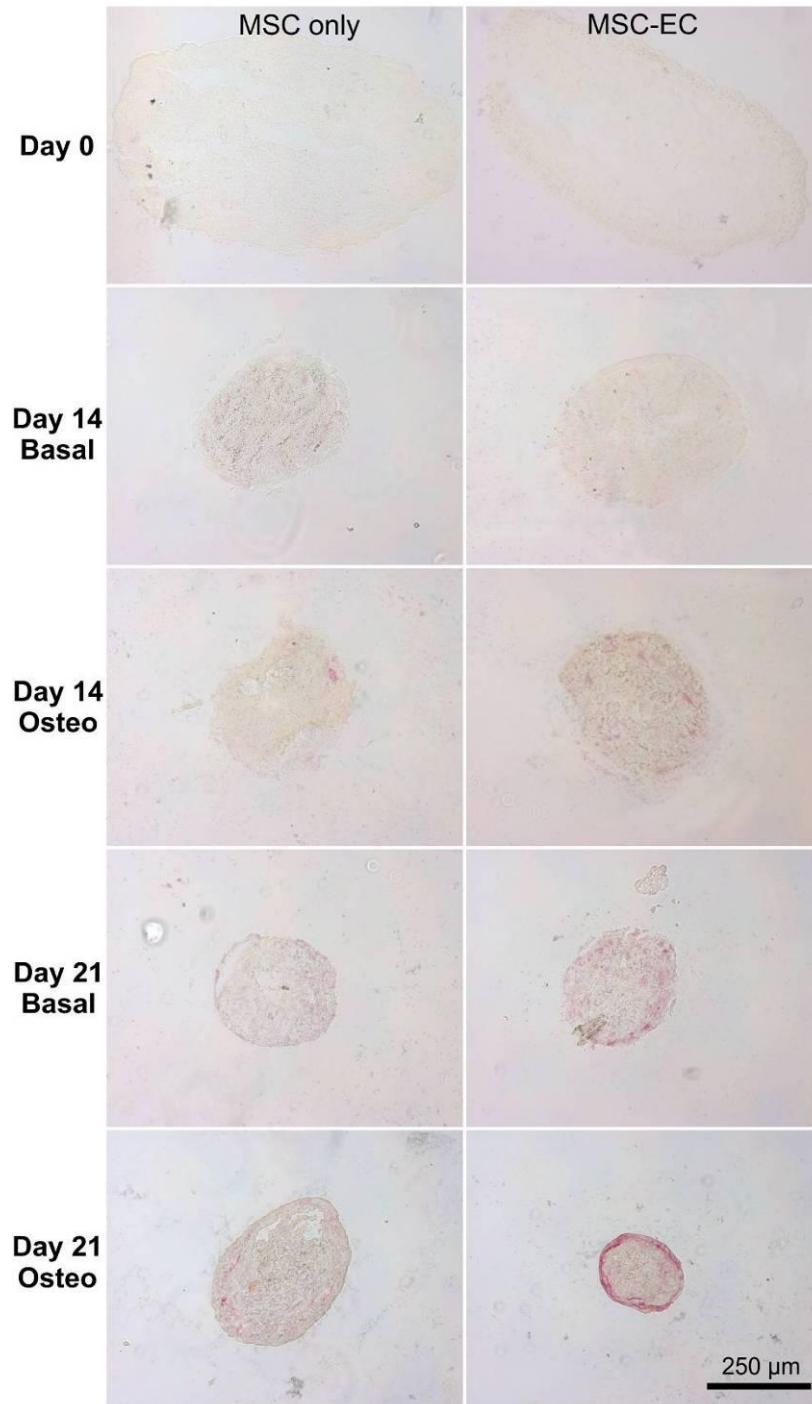
Figure 3.4.11 – ALP and von Kossa staining on MSC and MSC-EC spheroid sections

Representative sections of ALP and von Kossa staining performed on Donors 1 and 2 (K93 and K129) MSC-only and MSC-EC spheroids at various time points cultured in either basal or osteogenic conditions. Pink staining is positive ALP staining which is most strongly seen in MSC-EC sections day 21 osteogenic conditions. No positive brown/black von Kossa staining was observed.

Using the calcium quantification method, medium samples from 3D MSC-only and MSC-EC spheroids were collected every 96 hours for up to 20 days. Six individual medium samples were tested per time-point, per biological donor (n=6). The cumulative calcium depletion was then calculated for biological Donors 1 and 2 cultured in either basal or osteogenic 3D co-culture medium (Figure 3.4.12). These results showed that both Donors 1 and 2 had statistically greater calcium depletion for both MSC-only and MSC-EC spheroids when cultured in osteogenic conditions compared to basal controls. It was also observed that for both donors significantly greater calcium depletion was observed in MSC-EC osteogenic spheroids compared to MSC-only osteogenic spheroids at days 12, 16 and 20, despite MSC-EC spheroid containing half the number of MSCs.

Donor 3 (K107) was unique as during 2D analysis it appeared to be osteogenic insert, this donor was also cultured in 3D MSC-only and MSC-EC spheroids in either basal or osteogenic conditions. The spheroids were then sectioned and stained for ALP and von Kossa (Figure 3.4.13). Medium samples were also collected and cumulative calcium depletion was tabulated (Figure 3.4.14). Similar to 2D culture, Donor 3 showed no positive ALP, von Kossa staining or significant calcium depletion.
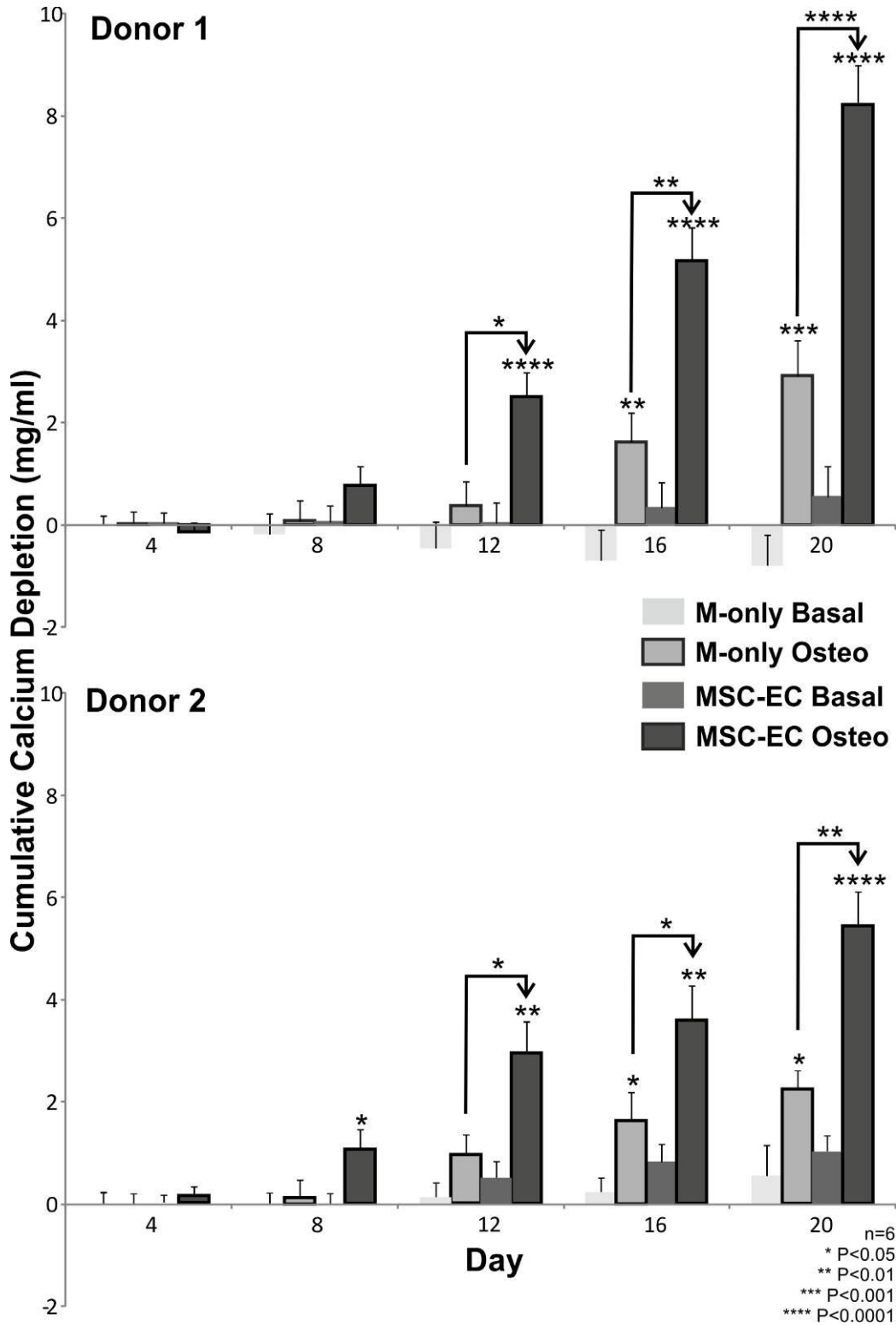
Figure 3.4.12 – 3D cumulative calcium depletion from basal and osteogenic culture medium in MSC-only and MSC-EC spheroids

MSC donors 1 and 2 (K93 and K129) were cultured in either basal or osteogenic 3D co-culture medium conditions for up to 20 days. Medium samples were collected every 96 hours and analysed to calculate calcium concentration compared to control medium. From this cumulative calcium depletion from the culture medium over a period of 20 days was calculated. Donor 1 osteogenic conditions shows significantly greater calcium depletion from day 12 compared to basal. Significantly greater calcium depletion in MSC-EC spheroids can be seen at days 12, 16 and 20 compared to MSC-only. Donor 2 had a similar cumulative calcium depletion patter to Donor 1; however, overall calcium depletion at day 20 was less. For each time point and biological donor six individual medium samples were tested (n=6).
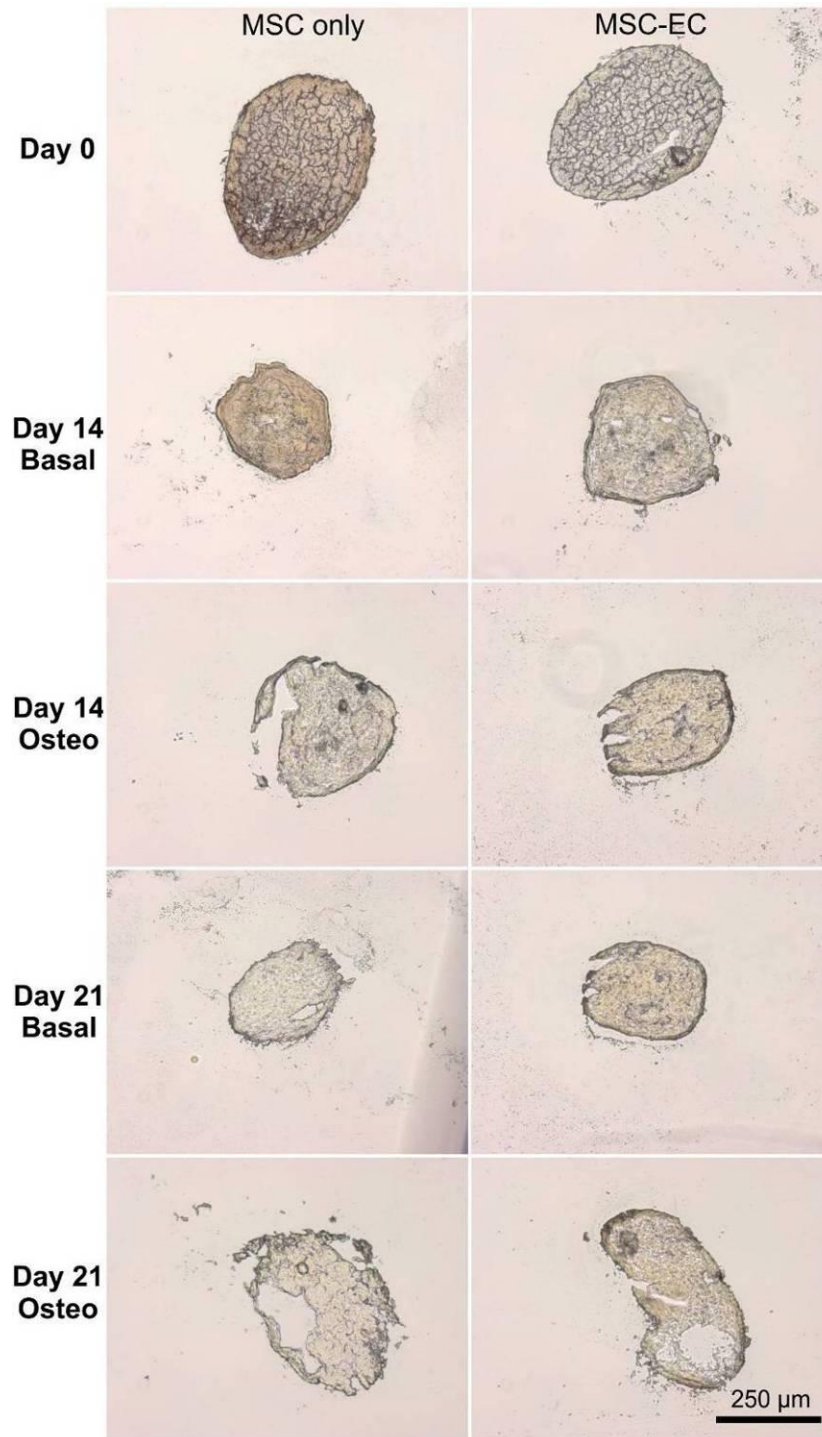
Figure 3.4.13 – ALP and von Kossa staining of Donor 3 MSC-only and MSC-EC spheroid sections

Representative sections of ALP and von Kossa staining performed on Donor 3 (K107) MSC-only and MSC-EC spheroids at various time points cultured in either basal or osteogenic conditions. No pink or brown/black staining was observed showing the samples were ALP and von Kossa negative.
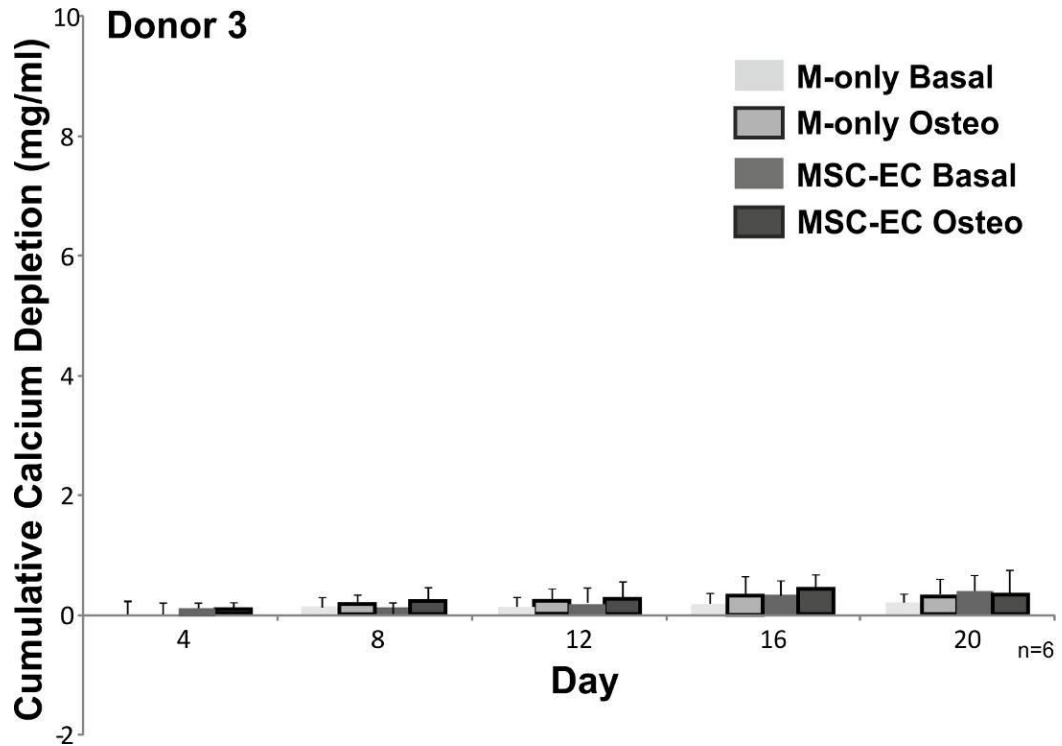
Figure 3.4.14 – Cumulative calcium depletion from Donor 3 MSC-only and MSC-EC spheroids culture in basal and osteogenic condition

MSC Donor 3 (K107) was cultured in either basal or osteogenic 3D co-culture medium conditions for up to 20 days. Medium samples were collected every 96 hours and analysed to calculate calcium concentration compared to a control. From this cumulative calcium depletion from the culture medium was tabulated. No statistically significant calcium depletion was observed at any time point in any condition. This further demonstrates biological Donor 3 osteogenic inert behaviour. For each time point, culture condition and spheroid type six individual media samples were tested (n=6).

Second harmonic generation (SHG) imaging was used to visualise collagen within spheroid sections. To act as a control a section of OCT and human bone tissue were analysed (Figure 3.4.15). OCT was used due to being a collagen-free material that was used in the process of sectioning both human bone and cell spheroids. In the SHG figures, a range indicator was applied to the images; blue represents background/negative whilst black and grey represents positive collagen imaging. The lightly porous structure of cancellous bone can be easily observed. SHG imaging was also performed on MSC-only and MSC-EC spheroid sections culture in either basal or osteogenic 3D co-culture conditions and representative images can be seen in Figure 3.4.16. Low collagen levels could be detected at the edges of the spheroid sections from day 1, however, by day 21 higher collagen levels were observed, particularly in spheroids cultured in osteogenic conditions. However, a collagen structure similar to human bone was not detected.

Image analysis was performed on the SHG images to quantify the intensity and subsequent collagen presence. Collagen type I is a marker of osteogenic differentiation of MSCs, therefore, this could be used as a novel quantitative technique to measure osteogenesis in 3D. Figure 3.4.17 shows the quantification of MSC-only and MSC-EC spheroids culture in either basal or osteogenic condition up to 21 days using human bone and OCT as a control. Human bone had significantly more SHG imaging pixel intensity compared to all other tested materials.

SHG imaging is a non-destructive technique to quantify collagen within materials; however, it is unable to identify the type of collagen present. Immunofluorescent labelling of MSC-only and MSC-EC spheroid sections for collagen type I and II were performed (Figure 3.4.18). Positive Collagen type I staining was observed in both MSC-only and MSC-EC spheroid sections cultured in osteogenic conditions after 21 days.
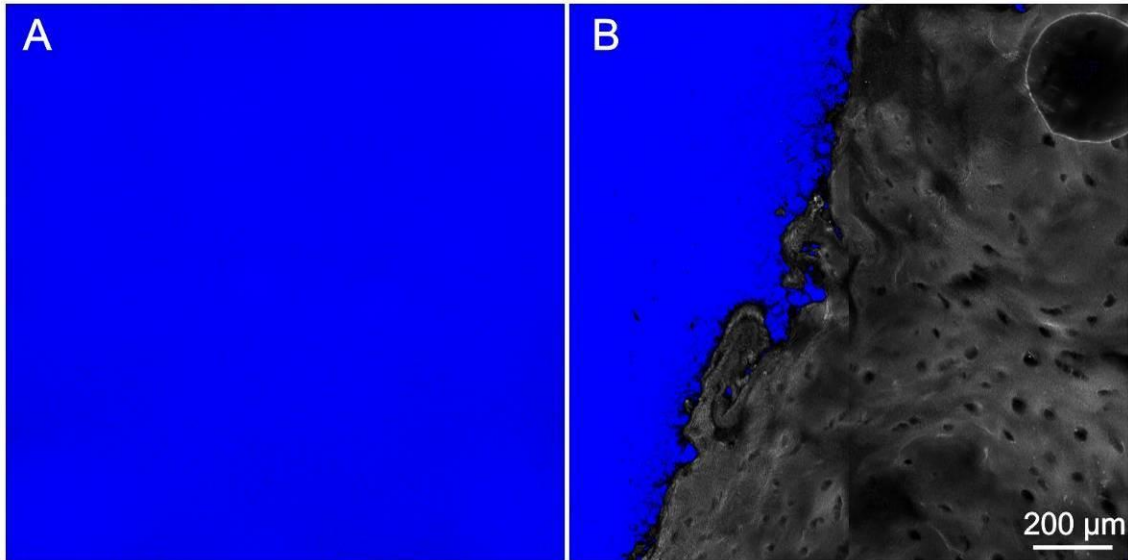
Figure 3.4.15 – Second harmonic generation imaging of an OCT section and a human bone marrow section

SHG imaging at 870nm was performed and expressed using a range indicator. Blue represents background or collagen-free material, whilst black/grey represents collagen containing material. A- Section of OCT, OCT was used as it is collagen free and was used to mount bone samples and cell spheroids for sectioning. B – 7µm section of human bone from the tibial plateau of the knee. The typical cancellous bone structure can be observed, which is slightly porous.
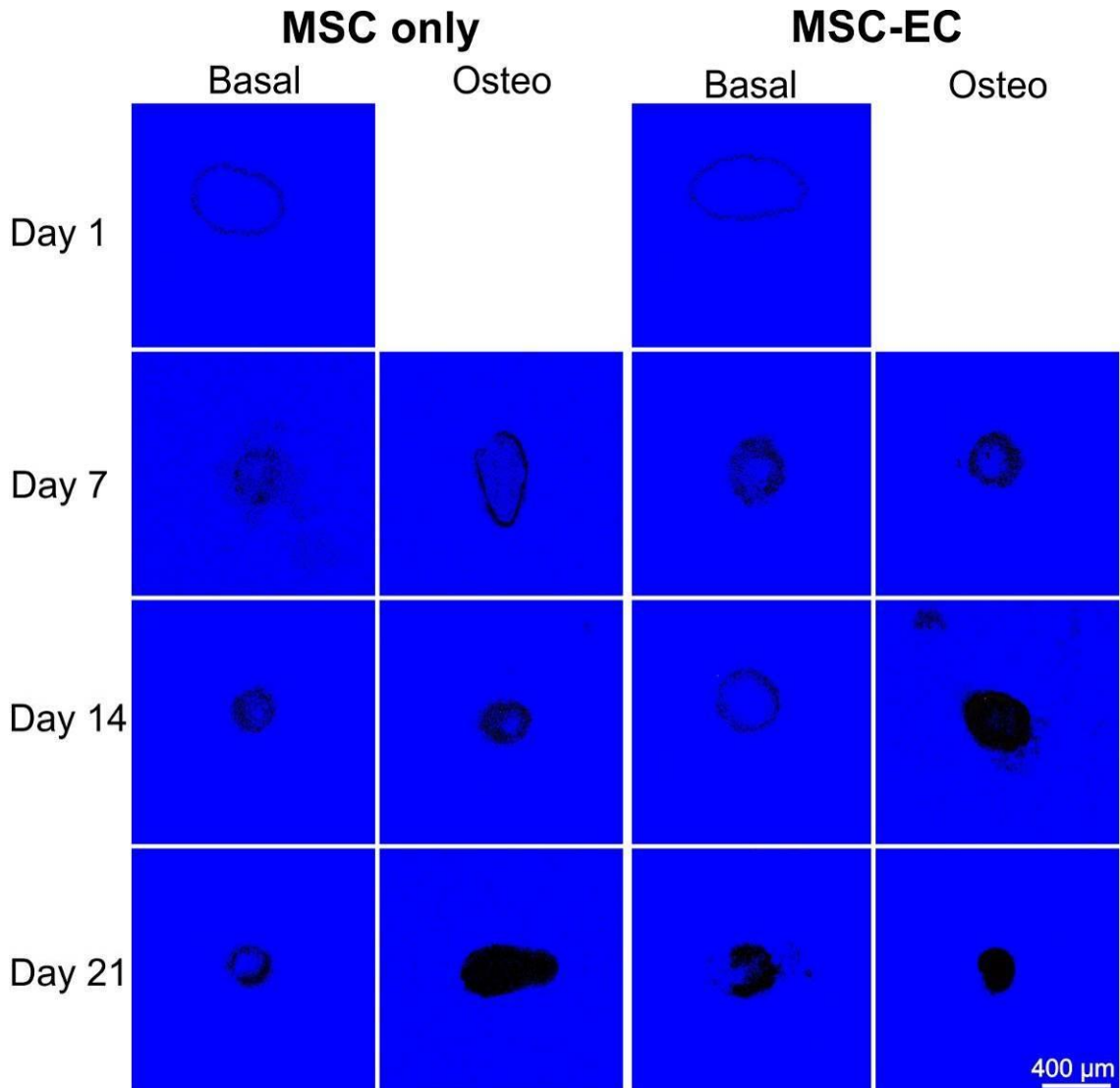
Figure 3.4.16 – Second harmonic generation imaging of MSC-only and MSC-EC spheroid sections at various time points

SHG imaging at 870nm was performed and expressed using a range indicator. Blue represents background or collagen-free material; grey/black represents collagen containing material. MSC-only and MSC-EC spheroids were cultured in either basal or osteogenic conditions for up to 21 days and representative images are shown. Spheroids were then snap frozen, sectioned at 7 µm before being SHG imaged. At Day 21 spheroid sections were clearly visible against the background; however, an organised structure was not detected.
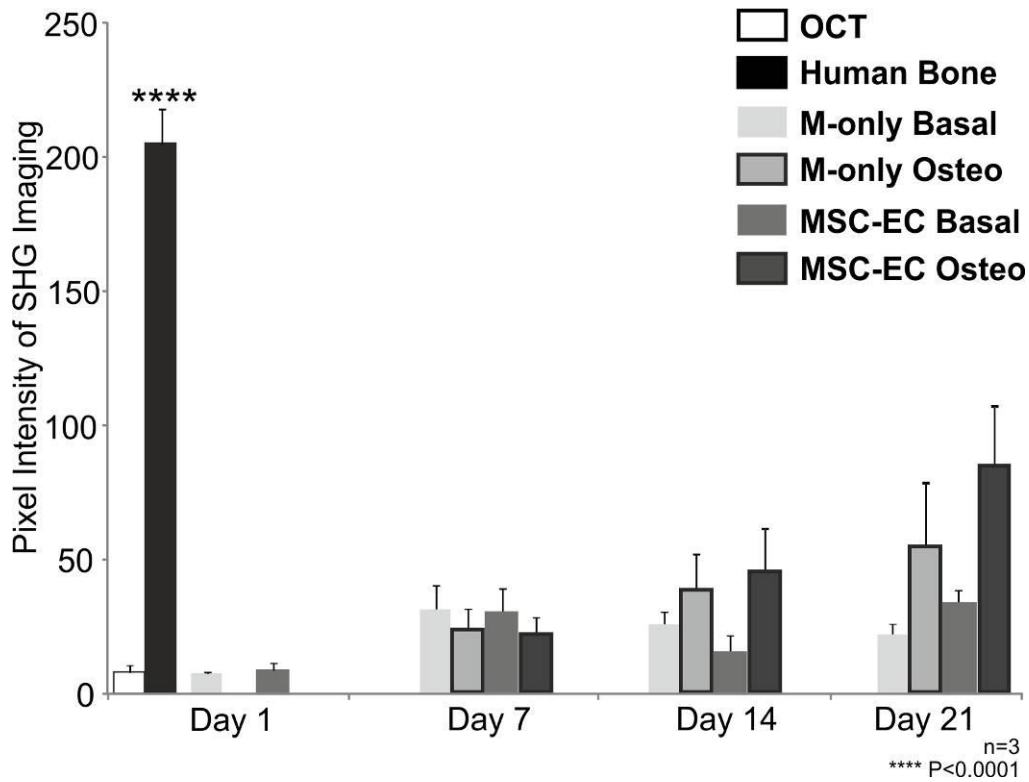
Figure 3.4.17 – Quantification of SHG imaging of MSC-only, MSC-EC spheroids, human bone and OCT

Using Image J analysis software the average pixel intensity for the various SHG imaged sections was calculated. Human bone was used as a positive collagen control, whilst OCT was used as a negative collagen control. MSC-only and MSC-EC spheroids cultured in either basal or osteogenic conditions at various time points were then analysed. Human bone was found to have a significantly greater pixel intensity compared to all other materials analysed. No significant differences were detected between MSC-only and MSC-EC spheroids. For each time point and culture condition three individual spheroids or samples were tested (n=3).
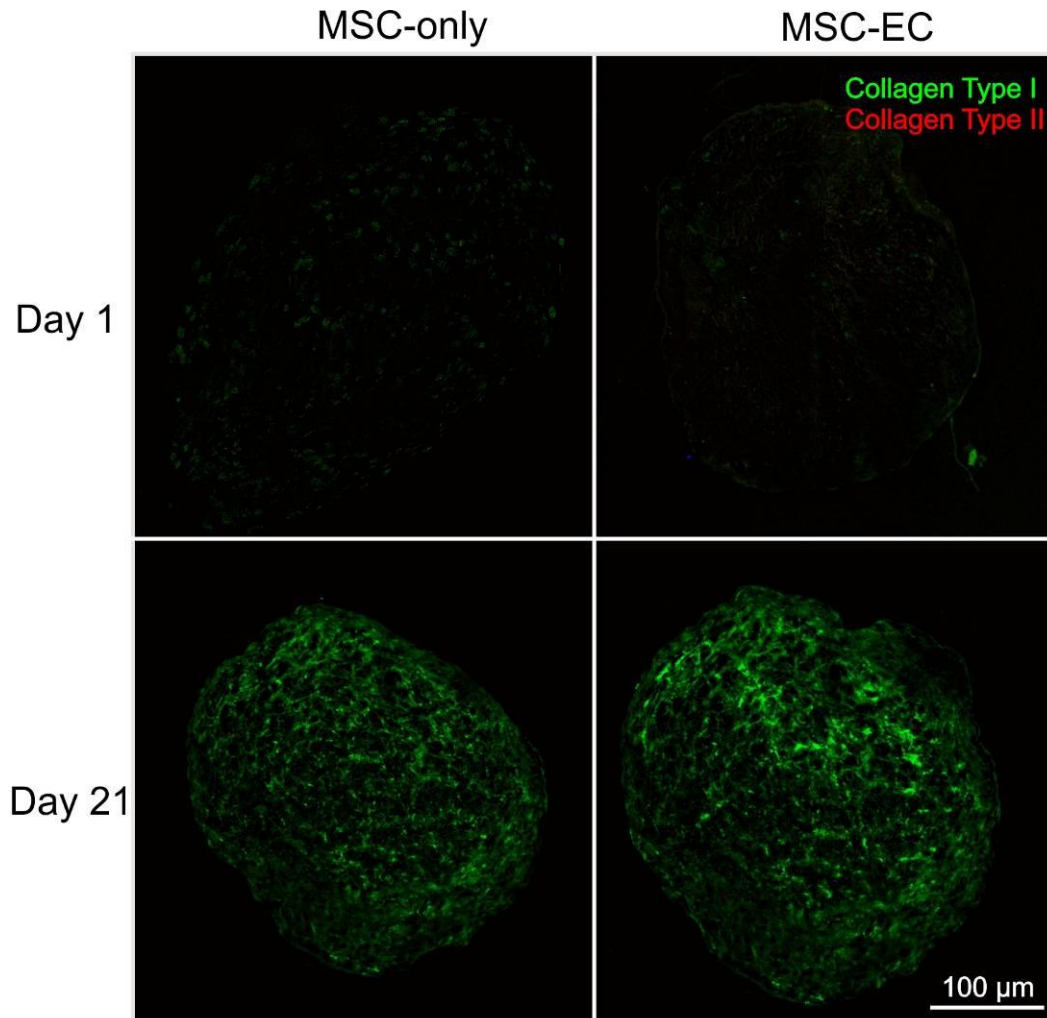
Figure 3.4.18 – Collagen type I and II immunostaining of MSC-only and MSC-EC spheroid sections

Spheroid sections from MSC only and MSC-EC spheroids cultured in osteogenic conditions for either 1 or 21 days were stained for collagen type I and II before being imaged via fluorescence microscopy. Positive collagen type I staining can be clearly observed at day 21. This confirmed that the collagen detected using SHG imaging is collagen type I.

3.4.5 Viability of Long-term 3D Culture of Mesenchymal Stromal Cells and Endothelial Cells

Live/dead staining was performed on MSC-only and MSC-EC spheroids cultured for up to 21 days to assess the long term viability of 3D culture (Figure 3.4.19). Cell spheroids were cultured in basal 3D co-culture medium and split fed twice a week. At days 1, 7, 14 and 21 post seeding spheroids were imaged using a confocal microscope. A dead control was produced by 10 minute incubation in 70% industrial methylated spirit (IMS)/dH$_2$O before application of live/dead stain. Spheroids cultured up to 21 days of both MSC-only and MSC-EC composition showed strong living (green) staining. A few nuclei within each sample have stained dead (red), however, the extent of red is not as severe as the dead control.

The percentage of dead cells within the MSC-only and MSC-EC spheroids was calculated using the images generated with live/dead staining and Image J analysis software (Figure 3.4.20). The dead control was found to have a significantly greater percentage of dead cells compared to all other MSC-only and MSC-EC spheroids. However, no differences were detected between MSC-only and MSC-EC spheroids.
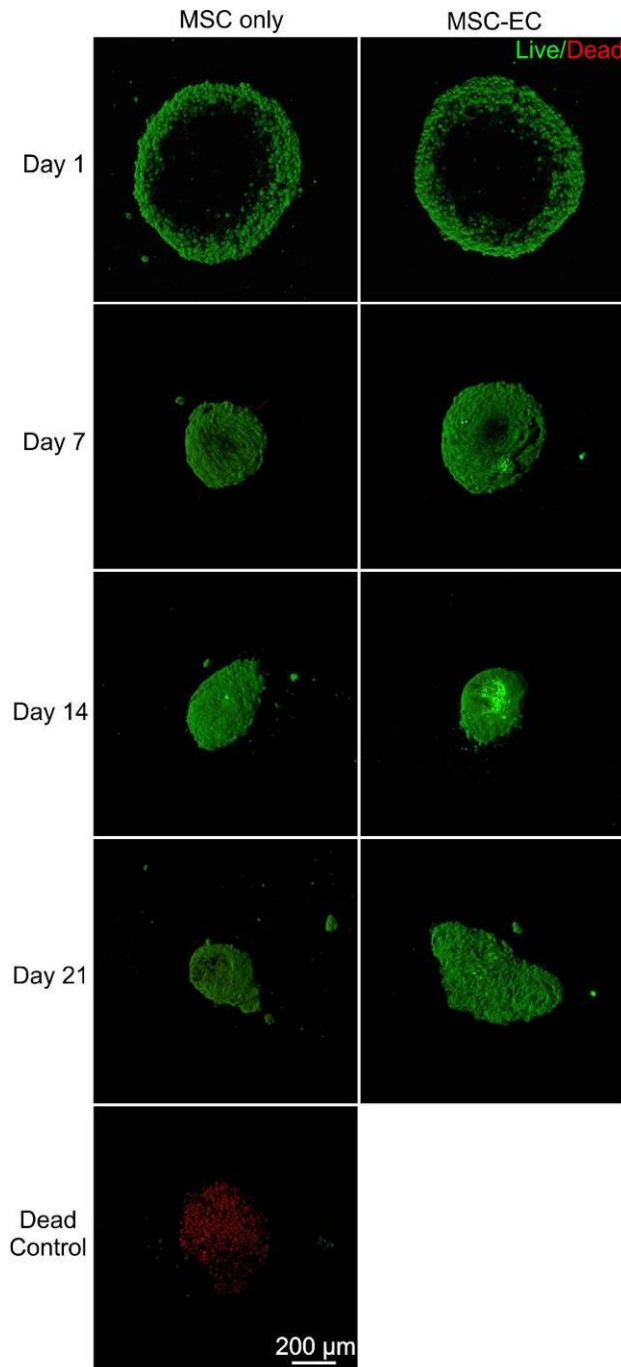
Figure 3.4.19 – Live/dead staining of MSC-only and MSC-EC spheroids over 21 days in culture

3D multi-photon confocal microscopy was used to image live/dead staining performed on MSC-only and MSC-EC spheroids after 1, 7, 14 and 21 days in culture. Active cells were able to uptake the dye into the cytoplasm and stain living cells green. Dead cells have damage nuclei and exposed DNA resulting in the nuclei being stained red. Within the dead control limited green was detected whilst many red nuclei were.
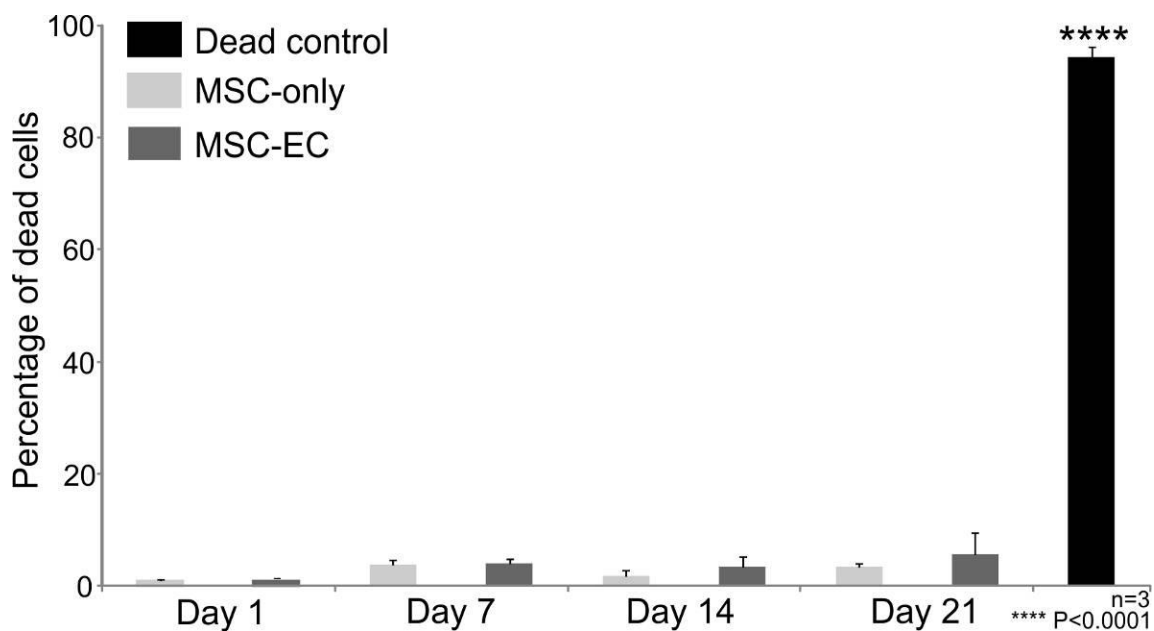
Figure 3.4.20 – Percentage of dead cells within MSC-only and MSC-EC spheroids using Live/Dead assay

Using the live-dead staining and Image J analysis software, the percentage of dead cells within MSC-only and MSC-EC spheroids cultured for 1, 7, 14 and 21 days was calculated. MSC-only or MSC-EC spheroids incubated in IMS for 10 minutes was used as a dead control. There were significantly more dead cells within the dead control compared to all other samples, no significant difference was observed between MSC-only and MSC-EC spheroids at any time point. For each time point and culture condition three individual spheroids were tested (n=3).

3.5 Discussion

Due to the lack of a specific cell surface marker, characterising MSCs is performed using a broad panel of cell surface markers. MSCs have been described as positive for many markers such as CD29, CD44, CD73, CD90, CD105 and CD166. They have also been described as negative for the markers CD11a, CD14, CD19, CD34, CD45, CD79a, CD144 and CD235a (Dvorakova et al., 2008, Karp and Leng Teo, 2009). MSCs extracted from both femoral heads and knees tested positive for MSC markers CD29, CD44, CD73, CD90 and CD105. However for all donors, MSCs sourced from both femoral heads and knees did not test positive for the frequently used MSC marker CD166. Overall, the MSCs expressed the majority of known markers whilst negatively expressing the haematopoietic markers CD34 and CD45, this negative expression is regarded as a strong indicator of bone marrow MSCs (Busser et al., 2015). Collectively, the data indicate that the MSC samples used in this study had a commonly recognised MSC immunophenotype.

Platelet endothelial cell adhesion molecule (PECAM-1) or CD31 is a cell surface marker used to identify endothelial cells (Ma et al., 2014). Within these experiments, ECs were frequently co-cultured with the MSCs. To prove the MSCs extracted from either femoral heads or knees were not contaminated with endothelial cells they were immunofluorescently labelled and analysed for the presence of CD31 and found to be negative. HUVECs were used as these are one of the most characterised and commonly used human primary endothelial cells. HUVECs were purchased from Promocell and were checked for CD31, they were found to positive expressed CD31 via immunofluorescence and flow cytometry. There are alternative endothelial cell sources such as; human cord blood and endothelial progenitor cells. However, these alternative cell sources were inferior to HUVECs for these experiments. Human cord blood endothelial cells are rare, therefore obtaining the numbers required for these experiments would be impractical (Kim et al., 2015, Henning et al., 2012). Endothelial progenitor cells have been directly compared to HUVECs when co-cultured with

adipose derived MSCs. Endothelial progenitor cells unable to produce a neovasculature, making these cells inferior of HUVECs when co-cultured *in vitro* (Haug et al., 2015).

Osteogenic differentiation of MSCs cultured in standard 2D cell culture conditions has been well documented. Assessment has been frequently examined using stains such as ALP, Alizarin Red S and von Kossa (Jones et al., 2002, Im et al., 2005). Quantification has also been performed through elution of Alizarin Red S staining and ALP activity by pNPP assessment (Shui and Scutt, 2001, Moreau and Xu, 2009). Using ALP and von Kossa staining osteogenesis within three biological MSC donors was assessed. Donors 1 and 2 both showed positive ALP staining but were negative for von Kossa staining. Von Kossa staining is used to identify mineralisation through phosphate deposits, due to these donors being cultured for up to 21 days it is possible that mineralisation would have occurred later. Uniquely Donor 3 (K107) was negative for both ALP and von Kossa staining after 21 days.

These three biological donors were also stained with Alizarin Red S and quantification performed using CPC elution. Donor 2 showed significance a little earlier than Donor 1 at day 7, both Donor 1 and 2 showed significant staining for days 14 and 21. Overall Donor 1 had higher Alizarin Red S levels compared to Donor 2 at day 21, indicating that this donor was slightly more osteogenic. Donor 3 showed limited osteogenesis through Alizarin Red S staining; a significant difference between basal and osteogenic conditions was detected at day 21. However, this is most likely a false positive; the highest elution with this donor was 0.5 ± 0.03. In contrast at the same time point Donors 1 and 2 had elution values of 2.7 ± 0.138 and 1.4 ± 0.137 respectively. Observations made using ALP and von Kossa staining indicate that Donor 3 was an osteogenic-inert MSC donor.

Despite the variety of techniques available to assess osteogenesis in 2D, these techniques have not always translated for 3D studies. The generation of a method that can be performed in both 2D and 3D could be used as a

complimentary assessment method. The importance of calcium within bone formation has long been known. Many cellular products associated with osteogenesis are calcium based (Wen et al., 2012). Previous research has also indicated a link between ALP and calcium, decreases in ALP activity were seen in conjunction with decreased intra and extra cellular calcium (Abnoshi et al., 2012). Therefore, quantifying calcium depletion within culture medium could be used to non-destructively assess osteogenic differentiation in both 2D and 3D cell culture conditions. Calcium depletion analysis from culture medium was performed on Donors 1, 2 and 3 cultured in 2D conditions for up to 20 days. Donor 2 showed significantly greater calcium depletion in osteogenic conditions compared to basal after 12 days, conversely Donor 1 significance was detected after 16 days. Overall, Donor 1 had higher calcium depletion after 20 days compared to Donor 2, these results are similar to those obtained through Alizarin Red S staining and elution. Donor 3 showed no significant difference in calcium depletion at any time, supporting evidence that Donor 3 is an osteogenic-inert biological donor.

Overall similar results were detected using both Alizarin Red S and calcium depletion on Donors 1, 2 and 3. Calcium depletion is a slightly advantageous technique as it is non-destructive making it easier to collect more data points. This technique also appeared to be more accurate. Alizarin Red S staining on Donor 3 showed a significant difference at day 21 between basal and osteogenic conditions. Indicating that Donor 3 underwent osteogenic differentiation, however, no positive ALP or von Kossa staining was detected at any time point making this highly unlikely. The false positive Alizarin Red S staining might have been caused by increased cell proliferation caused by the osteogenic induction medium. Dexamethasone a component within osteogenic induction medium has been shown to promote proliferation in MSCs (Wang et al., 2012).

Human bone is a complex 3D structure, to more closely represent this MSCs and ECs were cultured in cell spheroids using U-bottomed 96-well plates. Spheroids were sectioned and stained with Alizarin Red S, unlike 2D this method could not

be used quantitatively through CPC elution. Therefore, a quantitative technique for 3D osteogenic cell spheroid culture would be required. Alizarin Red S staining of spheroids sections was found to positively stain at both days 1 and 7 when cultured in basal conditions, making this stain inappropriate for both quantitative and qualitative assessment. pNPP is a procedure frequently used to assess osteogenic differentiation of MSCs. Translating this from traditional 2D to 3D resulted in large error bars and inconsistent results. These were most likely caused during the homogenisation process which generated heat and required extra stages compared to 2D. Generating heat during pNPP assessment can be detrimental due to this technique being used to quantify ALP, ALP is an enzyme making it sensitive to high temperature degradation.

ALP and von Kossa staining were performed on 3D MSC-only and MSC-EC spheroid sections. Donor 1 and 2 both showed positive ALP staining, however, both these donors were negative for von Kossa. Negative von Kossa staining was also observed using these donors in 2D and is most likely due to these donors having poor mineralisation properties. Observation of the ALP staining performed on Donors 1 and 2 showed stronger positive staining on MSC-EC spheroids compared to MSC-only. The positive ALP staining was also more prominent at the spheroid edges compared to the centre for all positive samples. This could be caused by a nutrient gradient caused by the 3D spheroid structure; peripheral cells will have more nutrients compared to central cells. An oxygen gradient will also occur, it has been previously demonstrated that a low oxygen concentration can inhibit osteogenesis (Malladi et al., 2005).

Cumulative calcium depletion from culture medium was calculated for Donor 1 and 2, MSC-only and MSC-EC spheroids. It was found that significantly greater calcium depletion was detected after 12 days in spheroids cultured in osteogenic conditions compared to basal conditions. MSC-EC spheroids showed significantly larger calcium depletion compared to MSC-only spheroids, indicating that the presence of ECs improved osteogenesis. These results are supported by previous research showing co-culture of MSCs and ECs in 2D, 2D scaffold and

3D scaffold conditions increasing osteogenic differentiation of MSCs. This increase is most likely due to a soluble factor produced by ECs (Saleh et al., 2011b, Gershovich et al., 2013, Pandula et al., 2014).

Despite MSC-EC spheroids containing half the number of MSCs compared to MSC-only spheroids, ALP staining, calcium depletion and SHG imaging all indicated greater osteogenesis. This is most likely attributed to the strength of a soluble factor released by the ECs. Known growth factors that enhance osteogenesis are VEGF, bone morphogenetic protein (BMP), FGF and TGF-β (Budiraharjo et al., 2013, Kim et al., 2012, Park et al., 2014, Geiger et al., 2005). VEGF, FGF-16 and FGF-18 are all known to be produced by ECs (Imaizumi et al., 2000, Antoine et al., 2006).

Donor 3 MSC-only and MSC-EC spheroids were also cultured in basal or osteogenic conditions for up to 21 days. ALP and von Kossa staining was negative for all conditions. Calcium depletion from the culture medium was also negative for all conditions. Biological Donor 3 appears to have limited osteogenic potential in 2D and 3D culturing systems. Variation between different biological donors is a common phenomenon with no correlation between age, gender or isolation source, previous studies have also found osteogenic-inert human MSCs (Siddappa et al., 2007, Phinney et al., 1999). These results also indicate that co-culturing MSCs with ECs does not give false positive results regarding ALP staining or calcium depletion.

SHG imaging has been used to non-destructively observe and quantify collagen within various tissues (Chen et al., 2012). Using a section of human bone marrow and OCT, SHG imaging was performed and optimised. SHG of human bone marrow was used to clearly image the complex slightly porous structure of cancellous bone. SHG imaging of MSC-only and MSC-EC spheroid sections was able to detect the collagen present at various time points and conditions. This was then quantified using Image J image analysis. Image analysis showed that human bone contained significantly more collagen compared to all other samples. No other significant differences were detected. Therefore, this

technique could not be used to demonstrate significant differences between MSC-only and MSC-EC spheroids cultured in either basal or osteogenic conditions, unlike cumulative calcium depletion.

SHG imaging has been used frequently to observed and quantify collagen, however, this technique is unable to distinguish between collagen type I and II (Chen et al., 2012). Immunofluorescence was performed on MSC-only and MSC-EC spheroids at days 1 and 21 for collagen type I and II. At day 21 both MSC-only and MSC-EC sections stain positive for collagen type I and a basic subtle lattice structure was observed. Therefore, the collagen imaged through SHG was most likely collagen type I.

Using U-bottomed 96-well plates as a 3D cell culture method has various advantages. Spheroid size, cell number, cell type and environment can all be controlled without the presence of scaffolds or other material. The long-term viability of MSCs and ECs within cell spheroids containing approximately 30,000 cells is unknown. Live/dead staining was performed on MSC-only and MSC-EC spheroids cultured after 1, 7, 14 and 21 days. Live/dead staining was used as this has been frequently reported as a method to assess cell viability (Lewus and Nauman, 2005, Zullo et al., 2015). The spheroids expressed strong living (green) staining at all time points, for day 1 the dye penetration was quite poor resulting in a dark centre. In contrast the dead control no positive living (green) stain was detected but many dead (red) nuclei were. The percentage of dead cells within the various spheroids was calculated. The dead control was found to have a significantly greater percentage of dead cells compared to all other spheroids. No significant difference in the percentage of dead cells was detected between MSC-only and MSC-EC spheroids for any time point. This demonstrates that culturing MSCs and ECs within 3D 30,000 cell spheroids in U-bottomed 96-well plates for up to 21 days has no detrimental effect of cell viability.

The ability for this novel 3D co-culture model to sustain cell viability is most likely due to the spheroid diameter being less than 1,000 µm. Early angiogenesis studies on cancer tumours observed that angiogenesis did not occur when

tumours were less than 1 mm^3 and during avascular phase of a tumour the diameter did not exceed 1 mm (Gimbrone et al., 1972, Knighton et al., 1977). Having a relatively low diameter is important as it allows sufficient diffusion of important molecules, such as nutrients, oxygen and waste products. Later studies expanded upon this analysis further using *in vitro* spheroid studies. It was found that the distance from the spheroid periphery at which cell-necrosis occurs depends upon cell type, cell consumption rate and cell density. This distance most commonly ranged between 100-220 μm when using human tumour cells (Sutherland, 1988). Bone marrow specifically is a highly vascularised tissue; most tissue regions of mouse bone marrow are within 15 μm from the nearest blood vessel. However, the oxygen tension within bone marrow is relatively low <32 mmHg, compared to arterial blood >600 mmHg (Spencer et al., 2014, Tanoue et al., 2002).

In summary the cells extracted from femoral heads and knees positively and negatively expressed the panel of cell surface markers associated with MSCs, therefore, these cells were identified as MSCs. HUVECs purchased from PromoCell were found to express the known endothelial cell marker PECAM-1 or CD31; therefore, these were identified as ECs. Using U-bottomed 96-well plates to create 3D cell spheroids was established and found to have no detrimental effects of cell viability during 21 day culture. Osteogenic differentiation of MSCs was proven in both 2D and 3D conditions and found to be enhanced by ECs. Calcium depletion from culture medium was found to be a new, non-destructive, real-time technique to assess osteogenic differentiation in both 2D and 3D environments. The next chapter will further examine the MSC-EC co-culture spheroid model specifically to observe; the cellular organisation, cell-cell relationships and possible signalling mechanisms.

Chapter 4

Chapter 4   : 3D Co-cultured MSCs and ECs – A Self-organising Spheroid Model

4.1 Introduction

A frequently observed organisation pattern within multi-cellular spheroids or aggregates is when one cell type migrates towards the periphery of the structure. For example this organisation pattern has been observed when co-culturing osteoblast cells with ECs in a collagen-based spheroid model (Stahl et al., 2004). This phenomenon is most likely the result of the differential adhesion hypothesis, where it is proposed that heterotypic cells within aggregates sort into isotypic groups (Steinberg, 1975). This theory has been tested by altering the number of cadherin cell-cell adhesion molecules on cells within aggregates. It was found that cells with lower cadherin expression enveloped those with higher cadherin expression. This resulted in the lower cadherin-expressing cells being located at the periphery of the spheroid, however when cadherin levels were equalised, the cells returned to an evenly intermixed organisation (Duguay et al., 2003, Foty and Steinberg, 2005, Thompson et al., 2012). Therefore, the differentiation adhesion hypothesis creates an organisation pattern due to the physical "stickiness" of the cells (Newman, 1996).

Cell signalling is a highly complex process of communication between cells and has many important functions; tissue development during embryonic development, adult tissue homeostasis and adult tissue repair. These functions all require cell migration and organisation to create and maintain functional tissues (O'Dea and King, 2013). Within humans there are many major signalling pathways that are known to control cell migration. Specifically three different signalling pathways are known to affect MSC and/or EC migration; FGF, Notch and ILK signalling and described further in Sections 4.1.1, 4.1.3, and 1.6.4. FGF signalling has been shown to affect EC migration, specifically HUVECs have

shown chemotaxis towards FGF-16 and FGF-18 *ex vivo* and application of FGF-2 has been shown to enhance HUVEC migration (Antoine et al., 2006, Dos Santos et al., 2014). Notch signalling has been shown to affect both EC and MSC migration. Using a combination of computational and experimental procedures it was demonstrated that Notch signalling was able to affect vascular-endothelial cadherin junctions on ECs, this subsequently limited their directional migratory ability (Bentley et al., 2014). Inhibition of Notch signalling in MSCs though γ-secretase inhibition or transcription factor knockout resulted in improved MSC migration (Xie et al., 2013). ILK is known to affect EC migration, novel ILK inhibitor treatment resulted in decreased EC migration and led to decreased capillary formation and angiogenesis *in vivo* and *ex vivo* (Tan et al., 2004). Cell signalling based migration and subsequent organisation is mainly attributed to biological rearrangement of the cytoskeleton and focal adhesions (Welf and Haugh, 2011).

Uniquely, work in our laboratory showed that when MSCs and ECs were co-cultured in 3D spheroids, the ECs self-organised into distinct segregated regions within the spheroid (Saleh et al., 2011b). Related research demonstrated that this self-organisation pattern was particularly prominent when MSCs, ECs and iPS cells were tri-cultured in matrigel, within this model it was found that ECs formed a primitive vascular like network throughout the spheroid structure (Takebe et al., 2013). Currently the mechanisms responsible for this distinct pattern are unknown. The unique pattern of ECs when co-cultured within MSCs has been described as a primitive vascular-like network. Therefore, research into angiogenesis (the formation of new blood vessels) could be used to understand the signalling mechanisms responsible (Moens et al., 2014). The study of angiogenesis has been highly popular within cancer studies, inhibition of this process could be used for therapeutic treatments. Recent studies have described that both VEGF and PDGF signalling play an important role in angiogenesis (Zhao and Adjei, 2015). PDGF suppression has been successfully used to limit angiogenesis within cancer and destabilise the vascular endothelium (Dong et al.,

2014, Roskoski, 2007). Additionally FGF, Notch and ILK signalling have all been described as affecting angiogenesis (Sections 4.1.1, 4.1.3 and 1.6.4).

Angiogenesis and bone formation have been linked, specifically deferoxamine mesylate (DFM) treatment was shown to enhance blood vessel formation and bone tissue in mice (Kusumbe et al., 2014). Additionally a wide range of growth factors are known to affect osteogenic differentiation of MSCs and/or bone formation these include; FGF, insulin like growth factor (IGF), PDGF, TGF-β, bone morphogenic protein (BMP) and VEGF (Stegen et al., 2015, Hengartner et al., 2013, Colciago et al., 2009, Rahman et al., 2015, Wu et al., 2013). Therapeutic application of FGF-1 and FGF-2 has been shown to enhance bone regeneration, specifically immobilisation of FGF-2 and BMP-2 on scaffolds was found to enhance the osteogenic differentiation of MSCs (Budiraharjo et al., 2013). PDGF is known to affect the differentiation potential of MSCs and has been reported as more effective than FGF; this is most likely attributed towards PDGF affecting the cellular morphology (Ng et al., 2008). Indeed, a large MSC morphology has been observed to result in enhanced osteogenic differentiation (Zhao et al., 2012). However, the use of growth factors therapeutically requires appropriate delivery system development; global application of growth factors can result in ectopic bone formation, overgrowth and severe inflammatory/immune response (Luginbuehl et al., 2004).

Conversely the use of a pharmacological agent does not require the development of an appropriate delivery system, for example DFM has been shown to enhance bone formation. DFM is a chelating agent frequently used within human medicine to remove excess iron from the blood; it is also a prolyl hydoxylase inhibitor leading to enhanced hypoxia inducible factor one alpha (HIF-1α) (Kusumbe et al., 2014). This study was conducted in conjunction with another that showed Notch signalling promoted EC proliferation and vessel growth. EC specific loss of Notch resulted in mice with impaired bone vessel morphology, growth, shortening of the long bones and decreased bone mass (Ramasamy et al., 2014). This result is supported by another study showing that Notch impaired osteogenesis, despite

Notch being activated during the differentiation process (Viale-Bouroncle et al., 2014).

4.1.1 FGF signalling in MSCs and ECs

FGF is such a diverse signalling pathway it has been shown to have numerous effects on MSCs. FGF is known to effect the proliferation, osteogenic differentiation, chondrogenic differentiation, potency, bone repair, skeletal development and maintenance of MSCs (Stegen et al., 2015). Specifically stimulation of FGFR1 is known to induce proliferation and positively regulate maintenance of MSCs, through c-Myc stimulation and cyclin-dependant kinase inhibition (Dombrowski et al., 2013). FGFR-2 acts as a regulator molecule that promotes osteogenic differentiation in MSCs through mediation of the MAPK signalling pathway (Miraoui et al., 2009). FGFR-2 also promotes chondrogenic differentiation of MSCs through inhibition of TGF-β and insulin-like growth factor (IGF) signalling (Ito et al., 2008). Multiple skeletal congenital disorders such as chondrodysplasia are associated with deregulation of the FGF pathway. FGFR-3 mutations are known to affect long bone development (endochondral ossification), leading to diseases such as hypochondroplasia and achondroplasia (Chen et al., 2013a, Di Rocco et al., 2014). Therefore, FGFR-3 is important in skeletal development. Therapeutic application of both FGF-1 and FGF-2 has been used in a variety of studies to improve bone regeneration (Iwaniec et al., 2002, Kuhn et al., 2013).

FGF is essential for the culture of ECs *ex vivo*; FGF-2 induces both proliferation and migration (Dos Santos et al., 2014). One of the most important cellular processes FGF is involved with is angiogenesis. Application of FGF-2 has been shown to enhance vascular sprouting, tube formation and decreased EC apoptosis through induced activation of Jagged-1 a ligand of Notch (Matsumoto et al., 2002). Due to the broad range of the FGF family understanding the specific role during vascular development is difficult. Indeed, FGF-1 and FGF-2 single and double knockout mice show no gross vascular defects (Javerzat et al., 2002).

However, it is known that both FGF-1 and FGF-2 can regulate the angiogenesis process. FGF-2 is able to induce angiogenesis indirectly through VEGF signalling (Auguste et al., 2001). FGF is able to enhance EC proliferation, migration, cadherin receptor expression and gap-junction communication (Hatanaka et al., 2012, Haddad et al., 2008).

4.1.2 PDGF signalling in MSCs and ECs

MSCs are known to abundantly express PDGFR and are subsequently influenced by PDGF signalling (Ball et al., 2007). PDGF signalling plays a crucial role in MSC commitment to osteogenesis, chondrogenesis and adipogenesis. PDGF signalling has been described as being more potent in MSC differentiation than fibroblast growth factor (FGF) signalling and TGF-β signalling. Specifically PDGF treatment enhanced MSC osteogenic differentiation further than FGF and TGF-β (Ng et al., 2008). This effect on MSC differentiation could be controlled by cell shape, cytoskeleton actin is known to be reorganised following PDGF stimulation and the differentiation potential of MSCs is known to be affected by MSC cell morphology (Woodring et al., 2003, McBeath et al., 2004). Specific inhibition of PDGFR has shown to result in MSCs with a more rounded morphology. Additionally PDGFR inhibition has resulted in increased MSC potency (Ball et al., 2012).

Little is known about the effects of PDGF signalling on ECs specifically; however, PDGF and PDGFR stimulation has been shown to produce a pro-angiogenesis phenotype (Wyler von Ballmoos et al., 2010). Global effects of PDGF signalling on angiogenesis are more well documented, PDGF signalling has recently been described as an alternative angiogenesis signalling pathway (Zhao and Adjei, 2015). Traditionally angiogenesis signalling has been related to VEGF specifically, however, combinational therapies of PDGF and VEGF inhibition have been shown to reduce blood vessel formation within cancer tumours (Dong et al., 2014). This result is complimented by the knowledge that a combination of PDGF and VEGF has been shown to enhance postnatal angiogenesis and used as a

successful therapy post myocardial infarction in animal models (Rehman et al., 2003).

4.1.3 Notch signalling in MSCs and ECs

Notch has been shown to have a range of effects on MSCs. Inhibition of Notch signalling within MSCs has been linked to decreased proliferation and survival, increased CXCR4, migration and stem cell potency (Liao et al., 2014, Xie et al., 2013). Using both small molecular inhibitors and transcription factors, Notch signalling was reduced within MSCs, surface protein and mRNA levels of CXCR4 were significantly increased. CXCR4 is believed to be one of the most important molecules responsible for MSC migration towards the site of injury. Within MSCs decreased Notch, leads to increased CXCR4 and subsequently increased migration. Co-culture of MSCs with other stem cells has shown MSCs are able to enhance the potency of other cells through Notch-1 and Hes-1 stimulation (Haragopal et al., 2015). Within bone tissue Notch signalling is linked to bone remodelling, rheumatoid arthritis, bone-loss and osteoblast inhibition. Within a mouse rheumatoid arthritis model, genes encoding Notch were markedly elevated within MSCs, subsequent treatment with Notch inhibitors resulted in improved bone formation and osteoblast activity. Therefore, Notch is associated with inflammatory mediated bone loss in diseases such as rheumatoid arthritis (Zhang et al., 2014).

Notch-1 and Notch-4 receptors and three Notch ligands are known to be expressed in ECs (Kume, 2009). Notch signalling has been reported as important in EC proliferation, migration, angiogenesis and survival (Liu et al., 2013, Kerr et al., 2015, Chang et al., 2013a). Increased Notch-3 expression in ECs leads to enhanced cell migration (Howard et al., 2013). Global expression of Notch within ECs is important, deletion of Notch-1 receptor within ECs results in severs vascular defects resulting in embryonic lethality (Gale et al., 2004). The specific roles of Notch within EC angiogenesis are highly complex, in brief Notch activity switches between the tip and stalk of the developing blood vessel stimulating

sprouting. During this process Notch signalling is closely linked with VEGF and both signalling mechanisms act as key regulators in angiogenesis (Thomas et al., 2013). Again, the importance of Notch and VEGF in the angiogenesis of tumours has also been reported. However, a greater understanding of the role of Notch within angiogenesis is required before anti tumour therapies can be developed (Liu et al., 2014).

4.2 Aims

The general aims of the work presented within this chapter are to characterise further the 3D co-culture model of MSCs and ECs, using a variety of different techniques to quantify self-organisation and to identify the possible mechanisms involved.

More specifically the objectives are to:

- Determine the optimal ratio of MSCs and ECs within 3D co-culture spheroids.
- Develop non-invasive real-time imaging strategies to quantify co-culture spheroid organisation.
- Characterise EC self-organisation patterns within co-culture spheroids and establish whether EC self-organisation is directed by MSCs.
- Identify cell signalling pathways responsible for EC self-organisation.
- Observe if known pharmacological agents affect EC self-organisation within the novel 3D co-culture model.

4.3 Methods

4.3.1 Formation of co-culture spheroids at various ratios

Various different ratios of MSCs:ECs were tested in the 3D co-culture method described in Section 2.1.7. All MSC-EC spheroids were cultured in 3D co-cultured medium containing 50% DMEM, 50% endothelial cell medium, 15% FBS, P/S and 0.25% (w/v) methyl cellulose. The MSC:EC ratios examined were 80:20, 65:35, 50:50, 35:65 and 20:80, all spheroids had a total of 30,000 cells. Therefore the 80:20 spheroid contained 24,000 MSCs and 6,000 ECs.

4.3.2 Formation of co-cultured human dermal fibroblast and endothelial cell spheroids

To test whether the self-organisation observed in MSC-EC spheroids was dependent on the presence of MSCs specifically, HDF-EC co-culture spheroids were created. The HDF-EC spheroids were cultured in 3D co-culture medium containing; 50% DMEM, 50% endothelial cell medium, 15% FBS, P/S and 0.25% (w/v) methyl cellulose, the same medium used in MSC-EC spheroid culture. The method used to create HDF-EC spheroids is the same as previously described in Section 2.1.7, however, MSCs were substituted with HDFs between passage 7-10.

4.3.3 Formation of co-cultured spheroids with various inhibitor and pharmacological treatments

To help determine the signalling mechanisms responsible for the self-organisation observed in the MSC:EC spheroids, various inhibitors were added to the cell suspension after the final stage of cell tracker labelling and prior to the suspension being placed into the U-bottomed well plate. The spheroids were then cultured for up to 7 days in the presence and absence of platelet-derived growth factor receptor inhibitor (PDGFRi), integrin-linked kinase inhibitor (ILKi), fibroblast

growth factor receptor inhibitor (FGFRi), Dibenzazepine (DBZ) and epidermal growth factor receptor inhibitor (EGFRi). Table 4.3.1 shows the various inhibitor treatments used on MSC-EC spheroids, the signalling pathways affected and the concentrations used. In Table 4.3.2 more specific information on the inhibitors such as chemical name and specificity are given. The pharmacological agent deferoxamine mesylate (DFM) (Cat no. D9533, Sigma-Aldrich, UK) was also added to various MSC-EC spheroids. DFM was added into appropriate culture medium to give a final concentration of 100 µM. For comparative purposes an MSC only spheroid with 50% of the population labelled red and 50% of the population labelled green was also produced.

Table 4.3.1 – Inhibitor treatments used on MSC-EC spheroids

Inhibitor name	Signalling Pathway	Concentration Used	Supplier	Cat No.
ILKi	ILK	2 µM	Millipore	407331
PDGFRi	PDGF	3 µM	Santa Cruz	sc 205794
EGFRi	EGF	100 nM	Tocris	1037
FGFRi	FGF	4 nM	Tocris	3044
DBZ	Notch	3 µM	Tocris	4489

Table 4.3.2 – Specific inhibitor information used on MSC-EC spheroids

Inhibitor name	Full name	Specificity
ILKi	N-methyl-3-(1-(4-(piperazin-1-yl)phenyl)-5-(4'-(trifluoromethyl)biphenyl-4-yl)-1H-pyrazol-3-yl)propanamide	Suppresses ILK-mediated phosphorylation of Akt at Ser473 site
PDGFRi	3-Fluoro-N-(6,7-dimethoxy-2,4-dihydroindeno[1,2-c]pyrazol-3-yl)phenylamine	Reversible ATP-competitive inhibitor of PDGFR-α and β
EGFRi	4-[(3-Bromophenyl)amino]-6,7-dimethoxyquinazoline hydrochloride	Potent inhibitor of EGF receptor tyrosine kinase
FGFRi	*N*-[2-[[4-(Diethylamino)butyl]amino]-6-(3,5-dimethoxyphenyl)pyrido[2,3-*d*]pyrimidin-7-yl]-*N'*-(1,1-dimethylethyl)urea	Selective FGFR-1 and FGFR-3 inhibitor,
DBZ	*N*-[(1*S*)-2-[[(7*S*)-6,7-Dihydro-5-methyl-6-oxo-5*H*-dibenz[*b*,*d*]azepin-7-yl]amino]-1-methyl-2-oxoethyl]-3,5-difluorobenzeneacetamide	Inhibitor of Notch γ-secretas, preventing cleavage of the Notch ICD

4.3.4 Pre-treatment with integrin-linked kinase inhibitor

Due to inhibitor treatments being applied to both MSCs and ECs when in 3D co-culture, the effect of pre-treatment of MSCs-only with ILKi was tested. MSCs were treated with ILKi at the same concentration shown in Table 4.3.1 for 96 hours in 2D before being used in labelled 3D co-culture MSC-EC spheroids. The spheroids were then analysed for up to 5 days to observe if MSC-only ILKi pre-treatment had any effect.

4.3.5   Imaging techniques and quantification

4.3.5.1 2D time-lapse imaging of co-culture spheroids

A 50-50 mixture of MSCs and ECs were placed as a random suspension into a U-bottomed 96-well plate. This cell culture plate was then placed into an incubator attached to a DMIRB Leica Light microscope. A needle was then inserted through the plate and attached to a 5% CO_2, 95% air gas cylinder. The light microscope was then automatically set-up to capture images every 15 minutes for up to 24 hours. This was done to preliminarily assess the time taken for the cell suspension to aggregate and form a spheroid.

4.3.5.2 4D imaging of co-culture spheroids

Using a Zeiss LSM 780 multiphoton inverted microscope with a 37°C incubator attachment and 5% CO_2 95% air cylinder it was possible to simultaneously culture cells whilst imaging them in 3D. Spheroids were produced using the method described in Section 2.1.7 and labelled as described in Section 2.2.1. MSC-EC spheroids were analysed and to act as a control MSC-only spheroids with 50% of the MSCs were fluorescently labelled green and the other 50% fluorescently labelled red. The appropriate cell suspension was added into the U-bottomed 96-well plate and surrounding wells were flooded with PBS to minimise evaporation. The cells were then incubated for 4 hours in a normal incubator at 37°C to allow early cellular aggregation. Immediate transfer and imaging of a cell suspension resulted in cell death due to damage caused by the laser light intensity. 3D imaging was then performed every 20 minutes for a total of 16 hours, during which time the cell suspension aggregated for form a spheroid.

4.3.5.3 Quantification of spheroid volume and spheroid surface

Spheroid volume was calculated using Volocity software (Perkin Elmer) using the quantification package. Specifically, the fluorescent volume was calculated as either μm^3 or mm^3 using pre-determined pixel to μm scale bars. It was possible to

calculate the percentage of either red or green cells at the spheroid surface. Using the Volocity quantification package surface analysis was performed and the area of green or red could be calculated, this was then converted into a percentage.

4.3.5.4 Internal organisation of spheroids

Using the plot profiler extension on Image J software (MBF – McMaster Biophotonics Facility, Canada) analysis of various cross-sections of spheroids was performed. Each spheroid section had a minimum of three different z-axes drawn across them; plot profile was then able to calculate the amount of either red or green at a specific point on the z-axis. At least three different sections of the same spheroid type were then analysed this way, before the data was averaged together to give an estimate of the internal organisation within the spheroid sections.

4.3.5.5 Quantification of endothelial cell networks

Using the freehand extension on Image J software the length and width of endothelial cell networks within spheroid section images were calculated. The number of branches was calculated manually.

4.4 Results

4.4.1 Characterisation of CellTracker™ green and red profiles

CellTracker™ green and red labels were applied to different cell types as described in Section 2.2.1 to enable tracking by fluorescence microscopy. Figure 4.4.1 shows individual spheroids labelled with CellTracker™ green (A) and red (B), these were used to optimise the excitation laser wavelength. Spectral analysis of the emission profiles were performed using this optimised laser wavelength (780 nm).

Figure 4.4.2 shows 2D MSCs and ECs labelled using CellTracker™ green and red respectively. Emission profiles were captured using a non-descan detector in three different regions. Region 1: 400-500nm, Region 2: 500-550nm and Region 3: 560-650nm, these correspond to the blue, green and red regions of the visible light spectrum. Individual cells can be easily identified within the relevant colour region; any bleeding between the two different CellTracker™ colours is undetectable by the human eye. These analyses validate the use of CellTracker™ green and red labels to distinguish different cell types in mixed cultures.
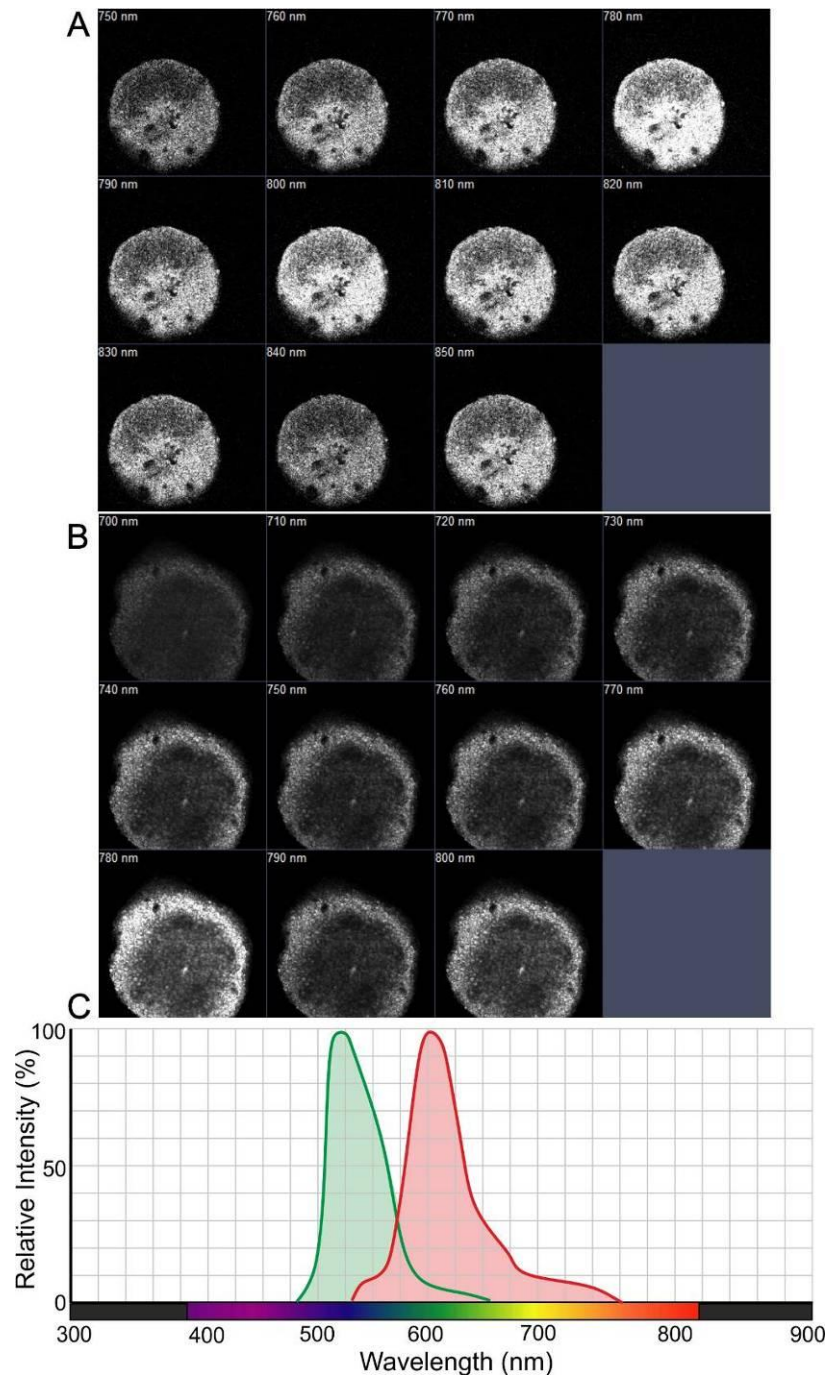
Figure 4.4.1 – Laser optimisation and spectral analysis using CellTracker™ Green and Red

A – Optimisation of laser excitation wavelength using a CellTracker™ green labelled spheroid. B – Optimisation of laser excitation wavelength using a CellTracker™ red labelled spheroid, optimised wavelength was found to be 780 nm. C – Spectral analysis of CellTracker™ green and red when excited with a laser at 780 nm. Emission profiles were detected by a non-descan detector ranging between 400-800 nm.
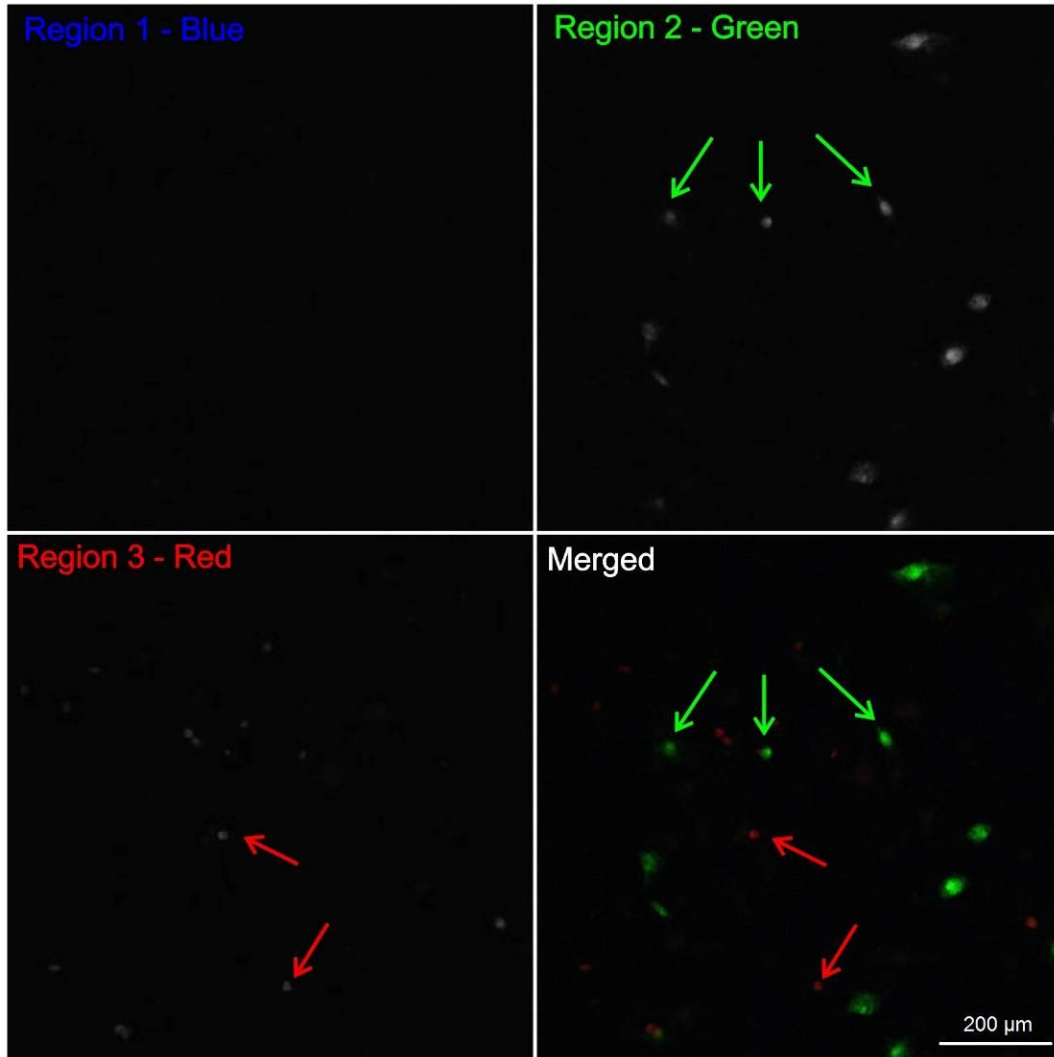
Figure 4.4.2 – 2D co-culture of fluorescently labelled MSCs and ECs

MSCs and ECs were labelled with fluorescent CellTracker™ green and red respectively before being co-cultured in 2D. Image was captured using a multiphoton confocal microscope using an excitation wavelength of 780 nm. The non-descan detector was split into three different regions. Region 1: 400-500 nm, Region 2: 500-550 nm and Region 3: 560-650 nm, these correspond with blue, green and red on the visible light spectrum. Clear separation can be seen between green MSCs and red ECs, highlighted with green and red arrows.

4.4.2 Characterisation of co-cultured spheroids

Five different ratios of MSC:EC were co-cultured to form spheroids, these were 20:80, 35:65, 50:50, 65:35 and 80:20. Within these experiments MSCs were always fluorescently labelled green and ECs red, the various MSC:EC spheroids were then cultured for up to 7 days. Fluorescent whole spheroid images can be seen in Figure 4.4.3. All combinations were able to form spheroids within 1 day; however, 20:80 spheroids had poor structural integrity after 7 days in culture.

Using the fluorescent whole spheroid images the diameter was measured for the various MSC:EC spheroids for up to 7 days in culture (Figure 4.4.4). Spheroid diameter decreased most dramatically between days 1 and 5 in culture as previously observed (Saleh et al., 2012). No significant differences in spheroid diameter at different ratios were detected, however, 20:80 spheroids appeared consistently smaller compared to 80:20. The various MSC:EC spheroids were sectioned after day 1, 3 and 5, self-organisation was only clearly detected in 50:50 MSC:EC spheroids, representative spheroid section images can be seen in Figure 4.4.5. Between approximately day 3 and 5, ECs self-organised to form a primitive vascular-like network evenly distributed throughout the spheroid. All other ratios resulted in ECs predominantly at the periphery of the spheroid at all time-points.
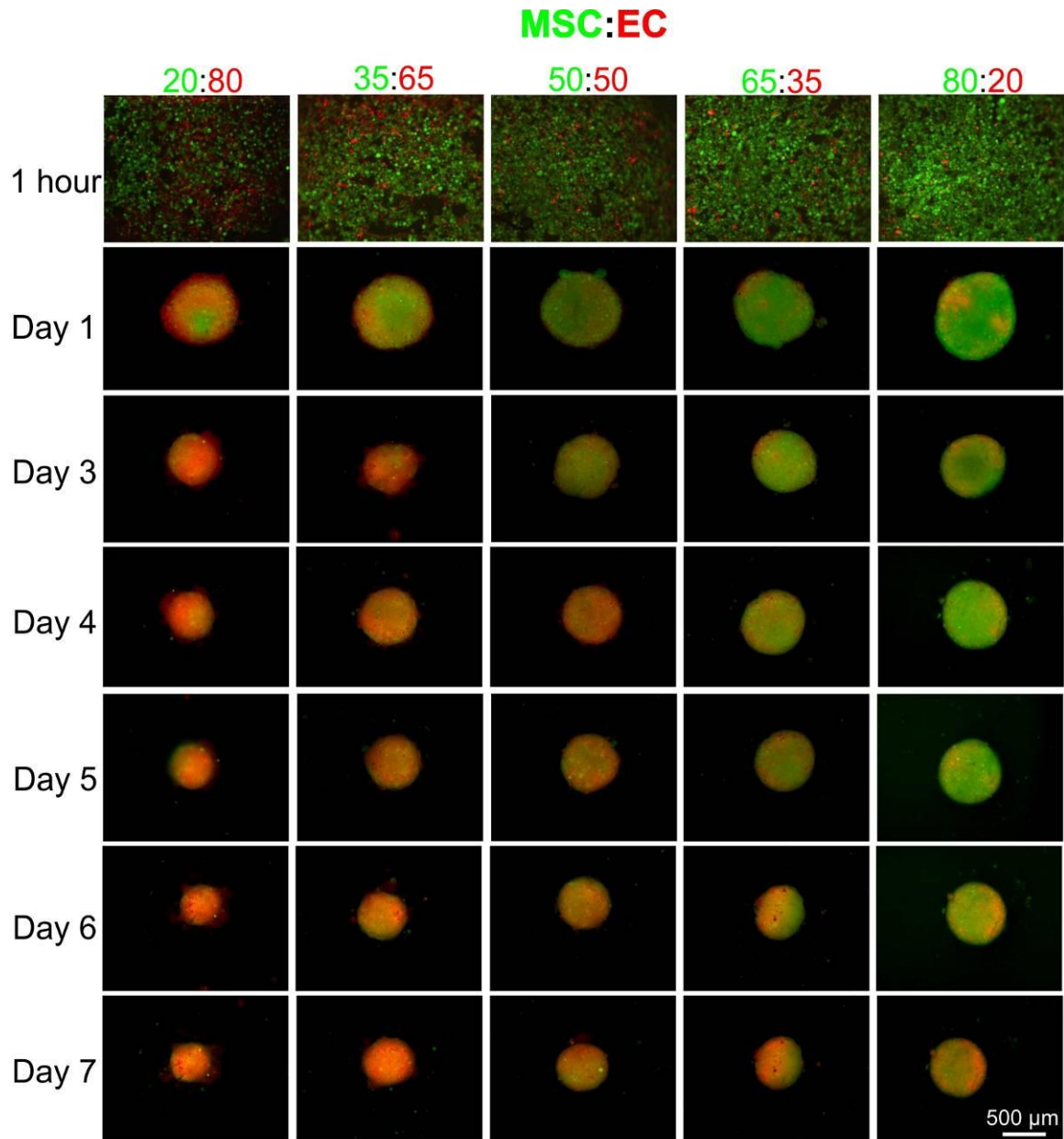
Figure 4.4.3 – Various fluorescently labelled whole MSC:EC spheroids cultured for up to 7 days

Whole fluorescently labelled MSC:EC spheroids were imaged using a fluorescent microscope. The various ratio co-culture spheroids were cultured for up to 7 days. MSCs were labelled green and ECs labelled red, all combinations were able to form spheroids within 1 day, however, the structural integrity of 20:80 spheroids after 7 days was poor.
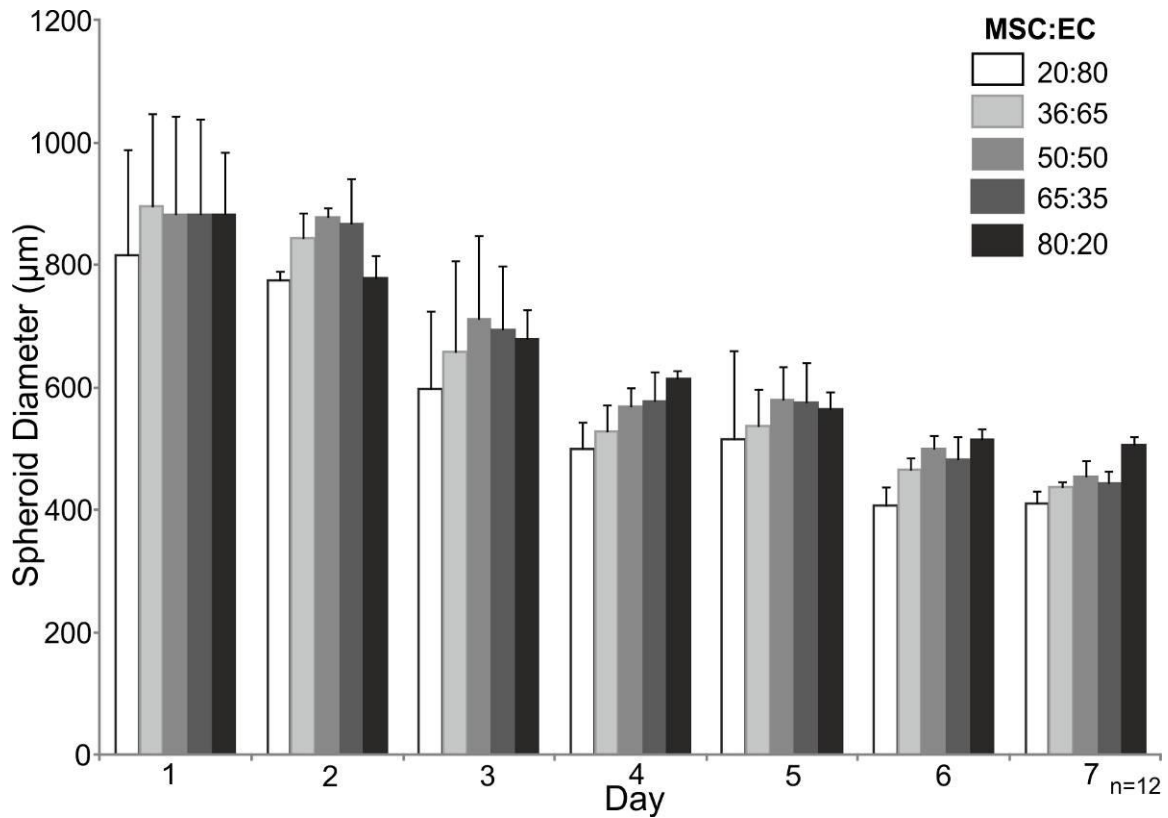
Figure 4.4.4 – Spheroid diameter of various MSC:EC spheroids cultured for up to 7 days

Spheroid diameter of various ratio MSC:EC spheroids was measured from fluorescent images using Image J software over a period of 7 days. Spheroid diameter decreased during culture, this is most striking between day 1 and 5. No significant differences between the various ratios were detected; however, 20:80 spheroids were consistently smaller compared to 80:20. For each time point and spheroid type, 12 individual spheroids from three different biological donors were measured (n=12)
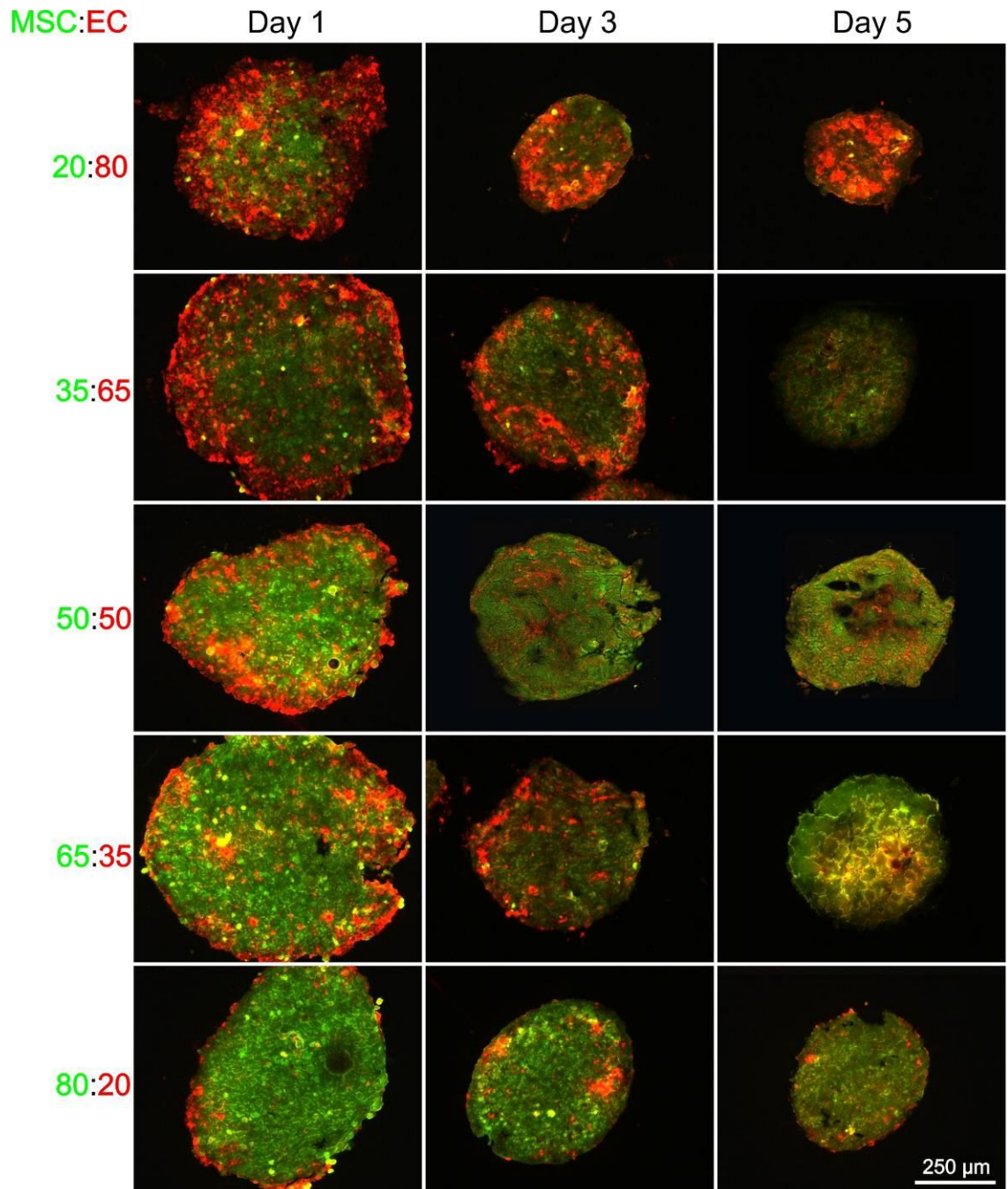
Figure 4.4.5 – Fluorescent spheroid sections of various MSC:EC ratios

The various fluorescently labelled MSC:EC spheroids were collected and snap frozen at days 1, 3 and 5. MSCs were labelled green and ECs red. Spheroids were sectioned and imaged using a fluorescence microscope to observe internal organisation patterns. 50:50 MSC:EC spheroids showed a unique primitive vascular-like network of ECs.

4.4.3 Three dimensional spheroid formation of co-cultured MSCs and ECs

Following these observations, from here on all MSC-EC spheroids used a 50:50 mixture of the two different cell types unless otherwise stated. To understand the self-organisation pattern observed, the spheroid formation process was analysed in more detail. Initial studies were performed using time-lapse imaging on a light microscope; this was done to assess the formation time between cell suspension to cell spheroid. Using this technique it was possible to observe the spheroid formation process, Figure 4.4.6 shows selected time coded images from this analysis. It was observed that from cell suspension to spheroid formation took approximately 15 hours.

This initial spheroid formation analysis was then developed into fluorescently labelled 4D imaging using a confocal microscope. A fluorescently labelled MSC-EC spheroid was analysed and 3D images were captured every 20 minutes. To reduce cell death caused by the laser light, the cell suspension was left for 4 hours before imaging was conducted. A selection of key time-points can be observed in Figure 4.4.7; MSCs were labelled green whilst ECs were labelled red. After 17 hours and 20 minutes after initial cell seeding a 3D cell spheroid was clearly observed. To act as a control for MSC-EC spheroid formation an MSC-only spheroid with half the population of MSCs labelled green and the other half red was created. This was then analysed using the same 4D imaging technique (Figure 4.4.8).
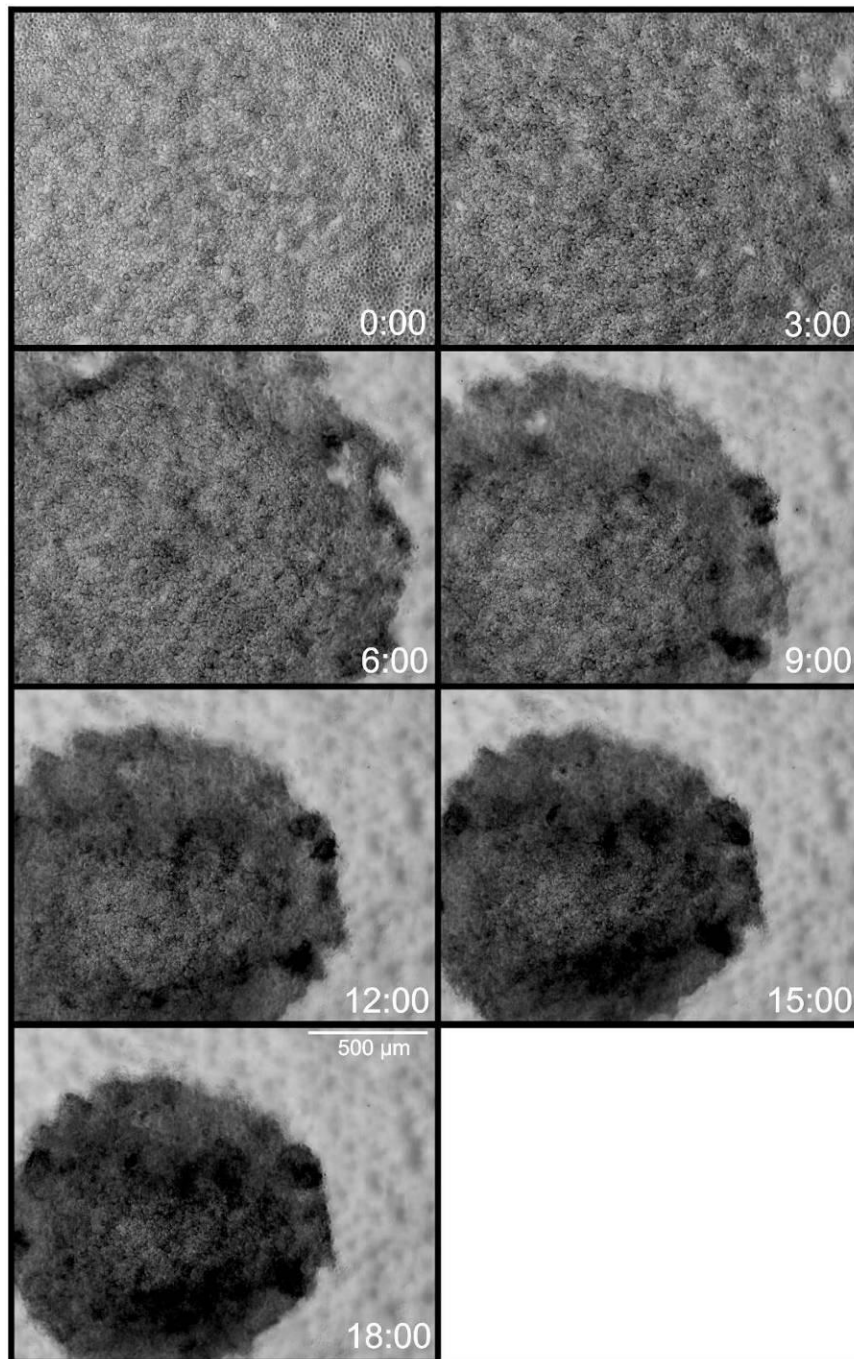
Figure 4.4.6 – Time-lapse of MSC-EC spheroid formation using a light microscope

Time-lapse analysis of MSC-EC spheroid formation was performed for up to 24 hours capturing images every 15 minutes. Here selected key time-points show the spheroid formation process. At 0:00 the cells are in a random suspension, at 6:00 the cells have begun to aggregate. By 15:00 a cell spheroid is clearly visible and by 18:00 the cell spheroid structure is still maintained. Therefore, the spheroid formation process took approximately 15 hours.
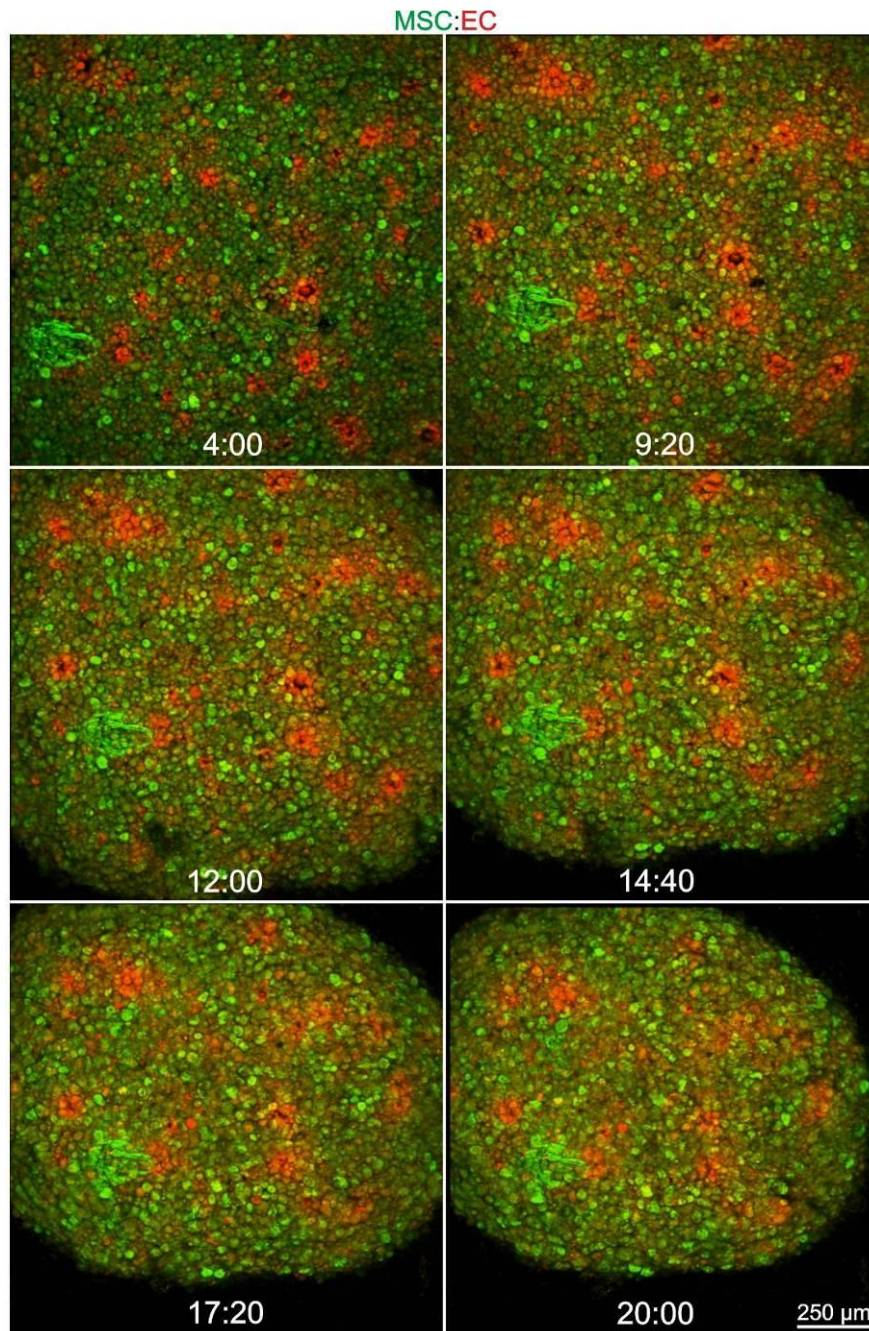
Figure 4.4.7 – Three-dimensional time-lapse analysis of a fluorescently labelled MSC-EC spheroid during formation

Three-dimensional time-lapse analysis or 4D imaging was performed on a fluorescently labelled MSC-EC spheroid, using a multi-photon confocal microscope. MSCs were labelled green and ECs red. 3D images were captured every 20 minutes for up to 16 hours. To reduce cell death caused by the laser light the cell suspension was incubated for 4 hours before being imaged. At this time point a random cell suspension can be observed, the cells begin to aggregate and a cell spheroid can be seen at 17:20.
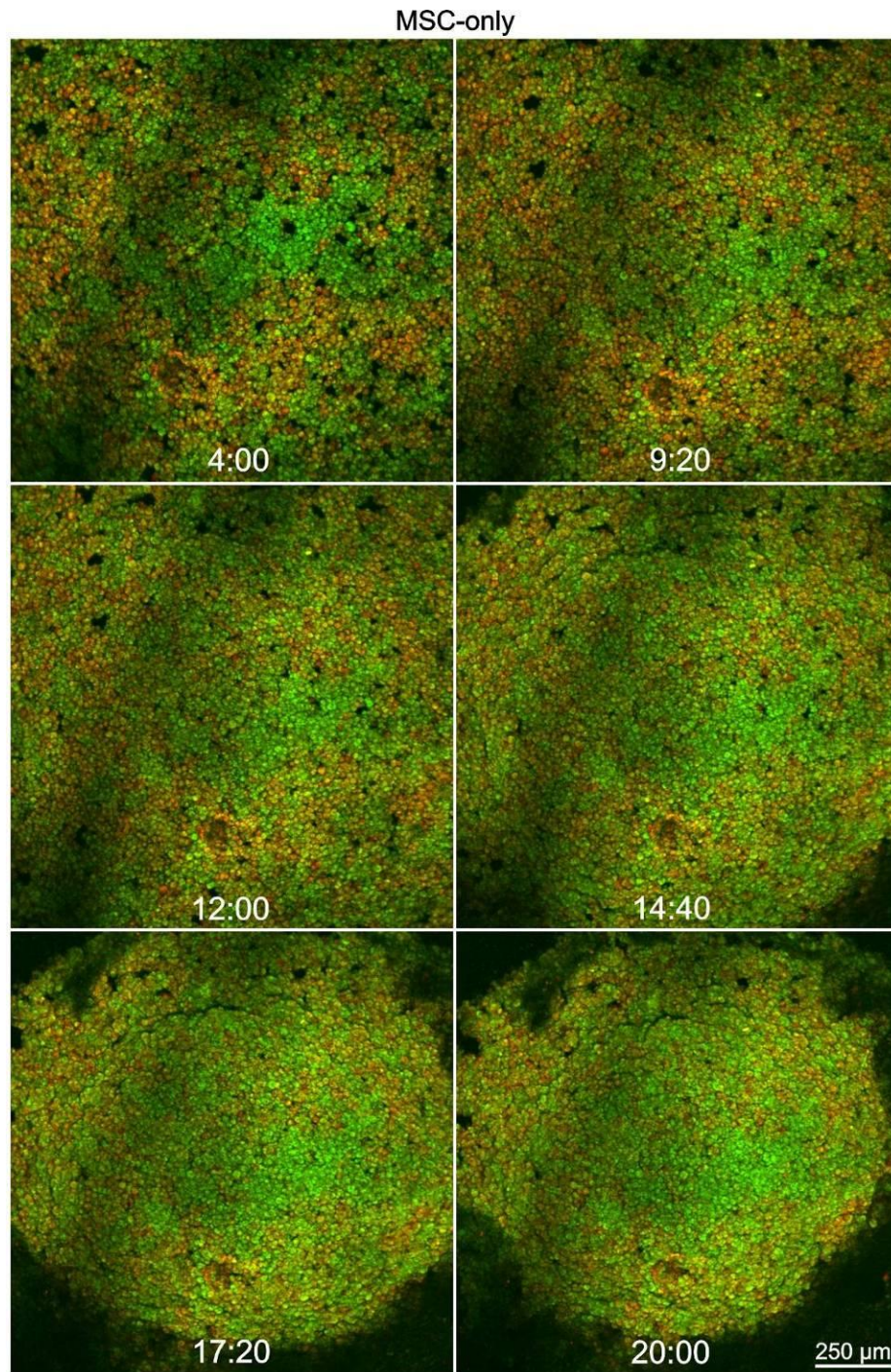
Figure 4.4.8 – Three dimensional time-lapse analysis of a fluorescently labelled MSC-only spheroid during formation

To act as a control three-dimensional time-lapse analysis or 4D imaging was performed on a fluorescently labelled MSC-only spheroid. Half of the MSCs were fluorescently labelled green whilst the other half were labelled red. A random cell suspension can be observed at time-point 4:00, the cells begin to aggregate and a spheroid can be seen at 17:20.

Using Volocity software the surface of the spheroid was analysed during the formation process. The percentage of either green or red cells at the spheroid surface was calculated every 20 minutes for a total of 16 hours (Figure 4.4.9). It can be seen that for the MSC-EC spheroid the percentage of red ECs increases during the spheroid formation, by contrast the MSC-only spheroid no increasing trend was observed. This spheroid surface analysis technique was then repeated using two additional biological donors. Both MSC-EC and MSC-only spheroids were analysed (Figure 4.4.10, Figure 4.4.11). For all MSC-EC spheroids, the percentage of red ECs increased at the surface by approximately 4% over the 15-hour analysis period. In contrast all MSC-only spheroids the percentage change was no greater than 2%.

Spheroid volume was also calculated using Volocity software during spheroid formation analysis (Figure 4.4.12). Both MSC-EC (50:50) and MSC-only spheroids had similar volumes that decreased at approximately the same rate over the same time period.
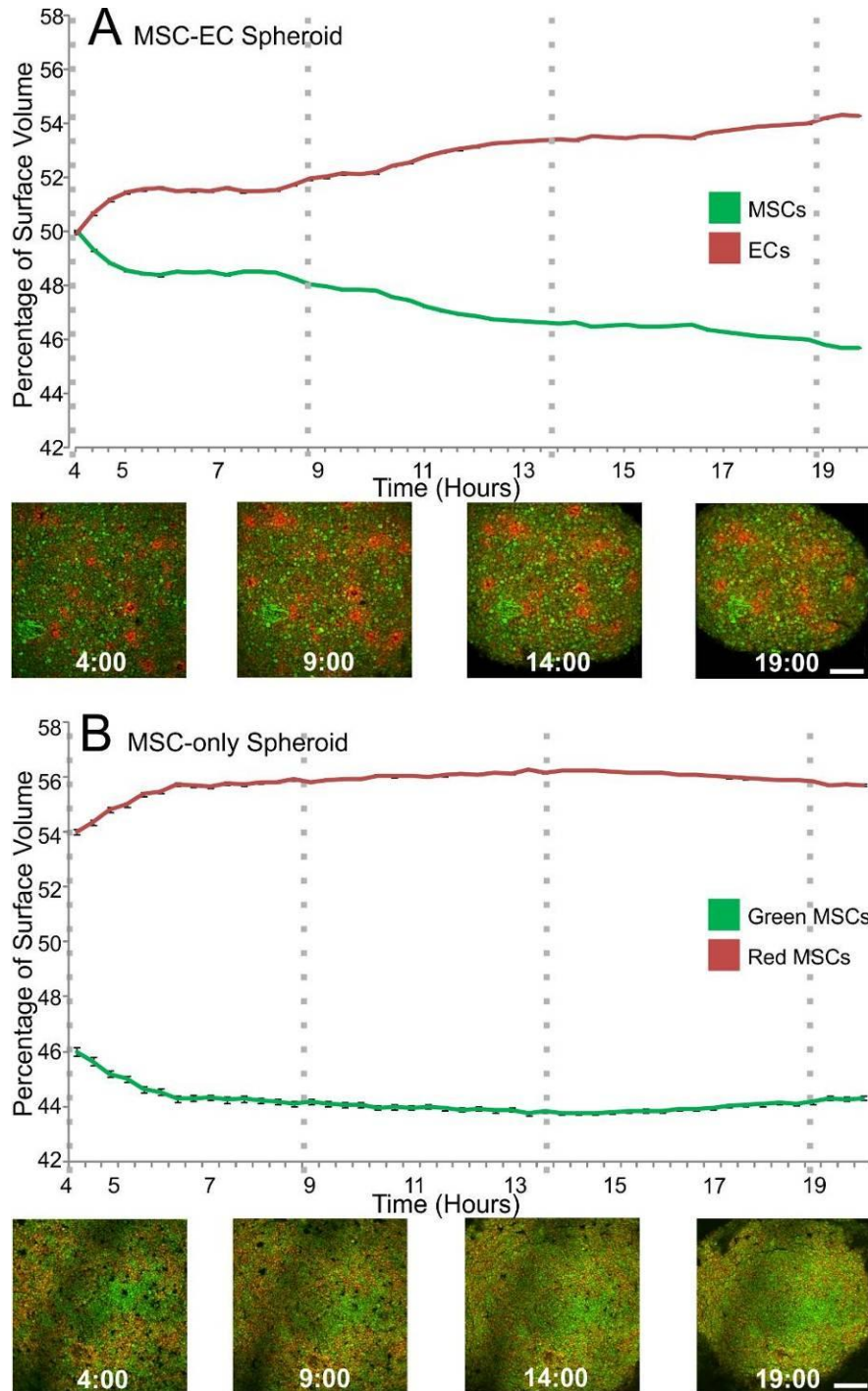
Figure 4.4.9 – Spheroid surface analysis during formation of MSC-EC and MSC-only spheroids

From the 4D imaging performed on the MSC-EC and MSC-only spheroid, surface analysis was performed. This was used to quantify the percentage of green or red cells at the spheroid surface. For the MSC-EC spheroid it was determined that the percentage of red (EC) cells at the surface increased with time. For the MSC-only spheroid no change in spheroid surface was observed.
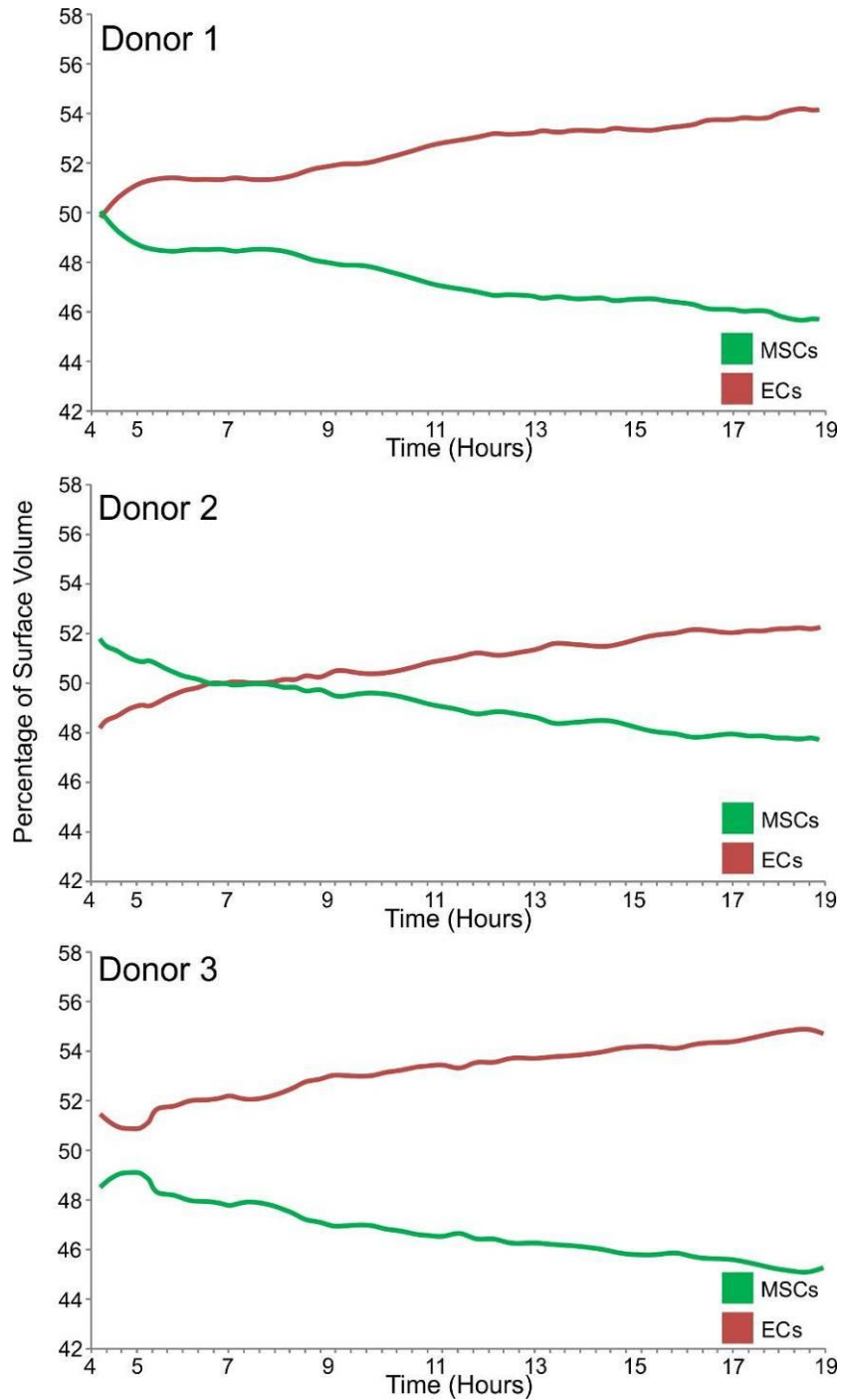
Figure 4.4.10 – Spheroid surface analysis during the formation of MSC-EC spheroids from Donors 1, 2 and 3

Surface analysis was performed using the 4D imaging of three MSC-EC spheroids from three different biological donors. This analysis quantified the percentage of green MSCs or red ECs at the spheroid surface. For all donors the percentage of ECs at the spheroid surface increases by approximately 4% over the 15-hour analysis.
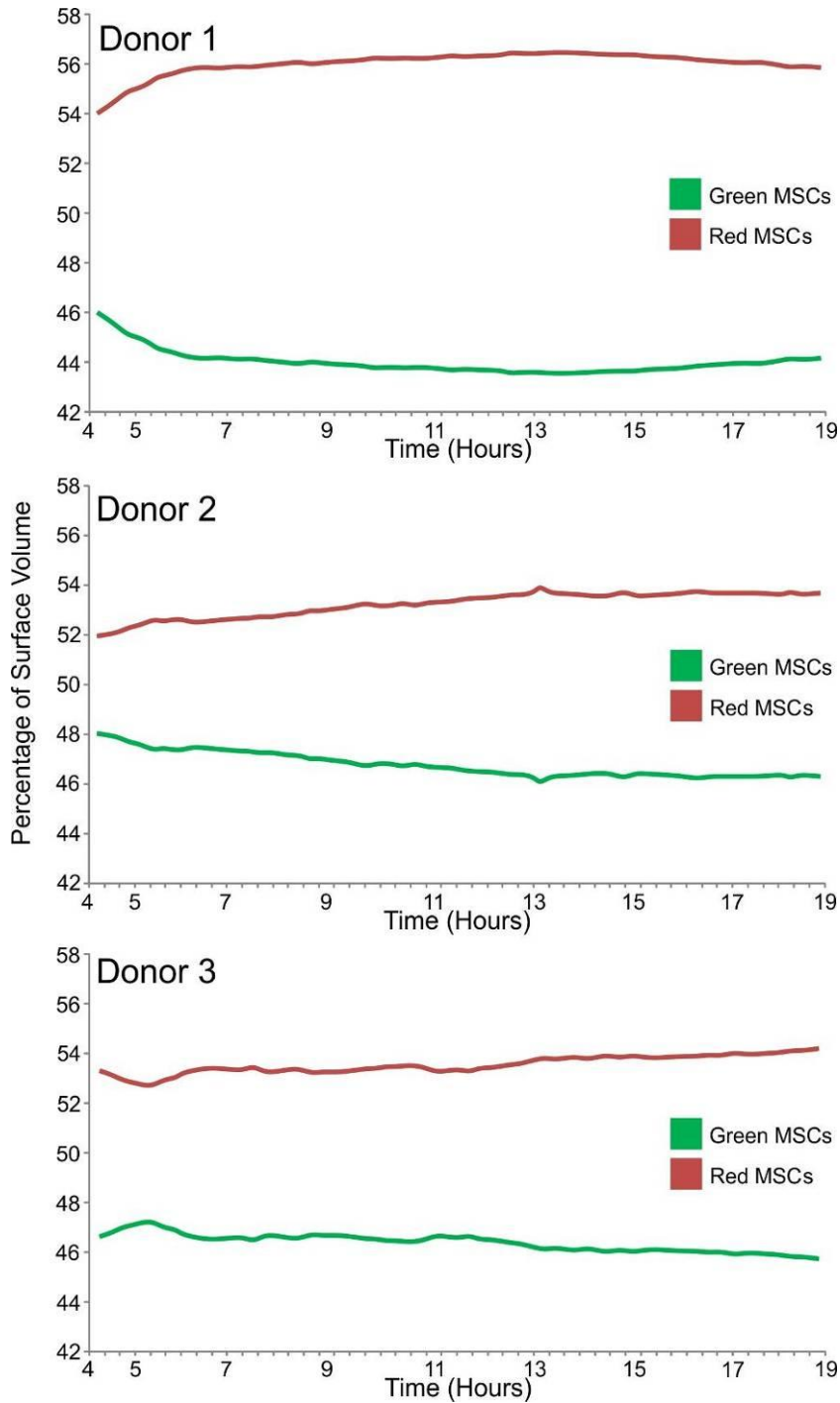
Figure 4.4.11 – Spheroid surface analysis during the formation of MSC-only spheroids from Donors 1, 2 and 3

Surface analysis was performed using the 4D imaging of three MSC-only spheroids from three different biological donors. This analysis quantified the percentage of either green MSCs or red MSCs at the spheroid surface. For all donors the percentage change of either red or green MSCs did not exceed 2% over the 15-hour analysis.
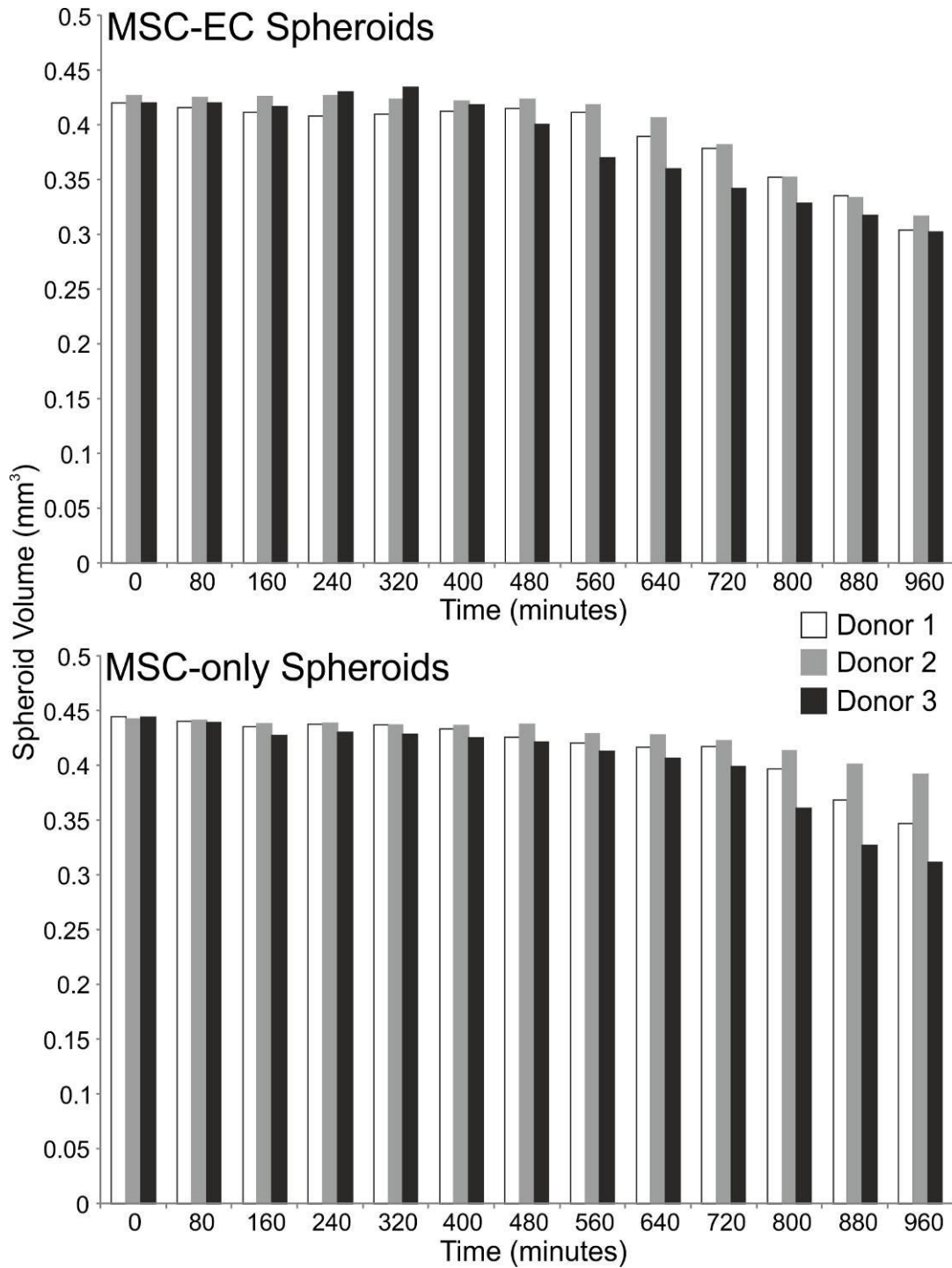
Figure 4.4.12 – Spheroid volume analysis of MSC-EC and MSC-only spheroids during formation

Spheroid volume was calculated using Volocity software for MSC-EC and MSC-only spheroid s during formation. Both MSC-EC and MSC-only spheroids had similar volumes that decreased at approximately the same rate over the same time period (n=1).

4.4.4 Three dimensional spheroid co-culture of HDFs and ECs

To determine whether the self-organisation relationship between MSCs and ECs was unique, HDFs were cultured with ECs in U-bottomed 96-well plates (Section 4.3.2). These HDF-EC spheroids were compared to MSC-EC spheroids, 3D confocal microscopy images can be seen in Figure 4.4.13. HDFs and MSCs were labelled green, whilst ECs were labelled red. These images show the whole spheroids over a period of 7 days, little difference can be observed by visual comparison. The spheroid diameter and spheroid surface of these two different spheroid types were calculated (Figure 4.4.14). It was found that HDF-EC spheroids were significantly smaller than MSC-EC spheroids at days 5 and 7 of culture. There were also significantly more green labelled cells (HDFs) at the spheroid surface of HDF-EC spheroids compared to the percentage of green labelled cells (MSCs) in MSC-EC spheroids at days 3 and 7 of culture.

The fluorescently labelled spheroids were snap frozen and sections to observed internal organisation, representative images from three different spheroids and three spheroid sections (N=9) can be seen in Figure 4.4.15. HDF-EC and MSC-EC spheroids were compared at various time-points in culture, HDFs and MSCs were labelled green whilst ECs were consistently labelled red. Little to no organisation was detected in HDF-EC spheroids, at day 1 and 3 ECs appear more prominently at the spheroid periphery. In contrast MSC-EC spheroids demonstrated a different organisation pattern; ECs did not appear more prominent at the spheroid edge. The ECs appeared to be associated forming a network that was evenly distributed throughout the spheroid by day 3. The EC-network length, width and branching was then calculated from these spheroid section images (Figure 4.4.16). A total of 24 spheroids sections from six spheroids were analysed (n=24). MSC-EC sections had a significantly greater EC-network length compared to HDF-EC sections at days 3 and 5. MSC-EC sections also had significantly more branching compared to HDF-EC spheroids at day 5.
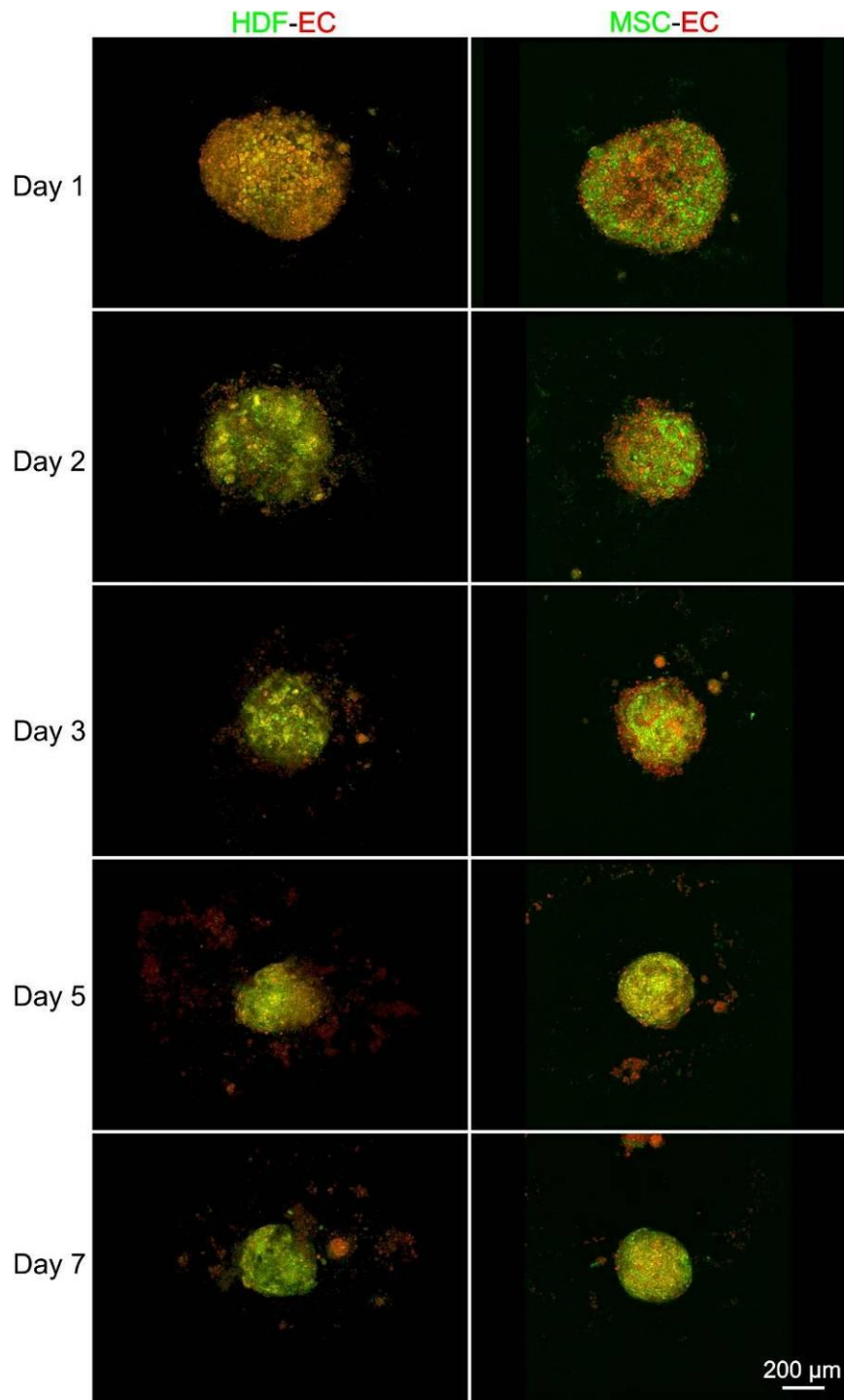
Figure 4.4.13 – 3D confocal images of whole fluorescently labelled HDF-EC and MSC-EC spheroids

Whole spheroid images of HDF-EC and MSC-EC spheroids were taken over a 7-day culture period using a multi-photon confocal microscope. HDFs and MSCs were labelled green whilst ECs were labelled red. These whole spheroid images show little difference via visual comparison.
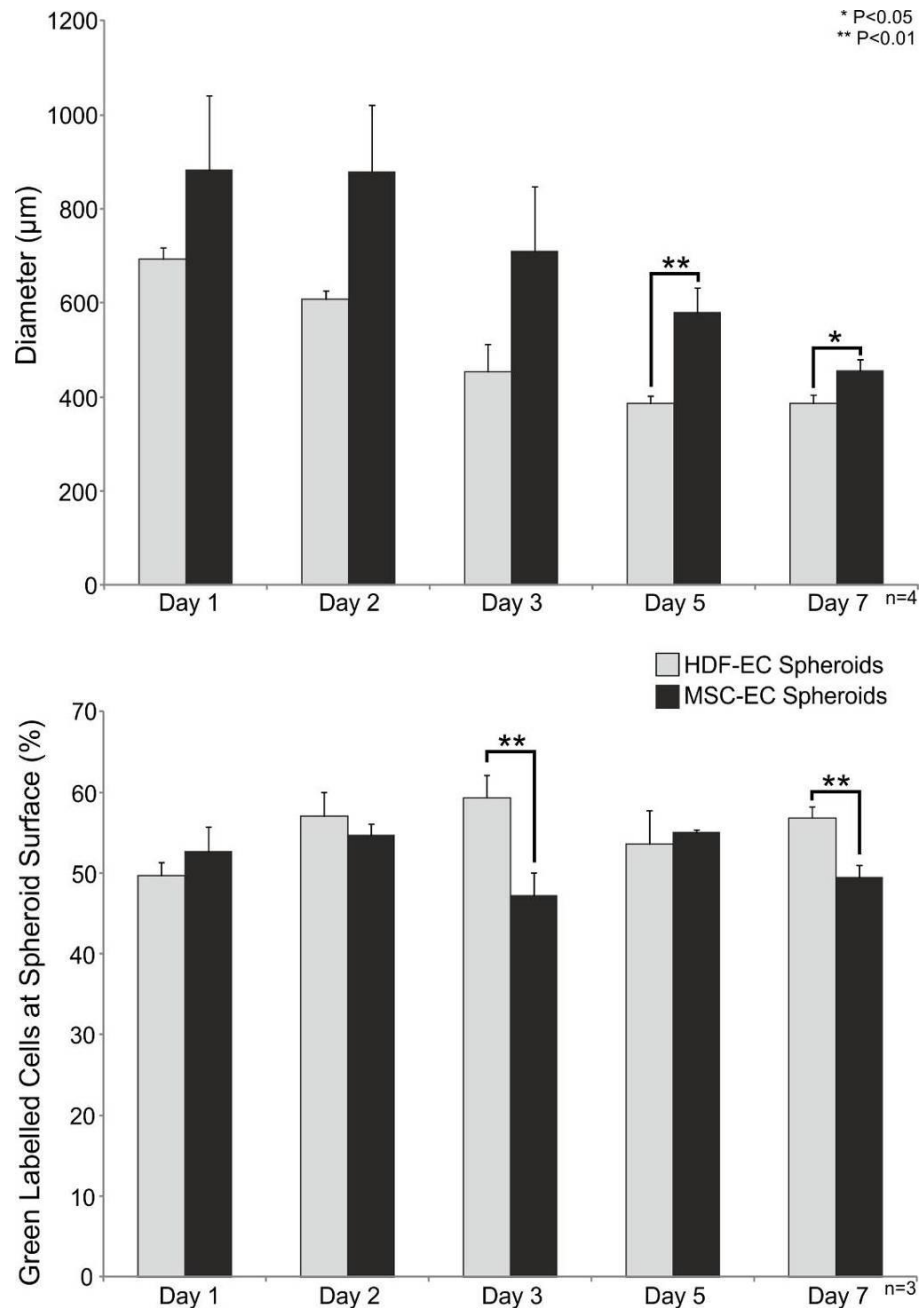
Figure 4.4.14 – Diameter and surface analysis of HDF-EC and MSC-EC spheroids

The spheroid diameter of HDF-EC and MSC-EC spheroids was calculated, it was found that HDF-EC spheroids were significantly smaller than MSC-EC spheroids at days 5 and 7 of culture. Surface analysis of green labelled cells (HDFs or MSCs) found that significantly more green cells were at the spheroid surface of HDF-EC spheroids compared to MSC-EC spheroids at days 3 and 7 of culture. Spheroid diameter was calculated from four individual spheroids per time point (n=4) and spheroid surface analysis was conducted on three individual spheroids per time-point (n=3).
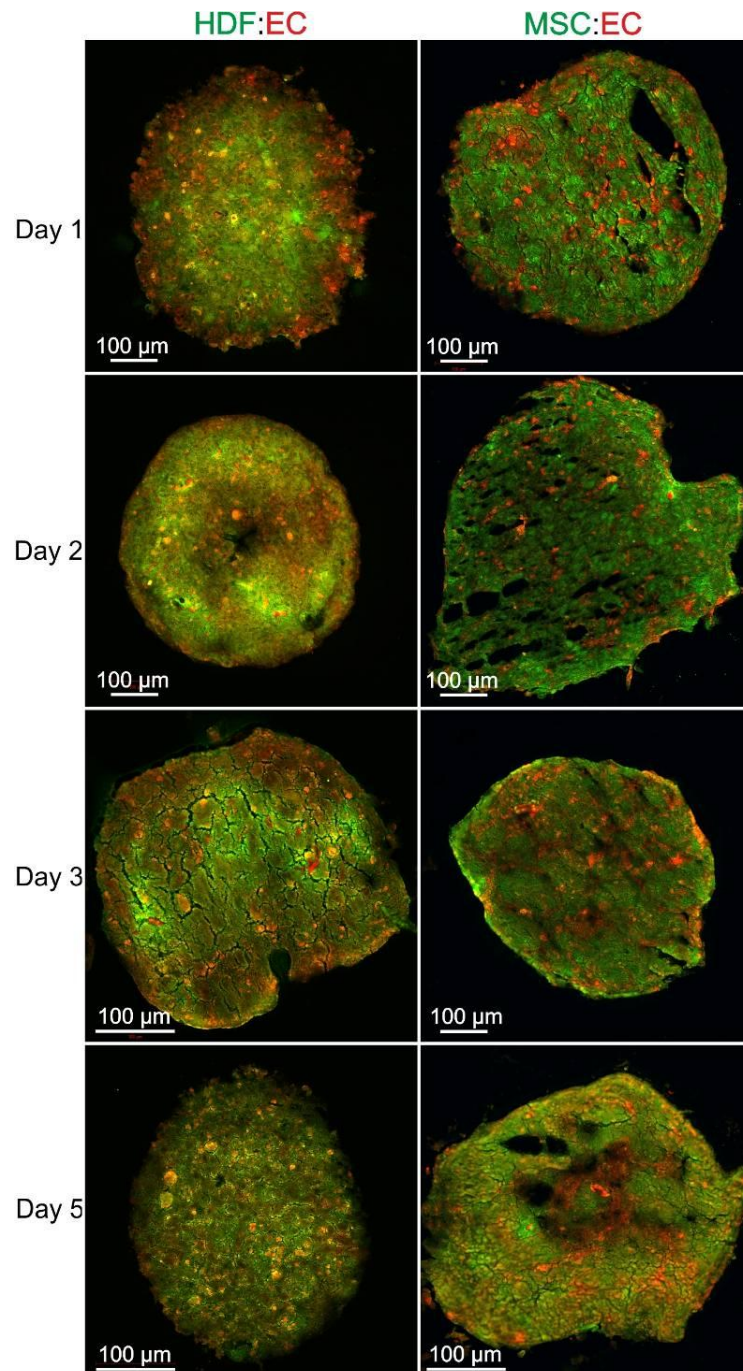
Figure 4.4.15 – Fluorescently labelled spheroid sections of HDF-EC and MSC-EC co-cultured spheroids

Spheroids were fluorescently labelled to identify the two different cell types and representative images are shown from n=24 independent observations. HDF-EC and MSC-EC spheroids were compared to observe if MSCs directed EC self-organisation. HDF or MSCs were labelled green and ECs were labelled red. Little self-organisation within HDF-EC spheroid sections was visibly detected, unlike MSC-EC spheroid sections where an EC network was observed from day 3.
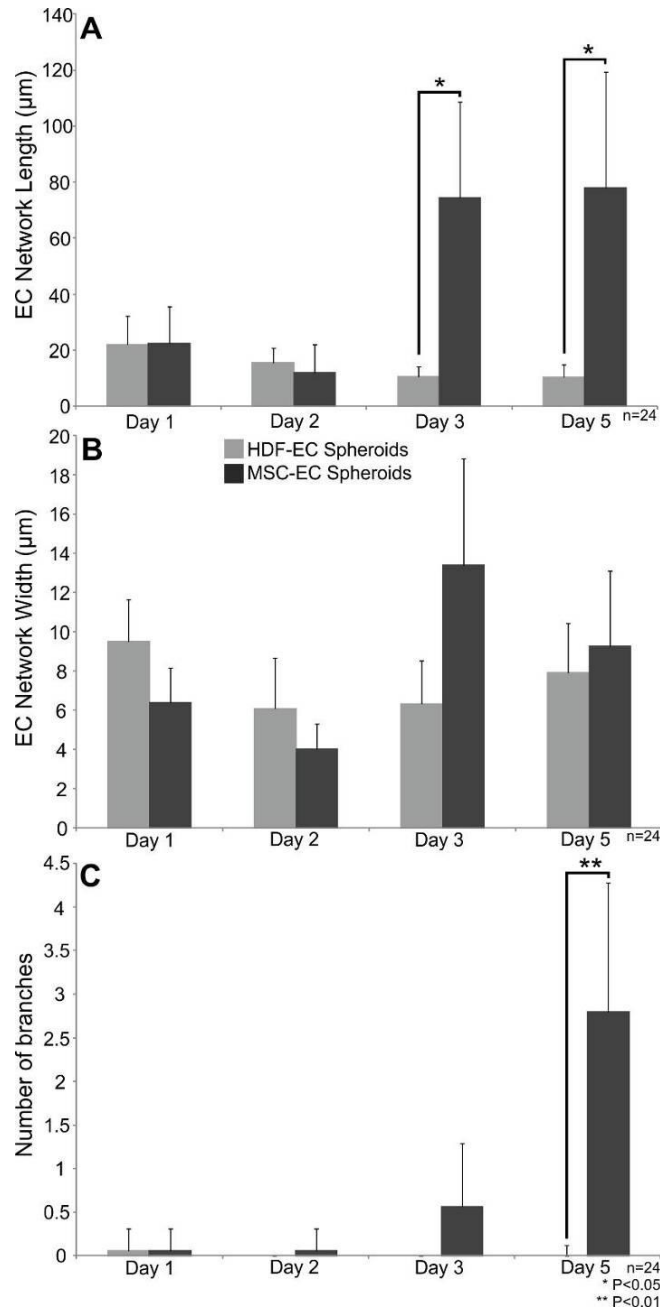
Figure 4.4.16 – Endothelial cell network length width and branching analysis of HDF-EC and MSC-EC spheroids

From the various HDF-EC and MSC-EC spheroid section images the EC networks within these sections were manually analysed using Image J software to quantify length (A), width (B) and branching (C). A significant increase in network length was detected in MSC-EC spheroids at days 3 and 5 compared to HDF-EC. A significant increase in the number of branches was detected in MSC-EC day 5 sections compared to HDF-EC sections at day 5. A total of 24 different spheroid sections from six spheroids were analysed (n=24).

4.4.5 Effects of various inhibitor treatments on co-culture spheroid formation and organisation

All experiments performed in this section were conducted using three different biological MSC donors; all images are representative of a minimum of three different spheroids from three different biological donors. All results are averages calculated from three biological donors. MSC-EC spheroids were treated with a variety of different inhibitor treatments to block key signalling pathways. Some of the signalling pathways, such as FGF and ILK are known to affect or be affected by EC migration. Whole spheroid images on these different inhibitor treatments and an MSC-only control (made of an equal mixture of green and red MSCs) can be seen in Figure 4.4.17. MSC-EC spheroids were treated with ILKi, PDGFRi, EGFRi, DBZ (Notch inhibitor) and FGFRi. Visual differences can be seen depending upon the inhibitor treatment; MSC-EC spheroids treated with ILKi clearly have more green MSCs at the spheroid surface compared to MSC-EC alone. Spheroids treated with PDGFRi also appear larger at Day 1. Using Volocity visualisation and rendering software an alternative whole spheroid images were generated, these images showed that both FGFRi and DBZ treated spheroids had more red labelled ECs at the spheroid surface (Figure 4.4.18). These whole spheroid images were then analysed to quantify diameter and percentage of green labelled MSCs at the spheroid surface (Figure 4.4.19).

From this analysis it was found that PDGFRi treated spheroids were significantly larger at days 1 and 2 of culture and FGFRi treated spheroids were larger at day 3. Spheroid surface analysis confirmed observations in Figure 4.4.17 and Figure 4.4.18, ILKi treatment resulted in significantly more green MSCs being at the spheroid surface at days 1, 2 and 3 compared to MSC-EC untreated spheroids. PDGFRi treatment resulted in significantly fewer MSCs at the spheroid surface at days 1, 2 and 5. DBZ treatment resulted in significantly fewer MSCs at the spheroid surface at days 1, 2 and 3. FGFRi treatment resulted in significantly fewer MSCs at the spheroid surface at days 1 and 2.
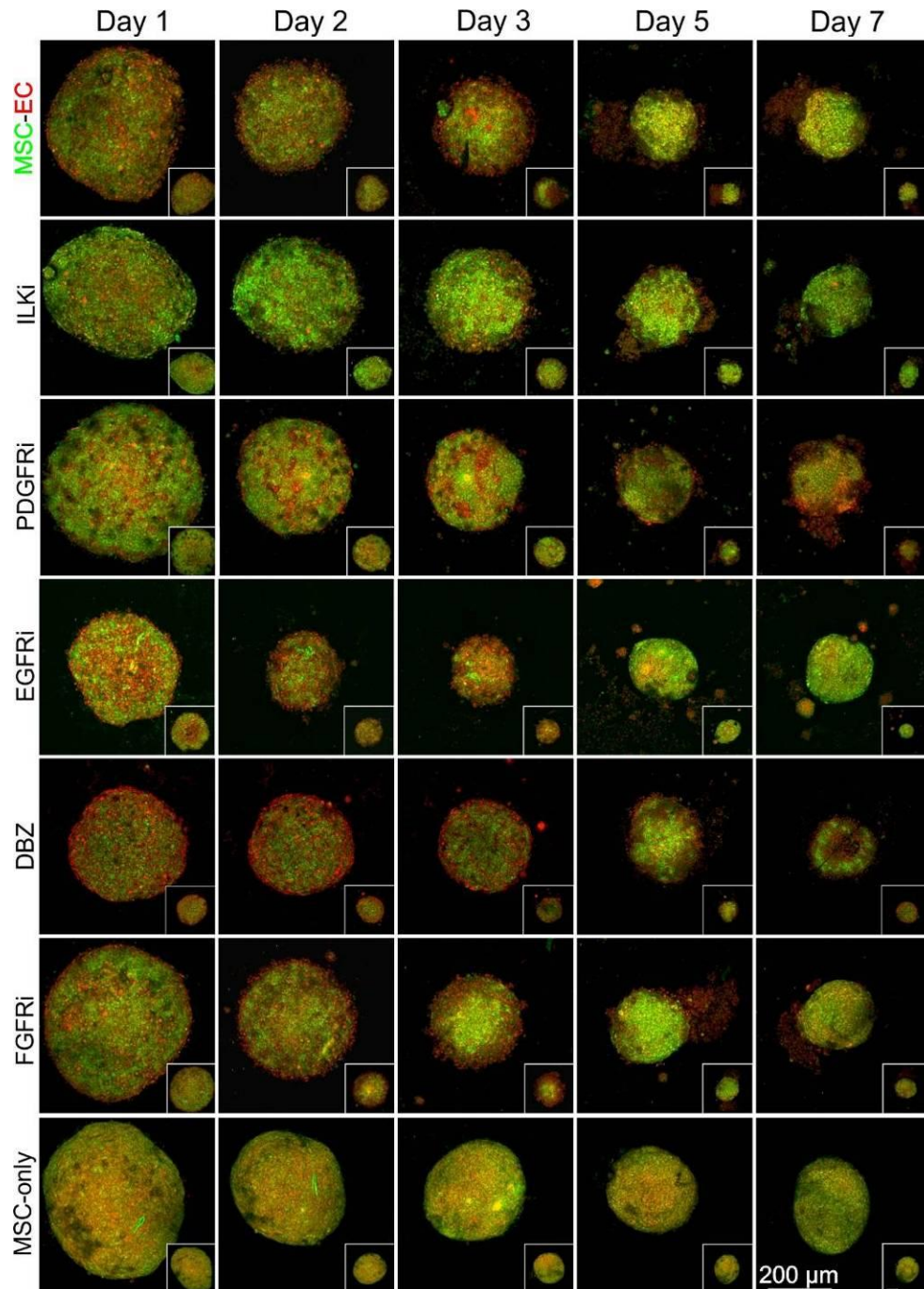
Figure 4.4.17 – Whole 3D MSC-EC spheroids treated with various inhibitors

Using 3D multi-photon confocal microscopy whole images of living MSC-EC spheroids were imaged. MSCs were labelled green and ECs red, except for the MSC-only control, 50% of the cells were labelled green and the other 50% red. Spheroids were treated with ILKi, PDGFRi, EGFRi, DBZ (Notch inhibitor) and FGFRi for up to 7 days in culture. PDGFRi treated spheroids appear larger, ILKi spheroids appear to have greater green and DBZ treated spheroids appear more red.
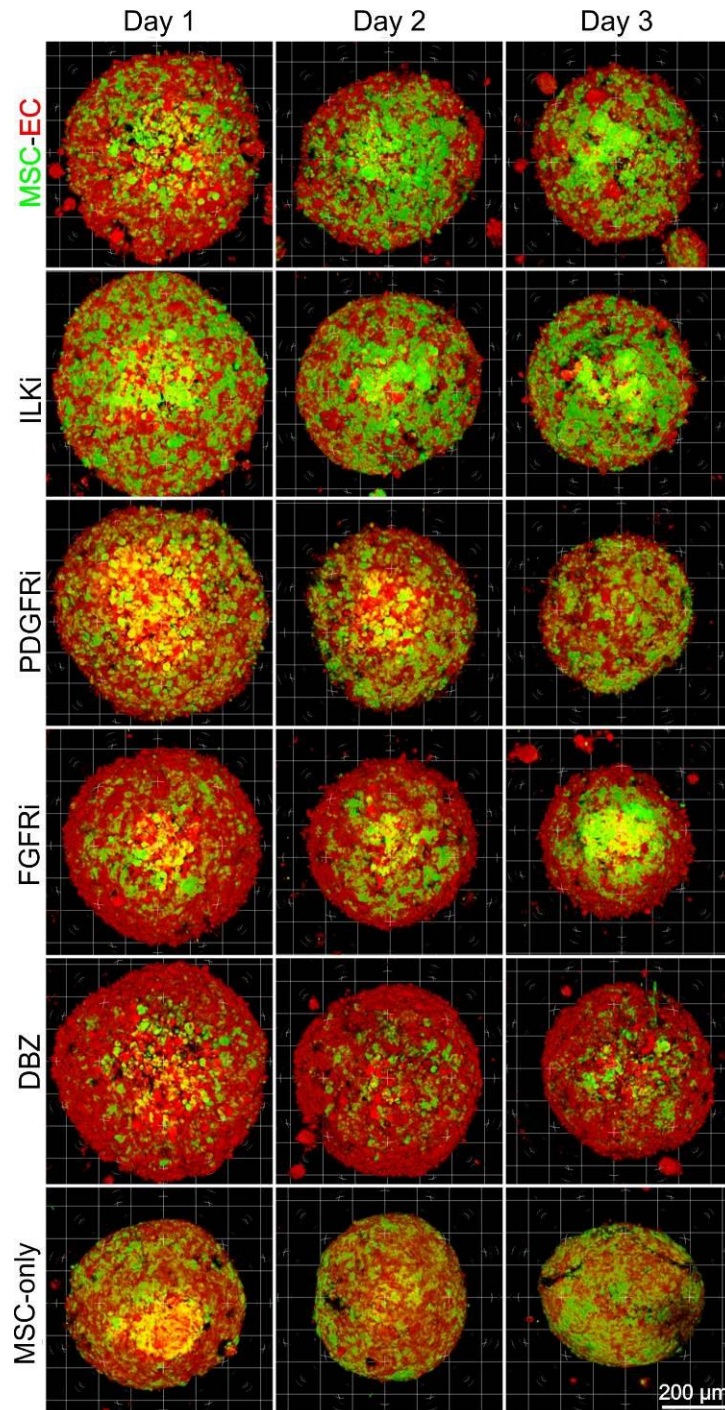
Figure 4.4.18 – Whole 3D MSC-EC spheroid images rendered using Volocity software

Whole MSC-EC spheroids treated with various inhibitors were imaged as shown in Figure 4.4.17. However, using Volocity image rendering these alternative images were created, highlighting that FGFRi and DBZ treatment resulted in more red labelled ECs at the spheroid surface compared to untreated control MSC-EC spheroids.
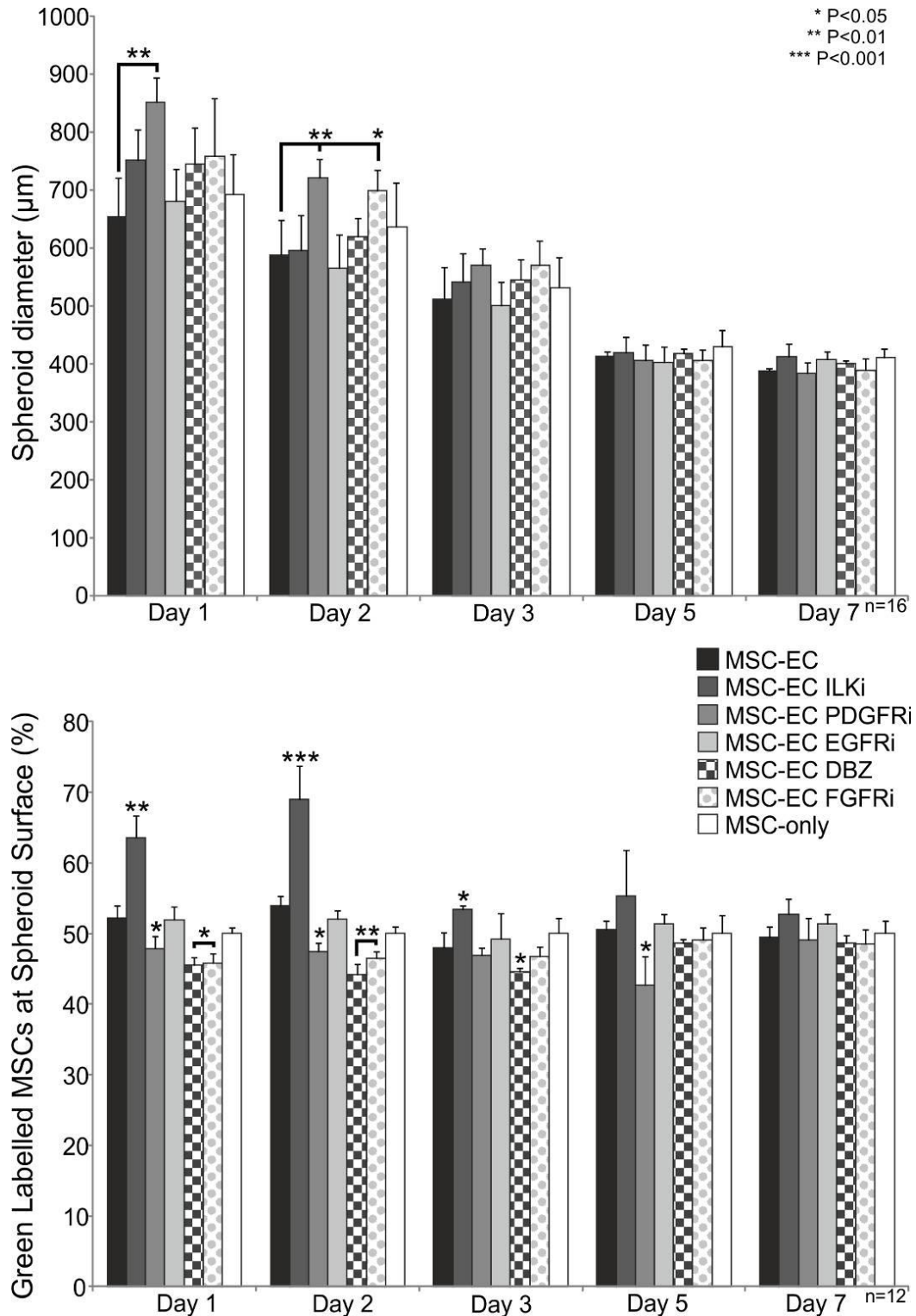
Figure 4.4.19 – Spheroid diameter and surface analysis of MSC-EC spheroids treated with various inhibitors

From the whole spheroid images analysis was performed to analyse spheroids diameter and the percentage of green cells (MSCs) at the spheroid surface. From

this analysis it was found that PDGFRi treated spheroids were significantly larger at days 1 and 2 of culture and FGFRi treated spheroids were larger at day 3, compared to MSC-EC untreated spheroids. Spheroid surface analysis confirmed observations in Figure 4.4.17, ILKi treatment resulted in significantly more green MSCs being at the spheroid surface at days 1, 2 and 3 compared to MSC-EC untreated spheroids. PDGFRi treatment resulted in significantly fewer MSCs at the spheroid surface at days 1, 2 and 5. DBZ treatment resulted in significantly fewer MSCs at the spheroid surface at days 1, 2 and 3. FGFRi treatment resulted in significantly fewer MSCs at the spheroid surface at days 1 and 2. Spheroid diameter was calculated from four individual spheroids, from three different biological donors per time point (n=16) and spheroid surface analysis was conducted on four individual spheroids, from three biological donors per time-point (n=12).

The spheroids were sectioned at various time-points to identify internal organisation patterns, a minimum of three sections were images per individual spheroid. In addition each treatment type was performed using three different biological donors. Untreated control MSC-EC spheroids had previously demonstrated a vascular-like network of ECs evenly distributed throughout the spheroid (Section 4.4.2). Figure 4.4.20 shows this pattern was observed again in untreated MSC-EC spheroids, MSCs were labelled green and ECs red. However, the various inhibitor treatments had clear effects of cellular organisation within the spheroids. ILKi treatment resulted in a layer of green MSCs at the periphery of the spheroid. PDGFRi treatment resulted in a much thicker vascular-like network of ECs, however, this was more concentrated towards the centre of the spheroid. EGFRi treatment appeared to have no effect and a similar organisation pattern was observed compared to MSC-EC untreated spheroids. DBZ treatment resulted in a layer of ECs at the periphery of the spheroid. FGFRi treatment resulted in a tight group of ECs within the centre of the spheroid. MSC-only spheroids were composed of an equal number of MSCs labelled either green or red to act as a control, a random distribution of the two different coloured cells was observed.

From these spheroid section images the EC network length, width and branching was calculated (Figure 4.4.21). A significant increase in network length was detected in PDGFRi treated spheroids at days 1 and 2. A significant increase in network width was detected in ILKi treated spheroids day 2 and PDGFRi treated spheroids days 1 and 2. For all time-points a significantly greater number of branches were detected with PDGFRi treatment. Overall EGFRi treatment appeared to have no effect of MSC-EC 3D spheroids, through the various qualitative and quantitative assessments no visual or significant differences were detected. Therefore, EGFRi was excluded from any further study.

Despite EC network length, width and branching showing some significant differences between various inhibitor treatments, manual Image J software analysis was unable to analyse the overall distribution of MSCs or ECs within the

spheroid. Therefore, plot profiling was performed on the spheroid section images (Figure 4.4.22). The graphs show the distribution of either positive value (green MSCs) or negative value (red cells ECs or MSCs) through the z-axis of the section. Neutral values relate to no fluorescence, this was caused by the z-axis being outside the spheroid section or damage to the spheroid section. This analysis showed that ILKi and FGFRi treatment resulted in ECs being predominantly at the centre of the spheroid. PDGFRi treatment resulted in ECs being more centrally located compared to MSC-EC untreated sections. DBZ treatment resulted in a distribution similar to untreated sections. MSC-only sections showed a random and even distribution of green and red labelled MSCs throughout the sections.
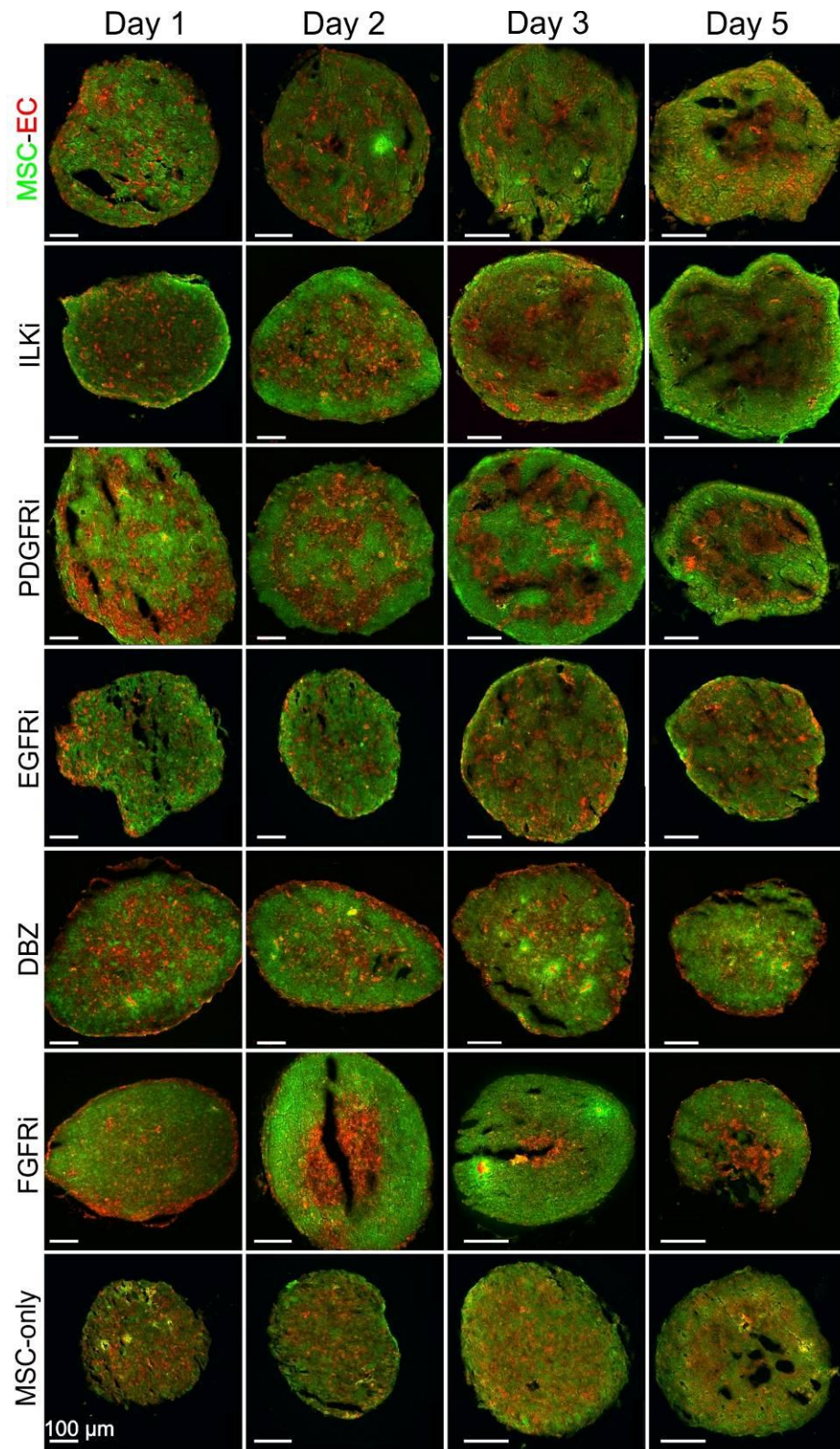
Figure 4.4.20 - Spheroid sections of fluorescently labelled MSC-EC spheroids treated with various inhibitors

Representative spheroid sections from n=24 independent observations of MSC-EC spheroids with various inhibitor treatments, MSCs were labelled green and ECs red. For the MSC-only control an equal ratio of MSCs were labelled green and red. Clear differences in the organisational patterns within the spheroid sections can be observed. PDGFRi treatment is most striking, with very large irregular EC-network arrangements when compared to MSC-EC untreated. ILKi treatment resulted in a thick peripheral layer of green MSCs at the spheroid surface. DBZ treatment resulted in the opposite and a thick peripheral layer of red ECs at the spheroid surface can be seen. FGFRi treatment resulted in a tight group of ECs at the centre of the spheroid. No organisation was detected in the MSC-only control spheroids.
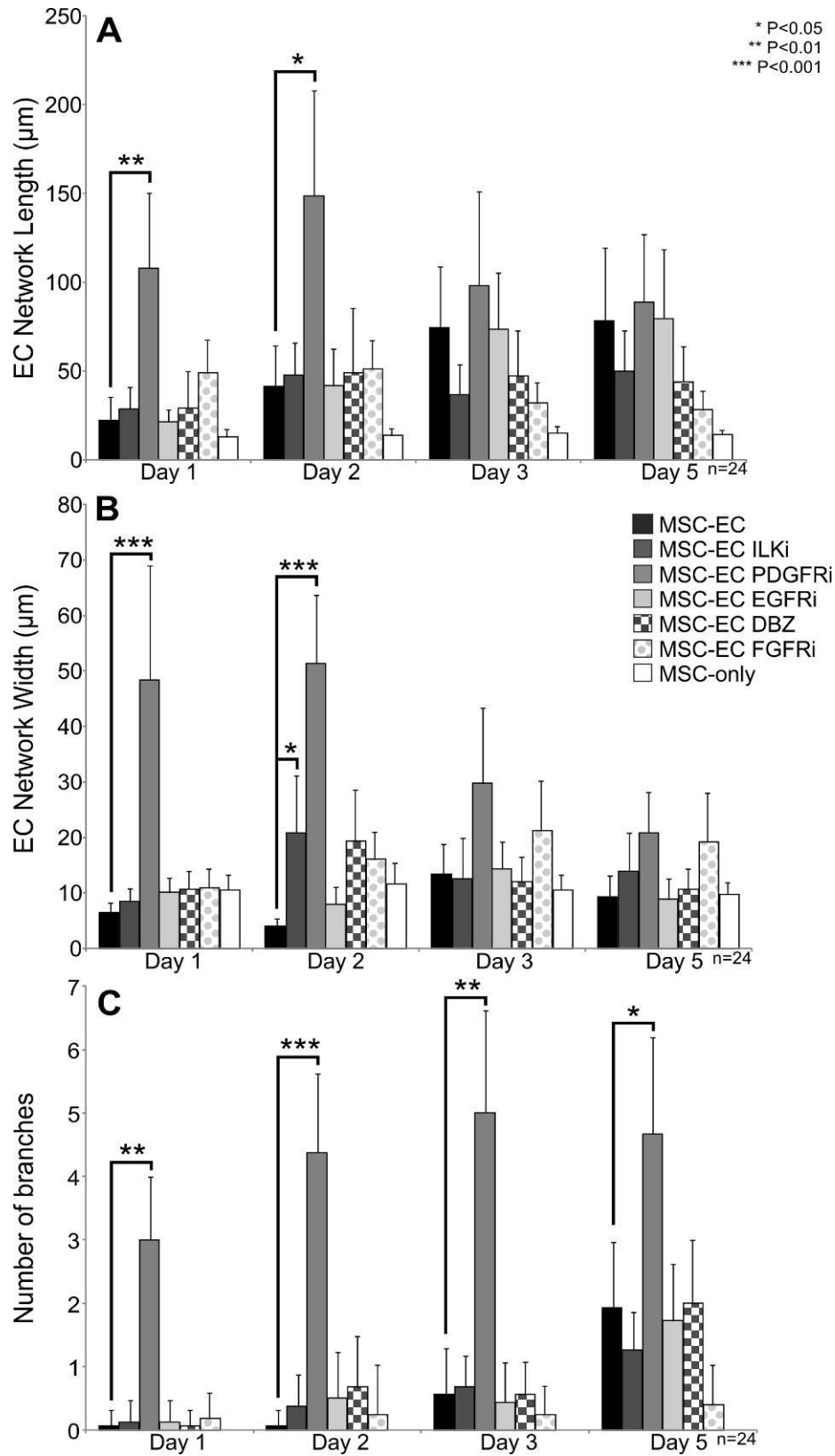
Figure 4.4.21 – Endothelial cell network length, width and branching from MSC-EC spheroid sections treated with various inhibitors

Using the various MSC-EC spheroid section images the EC networks were manually analysed using Image J software to quantify (A) length, (B) width and (C) branching. A significant increase in network length was detected in PDGFRi treated spheroids at days 1 and 2. A significant increase in network width was detected in ILKi treated spheroids day 2 and PDGFRi treated spheroids days 1 and 2. For all time-points a significantly greater number of branches were detected with PDGFRi treatment. EC network length, width and number of branches were calculated from observing a total of 8 spheroid sections from three different biological donors (n=24).
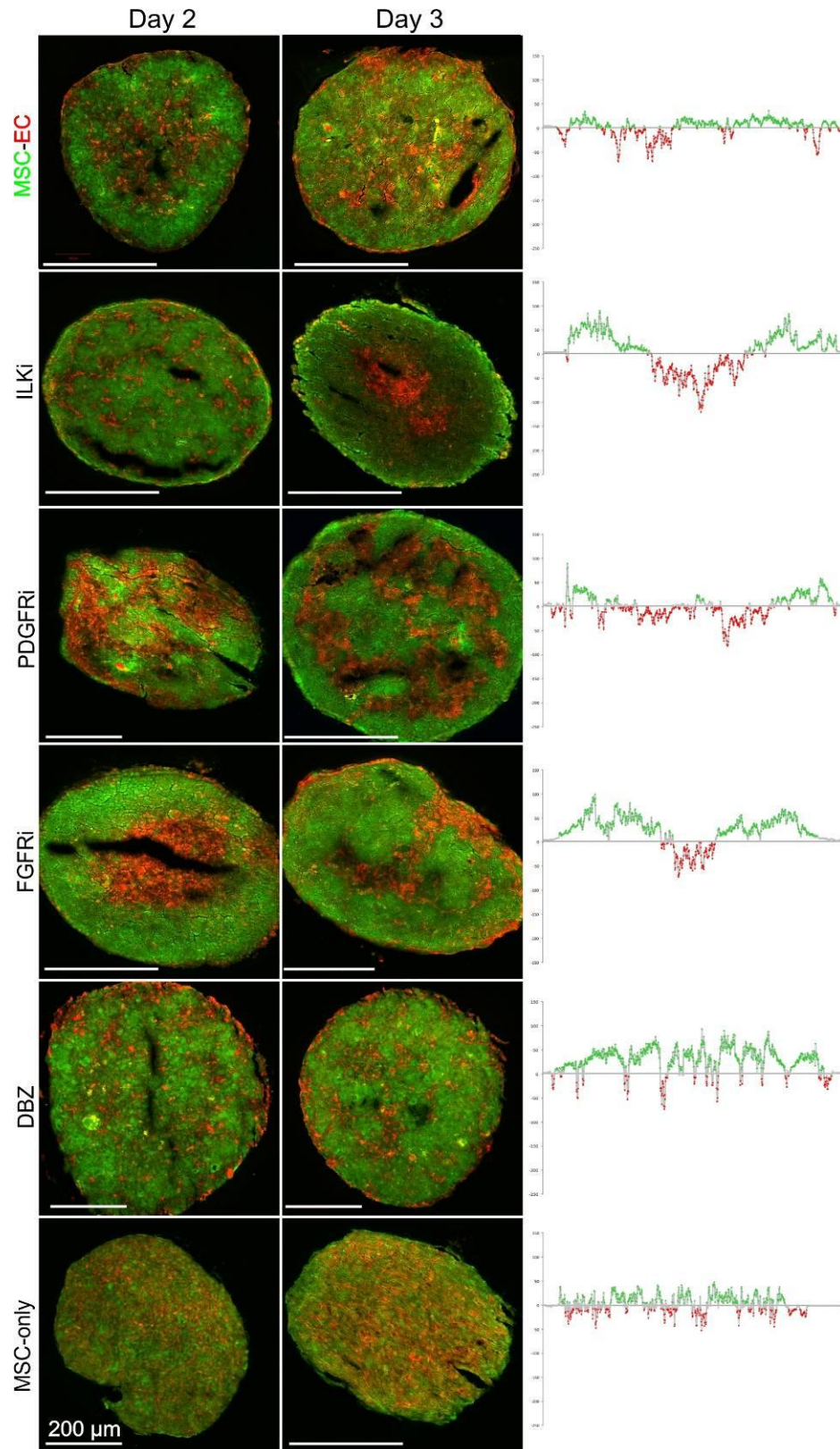
Figure 4.4.22 – Plot profiler analysis of MSC-EC spheroid sections treated with various inhibitors

Plot profiler analysis was performed to analyse the distribution of MSCs and ECs throughout the spheroid sections. The graphs show the distribution of either positive value (green cells) or negative value (red cells) throughout the z-axis of the section. Neutral values relate to no fluorescence caused by either areas outside the spheroid section or tears in the spheroid section. This analysis showed that ILKi and FGFRi treatment resulted in ECs being mainly in the centre of the spheroid. PDGFRi treatment resulted in ECs being more centrally located compared to MSC-EC untreated sections. DBZ treatment resulted in a distribution similar to untreated sections. MSC-only sections showed a random and even distribution of green and red labelled MSCs throughout the sections.

4.4.6 Deferoxamine mesylate treatment on co-culture inhibited spheroids

MSC-EC spheroids with the various inhibitors were also treated with DFM, a known pharmaceutical agent that enhanced blood vessel formation and subsequently bone formation in mice (Ramasamy et al., 2014). The inhibitors ILKi, PDGFRi, DBZ and FGFRi were used as these were found to effect organisation of MSCs and ECs within 3D spheroid culture, unlike EGFRi. Figure 4.4.23 shows whole 3D fluorescent MSC-EC spheroids treated with various inhibitors and DFM. From these whole spheroid images no visual differences due to DFM treatment were detected. These images were then analysed and the spheroid diameter and percentage of green labelled MSCs at the spheroid surface was quantified (Figure 4.4.24). This analysis revealed that PDGFRi+DFM spheroids were significantly smaller compared to PDGFRi only spheroids at day 1. Surface analysis showed that MSC-EC+DFM spheroids had significantly fewer green labelled MSCs at the spheroid surface compared to MSC-EC only at day 3.

The spheroids were then sectioned to observe if internal organisation was affected by the application of DFM. In Figure 4.4.25 these fluorescently labelled spheroid sections can be observed. The EC network, length, width and branching was then calculated from these spheroid sections (Figure 4.4.26). No significant differences in EC network length, width and branching were detected with DFM treatment. However, these results did show that inhibitor treatments resulted in similar organisation patterns previously observed (Section 4.4.5).
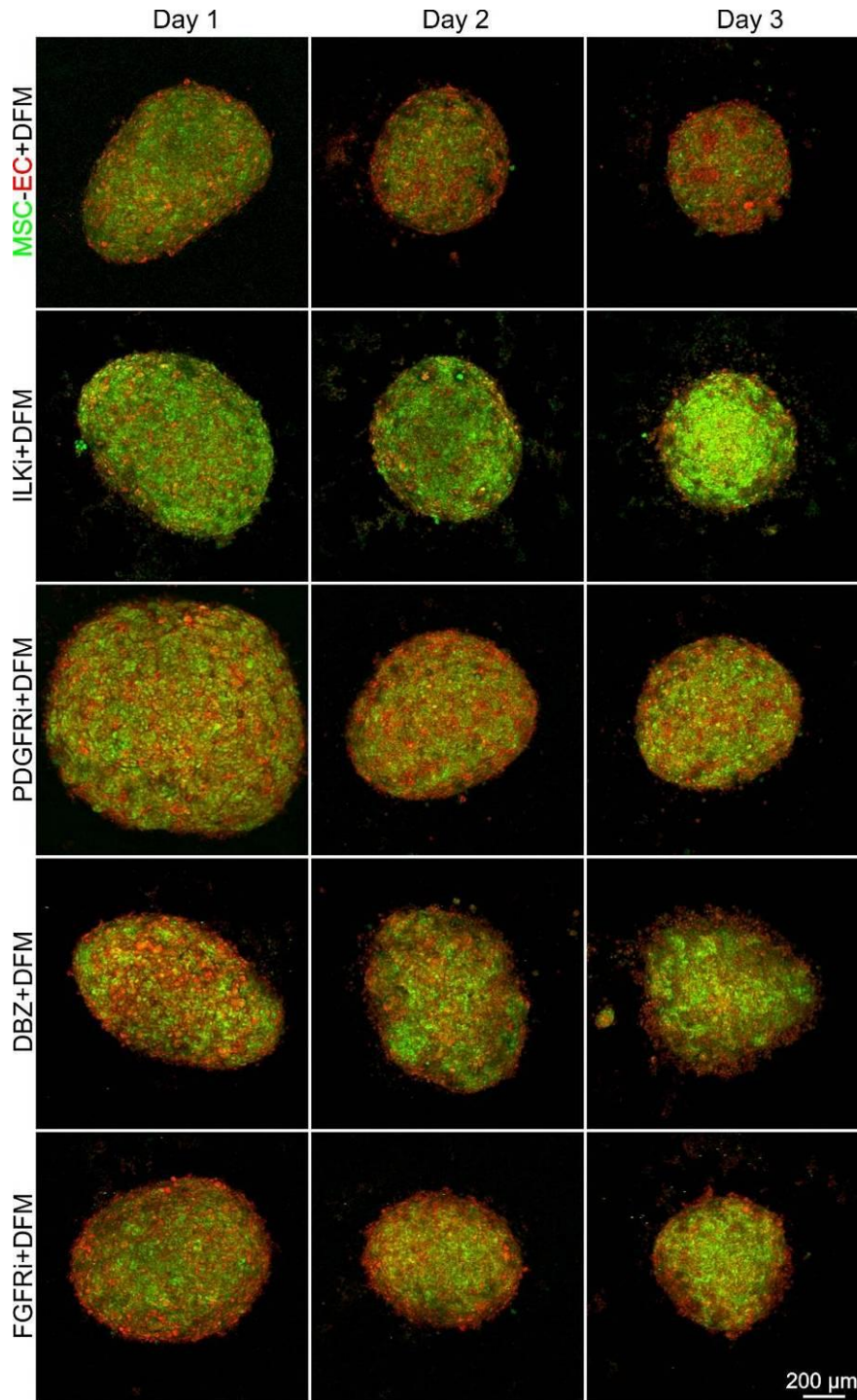
Figure 4.4.23 – 3D fluorescent images of whole MSC-EC spheroids treated with various inhibitors and DFM

MSC-EC spheroids were treated with various inhibitors in combination with DFM. 3D whole spheroid images were taken using a multi-photon confocal microscope. From the 3D whole spheroid images no visual differences occurred due to DFM treatment.
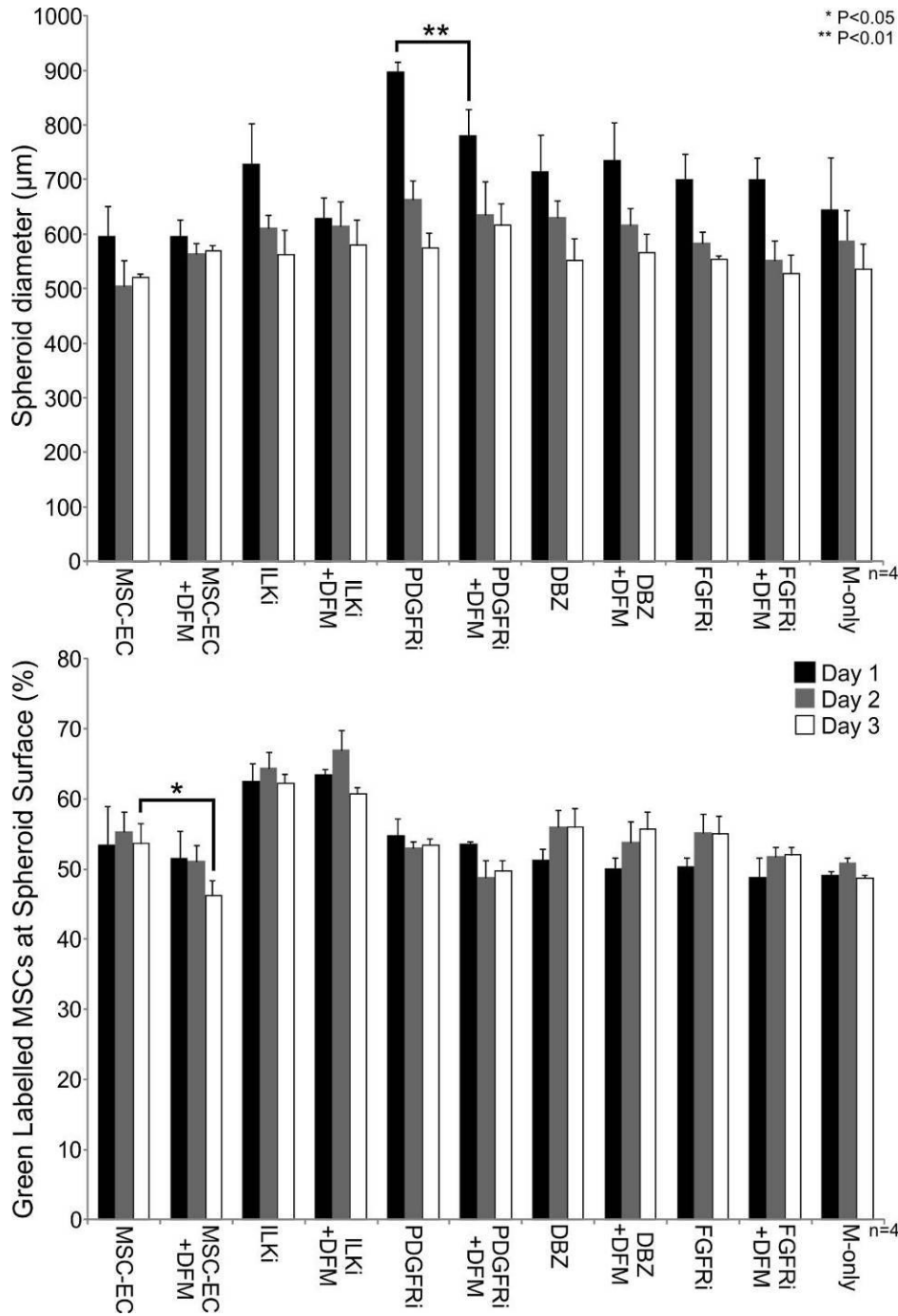
Figure 4.4.24 – Spheroid diameter and surface analysis of MSC-EC spheroids treated with various inhibitors and DFM

The diameter and surface of the spheroids was analysed, MSC-EC spheroids were cultured with various different inhibitors in combination with DFM. MSC-EC PDGFRi spheroids were significantly larger at day 1 compared to MSC-EC PDGFRi+DFM spheroids. DFM treatment also resulted in significantly fewer green labelled MSCs at the spheroid surface compared to MSC-EC untreated spheroids.
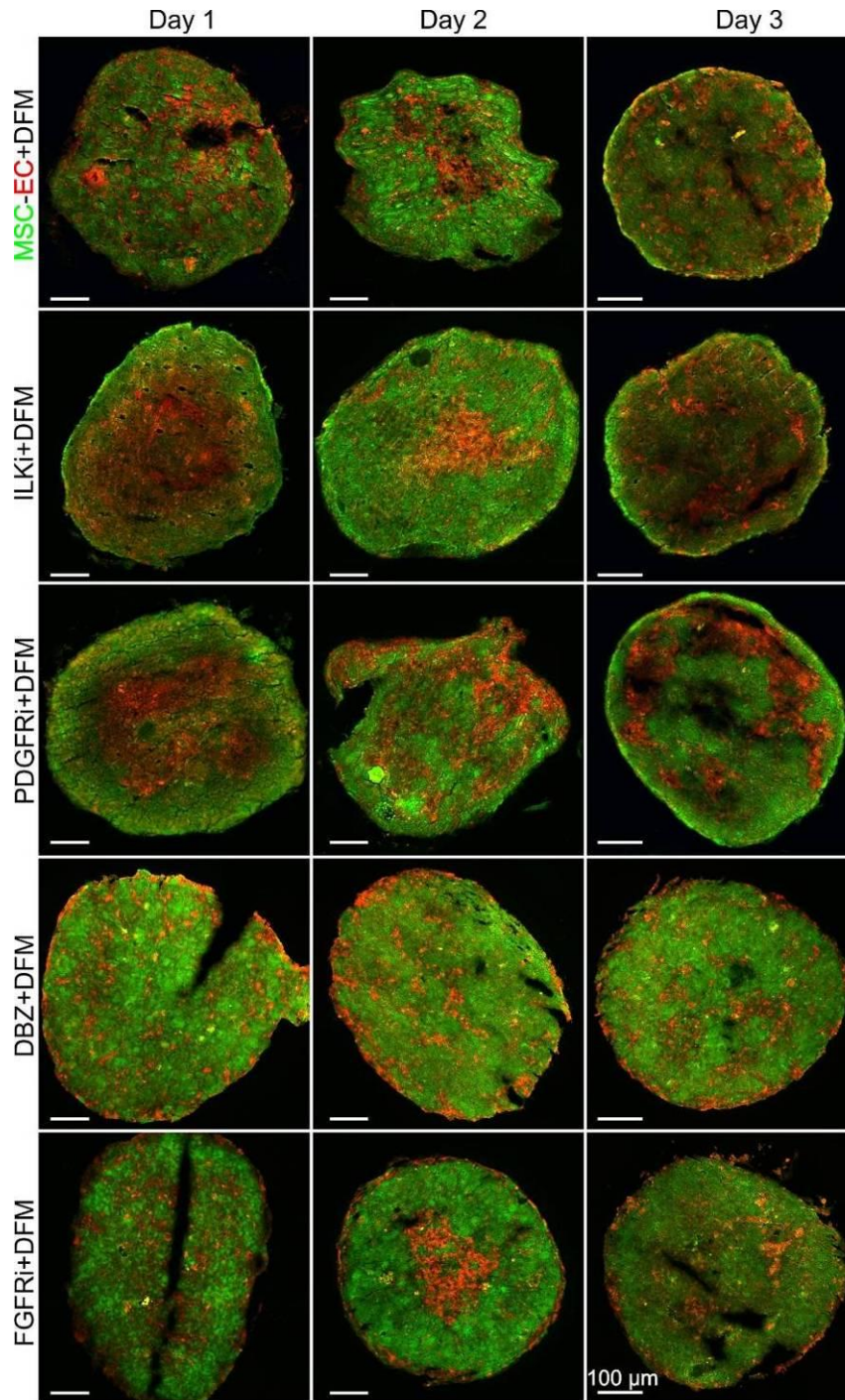
Figure 4.4.25 – Spheroid sections of various fluorescently labelled MSC-EC spheroids treated with inhibitors and DFM

Spheroid sections were taken to look at the internal organisation of green MSCs and red ECs within the co-culture spheroids treated with various inhibitors and DFM. The inhibitor treatments used were ILKi, PDGFRi, DBZ and FGFRi. Internal self-organisation of ECs within these spheroids was detected and differed depending upon inhibitor treatment but did not appear affect by DFM treatment.
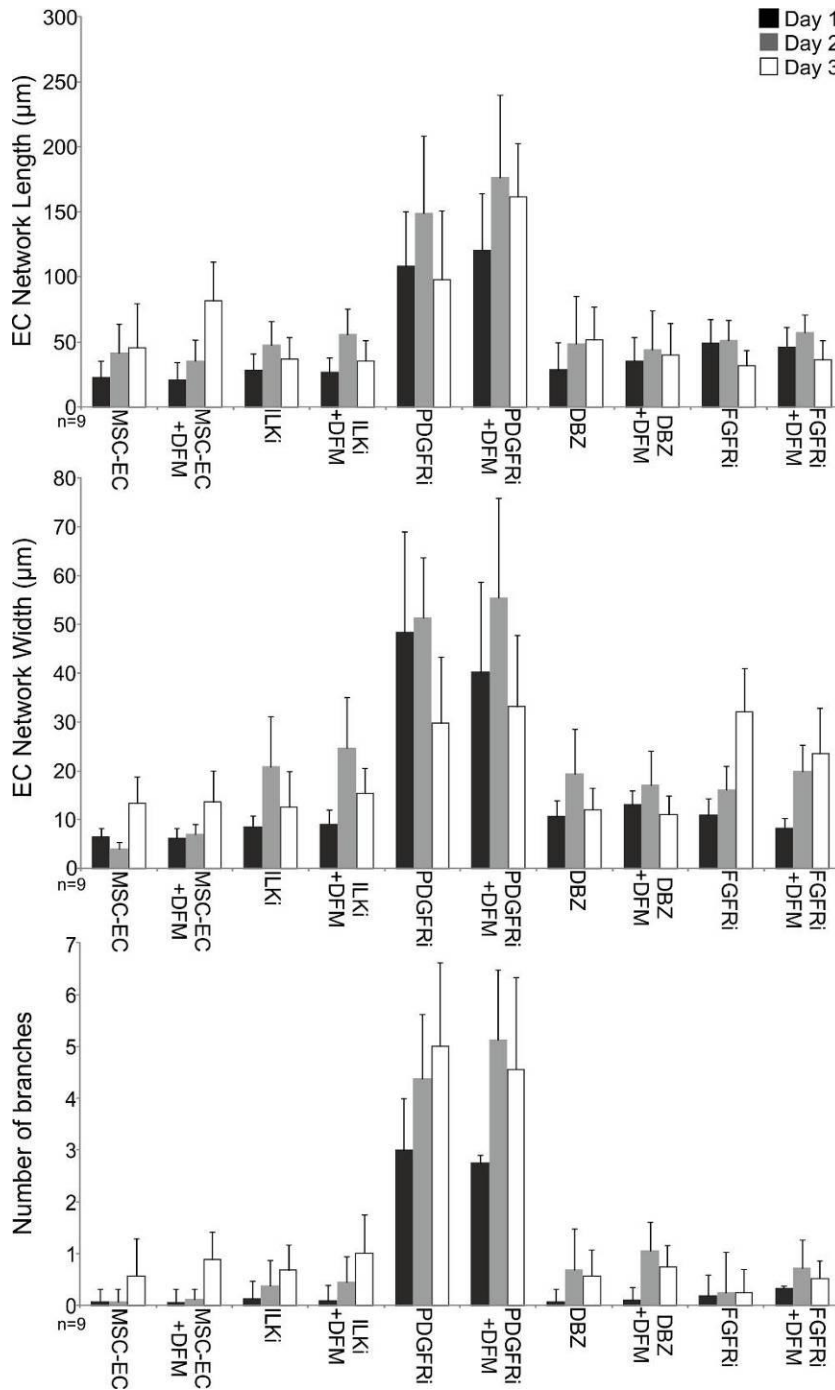
Figure 4.4.26 – EC network length, width and branching in MSC-EC spheroids treated with various inhibitors and DFM

Through manual Image J software analysis, quantification of the EC network length, width and branching was calculated in the various MSC-EC spheroid sections with and without DFM treatment. No significant differences due to the treatment of DFM were detected; however, similar organisation patterns previously observed due to inhibitor treatments were detected.

4.4.7 Pre-treatment of Mesenchymal Stromal cells with ILK inhibitor

To determine whether the organisation pattern observed in MSC-EC spheroids treated with ILKi was affecting primarily MSCs or ECs. MSCs were pre-treated with ILKi before generating pre-treated MSC-EC spheroids, within these spheroids ECs would not have been exposed to ILKi. ILKi was chosen due to effects on the spheroid surface being observed within 24 hours (Section 4.4.5). Fluorescently labelled whole spheroid images can be seen in Figure 4.4.27. Pre-treatment of MSCs with ILKi had a clear effect of spheroid organisation, at day 1 more green labelled MSCs can be seen at the spheroid surface compared to untreated control MSC-EC spheroids. These whole spheroid images were then analysed to calculate spheroid diameter and percentage of green MSCs at the surface (Figure 4.4.28). Spheroid diameter was unaffected by ILKi pre-treatment. However, the percentage of green labelled MSCs at the surface was significantly greater in ILKi pre-treated spheroids compared to untreated control MSC-EC spheroids for all time-points. ILKi treatment of MSCs resulted in significantly more MSCs at the spheroid surface at day 1 compared to untreated control MSC-EC spheroids. However, significantly fewer green labelled MSCs were at the spheroid surface in pre-treated spheroids compared to MSC-EC spheroids treated with ILKi for all time-points.

These various spheroids were then sectioned to determine internal organisation patterns. Figure 4.4.29, ILKi treatment resulted in a thick peripheral layer of green MSCs for all time-points. Untreated control MSC-EC spheroids showed a lattice-like network of ECs by day 3. ILKi pre-treatment resulted in a peripheral layer of green MSCs at day 1; this was not so obvious at days 2 and 3. No lattice-like network was detected in ILKi pre-treated spheroids, unlike untreated control MSC-EC spheroids. This demonstrated that ILKi pre-treatment had an effect on the organisation of ECs within the spheroid, to further examine this, EC networks were analysed to determine length, width and branching (Figure 4.4.30). This analysis showed no significant differences between untreated control MSC-EC spheroids, ILKi pre-treated MSC-EC spheroids and ILKi MSC-EC spheroids in

EC network length of branching. However, EC network width was significantly greater in ILKi treated spheroids compared to control untreated MSC-EC spheroids; this again confirms the results seen in Section 4.4.5.
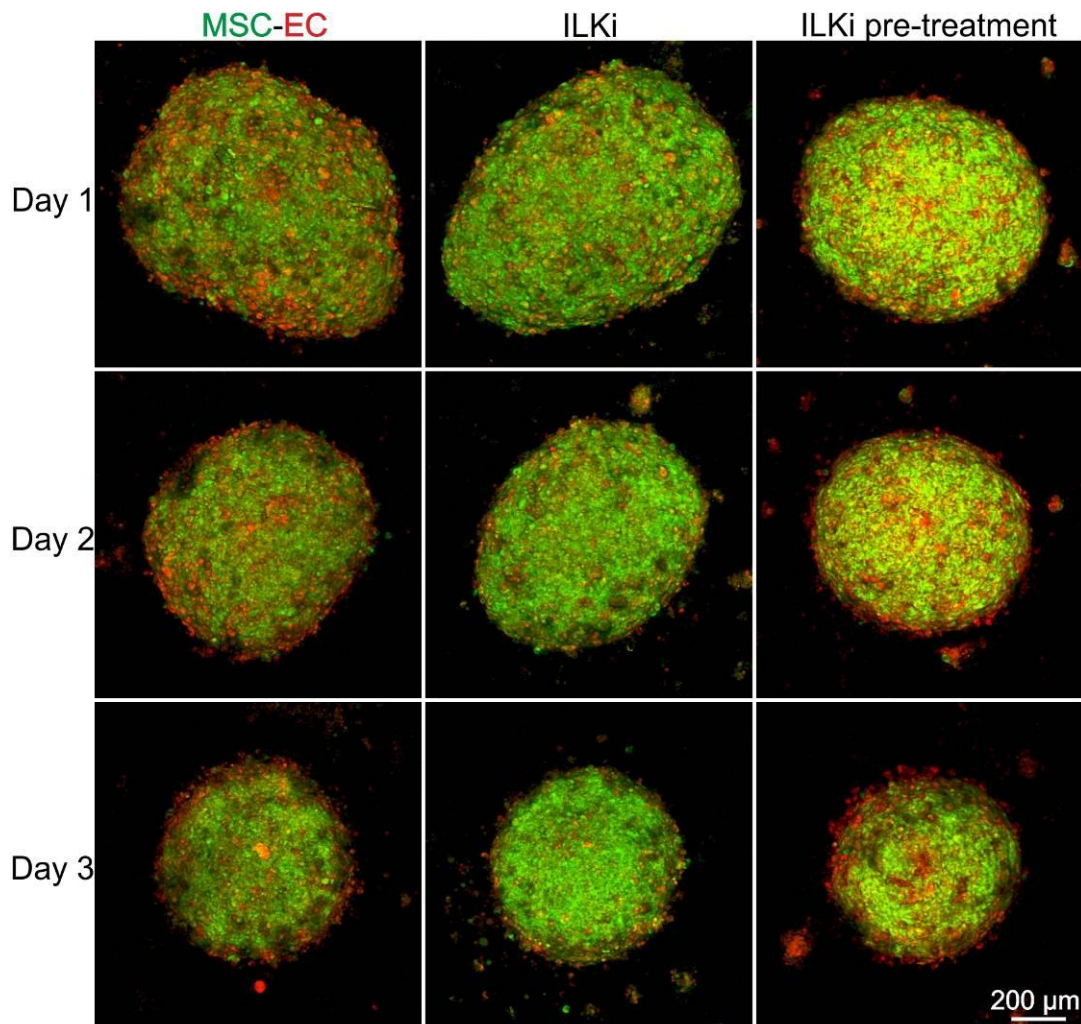
Figure 4.4.27 – Fluorescently labelled 3D whole MSC-EC spheroids pre-treated and treated with ILKi

Fluorescently labelled MSC-EC spheroids were pre-treated and treated with ILKi, MSCs were labelled green and ECs were labelled red. These 3D whole spheroid images were captured using a multi-photon confocal microscope. ILKi pre-treated spheroid images show at day 1 pre-treatment has had a clear effect on spheroid formation, more green labelled MSCs are at the surface compared to MSC-EC untreated.
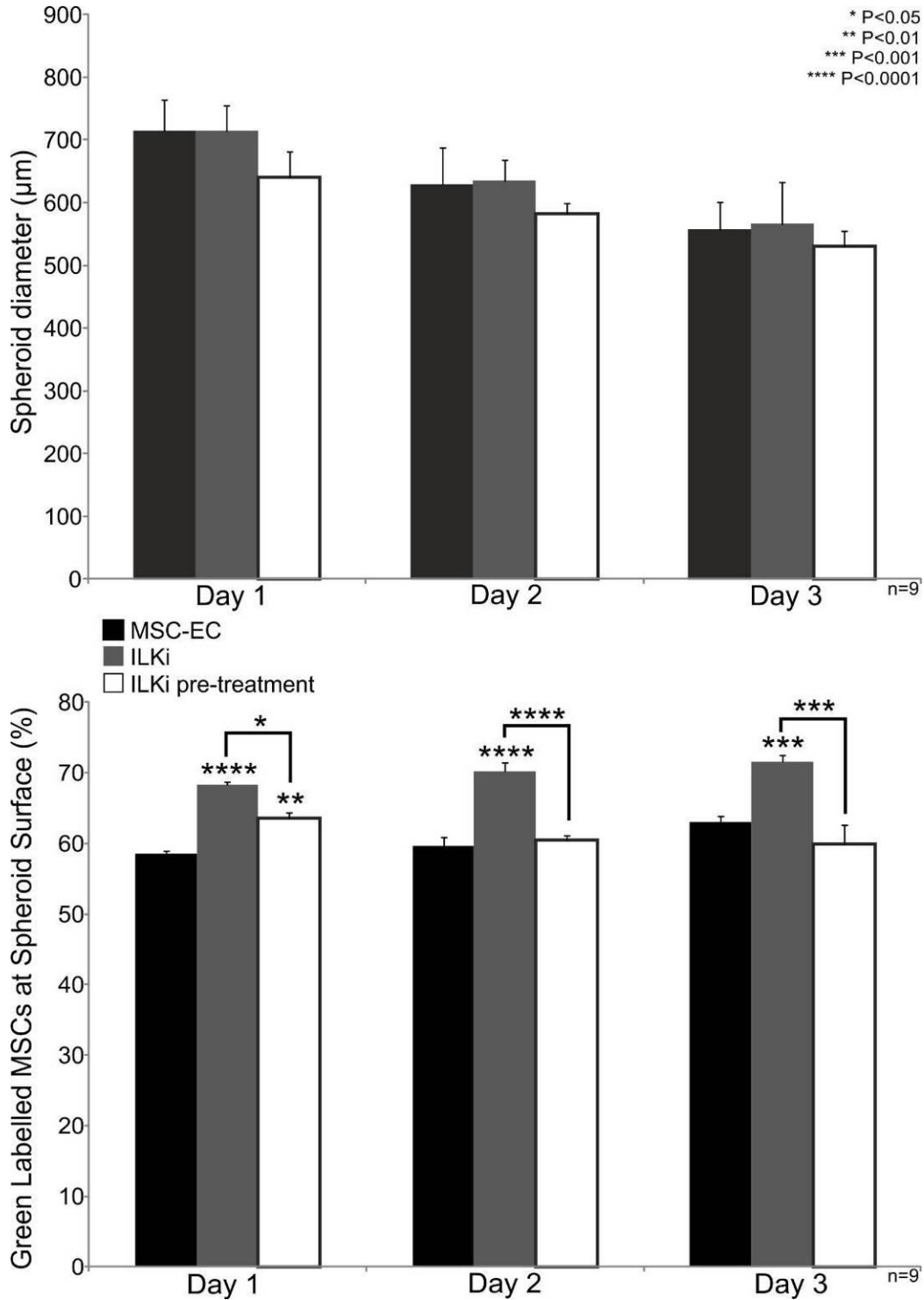
Figure 4.4.28 – Diameter and surface analysis of MSC-EC spheroids with and without ILKi pre-treatment

From the fluorescent 3D whole spheroid images the spheroid diameter and surface was analysed. No significant differences in spheroid diameter were detected depending upon treatment; this result is consistent with those previously

obtained with ILKi treatment (Section 4.4.5). Surface analysis revealed that ILKi treatment of the whole spheroid resulted in significantly more MSCs at the spheroid surface for all time-points compared to untreated control MSC-EC spheroids. ILKi pre-treated spheroids had significantly more MSCs at the spheroid surface compared to untreated control MSC-EC spheroids at day 1. However, pre-treated spheroids had significantly fewer green MSCs at the spheroid surface compared to MSC-EC ILKi treated spheroids for all time-points.
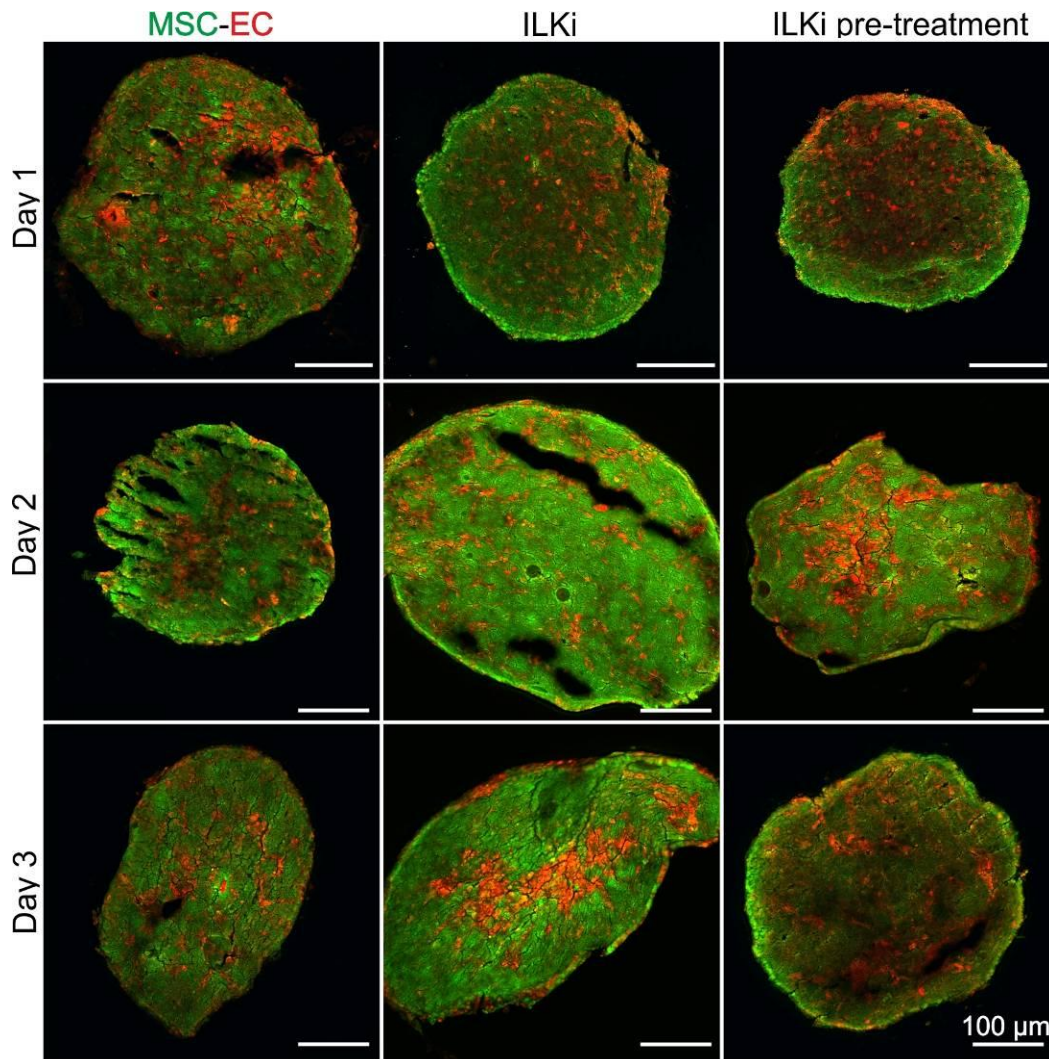
Figure 4.4.29 – Sections of fluorescently labelled MSC-EC spheroids with and without ILKi pre-treatment

Sectioning of the fluorescently labelled MSC-EC spheroids with and without ILKi pre-treatment were performed to observe internal organisation. MSC-EC untreated spheroids showed EC self-organisation into a lattice-like network at day 3. ILKi treated spheroids showed a thick peripheral layer of green MSCs at all time-points. ILKi pre-treatment resulted in a peripheral layer of green MSCs at day 1, however, this is then lost. However, no EC lattice-like organisation was detected.
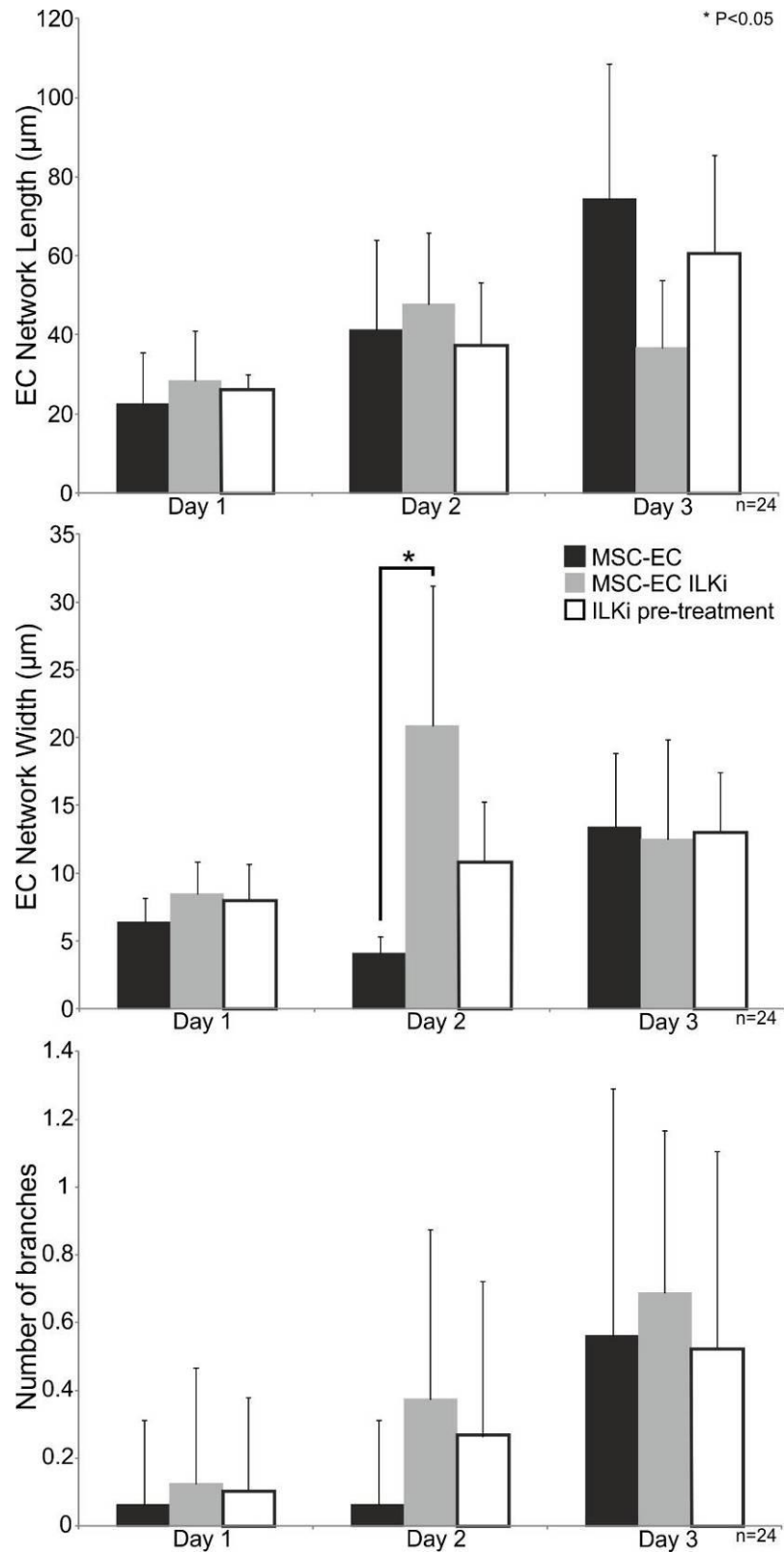
Figure 4.4.30 – EC network length, width and branching analysis of MSC-EC spheroid sections with and without ILKi pre-treatment

EC network analysis was performed using manual Image J software on the MSC-EC spheroid sections to with and without ILKi pre-treatment to quantify width, length and number of branches. No significant differences in EC network length were detected, however, at day 3 MSC-EC untreated and pre-treated spheroids showed greater network length compared to ILKi treated spheroids. A significant increase in EC-network width was detected in ILKi treated spheroids compared to MSC-EC untreated spheroids at day 2. No significant differences in network branching were detected at any time-point.

4.5 Discussion

The multiphoton confocal microscope used had an adjustable laser wavelength, which needed optimisation to ensure accurate use of CellTracker™ green and red for cell tracking. A wide range of different excitation wavelengths were tested, from 700-850 nm and it was found that 780 nm had strong emission for both green and red CellTracker™. Once the optimised wavelength was established, it was important to make sure there was limited colour bleeding; therefore spectral analysis of the emission wavelengths for the two different CellTracker™ colours was performed. This spectral analysis showed there was a small overlap in the emission profile, however, the emission peaks were at approximately 520 nm and 600 nm respectively so colour bleeding would be minimal. To confirm there was minimal bleeding and that region 2 and 3 of the non-descan detector were able to appropriate select between the two different CellTracker™ colours, MSCs and ECs were labelled green and red respectively before being analysed with the multiphoton confocal microscope. The analysis showed the individual labelled cells could easily be detected and separated into the appropriate spectral region with no visible bleeding between the two colours. The use of CellTracker™ labelling to identify two different cell types has been previously performed, however, variation between different equipment can occur (Burch et al., 2005). CellTracker™ labelling of cells has various advantages, for example mixed cell populations can be easily identified and tracked in real-time which would be difficult using end-point immunofluorescence staining.

CellTracker™ labelling was then used to identify two different cell types MSCs and ECs within the 3D co-culturing model. Previous research in this laboratory into co-culture of MSCs and ECs in 3D U-bottomed 96-well plates showed that when the cells were equally mixed (50:50) the EC population formed segregated regions, however different ratios were not tested (Saleh et al., 2011b). Therefore, the effect of MSC:EC ratio on cell spheroid organisation was not determined. Five different ratios were found to all form spheroids within 24 hours; however, the 20:80 spheroids by day 7 had poor structural integrity. This result could be due to

a reduced number of cell-cell adhesion molecules on ECs, co-culture of ECs with MSCs has been shown to reduce EC permeability through increased VE-cadherin and β-catenin expression (Pati et al., 2011). These cell-cell adhesion molecules are essential for cell spheroid formation and subsequent maintenance (Shimazui et al., 2004). An alternative method to monitor spheroid formation and maintenance is through observations into the spheroid diameter during culture. These measurements showed that the spheroid diameter decreased, with the most notable shrinkage occurring between days 1 and 5, however, no significant differences between the various ratios were detected. Previous research has shown that within spheroids diameter was linked with cell viability; specifically for cancer modelling an increased spheroid diameter is seen in conjunction with a successful tumour model (Wen et al., 2013, Ivascu and Kubbies, 2006). However, MSCs are not a cancerous cell line and therefore do not exhibit the same cellular proliferation. Therefore, an increased spheroid diameter for non-cancerous cell lines cannot be associated with cell viability. Indeed, a decrease in MSC-only spheroid diameter after 7 days in culture has been previously reported (Yamaguchi et al., 2014).

Fluorescently labelled spheroids were then sectioned to examine internal organisation, it was found at day 1 for all ratios ECs were predominantly at the periphery of the spheroid. This result is most likely due to the differential adhesion hypothesis, by which a heterogeneous population of cells will form into isotypic groups (Foty and Steinberg, 2005). This result also demonstrates that ECs probably have lower homotypic cell-cell mechanism compared to MSCs, emphasised by the lack of structural integrity in 20:80 high EC content spheroids. By day 3, differences depending upon ratio were detected, 50:50 spheroids showed EC self-organisation into a lattice-like network evenly distributed throughout the spheroid. The mechanisms behind this self-organisation pattern are currently unclear. However, this could be used as a method to model angiogenesis within a stromal environment including bone marrow. From this point on 3D co-culture of MSC-EC spheroids was performed using the 50:50 ratio as this gave the greatest evidence of the unique self-organisation pattern.

Previous research into 3D tumour models has demonstrated that real-time quantitative analysis for pharmaceutical analysis and validation is essential (Vinci et al., 2012). Therefore, time-lapse analysis was performed on MSC-EC spheroids to further investigate the spheroid formation process which evolved into 4D image analysis using a multiphoton confocal microscope. This analysis technique combined with CellTracker™ labelled of MSCs and ECs allowed the individual cells, type and location to be identified in 3D during the spheroid formation process. To act as a control MSC-only spheroids were analysed, these contained a 50-50 mixture of MSCs labelled green or red. This was done to determine whether CellTracker™ labelling gave false positive results in spheroid organisation. These results showed that MSC-EC spheroid formation was a dynamic process. The percentage of red labelled ECs at the spheroid surface increased by approximately 4% during the analysis period in three different biological donors. This confirmed previous observed internal organisation results of a predominantly EC peripheral layer at day 1 in spheroid sections. This initial EC migration is most likely due to the differential adhesion hypothesis (Steinberg, 1975). In contrast MSC-only formation analysis demonstrated that limited cell migration occurred within a homogenous cell type spheroid, for these spheroids the percentage change at the spheroid surface did not exceed 2% in three different biological donors. This small change at the spheroid surface might be due to the CellTracker™ green being more prone to photo bleaching than CellTracker™ red (De Los Santos et al., 2015). From the 4D imaging it was possible to calculate the spheroid volume throughout the formation process, both MSC-EC and MSC-only spheroids had a similar starting volume which decreased slightly towards the end of the formation process, this shows that the cell suspension was aggregating together.

To determine if the EC network within MSC-EC spheroids was due to MSCs directing ECs or due to a capacity ECs naturally posses, MSCs were replaced with HDFs. ECs such as HUVECs have been described as spontaneously forming a network in 2D on Matrigel, this network has structural and organisational similarities to those observed within MSC-EC spheroid sections

(Mezentsev et al., 2005, Chiew et al., 2015). HDFs were chosen as they have been described as similar to adipose derived MSCs, they express the same cell surface markers as MSCs (CD29, CD44, CD90 and CD105) and have been claimed to demonstrate a tri-differentiation potential (Blasi et al., 2011). HDF-EC spheroids were compared directly to MSC-EC spheroids, whole spheroid images showed these cells were capable of forming spheroids within 24 hours and visually they look comparable. Further analysis into diameter and the spheroid surface revealed that HDF-EC spheroids were significantly smaller than MSC-EC spheroids at days 5 and 7. HDF-EC spheroids also had significantly more green HDFs at the spheroid surface compared to green labelled MSCs at the spheroid surface at days 3 and 7. Therefore, subtle differences between the two spheroid types were detected early on using non-destructive techniques. Whole spheroids were then sectioned to examine the internal organisation patterns, MSC-EC sections showed an EC network throughout the spheroid at days 3 and 5. In HDF-EC spheroid sections no EC network was detected, ECs appeared to form a layer predominantly around the periphery of the spheroid at day 1 and 3. Further analysis of the EC network showed at days 3 and 5, EC network length and branching were significantly greater in MSC-EC sections compared to HDF-EC sections. These results establish that there is a unique relationship between MSCs and ECs in 3D cell spheroid culture. Specifically a 50-50 mixture of MSCs and ECs in direct co-culture spheroids results in an EC network described as a capillary like structure (Saleh et al., 2011b). A similar structural observation was made when a small percentage (8%) of ECs were co-cultured with MSCs in 3D spheroids. However, these experiments were performed using much larger spheroids (150,000 cells per spheroid) ultimately resulting in a similar total number of ECs per spheroid as those described by Saleh in 2011 (Rivron et al., 2012). Primitive vascular networks were also observed within a liver model containing MSCs, iPS cells and HUVECs tri-cultured spheroids on matrigel (Takebe et al., 2013). Unlike 2D culture, ECs do not possess an innate ability to spontaneously form a network within a 3D structure. Therefore, the next stage

was to evaluate possible MSC induced mechanisms responsible for this unique self-organisation pattern.

To determine possible signalling pathways responsible for the EC self-organisation pattern a variety of different inhibitor treatments were added to MSC-EC spheroids. Most of the signalling pathways had been linked as important for angiogenesis, MSC or EC migration. Unfortunately using these techniques, both MSCs and ECs were exposed to these inhibitor treatments; therefore, it is impossible to determine if they are acting in MSCs, ECs or both. Combinations of inhibitor treatments would also have enhanced the study, for example combining all inhibitor treatments could have demonstrated if a particular signalling pathway was more potent. Whole fluorescent spheroid images showed that inhibitor treatments had clear effects of MSC-EC spheroid formation and organisation. ILKi treated spheroids appeared greener compared to untreated control spheroids and DBZ treatment appeared to have the opposite effect, spheroids appeared redder. PDGFRi treatment appeared to make spheroids larger compared to control untreated MSC-EC spheroids. Spheroid diameter calculations showed that PDGFRi and FGFRi treated spheroids were significantly larger than untreated control MSC-EC spheroids. Strikingly a wide variety of differences were detected in the percentage of green MSCs at the spheroid surface. ILKi treatment resulted in significantly more MSCs at the spheroid surface; this result could be attributed to ILKi treatment having a greater effect on MSC cell-cell adhesion molecules, resulting in MSCs becoming less adhesive compared to ECs. Indeed, ILK transfected MSCs were shown to have a higher adhesion rate within a cardiac matrix compared to untreated control MSCs (Song et al., 2009). The differential adhesion hypothesis would then cause MSCs to envelope ECs causing an increase in MSCs at the spheroid surface (Lee et al., 2011, Gess et al., 2008). PDGFRi treatment resulted in significantly fewer MSCs at the spheroid surface. PDGF is known to play an important role in cell migration, specifically decreased PDGF expression has been seen in conjunction with reduced angiogenesis within tumours (Heldin and Westmark, 1999, Ho et al., 2013). Therefore, PDGFRi treatment might have prevented ECs from migrating

into the spheroid, resulting in them becoming located predominantly at the spheroid surface. DBZ treatment resulting in Notch inhibition resulted in significantly fewer MSCs at the spheroid surface. Notch signalling has been identified as important in both MSC and EC migration. Inhibition of Notch signalling *in vivo* has been shown to result in the loss of directional migration of ECs, conversely Notch inhibition in MSCs has been shown to result in enhanced migration (Bentley et al., 2014, Xie et al., 2013). These studies are further supported as increased Notch expression within ECs has been shown to enhance cell migration (Howard et al., 2013). Therefore, DBZ treated and subsequent Notch inhibition will have affected EC migration, most likely preventing them migrating from the spheroid periphery. FGFRi treatment resulted in significantly fewer MSCs at the spheroid surface. FGF is a diverse signalling pathway that has numerous effects on both MSCs and ECs. Specifically EC migration has been shown to be effected specifically by FGF, FGF is known to stimulate angiogenesis and FGF application has been shown to enhance EC migration (Kim et al., 2012, Hatanaka et al., 2012). Therefore, FGFRi treatment could hinder EC migration, resulting in ECs becoming immovable at the spheroid surface.

Internal organisation of MSCs and ECs within the spheroids was visualised through spheroid sections. ILKi inhibition resulted in a dense layer of peripheral MSCs, this result compliments those observed using non-destructive spheroid surface analysis. Within the core of the spheroid ECs were evenly distributed, and an EC network was not observed, this result could be linked to previous observations of reduced EC migration through ILKi treatment *in vivo* and *in vitro* (Lu et al., 2013, Chen et al., 2007). PDGFRi treatment resulted in a lattice-like EC network; however, it was much thicker and does not appear evenly distributed throughout the spheroid. Specifically PDGFR has been shown to be activated in response to chemotaxis (Popova et al., 2004). Therefore, loss or reduced chemotaxis within ECs could result in uncoordinated cell migration, ultimately preventing ECs being evenly distributed throughout the spheroid. Additionally PDGF has been shown to play an important role in angiogenesis, specifically in

the morphology of blood vessels (Dong et al., 2014, Robinson et al., 2008). Therefore, loss of PDGF could have resulted in the thicker EC network observed. EGFRi treatment appeared to have no effect on MSC-EC internal organisation. This result was expected as EGF has been shown to have no effect on MSC migration and only affect EC migration in combination with VEGF and FGF (Ponte et al., 2007, Maretzky et al., 2011). DBZ and FGFRi treatment appeared to completely prevent an EC lattice-like network, both these treatments are known to hinder angiogenesis (Fons et al., 2015, Kerr et al., 2015). Therefore, EC migration and organisation were hindered preventing network development. MSC-only spheroid sections show a random distribution of both green and red labelled MSCs. Demonstrating random self-organisation did not occur and CellTracker™ labelled had no effect on cellular organisation. From these spheroid sections the EC network length, width and branching were calculated. These calculations mainly showed that PDGFRi treatment had significant effects on EC length, width and branching compared to untreated control MSC-EC sections. PDGF has been shown to play an important part in stabilising the vascular endothelium (Roskoski, 2007). *In vivo* studies have found PDGF inhibition resulted in significantly shorter neovessel lifespan, therefore, these thicker EC networks could be attributed to a loss of a vessel formation checkpoint (Yao et al., 2014). Plot profiling was used to try and visualise the distribution of either MSCs or ECs within the spheroid sections. This technique was able to demonstrate that inhibitor treatments did effect cellular distribution. ILKi and FGFRi showed few red labelled ECs at the section periphery and the majority of ECs were at the core of the spheroid. MSC-only spheroid sections confirmed random cell distribution in the homogenous cell type spheroid section. Unfortunately, this technique could not be used for statistical evaluation.

DFM treatment was performed in addition to MSC-EC inhibitor treatments as this pharmacological agent had been shown to enhance angiogenesis in mouse bones exposed to Notch inhibition (Ramasamy et al., 2014). Therefore, it was hypothesised that DFM treatment might recover angiogenesis hindrance caused by inhibitor treatments. However, very few differences between untreated and

DFM treated spheroids were detected. DFM exposure did result in significantly smaller spheroids in conjunction with PDGFRi treatment and significantly fewer MSCs were at the spheroid surface in MSC-EC+DFM compared to untreated control MSC-EC spheroids at day 3. DFM treatment on human MSCs has been shown to enhance the expression of angiogenic factors such as VEGF and TGF-β, stimulating known alternative PDGF pathways (Potier et al., 2008). Additional studies using rat trachea in conjunction with DFM exposure showed increased gene expression of PDGF and TGF-β (Dai and Churg, 2001). Therefore, DFM treatment might have negated the effects of PDGFRi treatment. *In vitro* studies using human aortic ECs in conjunction with DFM exposure showed enhanced tube formation, cell proliferation and migration (Ikeda et al., 2011). Thus DFM treatment could have stimulated EC proliferation; subsequently resulting in the spheroid surface appearing redder in MSC-EC+DFM compared to untreated control MSC-EC spheroids. Spheroid section analysis of internal organisation patterns showed no visual differences due to DFM treatment, this was confirmed through EC network length, width and branching calculations. DFM was used at a concentration of 100 µM as this was below the cytotoxicity concentration (Chung et al., 2013). However, in Ramasamy et al. study a much higher concentration was injected into mice, therefore, the concentration for 3D spheroids might have been too low (Ramasamy et al., 2014). *In vitro* work is also performed in a closed system; therefore, DFM might have enhanced an alternative signalling pathway found *in vivo*.

To determine whether ILKi treatment primarily affected MSCs rather than ECs, MSCs were pre-treated with ILKi for 96-hours before being used in co-culture spheroids. To further confirm the results observed ILKi pre-treatment could be performed on ECs only. These ILKi pre-treated spheroids were then analysed compared to untreated control and ILKi control spheroids. Whole spheroid images and surface analysis showed that overall ILKi treatment does most likely principally affect MSCs. Significantly more fluorescent MSCs were at the spheroid surface of both ILKi pre-treated and ILKi control spheroids compared to untreated control spheroids. However, significantly fewer fluorescent MSCs were

at the spheroid surface of ILKi pre-treated spheroids compared to ILKi control spheroids. Indicating that pre-treatment affected the initial spheroid formation; however, the potency of the pre-treatment was transient. This result was expected as ILKi exposure was not continued during ILKi pre-treated spheroid formation and culture. Indeed, alternative ILKi treatments have shown to have a transient effect on tumour physiology (Kalra et al., 2015).

Overall the results within this chapter demonstrate the important relationship between MSCs and ECs within a 3D environment. Uniquely using CellTracker™ green and red labelling in combination with 3D and 4D imaging techniques resulted in a tractable *in vitro* 3D model being developed. Quantification of spheroid diameter and spheroid surface analysis were able to indirectly quantify tissue organisation within this complex 3D structure non-destructively. Additional spheroid sections were able to observe internal cellular organisation with greater specificity. These techniques showed that MSCs are able to direct EC self-organisation, resulting in a 3D lattice-like EC network that was evenly distributed throughout the spheroid. This EC network has been previously observed within similar studies and has been described as a primitive vascular-like network with links to angiogenesis. However, the underlying mechanism of this 3D EC network and a direct link to angiogenesis are currently undefined. Within 2D *in vitro* culture a similar network of ECs has been frequently used as an angiogenesis assay (Mezentsev et al., 2005). However, the use of a 3D *in vitro* culture system is able to more closely represent the *in vivo* environment compared to 2D. Therefore, a wide variety of different pharmacological agents were added to MSC-EC spheroids to determine the novelty of 3D MSC-EC spheroids as an angiogenesis model. It was found that 3D EC network organisation was affected by the known angiogenesis signalling pathways FGF, PDGF and Notch, however, currently the evidence shown is not definitive. Equally treatment with EGFRi that has no direct links with angiogenesis was found to have no affect on the EC network, further confirming the durability of this model. However, to fully confirm these effects inhibition or significant reduction of specific downstream markers are required. The next chapter will further evaluate the concept of using MSCs

and ECs in 3D spheroid culture as an *in vitro* tractable model, specifically for human osteochondral tissue.

Chapter 5

Chapter 5 : Pre-differentiation of MSCs and ECs - A 3D *in vitro* Osteochondral Model

5.1 Introduction

Many skeletal elements within the human body are primarily constructed of bone tissue with cartilage tissue on articulating surfaces. Consequently, combining these two tissues has often been the aim for the treatment of diseases such as osteoarthritis. Both natural and synthetic osteochondral plugs have been developed and used to successfully treat osteoarthritis. Autologous osteochondral plugs taken from non-load bearing regions of joints have been used to successfully treat patients suffering from severe arthritis (Berti et al., 2013). The combination of MSCs and triphasic scaffolds have also been used to artificially create osteochondral plugs; these were then used to successfully treat chronic defects within an ovine model (Marquass et al., 2010).

Another area of interest regarding bone formation is a process known as endochondral ossification. This is important for long bone development in the embryo (Chan et al., 2009). The process is not fully understood in humans due to the ethical controversy regarding the study of human foetal development (Klimanskaya, 2013). However, from the use of other mammalian models it is believed that primitive mesenchymal cells condense to form cartilage tissue; this tissue is then invaded by blood vessels triggering the cartilage tissue to differentiate into bone tissue (Kronenberg, 2003, Maes et al., 2002). During adult bone healing a highly similar process takes place; therefore, fully understanding endochondral ossification could also have significant impact in understanding bone healing (Sisask et al., 2013, Tannous et al., 2013).

The skeletal differentiation potential of MSCs has made them an attractive cell type in the field of tissue engineering and regenerative medicine of bone tissue. MSCs have been combined with growth factors and scaffolds to enhance their skeletal regenerative capacity (Tamama et al., 2010, Levorson et al., 2013). These combinations have been successful *in vitro*, however therapeutic translation has been poor, currently no MSC-based therapy has received FDA approval (Mendicino et al., 2014). This limitation is often associated with MSCs being a heterogeneous cell population that lacks a specific cell surface marker (Keating, 2012). However, the ability of MSCs to differentiate into both an osteogenic and chondrogenic lineage makes them a unique cell source for bone tissue modelling. Therefore, the use of MSCs as a model cell type to study skeletal diseases and therapies has strong potential

Recent studies have begun to combine both the osteogenic and chondrogenic potential of MSCs to create biphasic osteochondral tissues. However, one of the main challenges is the effective differentiation of MSCs in both an osteogenic and chondrogenic lineage is culture medium. Traditionally two separate medium formulations are required. Therefore, the concept of pre-differentiation of MSCs has been previously used to prime MSCs towards a lineage of choice. MSCs have been pre-differentiated for chondrogenic and osteogenic applications (Babur et al., 2015, Grayson et al., 2010, Genovese et al., 2009). Therefore, using pre-differentiated osteogenic and chondrogenic MSCs in conjunction with a supportive osteochondral medium could enhance this developing area of research (Guo et al., 2009).

Additionally osteochondral research has overlooked ECs. Within the native bone environment, ECs play an important role in tissue homeostasis and repair following injury. Specifically a lack of blood vessels or impair blood vessel formation within bone is seen in conjunction with degenerative diseases such as osteoporosis, osteoarthritis and non-union fracture healing (Prasad et al., 2014, Findlay, 2007, Dickson et al., 1994). ECs and blood vessels provide key regulatory cues that direct tissue function, indeed many factors have been found

that are angiogenesis stimulating and important in bone development and repair. These include PDGF, FGF, VEGF, TGF-β and BMPs (Stegen et al., 2015). Using cell spheroids provides a 3D novel approach to *in vitro* recreation of osteochondral tissue in a scaffold-free manner. This tractable system can be easily manipulated to look at a wide range of cell types in various combinations with the addition of pharmacological agents to influence key regulatory cues.

5.2 Aims

The general aims of the work presented in this chapter are to investigate the use of the novel 3D co-culture system described previously in combination with pre-differentiated MSCs and ECs as an osteochondral bone model.

More specifically the objectives are to:

- Determine the pre-differentiation time required for osteogenic and chondrogenic separation of MSCs.
- Use pre-differentiation osteogenic and chondrogenic MSCs in 3D co-culture and establish a 3D co-culture model.
- Use fluorescent labelling techniques to track three different cell types within 3D spheroid culture.
- Create various osteochondral spheroid combinations using osteogenic and chondrogenic MSCs with ECs.
- Determine possible mechanisms involved in osteochondral organisation.

5.3 Methods

5.3.1 Cell Culture Methods

5.3.1.1 Chondrogenic Differentiation of human MSCs

Chondrogenic differentiation of MSCs was induced by culturing the cells in chondrogenic induction medium. Chondrogenic induction medium was created by the addition of 50 µg/ml L-Ascorbic acid, 100 nM dexamethasone, 40 µg/ml L-proline (Sigma-Aldrich, UK, Cat no. P5607), 1% ITS+ Universal culture supplement premix (VWR International, Cat no. 47743) and 10 ng/ml TGF-β1 (PeproTech, Cat no. 100-21) to DMEM plus P/S. The culture medium was replaced twice a week for up to 21 days.

5.3.1.2 Pre-differentiation of MSCs in either osteogenic or chondrogenic culture medium

To determine the period of time required for MSCs to become differentiated enough for them to maintain either osteogenic or chondrogenic phenotype within osteochondral media. MSCs were pre-differentiated for either 7 or 14 days in osteogenic or chondrogenic differentiation medium before being placed into osteochondral differentiation medium (Section 5.3.1.3).

5.3.1.3 Osteochondral Differentiation of human MSCs

Osteochondral medium was used to support either an osteogenic or chondrogenic pre-differentiated MSCs. Osteochondral media contained DMEM, 5% FBS, P/S with the addition of 50 µg/ml L-Ascorbic acid, 5mM β-glycerophophate, 100 mM dexamethasone, 40 µg/ml L-proline and 1% ITS+ Universal culture supplement premix.

5.3.2 Formation of 3D osteochondral spheroids

5.3.2.1 3D osteochondral + endothelial cell medium

3D osteochondral medium contained 50% DMEM, 50% endothelial cell medium, 10% FBS, P/S, 0.25% (w/v) methyl cellulose with the addition of 50 µg/ml L-Ascorbic acid, 5mM β-glycerophosphate, 100 mM dexamethasone, 40 µg/ml L-proline and1% ITS+ Universal culture supplement premix.

5.3.2.2 3D spheroid formation of various osteochondral spheroids

MSCs were pre-differentiated with osteogenic or chondrogenic induction medium (Section 3.3.3 and 5.3.1.1) for 7 or 14 days before being used to create 3D spheroids. A schematic representation of this method can be seen in Figure 5.3.1. Osteogenic MSCs were labelled with CellTracker™ red, chondrogenic MSCs were labelled with CellTracker™ green and ECs were labelled with CellTracker™ blue. These three different cell types were then pooled in various combinations to make osteochondral spheroids. The cell spheroids were created by the same method described in Section 2.1.7, all spheroids contained a total of 30,000 cells. Cells were labelled using CellTracker™ using the method described in Section 2.2.1.

5.3.2.3 3D Osteo + Chondro spheroids

MSCs were pre-differentiated in osteogenic or chondrogenic induction medium for 7 or 14 days before being used to create individual 3D spheroids with a total of 15,000 cells per spheroid, using the method described in Section 2.1.7. A schematic representation of this method can be seen in Figure 5.3.2. These individual osteogenic or chondrogenic cell suspensions were left for 24 hours from initial seeding to form spheroids. After this incubation period the spheroids were then transferred into the same well to allow for combination of the two separate spheroids. 3D osteo+chondro spheroids totalling 30,000 cells were culture in the 3D osteochondral medium described in Section 5.3.2.1.
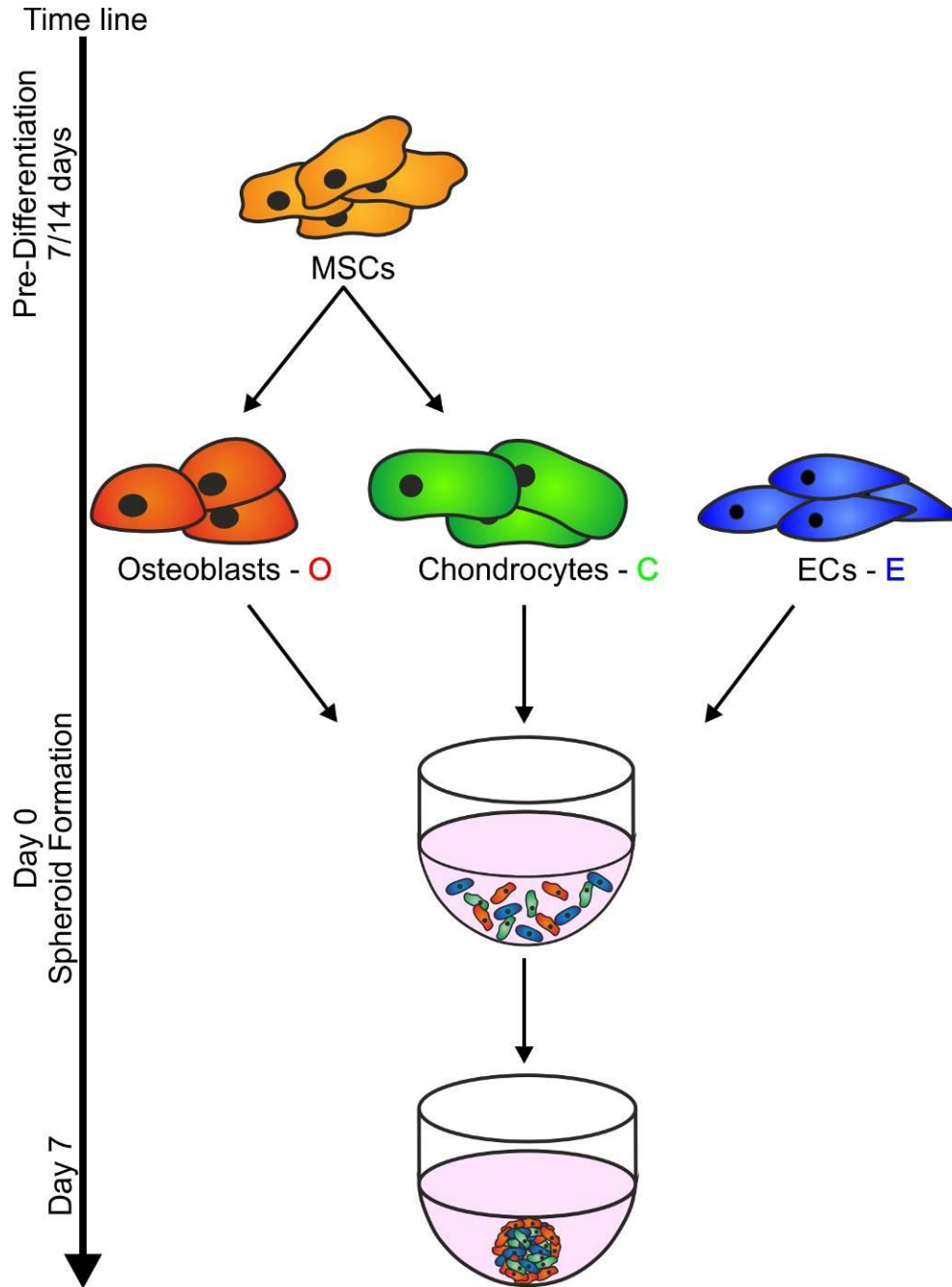
Figure 5.3.1 - Schematic representation of the procedure to produce an osteochondral spheroid

MSCs were pre-differentiated for 7 or 14 days before being consider either osteogenic or chondrogenic. Osteogenic MSCs were labelled with CellTracker™ red, chondrogenic MSCs were labelled with CellTracker™ green and ECs were labelled with CellTracker™ blue. These three different cell types were then pooled in various combinations to create osteochondral spheroids.
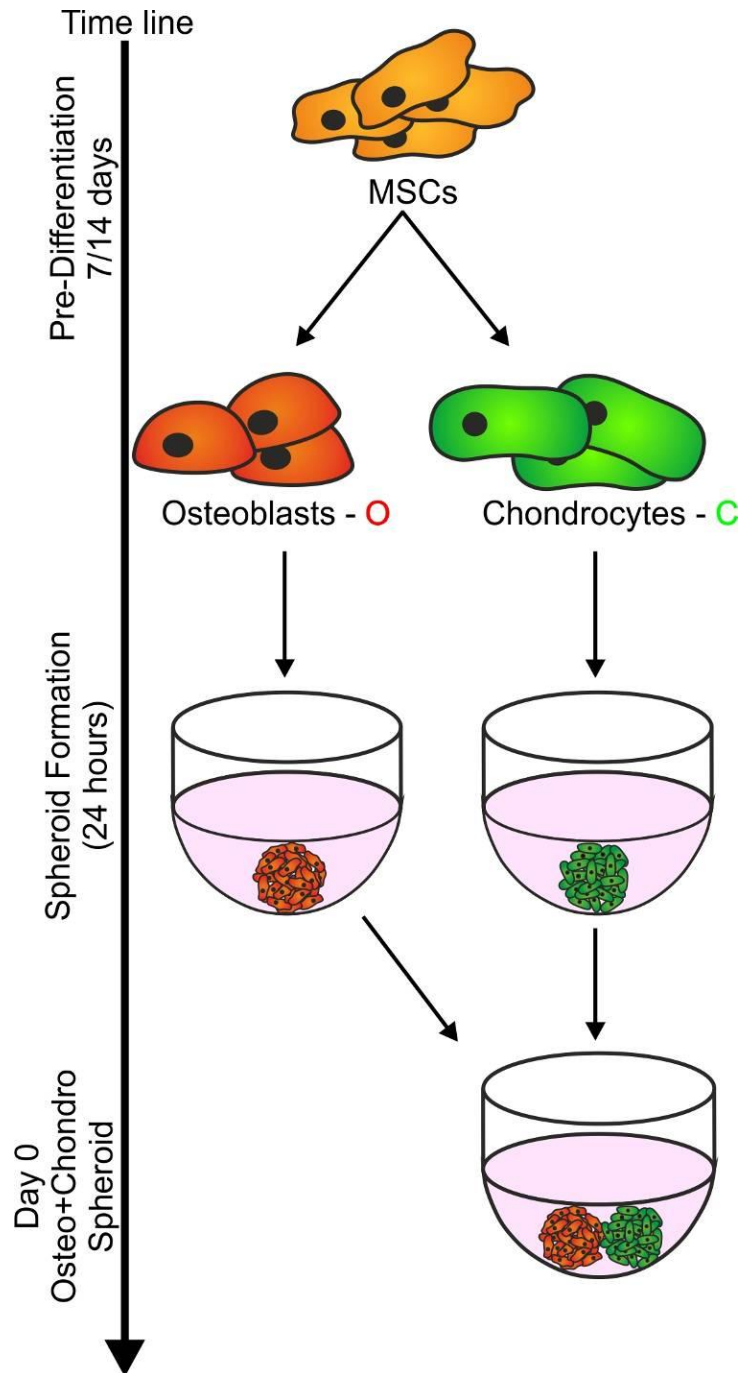
Figure 5.3.2 – Schematic representation of the procedure to produce an osteo+chondro spheroid

MSCs were pre-differentiated for 7 or 14 days before being consider either osteogenic or chondrogenic. Osteogenic MSCs were labelled with CellTracker™ red, chondrogenic MSCs were labelled with CellTracker™ green. 15,000 labelled osteogenic or chondrogenic MSCs were then placed in a U-bottomed well plate for 24 hours to create a spheroid. These two separate spheroids were then combined together to create an osteo+chondro spheroid totalling 30,000 cells.

5.3.3 Histological staining techniques

5.3.3.1 Alcian Blue staining

Alcian blue staining was performed to visualise glycosaminoglycans within chondrogenic differentiated MSCs. Samples were washed with PBS twice followed by fixation using 4% PFA incubated at room temperature for 5 minutes. The samples were then washed three times with PBS before being stained with 10 mg/ml Alcian blue solution pH<1 (Sigma-Aldrich, UK) for 30 minutes at room temperature. After the incubation, the samples were washed in dH_2O to remove non-specific staining. The samples were then imaged using a light microscope (Section 3.3.8).

5.3.4 Quantification of CellTracker™ within defined regions

Spheroid sections were analysed using ImageJ software to quantify the amount of CellTracker™ green, red or blue within a specific region. Regions were manually defined before the average pixel intensity of the specific colour was quantified. A minimum of three separate spheroid sections were used for all quantification studies with background staining subtracted.

5.4 Results

5.4.1 Characterisation of pre-differentiated MSCs in 2D towards an osteogenic or chondrogenic lineage

MSCs were cultured in either osteogenic or chondrogenic culture medium for 7 or 14 days before being cultured in osteochondral culture medium. Figure 5.4.1 shows 2D MSCs stained with Alizarin red, ALP and von Kossa for osteogenic differentiation and Alcian blue for chondrogenic differentiation. Both 7 and 14 days of pre-differentiation in either osteogenic or chondrogenic culture medium were able to cause separation between the two different lineages. This separation of the lineages was not lost when cultured in osteochondral medium. Alizarin red staining was positive for both osteogenic and chondrogenic lineages, however, ALP staining was only positive for osteogenic cells and Alcian blue was only positive for chondrogenic cells.

MSCs were pre-differentiated in standard 2D culture conditions for either 7 or 14 days. The MSCs were then transferred into U-bottomed well plates to assess whether pre-differentiation had effects on 3D osteochondral or osteo+chondro spheroid formation (Figure 5.4.2). 7 days of pre-differentiation had no detrimental effects on the ability of MSCs to form 3D spheroids in any combination. However, 14 day pre-differentiated chondrogenic MSCs were unable to form structurally individual spheroids. Therefore, 7 days of pre-differentiation was used for all future osteochondral and osteo+chondro spheroid experiments.
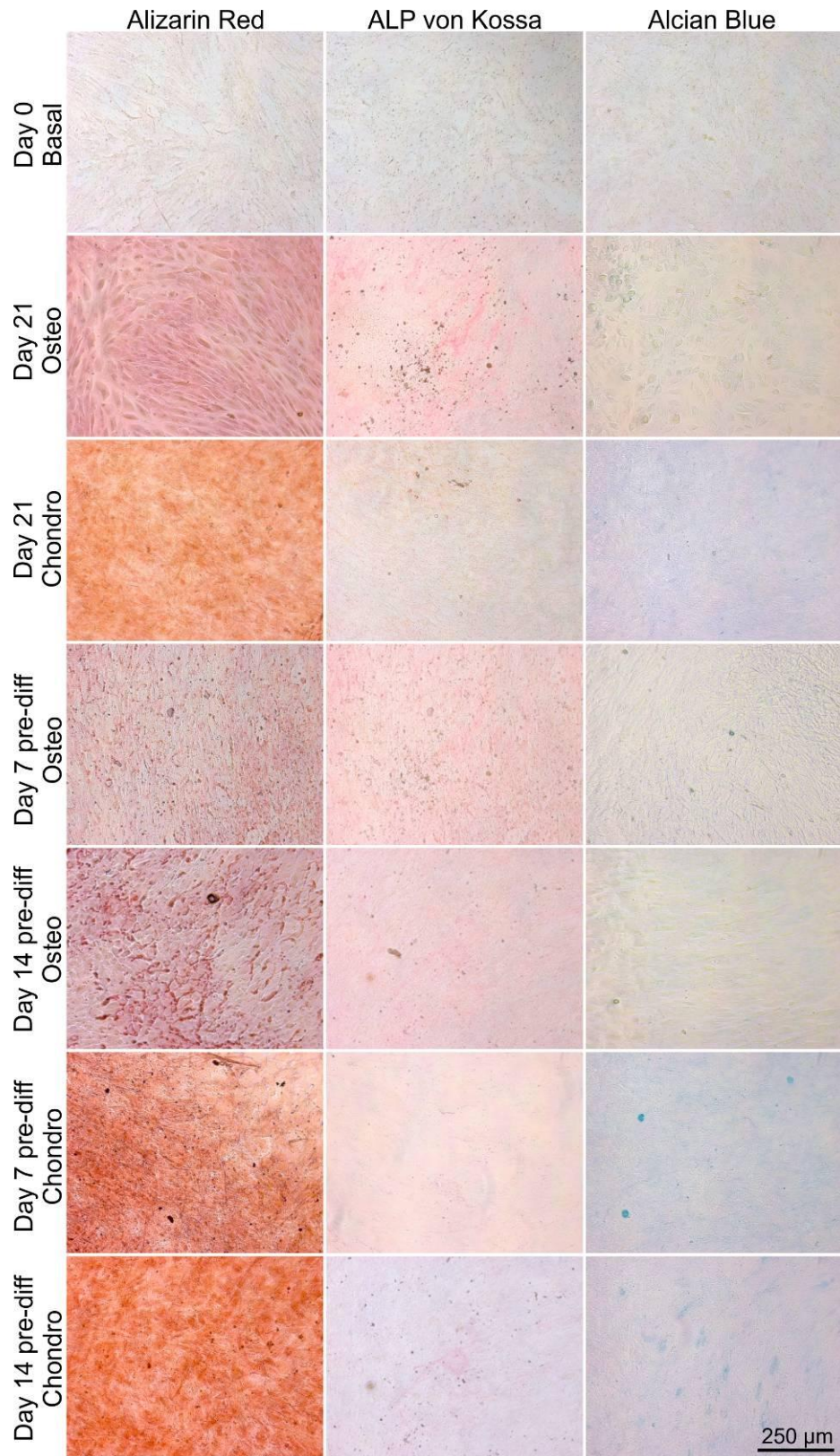
Figure 5.4.1 – Pre-differentiation of MSCs in either osteogenic or chondrogenic condition for 7 or 14 days

MSCs were cultured in either osteogenic or chondrogenic culture medium for 7 or 14 days before being cultured in osteochondral medium for a total of 21 days in culture. To act as controls, MSCs were also cultured in only osteogenic and chondrogenic culture medium for 21 days. All 2D MSC samples were stained with Alizarin Red and ALP/von Kossa for bone markers and Alcian blue for cartilage markers. Both 7 and 14 days of pre-differentiation were successfully able to produce either osteogenic or chondrogenic cells when transferred into osteochondral medium. Alizarin red staining was positive in all chondrogenic MSCs. However, Alizarin red stains calcium which is also present within cartilage. ALP and von Kossa staining was only positive for osteogenic samples and Alcian blue staining was only positive for chondrogenic samples.
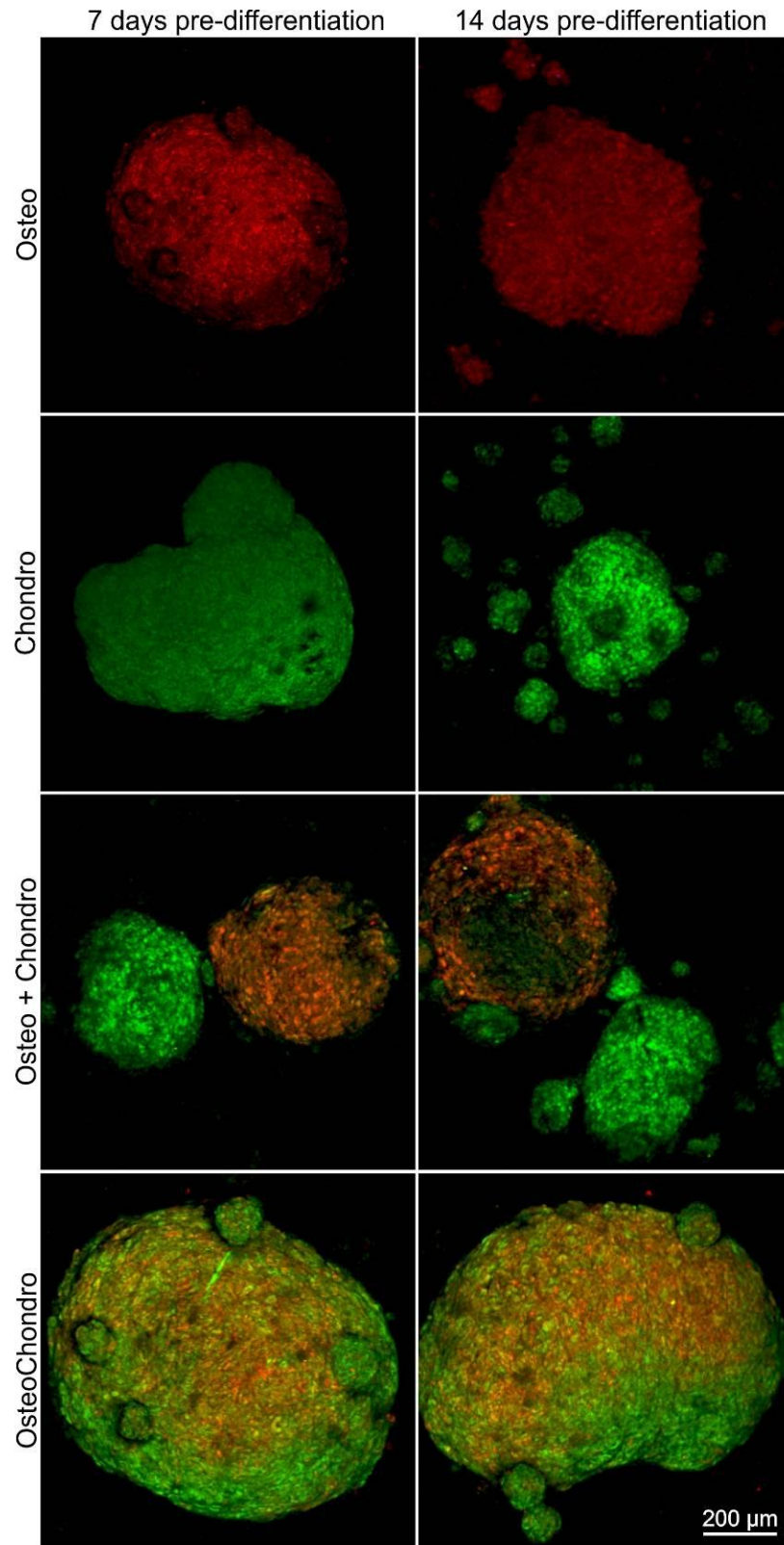
Figure 5.4.2 – 3D spheroids made with 7 or 14 day pre-differentiated osteogenic and chondrogenic MSCs

MSCs were pre-differentiated in either osteogenic or chondrogenic induction medium for 7 or 14 days before the cells were used to create 3D spheroids. After 24 hours from the initial cell suspension spheroids were imaged. 7 days of pre-differentiation was able to produce individual osteogenic, chondrogenic, osteo+chondro and osteochondral spheroids. However, MSCs pre-differentiated for 14 days in chondrogenic induction medium were unable to form individual spheroids, resulting in failed chondrogenic spheroids and osteo+chondro spheroids.

5.4.2 Generation of 3D osteochondral spheroids using pre-differentiated MSCs and ECs

ECs and blood vessels have been shown to play an important role in the maintenance of bone tissue and repair following injury (Findlay, 2007, Stegen et al., 2015). Pre-differentiated MSCs were combined with ECs to further assess osteochondral spheroids. Various combinations of cells were trialled, resulting in a maximum of three different cell types within one spheroid. Therefore, the use of CellTracker™ blue was introduced to indentify this additional cell type. Figure 5.4.3-A shows the use of CellTracker™ blue, green and red in 2D tri-culture to individually identify the different cell types of either; ECs (blue), chondrogenic MSCs (green) and osteogenic MSCs (red). The three different regions of the non-descan detector ranging between 400-800 nm were able to individually identify the three different cell types. Figure 5.4.3-B shows the spectral analysis of the three different CellTracker™ colours; all three have separate peak emission wavelengths with little emission spectrum overlap.

CellTracker™ blue, green and red were used to identify ECs, chondrogenic MSCs and osteogenic MSCs respectively throughout further experiments. Various combinations of the three different cell types were combined to create a variety of different 3D osteochondral spheroids, these were osteogenic and chondrogenic MSCs (OC), osteogenic MSCs and ECs (OE), chondrogenic MSCs and ECs (CE) and all three (OCE) (Figure 5.4.4). All four combinations were found to successfully produce 3D spheroids that were cultured for up to 7 days. The spheroids were then sectioned for further analysis of the internal organisation (Figure 5.4.5). All whole spheroid and spheroid section images show representatives of the observations made across multiple donors and multiple spheroids. These spheroid sections showed that OC and OCE spheroids had clear self-organisation patterns. OC spheroids had lateral-like separation of the osteogenic and chondrogenic MSCs, OCE spheroids had a predominantly green core region (chondrogenic MSCs) and a predominantly red outer region

(osteogenic MSCs). These various regions were highlighted in separate images using white dotted lines. OE and CE spheroids showed no clear self-organisation patterns.
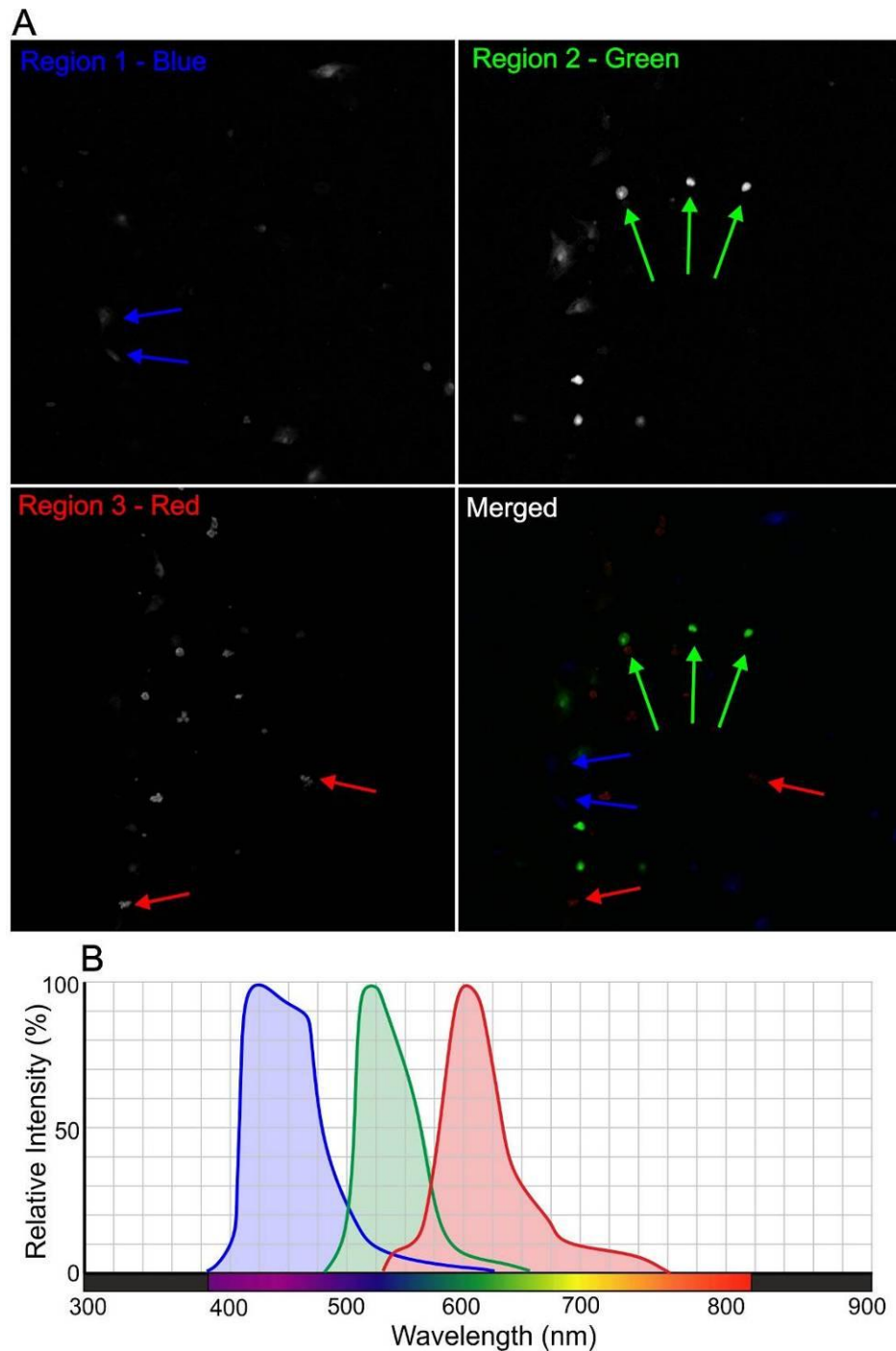
Figure 5.4.3 – 2D tri-culture of fluorescently labelled MSCs and ECs

A – 2D tri-culture of fluorescently labelled ECs (blue), chondrogenic MSCs (green) and osteogenic MSCs (red). These three different cell types were individually detected in the relevant region using a non-descan detector ranging between 400-800nm. B – Spectral analysis of the three different CellTracker™ fluorophores revealed separate emission peaks with little emission spectrum overlap.
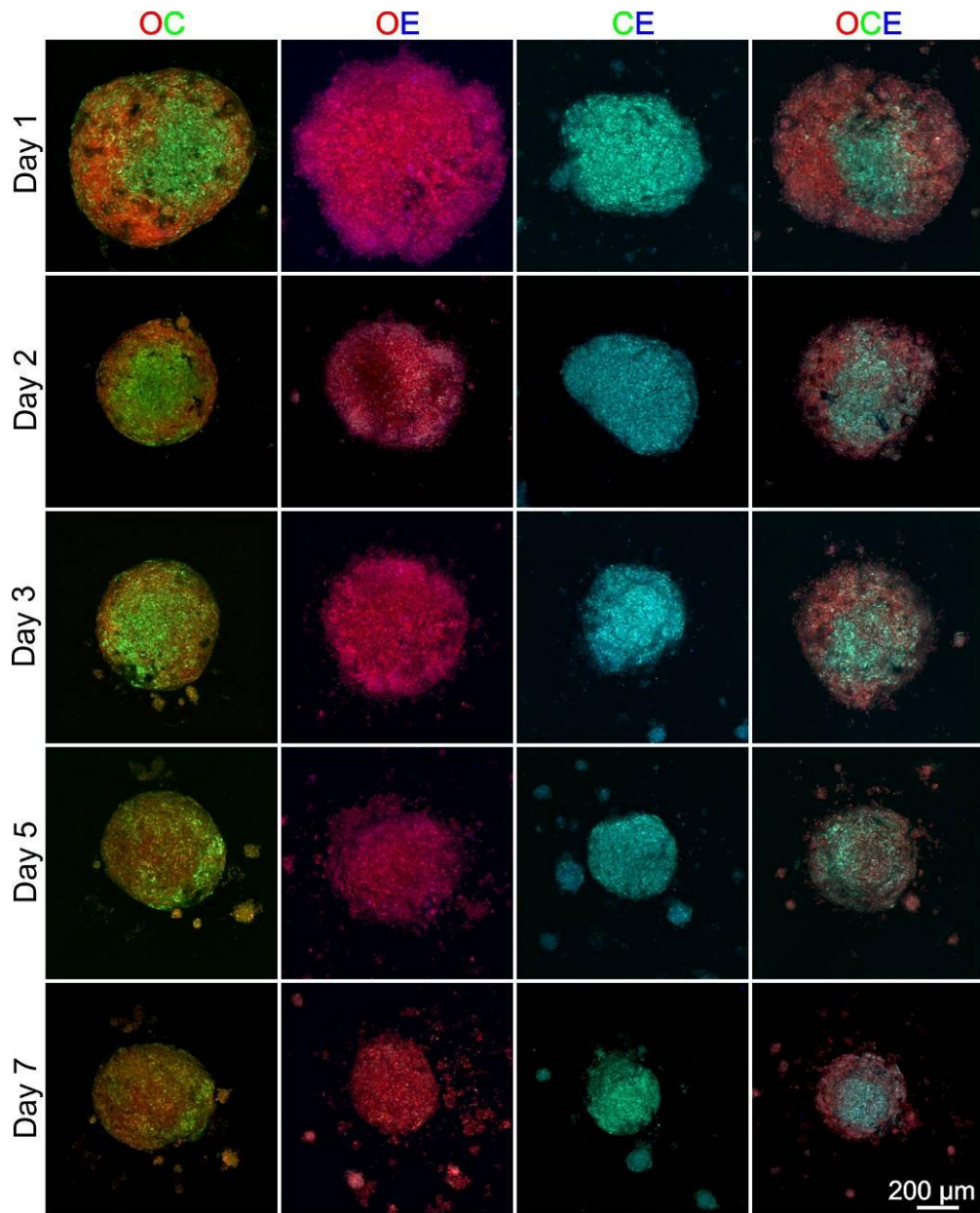
Figure 5.4.4 – Various 3D spheroid combinations using ECs, osteogenic and chondrogenic MSCs

MSCs were pre-differentiated in appropriate medium for 7 days before being used in combination with ECs to produce a variety of 3D osteochondral spheroids. Osteogenic MSCs (O) were labelled red, chondrogenic MSCs (C) were labelled green and ECs (E) were labelled blue. The various combinations created were OC, OE, CE and OCE. All four different combinations were able to successfully produce 3D spheroids that were cultured for up to 7 days. The images shown are representative of the observations made across various spheroids and biological donors.
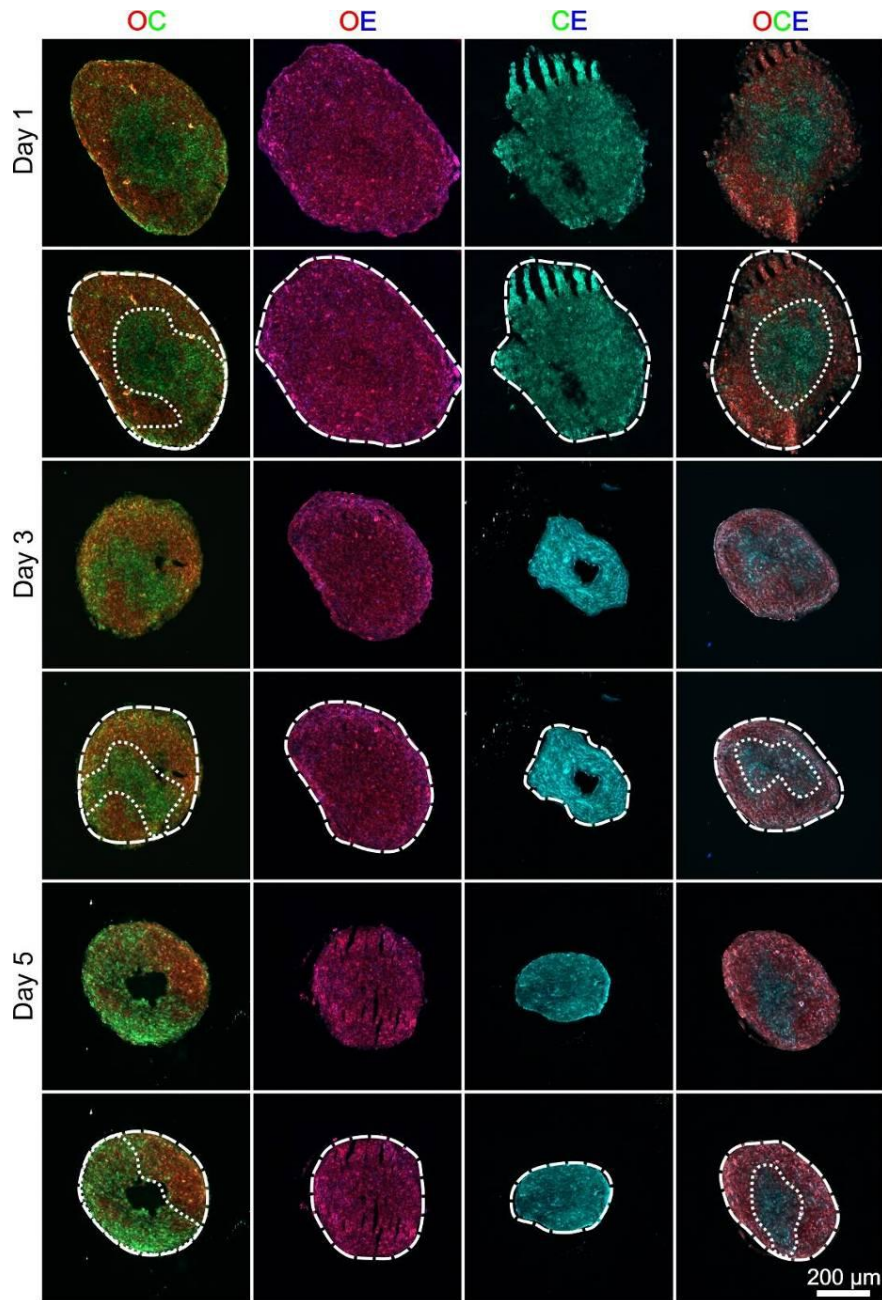
Figure 5.4.5 – Spheroid sections of various EC, osteogenic and chondrogenic MSC combinations

The various 3D osteochondral spheroid combinations were then sections to look at internal organisation patterns and representative images are shown from n=24 independent observations. No self-organisation was observed within OE and CE spheroids. However, OC spheroids showed a lateral-like separation of the osteogenic MSCs (O) and the chondrogenic MSCs (C). OCE spheroids also showed self-organisation of a core region that was predominantly green (chondrogenic MSCs) with an outer region that was predominantly red (osteogenic MSCs). The regions are highlighted using white dotted lines.

The self-organisation observed within the OC and OCE spheroid sections was further analysed. Figure 5.4.6-A shows a day 1 OC spheroid section that has been divided into an osteogenic region highlighted using the red dotted line and a chondrogenic region highlighted using a green dotted line. These regions were then analysed over 5 days to quantify the amount of CellTracker™ green or red present (Figure 5.4.6-B). Per time point and condition three spheroids from two different biological donors were analysed (n=6). This analysis confirmed that for all time points a significantly greater amount of CellTracker™ red was detected in the osteogenic regions and a significantly greater amount of CellTracker™ green was detected in the chondrogenic regions.

OCE spheroid sections showed a self-organisation pattern of a core of predominantly green (chondrogenic MSCs) and outer region of predominantly red (osteogenic MSCs). Figure 5.4.7-A shows a day 1 OCE spheroid section that has been highlighted to show the core region (yellow) and the outer region (white). The colours yellow and white were chosen to differentiate these regions from the osteogenic and chondrogenic regions seen in OC sections. OCE spheroid sections contained ECs, therefore, the regions could not be defined as osteogenic or chondrogenic. The quantity of either CellTracker™ green, red or blue within these two different regions was calculated at days 1, 3 and 5 of culture (Figure 5.4.7-B). Per time point and condition three spheroids from two different biological donors were analysed (n=6). For all time points the centre region had a greater quantity of CellTracker™ green (labelling chondrogenic MSCs) whilst the outer region had a significantly greater quantity of CellTracker™ red (osteogenic MSCs). No difference in CellTracker™ blue (ECs) was detected between the two regions.
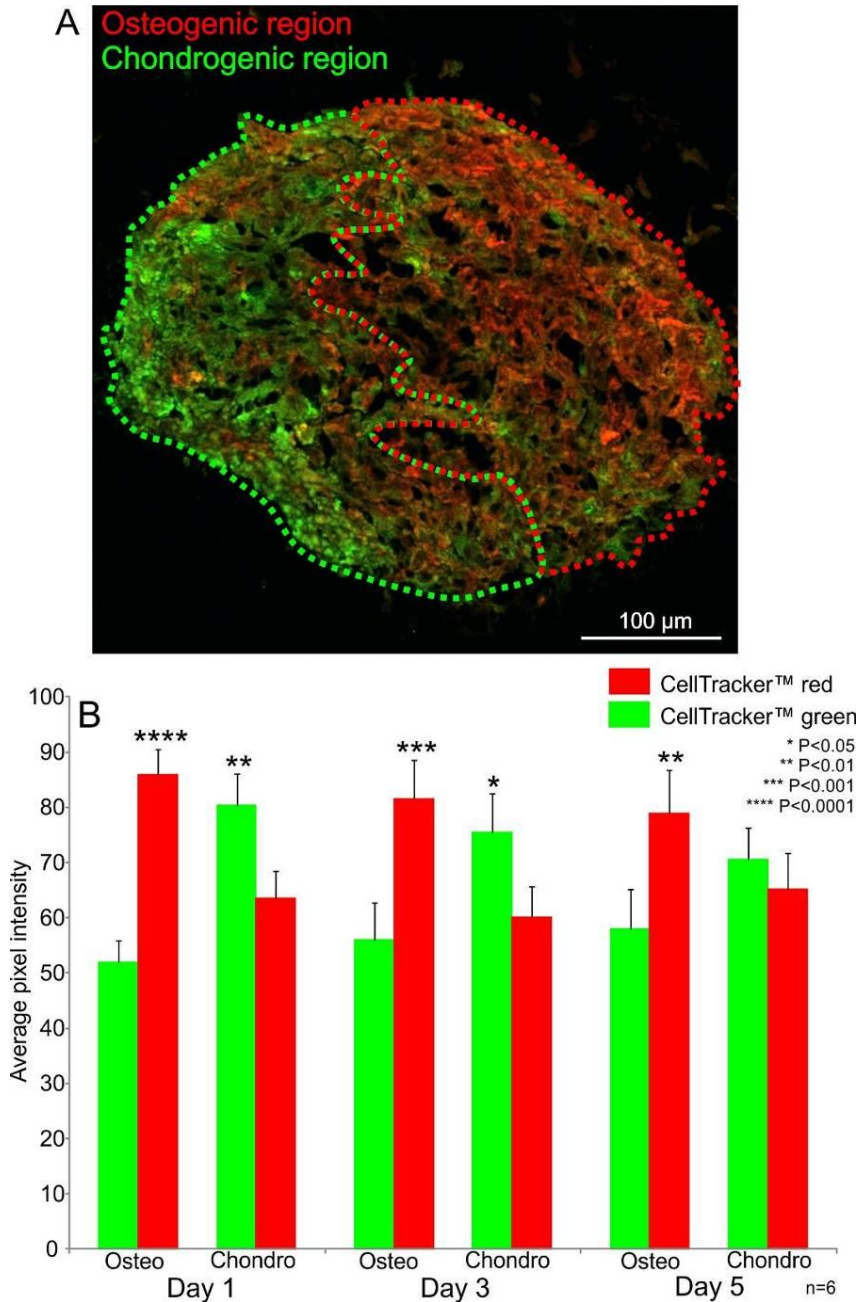
Figure 5.4.6 – OC spheroid section analysis of osteogenic and chondrogenic regions

A – Day 1 OC section separated into either osteogenic or chondrogenic regions using red or green dotted line. B – Spheroid sections at Days 1, 3 and 5 were analysed, CellTracker™ green or red present within either the osteogenic or chondrogenic regions were calculated. It was found for all time points significantly greater CellTracker™ red intensity was detected in osteogenic regions and significantly greater CellTracker™ green intensity was detected in chondrogenic regions. Per time point and condition three individual spheroids from two biological donors were analysed (n=6).
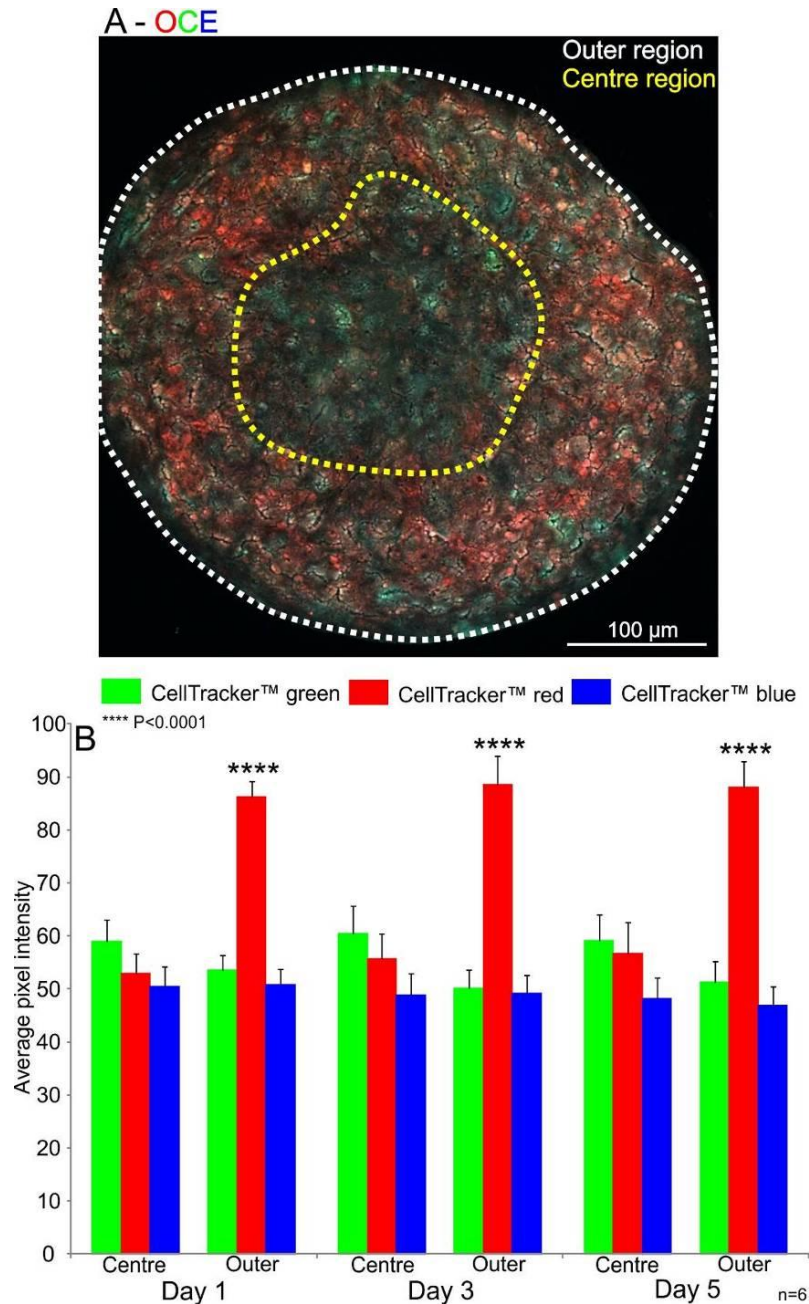
Figure 5.4.7 – OCE spheroid section analysis of central and outer regions

A – Day 1 OCE spheroid section separated into either a core region (yellow) or outer region (white) using dotted lines. B – Spheroid sections at days 1, 3 and 5 were analysed to quantify the amount of CellTracker™ green, red or blue present within the two different regions. For all time points a significantly greater quantity of CellTracker™ red was detected within the outer regions and a greater quantity of CellTracker™ green was detected within the core regions. No difference in CellTracker™ blue was detected between the regions. Per time point and condition three individual spheroids from two biological donors were analysed (n=6).

5.4.3 Further analysis of 3D Osteo+Chondro spheroids using pre-differentiated MSCs

MSCs were pre-differentiated for 7 days in either osteogenic or chondrogenic induction medium before being made into individual spheroids and combined to form osteo+chondro spheroids using the method described in Section 5.3.2.3. Figure 5.4.8 shows osteo+chondro spheroids from the initial combination of the two spheroids through to 3 days of culture. The two individual spheroids became connected within 8 hours, the spheroids then merged together to form a single spheroid by day 3, whilst retaining distinct red/green separation. These spheroids were then sectioned to examine the internal organisation (Figure 5.4.9). A clear separation between the two different spheroids is still visible at day 1; however, the spheroids have begun to merge together. The osteogenic MSCs (red) and chondrogenic MSCs (green) remain segregated, however, an integrated osteochondral boundary forms between the two cell types.

The osteo+chondro spheroids sections were then separated into osteogenic and chondrogenic regions, this is highlighted by the red and green dotted lines shown in Figure 5.4.10-A. The spheroid sections were the analysed after days 1, 2 and 3 in culture, a significantly greater pixel intensity of CellTracker™ red was detected in osteogenic regions whilst a significantly greater pixel intensity of CellTracker™ green was detected in chondrogenic regions (Figure 5.4.10-B). Per time point and condition three spheroids from two different biological donors were analysed (n=6)
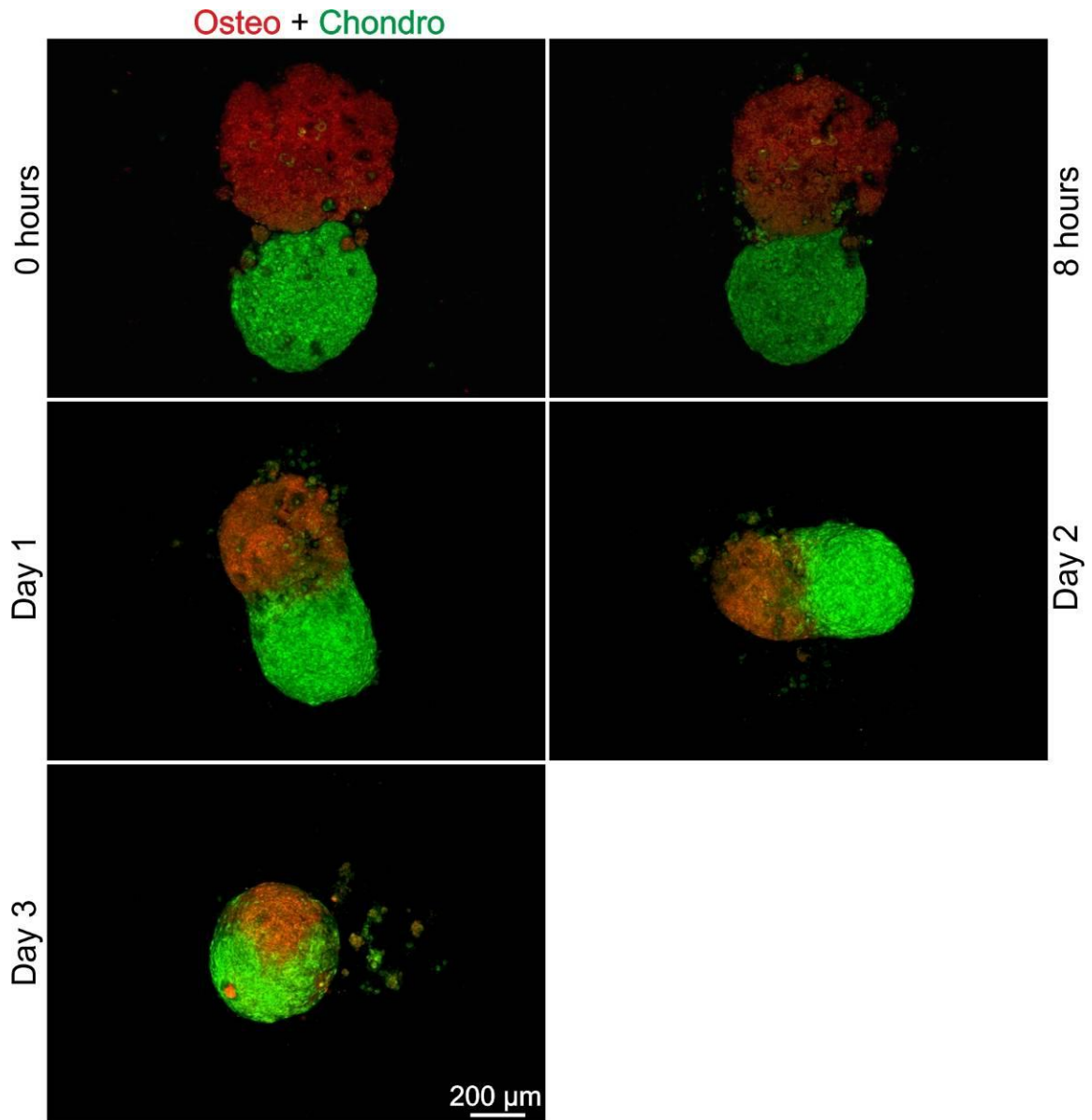
Figure 5.4.8 – Osteo+Chondro 3D spheroids during culture

Osteogenic MSC and chondrogenic MSC 3D spheroids containing a total of 15,000 cells were generated separately. After 24 hours in culture, these two spheroids were then combined in the same well, within 8 hours the two separate spheroids connect, by day 3 they have merged together to form a single spheroid.
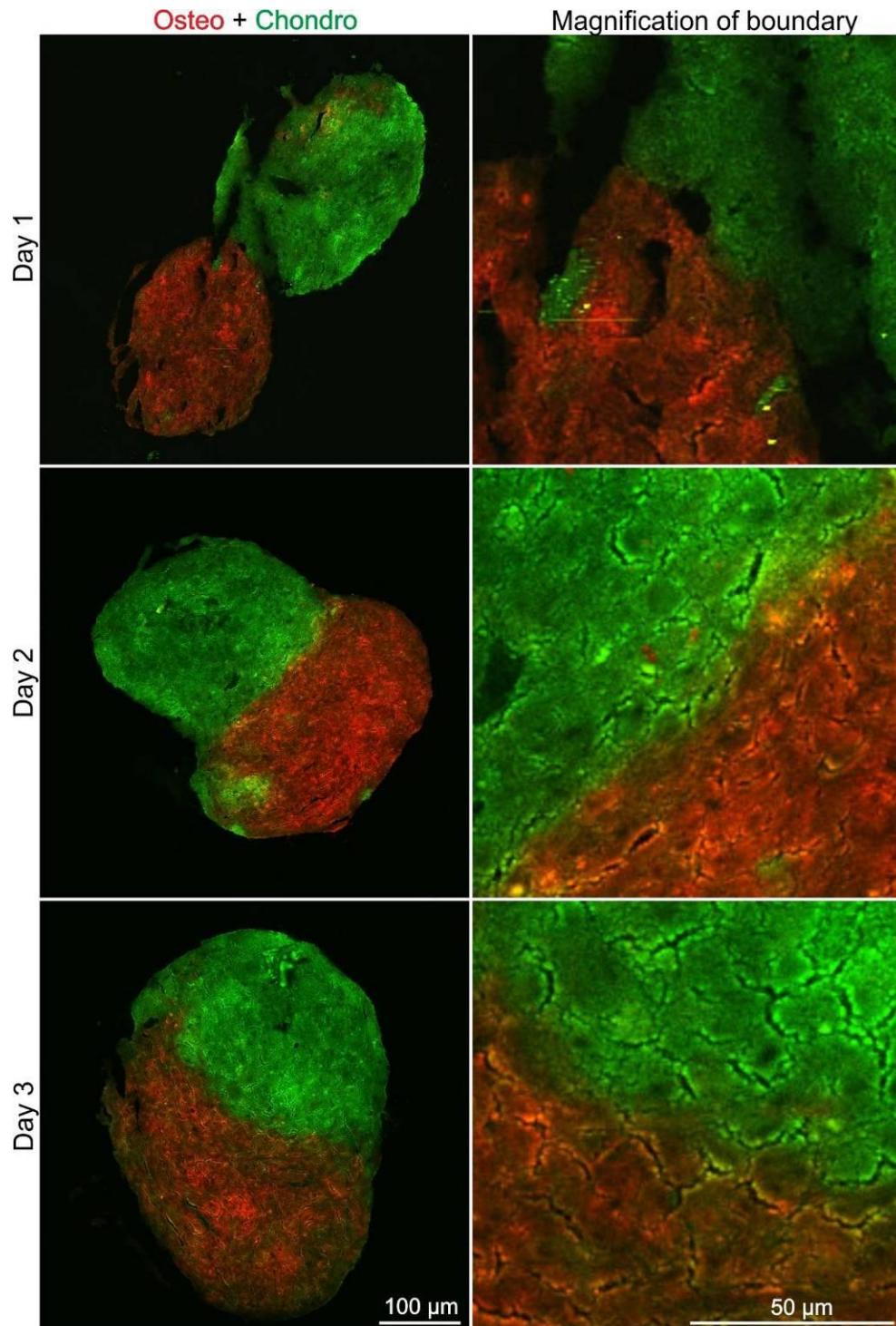
Figure 5.4.9 – Osteo + Chondro spheroid sections with magnification of osteochondral boundary

Osteo + chondro spheroid were sections to observe internal organisation. Clear distinction between the two spheroids can be seen at day 1, however, by day 3 the spheroids have merged together to form a single spheroid.
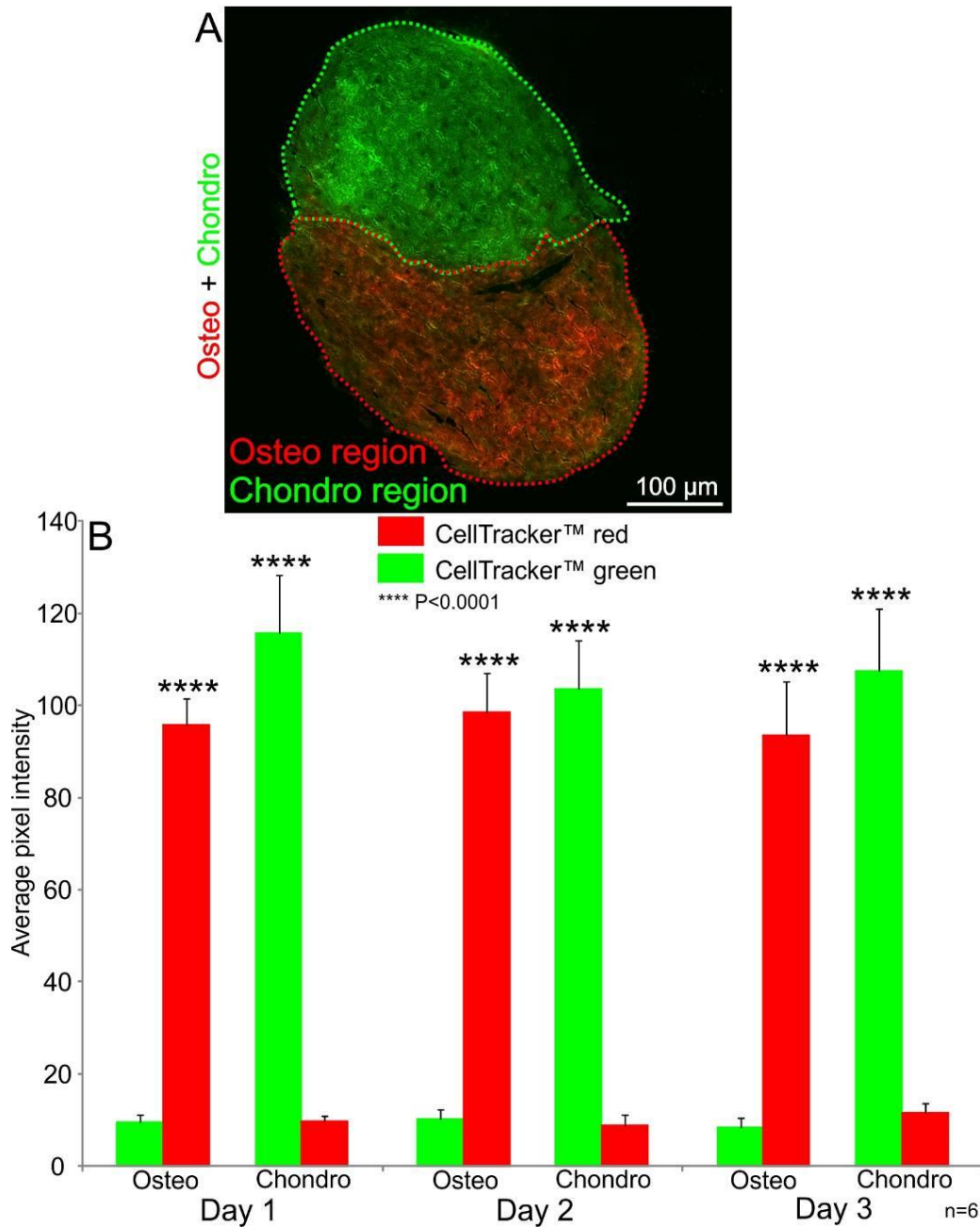
Figure 5.4.10 – Osteo + Chondro spheroid section analysis of osteogenic and chondrogenic regions

A – Day 3 osteo + chondro spheroid section separated into osteogenic and chondrogenic regions using red and green dotted lines respectively. B – Quantification of the CellTracker™ red or green intensity within the osteogenic or chondrogenic regions at days 1, 2 and 3. A significantly greater quantity of CellTracker™ red was detected in osteogenic regions and a significantly greater quantity of CellTracker™ green was detected in chondrogenic regions. Per time point and condition three individual spheroids from two biological donors were analysed (n=6).

5.4.4 Expression of bone, cartilage and endothelial cell markers in various osteochondral spheroid during long term *in vitro* culture

From these initial studies, three spheroid combinations were assessed for expression of bone, cartilage and endothelial markers through immunofluorescent labelling (Section 2.3.2). This was done to independently verify the distribution and function of osteogenic MSCs, chondrogenic MSCs and ECs with the spheroids. The spheroids studied were osteochondral (OC) spheroids composed of a 50-50 mixture osteogenic and chondrogenic MSCs; osteo+chondro (O+C) spheroids these were created through the combination of an osteogenic MSC spheroid and a chondrogenic MSC spheroid (Section5.3.2.3); and osteochondral and endothelial (OCE) spheroids containing an equal mixture of endothelial cells, osteogenic and chondrogenic MSCs. To act as a control MSC-only spheroids were cultured in basal conditions. All other spheroids were cultured in 3D osteochondral medium.

The various osteochondral spheroid combinations were cultured for 21 days before being sectioned and immunofluorescently labelled for collagen type I, collagen type II, CD31, Sox 9 and osteonectin (Figure 5.4.11). Collagen type I and osteonectin are bone markers; collagen type II and Sox 9 are cartilage markers. Positive collagen type I staining and limited collagen type II staining were observed within OC, OCE and O+C spheroid sections. Within OC and O+C sections collagen type I and II staining appeared laterally separated. OCE sections collagen type II appeared more predominantly within the centre of the section whilst collagen type I was predominant at the spheroid surface. Positive CD31 staining was only observed within OCE spheroid sections; this staining appeared evenly distributed throughout the spheroid. No positive Sox 9 staining was observed within any spheroid section. Positive osteonectin staining was observed within OC, OCE and O+C spheroid sections; this staining appeared to

be evenly distributed through the spheroid. These observations confirm the cellular distribution observed within Section 5.4.2 and 5.4.3.
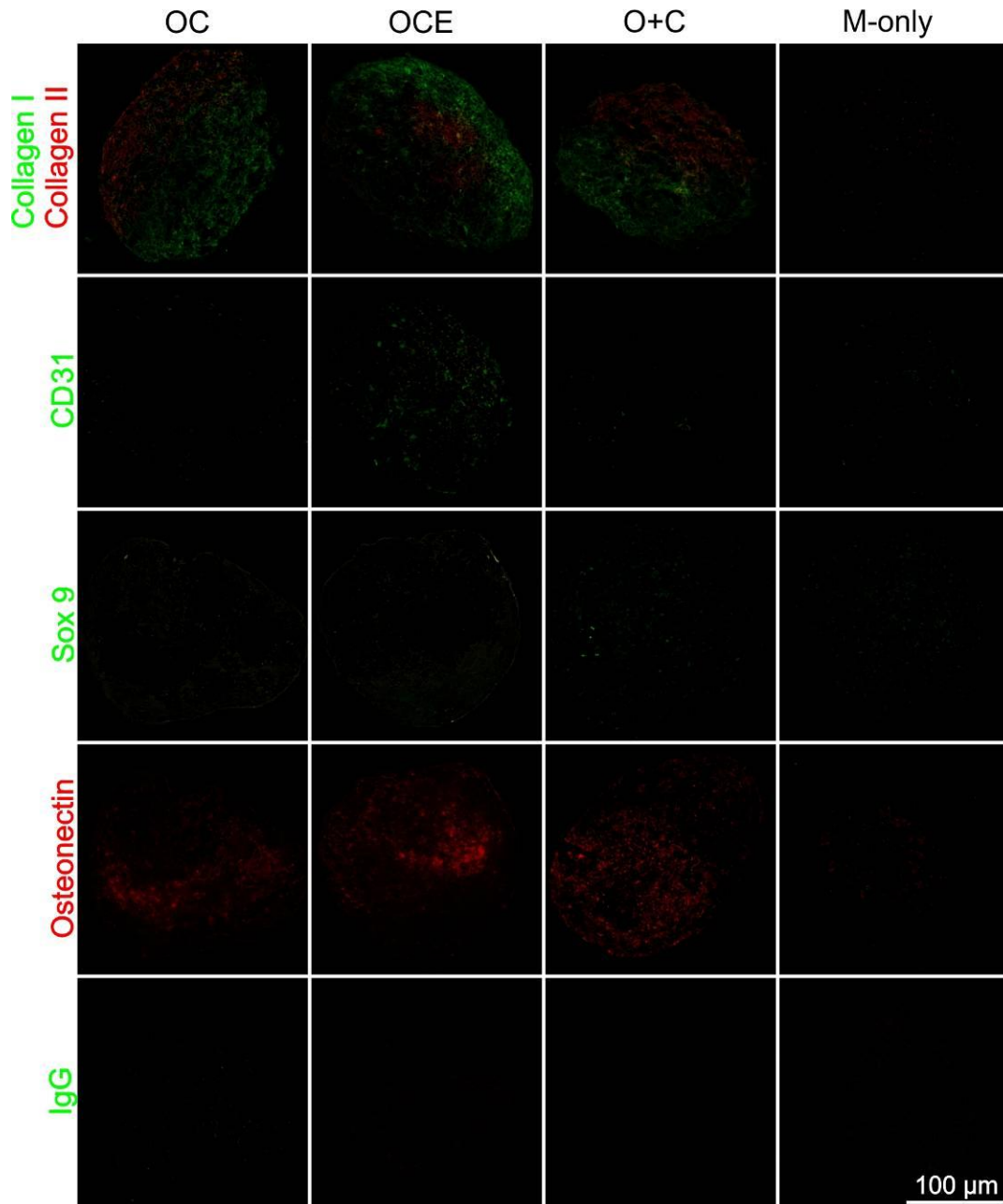
Figure 5.4.11 – Immunofluorescent labelled of various osteochondral spheroid combinations for bone, cartilage and endothelial markers

Immunofluorescent labelling of various osteochondral spheroid combinations was performed after 21 days in culture. Collagen type I and osteonectin are bone markers; collagen type II and Sox9 are cartilage markers. Positive collagen type I staining was observed in OC, OCE and O+C spheroid sections. Minimal collagen type II staining was observed in OCE and O+C spheroid sections. CD31 staining was only observed in OCE spheroid sections. Sox 9 staining was not observed for any osteochondral spheroid combination. Osteonectin staining was observed in OC, OCE and O+C spheroid sections.

5.4.5 Effects of PDGFR, FGFR and Notch inhibition on osteochondral spheroids

To determine the role of signalling mechanisms in osteochondral spheroids, specifically the mechanisms involved in the lateral self-organisation pattern previously observed (Section 5.4.2). Whole spheroids were cultured with the addition of various inhibitors of PDGF, FGF and Notch signalling pathways at the concentrations described in Section 4.3.3. Inhibitor treatment was added to the cell suspension prior spheroid formation. To act as a control MSC-only (M-only) spheroids were produced, these contained a 50-50 mixture of MSCs stained with CellTracker™ green and red. The inhibitors used were PDGFRi, FGFRi and DBZ (Notch inhibitor) more details of these can be found on Table 4.3.2; these three inhibitor treatments were used as PDGF, FGF and Notch signalling have been linked with osteochondral defects. PDGF and FGF have been shown to enhance healing of osteochondral defects (Younger et al., 2015, Maehara et al., 2010). In contrast, Notch signalling has been shown to inhibit osteochondral healing through hindering osteogenic differentiation of MSCs (Matthews et al., 2014). The spheroids were culture for up to 3 days with the various inhibitor treatments and representative images can be seen in Figure 5.4.12. PDGFRi treatment resulted in much larger spheroids; however, no visual differences were observed with the other inhibitor treatments.

The whole spheroid images were analysed to calculate the spheroid diameter and the percentage of green labelled MSCs at the spheroid surface (Figure 5.4.13). The whole spheroid image analysis provides a rapid high throughput technique to quantify spheroid organisation. PDGFRi treatment resulted in a significantly greater spheroid diameter compared to untreated control OC spheroids at days 1, 2 and 3. No significant differences were observed for any other inhibitor treatment. The percentage of green labelled MSCs at the spheroid surface was not affected by the various inhibitor treatments.

To observe internal organisation the spheroids were sectioned (Figure 5.4.14). Untreated control OC spheroids appeared to have a lateral separation, osteogenic MSCs (red) appeared to separate from chondrogenic MSCs (green). This separation of the two different cell types occurred within untreated control OC spheroids and with PDGFRi, FGFRi and DBZ inhibitor treatments. Therefore, inhibitor treatments appeared to not affect the organisation of osteogenic or chondrogenic MSCs in osteochondral spheroids. MSC-only sections showed a random distribution of green and red labelled MSCs.
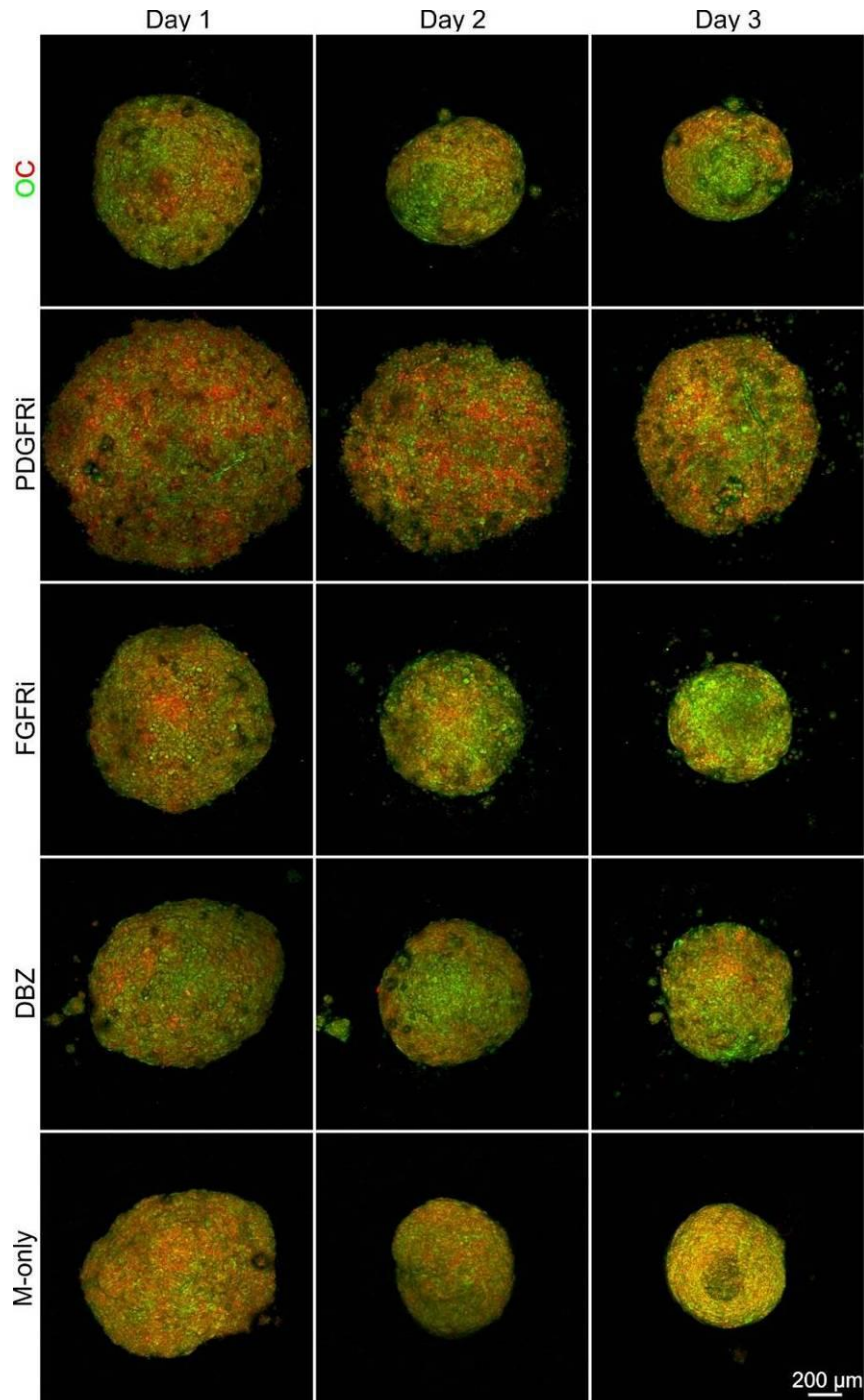
Figure 5.4.12 – Whole 3D osteochondral spheroids treated with various inhibitors

Whole 3D osteochondral spheroids were treated with the various inhibitors; PDGFRi, FGFRi and DBZ (Notch inhibitor) and representative images are shown from n=6 independent observations. The inhibitor was added to the cell suspension, prior to spheroid formation. PDGFRi treatment appeared to result in larger spheroids; however, no additional visual differences were observed.
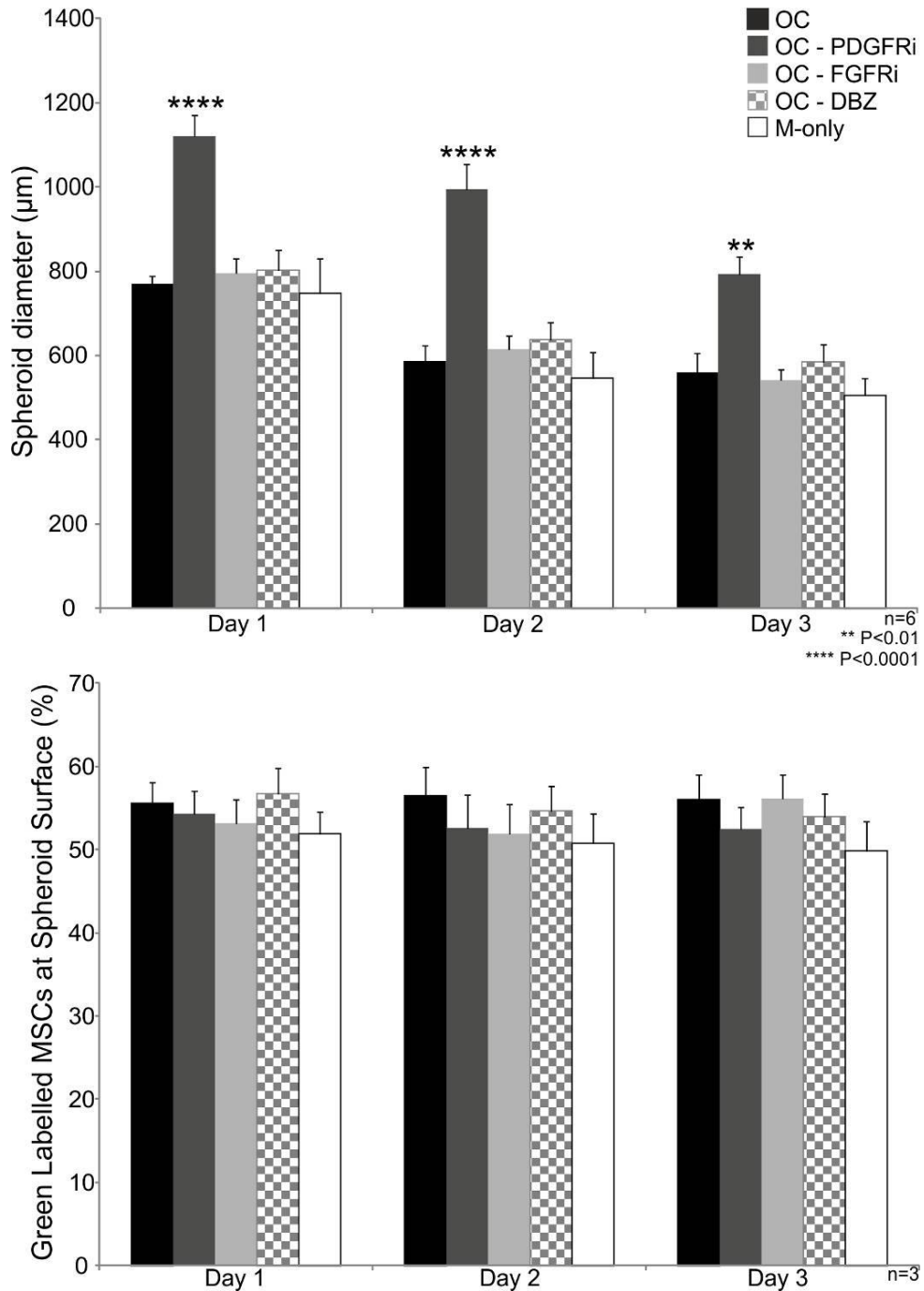
Figure 5.4.13 – Spheroid diameter and surface analysis of osteochondral spheroids treated with various inhibitors

Spheroid diameter of the osteochondral spheroids treated with various inhibitors, showed PDGFRi treatment resulted in significantly larger spheroids at days 1, 2 and 3. No other significant differences in spheroid diameter or percentage of green labelled MSCs at the spheroid surface were detected. Per time point and condition three spheroids from two different biological donors were analysed (n=6).
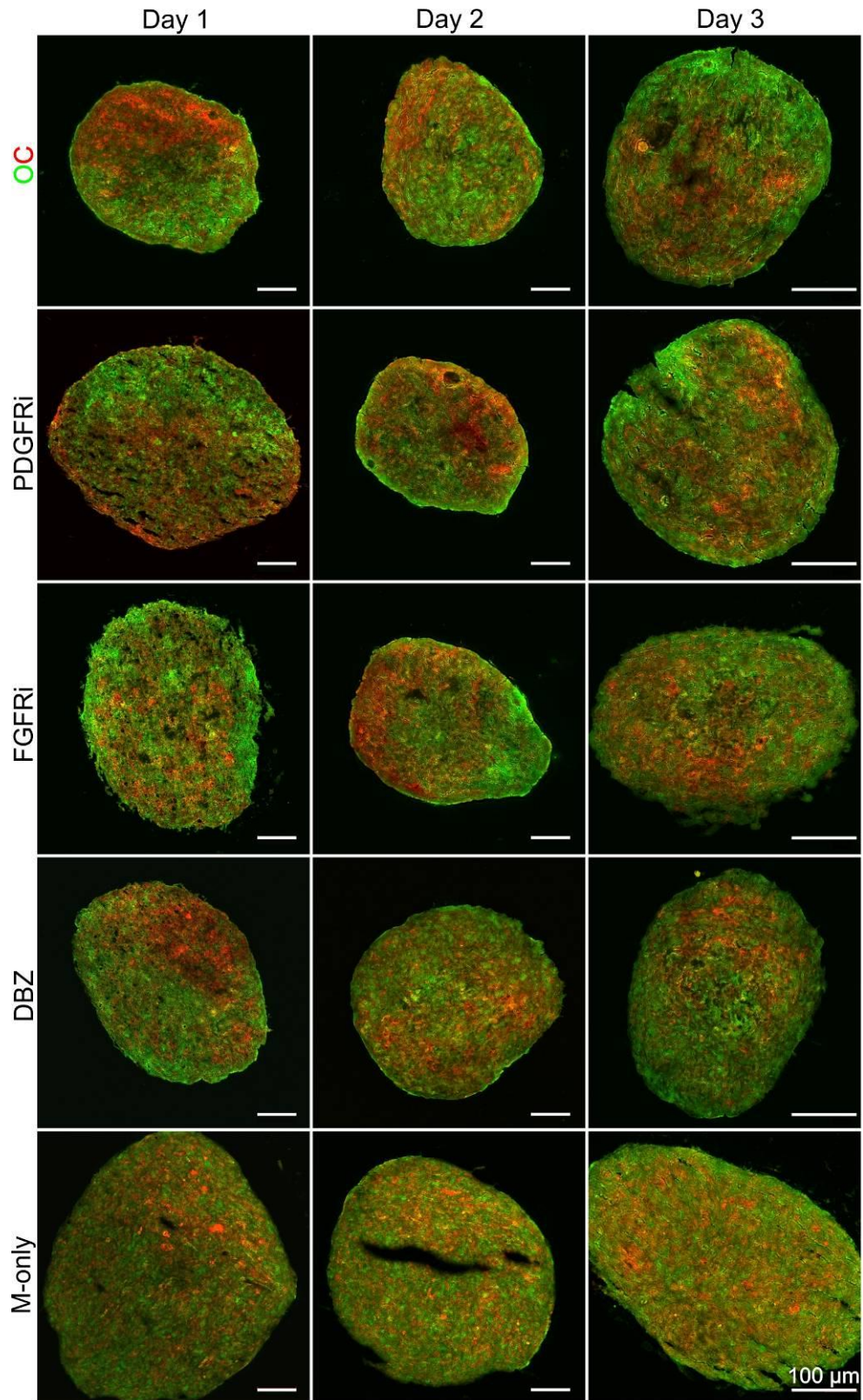
Figure 5.4.14 – Osteochondral spheroid sections treated with various inhibitors

Osteochondral spheroids treated with various inhibitors were sectioned to observed internal organisation and representative images are shown from n=6 independent observations. Osteochondral (OC) spheroids appeared to have a lateral separation, osteogenic MSCs (red) appeared to separate from chondrogenic MSCs (green). This separation of the two different cell types occurred within untreated control OC spheroids and with various inhibitor treatments (PDGFRi, FGFRi and DBZ). MSC-only sections appeared to show a random distribution of green and red labelled MSCs.

5.5 Discussion

MSCs were pre-differentiated for either 7 or 14 days to determine the period of time required to sustain either an osteogenic or chondrogenic lineage within an osteochondral medium developed to maintain both differentiated phenotypes. An osteochondral medium able to support both osteogenic and chondrogenic MSCs in culture has yet to be fully established (Rodrigues et al., 2012). However, attempts have been made by combining the components of both osteogenic and chondrogenic culture media (Li et al., 2009).

MSCs were pre-differentiated in osteogenic or chondrogenic medium for 7 or 14 days followed by a further 14 or 7 days in osteochondral medium respectively. All pre-differentiated samples and control samples were cultured for a total of 21 days unless otherwise stated. Pre-differentiated osteogenic MSCs stained positively for the osteogenic stains Alizarin red, ALP and von Kossa. However, pre-differentiated osteogenic MSCs stained negatively for the chondrogenic stain Alcian blue. The same positive and negative staining was observed in control osteogenic MSCs. Pre-differentiated chondrogenic MSCs stained positively for the osteogenic stain Alizarin red, however, ALP and von Kossa staining were negative; the chondrogenic stain Alcian blue was positive. The same positive and negative staining patterns were also observed in control chondrogenic MSCs. Positive Alizarin red staining can be attributed to staining calcium, therefore, this is not an osteogenic specific stain (Paul et al., 1983).

To identify if pre-differentiation had an effect on the spheroid formation capacity of MSCs, 7 and 14 day pre-differentiated MSCs were placed in U-bottomed well plates. 3D whole spheroid imaging was performed after 24 hours to allow structural observations. Four different combinations using osteogenic and chondrogenic pre-differentiated MSCs were performed, it was found that 14 days of pre-differentiation had a detrimental effect on spheroid formation for chondrogenic MSCs. This made 14 day pre-differentiation unsuitable for future studies, therefore, 7 days of pre-differentiation was used for all further

experiments. Pre-differentiation of MSCs has been previously described as having detrimental effects on their proliferation and cell attachment potential (Fensky et al., 2014). Therefore, pre-differentiation may have decreased the cell adhesion molecules on the cell membrane of MSCs, these are essential for spheroid formation. Indeed the loss of the cell adhesion molecule α5-integrin has been shown to result in complete spheroid failure in ovarian cancer models (Casey et al., 2001).

Previous osteochondral models have specifically only used osteogenic and chondrogenic MSCs (Babur et al., 2015, Guo et al., 2009, Marquass et al., 2010). However, native bone is a highly vascularised tissue and ECs play a key role in bone tissue homeostasis and repair following injury (Findlay, 2007, Stegen et al., 2015). Therefore, combining osteogenic and chondrogenic MSCs with ECs would more closely represent the native environment. This resulted in up to three different cell types being cultured in 3D spheroids. Using the CellTracker™ labelling techniques previously described CellTracker™ blue was used to identify the additional cell type. CellTracker™ blue in combination with CellTracker™ green and red were able to individual identify fluorescently labelled ECs, chondrogenic and osteogenic MSCs. Spectral analysis of the three different CellTracker™ colours, showed separated peak emission wavelengths with little emission overlap. Tri-culture of 3D cell aggregates has been previously performed, however, within this system only two cell types were fluorescently labelled (Takebe et al., 2013).

The three different cell types; osteogenic MSCs, chondrogenic MSCs and ECs were used to produce various osteochondral spheroid combinations, these combinations were: OC, OE, CE and OCE. These combinations were able to successfully produce 3D spheroids; however, observations of internal organisation demonstrated that OC and OCE spheroids underwent spontaneous cellular self-organisation. OC spheroids demonstrated a lateral separation of the osteogenic and chondrogenic MSCs. In contrast OCE spheroids demonstrated a central region that was predominantly green (chondrogenic MSCs) and outer

region that was predominantly red (osteogenic MSCs). Similar organisation to OCE spheroids has been artificially created through the addition of cell suspensions to existing cell spheroids (Urich et al., 2013). Further analysis of this organisation patterns through quantification of CellTracker™ green, red or blue confirmed these organisation patterns. Specifically OC spheroid sections were confirmed to have significantly more red labelled osteogenic MSCs within the manually defined osteogenic regions and significantly more green labelled chondrogenic MSCs in the chondrogenic regions. This demonstrates that manual CellTracker™ quantification was able to identify the osteogenic and chondrogenic MSC distribution within the spheroids. This technique had even greater importance when analysing OCE spheroid sections. Within these spheroid sections a core and outer region was manually identified, however, through CellTracker™ quantification of these regions it was possible to identify that ECs were evenly distributed between these regions. Therefore, the core region was a combination of mainly chondrogenic MSCs and ECs, whilst the outer region was mainly osteogenic MSCs and ECs. The organisation pattern observed within OCE spheroid sections shows similarities to those within early endochondral ossification. Specifically a cartilage core surrounded by a bone outer layer; this cartilage core is then infiltrated by new blood vessels triggering resorption of the cartilage core matrix and replacement with functional vascularised bone tissue.(Rodrigues et al., 2012, Scotti et al., 2010, Scotti et al., 2013).

The concept of creating osteochondral tissue has been performed using a variety of different techniques; *in vitro* these have usually been conducted using scaffolds (Angele et al., 1999, Fensky et al., 2014). However, these *in vitro* techniques are often limited due to the requirement of two separate medium sources and/or complex scaffold design. Therefore, generating a cell-only osteochondral model using an osteogenic MSC spheroid combined with a chondrogenic MSC spheroid could be beneficial. Osteogenic MSC spheroids and chondrogenic MSC spheroids were combined together after 24 hours in culture; within 8 hours the two separate spheroids formed an integrated osteochondral boundary. Within 3 days the two separate spheroids merged together to form a

single spheroid. A similar study was successfully performed using bone-like and cartilage-like cells derived from MSCs in a micropellet or microspheroid formation;, 24,000 of these individual micropellets were then layered together to create a biphasic structure. The micropellets amalgamated to form a continuous structure with bone-like and cartilage-like regions (Babur et al., 2015). This proof of concept study showed that bone-like and cartilage-like MSCs could be cultured together, however, the method used to produce the cellular structure was highly complex and labour intensive.

Spheroid section analysis of osteo+chondro spheroids showed a distinct separation between the two spheroids after 24 hours in culture together, after 3 days the osteochondral boundary was still well defined. Through quantification of CellTracker™ green and red within the osteogenic and chondrogenic regions this distinction between the two regions was significantly different for all time points. With single and multi-cellular aggregates limited cellular migration has been reported (Thompson et al., 2012, Bauer et al., 2012). This limitation migration is attributed towards a dense cellular network and strong cell-cell contacts. Within the context of an osteochondral boundary this limited cell migration is desired, within the native environment bone and cartilage tissue are clearly separated, however, the diffusion of oxygen, nutrients and waste products is essential for both tissues homeostasis (Smith and Mansour, 2000).

To determine the long-term bone and cartilage formation within various osteochondral spheroid combinations, immunofluorescent labelling was performed on day 21 spheroid sections. Spheroid sections were stained for the bone markers collagen type I and osteonectin, cartilage markers collagen type II and Sox 9 and CD31 for ECs. Positive collagen type I staining was observed in OC, OCE and O+C spheroid sections, limited collagen type II staining was observed within the same sections. Within OC and O+C sections collagen type I and II staining appeared more laterally separated, whilst within OCE section collagen type I appeared more predominantly at the spheroid surface and collagen type II appeared more predominantly at the spheroid core. This

organisation confirms the organisation patterns seen within CellTracker™ labelled spheroids. No positive Sox 9 staining was observed within any spheroid section, however, Sox 9 is a transient marker of chondrogenic differentiation and is frequently described as an early marker (Antunes et al., 2015, Hardingham et al., 2006). Therefore, Sox 9 expression could have been missed. Positive CD31 staining was only observed within OCE spheroids, this result was expected as these were the only spheroids that contained ECs. The CD31 staining appeared to be evenly distributed throughout the spheroid, confirming the results previous observed through CellTracker™ analysis. Positive osteonectin staining appeared evenly distributed within OC, OCE and O+C spheroid sections. Osteonectin is a traditional bone marker, however, it has been observed within both senescent MSCs and cartilage tissue (Juhasova et al., 2011, Vidal et al., 2012, Chandrasekhar et al., 1994). Within OCE sections this osteonectin staining was particularly strong; this might have been attributed towards chondrogenic MSCs in the presence of both osteogenic MSCs and ECs undergoing a transition into bone tissue. Within the native bone following injury cartilage tissue initially forms before being replaced with vascularised bone tissue, a similar process also occurs in endochondral ossification (Tannous et al., 2013, Sisask et al., 2013, Chan et al., 2009). A similar transition might have occurred in OC and O+C; however, due to a lack of ECs osteonectin staining was not as strong. Indeed, ECs have been shown to enhance the osteogenic differentiation potential of MSCs (Saleh et al., 2011a, Gershovich et al., 2013). Overall the immunohistochemical staining was poor, these results were mainly attributed towards problems with the primary antibodies. Positive controls such as HeLa were stained and negative results were observed for many of the primary antibodies. A positive control of human bone sections was also trialled, however, human bone is highly auto-fluorescent preventing confirmation of the primary antibody.

To determine possible signalling mechanisms responsible for the organisation pattern observed within osteochondral spheroids, PDGFRi, FGFRi and DBZ were added to OC cell suspensions prior to spheroid formation. 3D whole spheroid

images were taken and analysed to assess spheroid diameter and percentage of green labelled MSCs at the spheroid surface. PDGFRi treatment resulted in a significantly greater spheroid diameter at all time points compared to untreated control OC spheroids. This result is consistent with the effects of PDGFRi treatment on co-cultured MSC-EC spheroids (Section 4.4.5). PDGF signalling has been shown to affect the shape of MSCs in 2D culture, the addition of a similar small molecular inhibitor of PDGFR resulted in MSCs having a more rounded shape (Ball et al., 2012). More specifically PDGF signalling has been linked to controlling cell size within Drosophila, therefore, inhibition of this cell signalling pathway could result in larger cells and subsequently larger spheroids (Sims et al., 2009). To observe internal organisation, the OC spheroids treated with the various inhibitors were sectioned and no differences in spheroid organisation were observed with inhibitor treatments. All spheroid sections appeared to demonstrate a lateral separation of osteogenic and chondrogenic MSCs. Increased PDGF expression has been observed within the osteochondral region of patients with osteoarthritis, however, this occurred in conjunction with increased VEGF expression. Therefore, PDGF expression could be a consequence of VEGF (Walsh et al., 2010). FGF treatment has been successfully used to improve osteochondral defects within rabbits (Maehara et al., 2010). However, FGF treatment is known to increase cell proliferation and improve wound healing (Budiraharjo et al., 2013). Notch signalling modulation has been shown to effect osteochondral fracture healing, however, Notch is believed to regulate osteogenic differentiation (Matthews et al., 2014). The regulatory role of a signalling pathway in osteochondral cell organisation is currently unknown.

Overall the results within this chapter demonstrate that MSCs are a useful cell source for *in vitro* modelling of osteochondral tissues. Specifically MSCs require only 7 days of pre-differentiation in either osteogenic or chondrogenic conditions to generate distinctive and separate osteogenic MSCs or chondrogenic MSCs. These cells could then be used in a variety of combinations with the addition of ECs to create an osteochondral spheroid. Using these cells it was possible to

recreate *in vitro* an osteochondral boundary and by specifically combining all three cell types produced a unique self-organised endochondral ossification-like model. Where chondrogenic MSCs were at the core of the spheroid, osteogenic MSCs were at the periphery of the spheroid and ECs were evenly distributed throughout. The organisation and function of these regions was confirmed using immunofluorescent labelling; OCE spheroids expressed the known bone markers collagen type I and osteonectin and the cartilage marker collagen type II.

Chapter 6

Chapter 6 : Discussion

The work within this thesis has primarily focused on using MSCs and ECs in a novel 3D co-culture to generate *in vitro* models. MSCs were chosen due to them being a stem cell with great potential for tissue engineering and regenerative medicine. MSCs have been successfully used within a wide variety of studies such as; bone repair, immunity disorders and ischemia (Lu et al., 2014, Introna et al., 2014, Bhang et al., 2012b). ECs were specifically chosen due to MSCs principally residing within vascularised tissues; indeed this relationship with the vasculature is so important it has been hypothesised that MSCs reside within a perivascular niche (Crisan et al., 2008, Shi and Gronthos, 2003). Therefore, direct co-culture of MSCs and ECs in 3D would more closely represent the native environment. Direct co-culture of MSCs and ECs in 3D was found to enhance the osteogenic potential of MSCs using qualitative staining and quantitatively using the novel calcium depletion from culture medium method (Chapter 3). Using fluorescent labelling in combination with 3D co-culture it was possible to track and identify cell types within the spheroids using non-destructive 3D confocal imaging and destructive spheroid sectioning. These techniques were then utilised to understand the possible mechanisms responsible for the unique lattice-like self-organisation pattern observed in 3D spheroid co-culture of MSCs and ECs specifically (Chapter 4). This fluorescent labelling was then used in conjunction with osteogenic and chondrogenic differentiation of MSCs and ECs to create a variety of osteochondral models (Chapter 5).

6.1 ECs enhance the osteogenic differentiation potential of MSCs in 3D

Studies have previously observed that direct and in-direct culture of ECs enhanced the osteogenic differentiation potential of MSCs; this effect is attributed towards a paracrine factor secreted by ECs (Saleh et al., 2011a, Saleh et al., 2011b, Gershovich et al., 2013). However, these studies relied upon qualitative

staining in 3D studies; consequently statistical analysis was not performed. Therefore, a novel method to quantitatively assess MSC osteogenic differentiation specifically in 3D and also 2D was developed. Calcium deposition is an important factor in the osteogenic differentiation of MSCs, bone ECM is primarily composed of calcium based compounds and Alizarin Red S a common bone stain specifically binds to calcium (Wen et al., 2012, Paul et al., 1983). Therefore, it was hypothesised that during osteogenic differentiation of MSCs, soluble calcium within the culture medium would be converted into insoluble calcium salt deposits. Therefore, calcium ion depletion from culture medium was quantified and found to quantitatively assess osteogenic differentiation of MSCs in both 2D and 3D culture.

Using this method in conjunction with traditional staining it was observed that ECs were able to significantly improve the osteogenic differentiation potential of MSCs in 3D co-culture (Figure 3.4.11and Figure 3.4.12). Calcium depletion offers a non-destructive, sensitive and real-time technique to assess osteogenic differentiation. Indeed alternative methods such as Alizarin Red S staining and quantification were found to produce false positive results in unique circumstances. Specifically it was found that Donor 3 (K107) was an osteogenic inert donor, however, Alizarin Red S staining and quantification found significant differences between basal and osteogenic medium at day 21. However, using calcium depletion no statistically significant differences were observed, further verifying this method to quantitatively assess osteogenic differentiation in both 2D and 3D.

6.2 Fluorescent labelled of MSCs and ECs for spheroid organisation assessment

Previous work within the laboratory found that when MSCs and ECs were co-cultured together in 3D, a unique self-organisation pattern of ECs developed. This pattern was described as a capillary-like structure and comparable

observations have been made in other studies involving the co-cultures of MSCs and ECs (Saleh et al., 2011b, Takebe et al., 2013, Rivron et al., 2012). However, the underlying mechanisms and if MSCs are directing ECs remained unclear. In this study fluorescent labelling using CellTracker™ green, red and blue were used in conjunction with 3D and 4D imaging techniques to track multiple cell types within a spheroid. Using these techniques, it was possible to non-destructively quantify the spheroid diameter, volume and surface. These measurements in conjunction with spheroid sections to observe internal organisation and subsequent quantification of the EC network resulted in a tractable model. Untreated control MSC-EC spheroid formation was assessed and found to initially be controlled by the differential adhesion hypothesis, resulting in ECs migrating towards the periphery of the spheroid during formation. However, after this ECs began to migrate into the spheroid producing a lattice-like network (Figure 4.4.5). From direct comparison of untreated control MSC-EC and HDF-EC spheroids it was determined that MSCs were able to direct ECs into forming a lattice-like network, within HDF-EC spheroids no EC network was detected. Therefore, the EC network observed within MSC-EC spheroids was not caused by an innate ability.

Subsequently the *in vitro* model was used to determine the possible underlying cell signalling mechanism responsible. Five different small molecule inhibitors were trialled; FGFRi, PDGFRi, EGFRi, ILKi and DBZ, these were chosen due to their association with MSC migration, EC migration or angiogenesis (Dos Santos et al., 2014, Wyler von Ballmoos et al., 2010, Liao et al., 2014, Lu et al., 2013). These were found to have a various effects; FGFRi appeared to most predominantly affect EC migration, PDGFRi strongly affected EC network organisation and spheroid size, EGFRi had no effect, ILKi principally affected MSC migration and DBZ mainly affected EC migration. However, this model could not be used to directly confirm effects specific to these signalling pathways, to do this inhibition or significant decrease of specific downstream signalling molecules would be required. This model was then developed further to incorporate osteogenic MSCs, chondrogenic MSCs and ECs to create various

osteochondral models. Different cell combinations were trialled and three strong candidates were established; OC, osteo+chondro and OCE. All three of these combinations produced unique organisation patterns of distinct functional regions. OC spheroids self-organised into separated regions of osteogenic MSCs and chondrogenic MSCs (Figure 5.4.6). Osteo+chondro spheroids were formed from the combination of two individual spheroids to produce a distinct osteochondral boundary (Figure 5.4.10). OCE spheroids self-organised into an outer and core region, further analysis found the outer region containing mainly osteogenic MSCs, the core region predominantly contained chondrogenic MSCs and ECs were evenly distributed throughout (Figure 5.4.7).

6.3 Future Directions

There are two main areas of further research that have been highlighted in this work. Firstly, the use of 3D spheroid co-cultures of MSCs and ECs as a high throughput screening technique. The self-organisation observed within these spheroids was highly similar to those observed in 2D culture of ECs on matrigel, the culture of ECs on matrigel is commonly used as an angiogenesis model (Mezentsev et al., 2005). Additional experiments would be required to confirm the effects of inhibiting specific signalling pathways, specifically known downstream signalling molecules would need to be inhibited or significantly reduced. Enhancement of the specific signalling pathways could also be used to further clarify these effects. However, overall the 3D spheroid co-culture of MSCs and ECs could be utilised as a possible 3D *in vitro* angiogenesis model. Further analysis of this model could be performed using genome editing technologies such as clustered regularly interspaced short palindromic repeats (CRIPSR) or transcription activator-like effector nucleases (TALENs) to knockout specific signalling molecules in only MSCs or ECs (Park and Telugu, 2013).

The second area of interest is in the further development of osteogenic MSCs and chondrogenic MSCs for osteochondral and endochondral ossification applications. Functional observations into known markers such as collagen type

X, osteocalcin and osteonectin could be used to verify the functionality and ratify these cells within an osteochondral and/or endochondral ossification model (Scotti et al., 2013). These results could be further confirmed through the use of the inhibitor molecules such as; FGFRi or PDGFRi to hinder osteogenic and chondrogenic differentiation of MSCs during long term culture.

6.4 Conclusions

The work present here demonstrates how MSCs are a highly versatile stem cell source. MSCs combined with ECs in the 3D spheroid culture system were able to enhance the osteogenic potential of MSCs; this was quantified and confirmed using the novel calcium depletion from culture medium method. The culture system was then developed to incorporate fluorescent labelling to identify and track a specific cell type within the 3D spheroid for up to 7 days. Using these techniques it was possible to identify that MSCs direct ECs to self-assembling into a lattice-like network with organisational similarities to angiogenesis. The underlying mechanisms responsible for this were found to be strongly linked to FGF, PDGF and Notch signalling. Finally MSC pre-differentiation to either an osteogenic or chondrogenic lineage was found to create osteochondral tissue with a defined boundary. Combination of these MSCs with ECs was found to result in a unique self-organisation pattern with structural and functional similarities to adult bone repair and endochondral ossification.

List of Abbreviations

ALP – Alkaline Phosphatise

BMP – Bone morphogenetic protein

BSA – Bovine Serum Albumin

CPC - Cetylpyridinium chloride

CRISPR - Clustered regularly interspaced short palindromic repeats

DAPI - 4', 6- diamidino-2-phenylindole

DBZ – Dibenzazepine (Notch inhibitor)

DFM - Deferoxamine mesylate

DMEM – Dulbecco's modified Eagle medium

ECM – Extra cellular matrix

ECs – Endothelial cells

EGF – Epidermal growth factor

EGFR – Epidermal growth factor receptor

EGFRi – Epidermal growth factor receptor inhibitor

ESCs – Embryonic stem cells

FBS – Foetal bovine serum

FGF – Fibroblast growth factor

FGFR – Fibroblast growth factor receptor

FGFRi – Fibroblast growth factor receptor inhibitor

HDFs – Human Dermal Fibroblasts

HIF-1α - Hypoxia inducible factor one alpha

HSCs – Haematopoietic stem cells

HUVECs – Human umbilical vein endothelial cells

IGF – Insulin-like growth factor

ILK – Integrin-linked kinase

ILKi – Integrin-linked kinase inhibitor

ICD – Intracellular domain

iPS – Induced pluripotent stem cells

JAK - Janus Kinase

LIF – Leukaemia inhibitor factor

MAPK – Mitogen activated protein kinase

MHC – Major histocompatible complex

MSCs – Mesenchymal stromal cells or Mesenchymal stem cells

OC – Osteochondral

OCE – Osteochondral endothelial

OCT – Optimised cutting tissue

ON - Osteonectin

PBS – Phosphate buffer saline

PDGF – Platelet-derived growth factor

PDGFR – Platelet-derived growth factor receptor

PDGFRi – Platelet-derived growth factor receptor inhibitor

PECAM-1 - Platelet endothelial cell adhesion molecule

PFA – Paraformaldehyde

PI3K - Phosphoinositide 3-kinase

PLC-γ - Phosphoinositide phospholipase C-γ

P/S – Penicillin-streptomycin

SHG – Second harmonic generation

TALENs - Transcription activator-like effector nucleases

TGF-β – Transforming growth factor β

VE – Vascular endothelial

VEGF – Vascular endothelial growth factor

vWF – von Willebrand Factor

w/v – Weight/volume

References

ABDALLA, H. I. 2009. The role of the Human Fertilisation and Embryology Authority. *Obstetrics, Gynaecology & Reproductive Medicine,* 19**,** 53-56.

ABNOSHI, M. H., MEHRANJANI, M. S., SHARIATZADEH, M. A. & DEHDEHI, L. 2012. Para-nonylphenol Impairs Osteogenic Differentiation of Rat Bone Marrow Mesenchymal Stem Cells by Influencing the Osteoblast Mineralization. *Iranian Journal of Basic Medical Sciences,* 15**,** 1131-1139.

ADAMO, L. & GARCÍA-CARDEÑA, G. 2012. The vascular origin of hematopoietic cells. *Developmental Biology,* 362**,** 1-10.

ADAMO, L., NAVEIRAS, O., WENZEL, P. L., MCKINNEY-FREEMAN, S., MACK, P. J., GRACIA-SANCHO, J., SUCHY-DICEY, A., YOSHIMOTO, M., LENSCH, M. W., YODER, M. C., GARCÍA-CARDEÑA, G. & DALEY, G. Q. 2009. Biomechanical forces promote embryonic haematopoiesis. *Nature,* 459**,** 1131-1135.

ALVAREZ, C. V., GARCIA-LAVANDEIRA, M., GARCIA-RENDUELES, M. E., DIAZ-RODRIGUEZ, E., GARCIA-RENDUELES, A. R., PEREZ-ROMERO, S., VILA, T. V., RODRIGUES, J. S., LEAR, P. V. & BRAVO, S. B. 2012. Defining stem cell types: understanding the therapeutic potential of ESCs, ASCs, and iPS cells. *J Mol Endocrinol,* 49**,** 12-0072.

ANGELE, P., KUJAT, R., NERLICH, M., YOO, J., GOLDBERG, V. & JOHNSTONE, B. 1999. Engineering of Osteochondral Tissue with Bone Marrow Mesenchymal Progenitor Cell in a Derivatized Hyaluronan-Gelatin Composite Sponge. *Tissue Engineering,* 5**,** 545-53.

ANTEBI, B., PELLED, G. & GAZIT, D. 2014. Stem cell therapy for osteoporosis. *Curr Osteoporos Rep,* 12**,** 41-7.

ANTOINE, M., WIRZ, W., TAG, C. G., GRESSNER, A. M., WYCISLO, M., MULLER, R. & KIEFER, P. 2006. Fibroblast growth factor 16 and 18 are expressed in human cardiovascular tissues and induce on endothelial cells migration but not proliferation. *Biochemical and biophysical research communications,* 346**,** 224-33.

ANTUNES, J. C., TSARYK, R., GONCALVES, R. M., PEREIRA, C. L., LANDES, C., BROCHHAUSEN, C., GHANAATI, S., BARBOSA, M. A. & KIRKPATRICK, C. J. 2015. Poly(gamma-Glutamic Acid) as an Exogenous Promoter of Chondrogenic Differentiation of Human Mesenchymal Stem/Stromal Cells. *Tissue engineering. Part A,* 21**,** 1869-85.

ASARI, S., ITAKURA, S., FERRERI, K., LIU, C. P., KURODA, Y., KANDEEL, F. & MULLEN, Y. 2009. Mesenchymal stem cells suppress B-cell terminal differentiation. *Exp Hematol,* 37**,** 604-15.

ASTASHKINA, A., MANN, B. & GRAINGER, D. W. 2012. A critical evaluation of in vitro cell culture models for high-throughput drug screening and toxicity. *Pharmacol Ther,* 134**,** 82-106.

AUGUSTE, P., GURSEL, D. B., LEMIERE, S., REIMERS, D., CUEVAS, P., CARCELLER, F., DI SANTO, J. P. & BIKFALVI, A. 2001. Inhibition of

fibroblast growth factor/fibroblast growth factor receptor activity in glioma cells impedes tumor growth by both angiogenesis-dependent and -independent mechanisms. *Cancer Res,* 61**,** 1717-26.

BABUR, B. K., FUTREGA, K., LOTT, W. B., KLEIN, T. J., COOPER-WHITE, J. & DORAN, M. R. 2015. High-throughput bone and cartilage micropellet manufacture, followed by assembly of micropellets into biphasic osteochondral tissue. *Cell Tissue Res*.

BALDUINO, A., MELLO-COELHO, V., WANG, Z., TAICHMAN, R. S., KREBSBACH, P. H., WEERARATNA, A. T., BECKER, K. G., DE MELLO, W., TAUB, D. D. & BOROJEVIC, R. 2012. Molecular signature and in vivo behavior of bone marrow endosteal and subendosteal stromal cell populations and their relevance to hematopoiesis. *Exp Cell Res,* 318**,** 2427-37.

BALL, S. G., SHUTTLEWORTH, A. & KIELTY, C. M. 2012. Inhibition of platelet-derived growth factor receptor signaling regulates Oct4 and Nanog expression, cell shape, and mesenchymal stem cell potency. *Stem cells,* 30**,** 548-60.

BALL, S. G., SHUTTLEWORTH, C. A. & KIELTY, C. M. 2007. Platelet-derived growth factor receptor-α is a key determinant of smooth muscle α-actin filaments in bone marrow-derived mesenchymal stem cells. *The International Journal of Biochemistry & Cell Biology,* 39**,** 379-391.

BARBERO, A., PLOEGERT, S., HEBERER, M. & MARTIN, I. 2003. Plasticity of clonal populations of dedifferentiated adult human articular chondrocytes. *Arthritis and rheumatism,* 48**,** 1315-25.

BAUER, M., KANG, L., QIU, Y., WU, J., PENG, M., CHEN, H. H., CAMCI-UNAL, G., BAYOMY, A. F., SOSNOVIK, D. E., KHADEMHOSSEINI, A. & LIAO, R. 2012. Adult cardiac progenitor cell aggregates exhibit survival benefit both in vitro and in vivo. *PLoS One,* 7**,** 30.

BAZZONI, G. & DEJANA, E. 2004. *Endothelial Cell-to-Cell Junctions: Molecular Organization and Role in Vascular Homeostasis*.

BECKERMANN, B. M., KALLIFATIDIS, G., GROTH, A., FROMMHOLD, D., APEL, A., MATTERN, J., SALNIKOV, A. V., MOLDENHAUER, G., WAGNER, W., DIEHLMANN, A., SAFFRICH, R., SCHUBERT, M., HO, A. D., GIESE, N., BUCHLER, M. W., FRIESS, H., BUCHLER, P. & HERR, I. 2008. VEGF expression by mesenchymal stem cells contributes to angiogenesis in pancreatic carcinoma. *Br J Cancer,* 99**,** 622-31.

BELOV, A. A. & MOHAMMADI, M. 2013. Molecular mechanisms of fibroblast growth factor signaling in physiology and pathology. *Cold Spring Harb Perspect Biol,* 5.

BENTLEY, K., FRANCO, C. A., PHILIPPIDES, A., BLANCO, R., DIERKES, M., GEBALA, V., STANCHI, F., JONES, M., ASPALTER, I. M., CAGNA, G., WESTROM, S., CLAESSON-WELSH, L., VESTWEBER, D. & GERHARDT, H. 2014. The role of differential VE-cadherin dynamics in cell rearrangement during angiogenesis. *Nat Cell Biol,* 16**,** 309-21.

BERCHTOLD, D., FESSER, S., BACHMANN, G., KAISER, A., EILERT, J. C., FROHNS, F., SADONI, N., MUCK, J., KREMMER, E., EICK, D., LAYER, P. G. & ZINK, D. 2011. Nuclei of chicken neurons in tissues and three-

dimensional cell cultures are organized into distinct radial zones. *Chromosome Res,* 19**,** 165-82.

BERTI, L., VANNINI, F., LULLINI, G., CARAVAGGI, P., LEARDINI, A. & GIANNINI, S. 2013. Functional evaluation of patients treated with osteochondral allograft transplantation for post-traumatic ankle arthritis: one year follow-up. *Gait Posture,* 38**,** 945-50.

BHANG, S. H., LEE, S., LEE, T. J., LA, W. G., YANG, H. S., CHO, S. W. & KIM, B. S. 2012a. Three-dimensional cell grafting enhances the angiogenic efficacy of human umbilical vein endothelial cells. *Tissue Eng Part A,* 18**,** 310-9.

BHANG, S. H., LEE, S., SHIN, J. Y., LEE, T. J. & KIM, B. S. 2012b. Transplantation of cord blood mesenchymal stem cells as spheroids enhances vascularization. *Tissue engineering. Part A,* 18**,** 2138-47.

BILODEAU, K. & MANTOVANI, D. 2006. Bioreactors for tissue engineering: focus on mechanical constraints. A comparative review. *Tissue Eng,* 12**,** 2367-83.

BLASI, A., MARTINO, C., BALDUCCI, L., SALDARELLI, M., SOLETI, A., NAVONE, S. E., CANZI, L., CRISTINI, S., INVERNICI, G., PARATI, E. A. & ALESSANDRI, G. 2011. Dermal fibroblasts display similar phenotypic and differentiation capacity to fat-derived mesenchymal stem cells, but differ in anti-inflammatory and angiogenic potential. *Vasc Cell,* 3**,** 5.

BOTHAM, C. M., BENNETT, W. L. & COOKE, J. P. 2013. Clinical trials of adult stem cell therapy for peripheral artery disease. *Methodist Debakey Cardiovasc J,* 9**,** 201-5.

BRADLEY, A. 1990. Embryonic stem cells: proliferation and differentiation. *Curr Opin Cell Biol,* 2**,** 1013-7.

BRANDI, M. L. & COLLIN-OSDOBY, P. 2006. Vascular biology and the skeleton. *J Bone Miner Res,* 21**,** 183-92.

BRENNAN, M. A., RENAUD, A., GAMBLIN, A. L., D'ARROS, C., NEDELLEC, S., TRICHET, V. & LAYROLLE, P. 2015. 3D cell culture and osteogenic differentiation of human bone marrow stromal cells plated onto jet-sprayed or electrospun micro-fiber scaffolds. *Biomed Mater,* 10**,** 1748-6041.

BUDIRAHARJO, R., NEOH, K. G. & KANG, E. T. 2013. Enhancing bioactivity of chitosan film for osteogenesis and wound healing by covalent immobilization of BMP-2 or FGF-2. *Journal of biomaterial science, Polymer edition,* 24**,** 645-62.

BURCH, M. G., PEPE, G. J., DOBRIAN, A. D., LATTANZIO, F. A., JR. & ALBRECHT, E. D. 2005. Development of a coculture system and use of confocal laser fluorescent microscopy to study human microvascular endothelial cell and mural cell interaction. *Microvasc Res,* 70**,** 43-52.

BUSSER, H., NAJAR, M., RAICEVIC, G., PIETERS, K., VELEZ, P., PHILIPPART, P., MEULEMAN, N., BRON, D. & LAGNEAUX, L. 2015. Isolation and characterisation of human mesenchymal stromal cells subpopulations: comparison of bone marrow and adipose tissue. *Stem cells and development,* Ahead of print.

CAMPAGNOLA, P. 2011. Second harmonic generation imaging microscopy: applications to diseases diagnostics. *Anal Chem,* 83**,** 3224-31.

CASEY, R. C., BURLESON, K. M., SKUBITZ, K. M., PAMBUCCIAN, S. E., OEGEMA, T. R., JR., RUFF, L. E. & SKUBITZ, A. P. 2001. Beta 1-integrins regulate the formation and adhesion of ovarian carcinoma multicellular spheroids. *Am J Pathol,* 159**,** 2071-80.

CHA, H. M., KIM, S. M., CHOI, Y. S. & KIM, D. I. 2015. Scaffold-free three-dimensional culture systems for mass production of periosteum-derived progenitor cells. *J Biosci Bioeng,* 120**,** 218-22.

CHAN, C. K., CHEN, C. C., LUPPEN, C. A., KIM, J. B., DEBOER, A. T., WEI, K., HELMS, J. A., KUO, C. J., KRAFT, D. L. & WEISSMAN, I. L. 2009. Endochondral ossification is required for haematopoietic stem-cell niche formation. *Nature,* 457**,** 490-4.

CHAN, J. K. & GOTHERSTROM, C. 2014. Prenatal transplantation of mesenchymal stem cells to treat osteogenesis imperfecta. *Front Pharmacol,* 5.

CHANDRASEKHAR, S., HARVEY, A. K., JOHNSON, M. G. & BECKER, G. W. 1994. Osteonectin/SPARC is a product of articular chondrocytes/cartilage and is regulated by cytokines and growth factors. *Biochim Biophys Acta,* 10**,** 7-14.

CHANG, L., WONG, F., NIESSEN, K. & KARSAN, A. 2013a. Notch activation promotes endothelial survival through a PI3K-Slug axis. *Microvasc Res,* 89**,** 80-5.

CHANG, P. Y., CHEN, Y. J., CHANG, F. H., LU, J., HUANG, W. H., YANG, T. C., LEE, Y. T., CHANG, S. F., LU, S. C. & CHEN, C. H. 2013b. Aspirin protects human coronary artery endothelial cells against atherogenic electronegative LDL via an epigenetic mechanism: a novel cytoprotective role of aspirin in acute myocardial infarction. *Cardiovasc Res,* 99**,** 137-45.

CHEN, C. P., SU, Y. N., LIN, T. H., CHANG, T. Y., SU, J. W. & WANG, W. 2013a. Detection of a de novo Y278C mutation in FGFR3 in a pregnancy with severe fetal hypochondroplasia: prenatal diagnosis and literature review. *Taiwan J Obstet Gynecol,* 52**,** 580-5.

CHEN, D. Y., WEI, H. J., LIN, K. J., HUANG, C. C., WANG, C. C., WU, C. T., CHAO, K. T., CHEN, K. J., CHANG, Y. & SUNG, H. W. 2013b. Three-dimensional cell aggregates composed of HUVECs and cbMSCs for therapeutic neovascularization in a mouse model of hindlimb ischemia. *Biomaterials,* 34**,** 1995-2004.

CHEN, H., BAI, J., YE, J., LIU, Z., CHEN, R., MAO, W., LI, A. & ZHOU, J. 2007. JWA as a functional molecule to regulate cancer cells migration via MAPK cascades and F-actin cytoskeleton. *Cell Signal,* 19**,** 1315-27.

CHEN, S., LEWALLEN, M. & XIE, T. 2013c. Adhesion in the stem cell niche: biological roles and regulation. *Development,* 140**,** 255-65.

CHEN, X., NADIARYNKH, O., PLOTNIKOV, S. & CAMPAGNOLA, P. J. 2012. Second harmonic generation microscopy for quantitative analysis of collagen fibrillar structure. *Nature protocols,* 7**,** 654-69.

CHIEW, G. G., FU, A., LOW, K. P. & LUO, K. Q. 2015. Physical supports from liver cancer cells are essential for differentiation and remodeling of

endothelial cells in a HepG2-HUVEC co-culture model. *Scientific reports,* 5.

CHUNG, J. H., KIM, Y. S., NOH, K., LEE, Y. M., CHANG, S. W. & KIM, E. C. 2013. Deferoxamine promotes osteoblastic differentiation in human periodontal ligament cells via the nuclear factor erythroid 2-related factor-mediated antioxidant signaling pathway. *J Periodontal Res.*

COLCIAGO, A., CELOTTI, F., CASATI, L., GIANCOLA, R., CASTANO, S. M., ANTONINI, G., SACCHI, M. C. & NEGRI-CESI, P. 2009. In Vitro Effects of PDGF Isoforms (AA, BB, AB and CC) on Migration and Proliferation of SaOS-2 Osteoblasts and on Migration of Human Osteoblasts. *Int J Biomed Sci,* 5**,** 380-9.

COLLINS, C. & NELSON, W. J. 2015. Running with neighbors: coordinating cell migration and cell-cell adhesion. *Curr Opin Cell Biol,* 36**,** 62-70.

COLMONE, A. & SIPKINS, D. A. 2008. Beyond angiogenesis: the role of endothelium in the bone marrow vascular niche. *Translational research : the journal of laboratory and clinical medicine,* 151**,** 1-9.

COLOMBO, J. S., HOWARD-JONES, R. A., YOUNG, F. I., WADDINGTON, R. J., ERRINGTON, R. J. & SLOAN, A. J. 2015. A 3D ex vivo mandible slice system for longitudinal culturing of transplanted dental pulp progenitor cells. *Cytometry. Part A : the journal of the International Society for Analytical Cytology,* 87**,** 921-8.

COOK, D. & GENEVER, P. 2013. Regulation of mesenchymal stem cell differentiation. *Adv Exp Med Biol,* 786**,** 213-29.

CORDEIRO-SPINETTI, E., TAICHMAN, R. S. & BALDUINO, A. 2015. The bone marrow endosteal niche: how far from the surface? *J Cell Biochem,* 116**,** 6-11.

COULTAS, L., CHAWENGSAKSOPHAK, K. & ROSSANT, J. 2005. Endothelial cells and VEGF in vascular development. *Nature,* 438**,** 937-945.

CRISAN, M., YAP, S., CASTEILLA, L., CHEN, C. W., CORSELLI, M., PARK, T. S., ANDRIOLO, G., SUN, B., ZHENG, B., ZHANG, L., NOROTTE, C., TENG, P. N., TRAAS, J., SCHUGAR, R., DEASY, B. M., BADYLAK, S., BUHRING, H. J., GIACOBINO, J. P., LAZZARI, L., HUARD, J. & PEAULT, B. 2008. A perivascular origin for mesenchymal stem cells in multiple human organs. *Cell Stem Cell,* 3**,** 301-13.

DAI, J. & CHURG, A. 2001. Relationship of fiber surface iron and active oxygen species to expression of procollagen, PDGF-A, and TGF-beta(1) in tracheal explants exposed to amosite asbestos. *Am J Respir Cell Mol Biol,* 24**,** 427-35.

DE LOS SANTOS, C., CHANG, C. W., MYCEK, M. A. & CARDULLO, R. A. 2015. FRAP, FLIM, and FRET: Detection and analysis of cellular dynamics on a molecular scale using fluorescence microscopy. *Mol Reprod Dev.*

DE MUNTER, J. P. & WOLTERS, E. C. 2013. Autologous stem cells in neurology: is there a future? *J Neural Transm,* 120**,** 65-73.

DI ROCCO, F., BIOSSE DUPLAN, M., HEUZE, Y., KACI, N., KOMLA-EBRI, D., MUNNICH, A., MUGNIERY, E., BENOIST-LASSELIN, C. & LEGEAI-

MALLET, L. 2014. FGFR3 mutation causes abnormal membranous ossification in achondroplasia. *Hum Mol Genet,* 23**,** 2914-25.

DICKSON, K., KATZMAN, S., DELGADO, E. & CONTRERAS, D. 1994. Delayed unions and nonunions of open tibial fractures. Correlation with arteriography results. *Clinical orthopaedics and related research,* 302**,** 189-93.

DOMBROWSKI, C., HELLEDIE, T., LING, L., GRUNERT, M., CANNING, C. A., JONES, C. M., HUI, J. H., NURCOMBE, V., VAN WIJNEN, A. J. & COOL, S. M. 2013. FGFR1 signaling stimulates proliferation of human mesenchymal stem cells by inhibiting the cyclin-dependent kinase inhibitors p21(Waf1) and p27(Kip1). *Stem cells,* 31**,** 2724-36.

DONG, A., SEIDEL, C., SNELL, D., EKAWARDHANI, S., AHLSKOG, J. K., BAUMANN, M., SHEN, J., IWASE, T., TIAN, J., STEVENS, R., HACKETT, S. F., STUMPP, M. T. & CAMPOCHIARO, P. A. 2014. Antagonism of PDGF-BB suppresses subretinal neovascularization and enhances the effects of blocking VEGF-A. *Angiogenesis,* 17**,** 553-62.

DONG, Z., IMAI, A., KRISHNAMURTHY, S., ZHANG, Z., ZEITLIN, B. D. & NOR, J. E. 2013. Xenograft tumors vascularized with murine blood vessels may overestimate the effect of anti-tumor drugs: a pilot study. *PLoS One,* 8**,** e84236.

DOREY, K. & AMAYA, E. 2010. FGF signalling: diverse roles during early vertebrate embryogenesis. *Development,* 137**,** 3731-42.

DOS SANTOS, C., BLANC, C., ELAHOUEL, R., PRESCOTT, M., CARPENTIER, G., ORI, A., COURTY, J., HAMMA-KOURBALI, Y., FERNIG, D. G. & DELBÉ, J. 2014. Proliferation and migration activities of fibroblast growth factor-2 in endothelial cells are modulated by its direct interaction with heparin affin regulatory peptide. *Biochimie,* 107, Part B**,** 350-357.

DUGUAY, D., FOTY, R. A. & STEINBERG, M. S. 2003. Cadherin-mediated cell adhesion and tissue segregation: qualitative and quantitative determinants. *Developmental Biology,* 253**,** 309-323.

DURAY, P. H., HATFILL, S. J. & PELLIS, N. R. 1997. Tissue culture in microgravity. *Sci Med,* 4**,** 46-55.

DVORAKOVA, J., HRUBA, A., VELEBNY, V. & KUBALA, L. 2008. Isolation and characterization of mesenchymal stem cell population entrapped in bone marrow collection sets. *Cell Biology International,* 32**,** 1116-1125.

EGLOFF, A. M. & GRANDIS, J. R. 2012. Molecular pathways: context-dependent approaches to Notch targeting as cancer therapy. *Clin Cancer Res,* 18**,** 5188-95.

EL-GENDY, R., YANG, X. B., NEWBY, P. J., BOCCACCINI, A. R. & KIRKHAM, J. 2013. Osteogenic differentiation of human dental pulp stromal cells on 45S5 Bioglass(R) based scaffolds in vitro and in vivo. *Tissue engineering. Part A,* 19**,** 707-15.

EVANS, M. J. & KAUFMAN, M. H. 1981. Establishment in culture of pluripotent cells from mouse embryos. *Nature,* 292**,** 154-156.

FAN, L., YU, Z., LI, J., DANG, X. & WANG, K. 2014. Schwann-like cells seeded in acellular nerve grafts improve nerve regeneration. *BMC musculoskeletal disorders,* 15**,** 1471-2474.

FARRELL, E., BOTH, S. K., ODORFER, K. I., KOEVOET, W., KOPS, N., O'BRIEN, F. J., BAATENBURG DE JONG, R. J., VERHAAR, J. A., CUIJPERS, V., JANSEN, J., ERBEN, R. G. & VAN OSCH, G. J. 2011. In-vivo generation of bone via endochondral ossification by in-vitro chondrogenic priming of adult human and rat mesenchymal stem cells. *BMC musculoskeletal disorders,* 12**,** 31.

FENSKY, F., REICHERT, J. C., TRAUBE, A., RACKWITZ, L., SIEBENLIST, S. & NOTH, U. 2014. Chondrogenic predifferentiation of human mesenchymal stem cells in collagen type I hydrogels. *Biomed Tech,* 59**,** 375-83.

FINDLAY, D. M. 2007. Vascular pathology and osteoarthritis. *Rheumatology,* 46**,** 1763-8.

FONS, P., GUEGUEN-DORBES, G., HERAULT, J. P., GERONIMI, F., TUYARET, J., FREDERIQUE, D., SCHAEFFER, P., VOLLE-CHALLIER, C., HERBERT, J. M. & BONO, F. 2015. Tumor vasculature is regulated by FGF/FGFR signaling-mediated angiogenesis and bone marrow-derived cell recruitment: this mechanism is inhibited by SSR128129E, the first allosteric antagonist of FGFRs. *J Cell Physiol,* 230**,** 43-51.

FOTY, R. A. & STEINBERG, M. S. 2005. The differential adhesion hypothesis: a direct evaluation. *Developmental Biology,* 278**,** 255-63.

FRIEDENSTEIN, A. J., GORSKAJA, U. F. & KULAGINA, N. N. 1976. FIBROBLAST PRECURSORS IN NORMAL AND IRRADIATED MOUSE HEMATOPOIETIC ORGANS. *Experimental Hematology,* 4**,** 267-274.

FURDUI, C. M., LEW, E. D., SCHLESSINGER, J. & ANDERSON, K. S. 2006. Autophosphorylation of FGFR1 kinase is mediated by a sequential and precisely ordered reaction. *Mol Cell,* 21**,** 711-7.

GALE, N. W., DOMINGUEZ, M. G., NOGUERA, I., PAN, L., HUGHES, V., VALENZUELA, D. M., MURPHY, A. J., ADAMS, N. C., LIN, H. C., HOLASH, J., THURSTON, G. & YANCOPOULOS, G. D. 2004. Haploinsufficiency of delta-like 4 ligand results in embryonic lethality due to major defects in arterial and vascular development. *Proceedings of the National Academy of Sciences of the United States of America,* 101**,** 15949-54.

GARCIA-JEREZ, A., LUENGO, A., CARRACEDO, J., RAMIREZ-CHAMOND, R., RODRIGUEZ-PUYOL, D., RODRIGUEZ-PUYOL, M. & CALLEROS, L. 2015. Effect of uraemia on endothelial cell damage is mediated by the integrin linked kinase pathway. *J Physiol,* 593**,** 601-18.

GEIGER, F., BERTRAM, H., BERGER, I., LORENZ, H., WALL, O., ECKHARDT, C., SIMANK, H. G. & RICHTER, W. 2005. Vascular endothelial growth factor gene-activated matrix (VEGF165-GAM) enhances osteogenesis and angiogenesis in large segmental bone defects. *J Bone Miner Res,* 20**,** 2028-35.

GENOVESE, J. A., SPADACCIO, C., CHACHQUES, E., SCHUSSLER, O., CARPENTIER, A., CHACHQUES, J. C. & PATEL, A. N. 2009. Cardiac

pre-differentiation of human mesenchymal stem cells by electrostimulation. *Front Biosci,* 14**,** 2996-3002.

GERSHOVICH, J. G., DAHLIN, R. L., KASPER, F. K. & MIKOS, A. G. 2013. Enhanced Osteogenesis in Cocultures with Human Mesenchymal Stem Cells and Endothelial Cells on Polymeric Microfiber Scaffolds. *Tissue engineering. Part A.*

GESS, B., HALFTER, H., KLEFFNER, I., MONJE, P., ATHAUDA, G., WOOD, P. M., YOUNG, P. & WANNER, I. B. 2008. Inhibition of N-cadherin and beta-catenin function reduces axon-induced Schwann cell proliferation. *Journal of neuroscience research,* 86**,** 797-812.

GHAJAR, C. M., PEINADO, H., MORI, H., MATEI, I. R., EVASON, K. J., BRAZIER, H., ALMEIDA, D., KOLLER, A., HAJJAR, K. A., STAINIER, D. Y., CHEN, E. I., LYDEN, D. & BISSELL, M. J. 2013. The perivascular niche regulates breast tumour dormancy. *Nat Cell Biol,* 15**,** 807-17.

GIMBRONE, M. A., LEAPMAN, S. B., COTRAN, R. S. & FOLKMAN, J. 1972. Tumour dormancy in vivo by prevention of neovascularization. *The Journal of Experimental Medicine,* 136**,** 261-277.

GOESSLER, U. R., BIEBACK, K., BUGERT, P., HELLER, T., SADICK, H., HORMANN, K. & RIEDEL, F. 2006. In vitro analysis of integrin expression during chondrogenic differentiation of mesenchymal stem cells and chondrocytes upon dedifferentiation in cell culture. *Int J Mol Med,* 17**,** 301-7.

GOESSLER, U. R., BUGERT, P., BIEBACK, K., STERN-STRAETER, J., BRAN, G., SADICK, H., HORMANN, K. & RIEDEL, F. 2009. In vitro analysis of integrin expression in stem cells from bone marrow and cord blood during chondrogenic differentiation. *J Cell Mol Med,* 13**,** 1175-84.

GOTOH, N. 2008. Regulation of growth factor signaling by FRS2 family docking/scaffold adaptor proteins. *Cancer science,* 99**,** 1319-25.

GRANCHI, D., DEVESCOVI, V., BAGLIO, S. R., MAGNANI, M., DONZELLI, O. & BALDINI, N. 2012. A regenerative approach for bone repair in congenital pseudarthrosis of the tibia associated or not associated with type 1 neurofibromatosis: correlation between laboratory findings and clinical outcome. *Cytotherapy,* 14**,** 306-14.

GRAYSON, W. L., BHUMIRATANA, S., GRACE CHAO, P. H., HUNG, C. T. & VUNJAK-NOVAKOVIC, G. 2010. Spatial regulation of human mesenchymal stem cell differentiation in engineered osteochondral constructs: effects of pre-differentiation, soluble factors and medium perfusion. *Osteoarthritis and cartilage / OARS, Osteoarthritis Research Society,* 18**,** 714-23.

GREENBAUM, A., HSU, Y. M., DAY, R. B., SCHUETTPELZ, L. G., CHRISTOPHER, M. J., BORGERDING, J. N., NAGASAWA, T. & LINK, D. C. 2013. CXCL12 in early mesenchymal progenitors is required for haematopoietic stem-cell maintenance. *Nature,* 495**,** 227-30.

GUETTIER, C. 2005. Which stem cells for adult liver? *Annales De Pathologie,* 25**,** 33-44.

GUO, X., PARK, H., LIU, G., LIU, W., CAO, Y., TABATA, Y., KASPER, F. K. & MIKOS, A. G. 2009. In vitro generation of an osteochondral construct

using injectable hydrogel composites encapsulating rabbit marrow mesenchymal stem cells. *Biomaterials,* 30**,** 2741-52.

HADDAD, L., EL HAJJ, H., ABOU-MERHI, R., KFOURY, Y., MAHIEUX, R., EL-SABBAN, M. & BAZARBACHI, A. 2008. KSHV-transformed primary effusion lymphoma cells induce a VEGF-dependent angiogenesis and establish functional gap junctions with endothelial cells. *Leukemia : official journal of the Leukemia Society of America, Leukemia Research Fund, U.K,* 22**,** 826-34.

HARAGOPAL, H., YU, D., ZENG, X., KIM, S. W., HAN, I. B., ROPPER, A. E., ANDERSON, J. E. & TENG, Y. D. 2015. Stemness enhancement of human neural stem cells following bone marrow MSC coculture. *Cell Transplant,* 24**,** 645-59.

HARDINGHAM, T. E., OLDERSHAW, R. A. & TEW, S. R. 2006. Cartilage, SOX9 and Notch signals in chondrogenesis. *J Anat,* 209**,** 469-80.

HASS, R., KASPER, C., BÖHM, S. & JACOBS, R. 2011. Different populations and sources of human mesenchymal stem cells (MSC): A comparison of adult and neonatal tissue-derived MSC. *Cell Communication and Signaling,* 9**,** 12.

HATANAKA, K., LANAHAN, A. A., MURAKAMI, M. & SIMONS, M. 2012. Fibroblast growth factor signaling potentiates VE-cadherin stability at adherens junctions by regulating SHP2. *PLoS One,* 7**,** 22.

HAUG, V., TORIO-PADRON, N., STARK, G. B., FINKENZELLER, G. & STRASSBURG, S. 2015. Comparison between endothelial progenitor cells and human umbilical vein endothelial cells on neovascularization in an adipogenesis mouse model. *Microvasc Res,* 97**,** 159-66.

HAYCOCK, J. W. 2011. 3D cell culture: a review of current approaches and techniques. *Methods Mol Biol,* 695**,** 1-15.

HELDIN, C. H. & WESTMARK, B. 1999. Mechanism of Action and In Vivo Role of Platelet-Derived Growth Factor. *Physiological reviews,* 79**,** 1283-1316.

HENGARTNER, N. E., FIEDLER, J., IGNATIUS, A. & BRENNER, R. E. 2013. IL-1beta inhibits human osteoblast migration. *Mol Med,* 19**,** 36-42.

HENNING, R. J., DENNIS, S., SAWMILLER, D., HUNTER, L., SANBERG, P. & MILLER, L. 2012. Human umbilical cord blood mononuclear cells activate the survival protein Akt in cardiac myocytes and endothelial cells that limits apoptosis and necrosis during hypoxia. *Translational research : the journal of laboratory and clinical medicine,* 159**,** 497-506.

HILDEBRANDT, C., BÜTH, H. & THIELECKE, H. 2011. A scaffold-free in vitro model for osteogenesis of human mesenchymal stem cells. *Tissue and Cell,* 43**,** 91-100.

HILL-FELBERG, S., WU, H. H., TOMS, S. A. & DEHDASHTI, A. R. 2015. Notch receptor expression in human brain arteriovenous malformations. *J Cell Mol Med,* 19**,** 1986-93.

HO, I. A. W., TOH, H. C., NG, W. H., TEO, Y. L., GUO, C. M., HUI, K. M. & LAM, P. Y. P. 2013. Human Bone Marrow-Derived Mesenchymal Stem Cells Suppress Human Glioma Growth Through Inhibition of Angiogenesis. *Stem cells,* 31**,** 146-155.

HONG, S., ALAPURE, B. V., LU, Y., TIAN, H. & WANG, Q. 2014. Immunohistological localization of endogenous unlabeled stem cells in wounded skin. *J Histochem Cytochem,* 62**,** 276-85.

HOWARD, J. D., MORIARTY, W. F., PARK, J., RIEDY, K., PANOVA, I. P., CHUNG, C. H., SUH, K. Y., LEVCHENKO, A. & ALANI, R. M. 2013. Notch signaling mediates melanoma-endothelial cell communication and melanoma cell migration. *Pigment Cell Melanoma Res,* 26**,** 697-707.

HSU, E. C., KULP, S. K., HUANG, H. L., TU, H. J., SALUNKE, S. B., SULLIVAN, N. J., SUN, D., WICHA, M. S., SHAPIRO, C. L. & CHEN, C. S. 2015. Function of Integrin-Linked Kinase in Modulating the Stemness of IL-6-Abundant Breast Cancer Cells by Regulating gamma-Secretase-Mediated Notch1 Activation in Caveolae. *Neoplasia,* 17**,** 497-508.

HUI, E. E. & BHATIA, S. N. 2007. Micromechanical control of cell-cell interactions. *Proceedings of the National Academy of Sciences of the United States of America,* 104**,** 5722-6.

IKEDA, Y., TAJIMA, S., YOSHIDA, S., YAMANO, N., KIHIRA, Y., ISHIZAWA, K., AIHARA, K., TOMITA, S., TSUCHIYA, K. & TAMAKI, T. 2011. Deferoxamine promotes angiogenesis via the activation of vascular endothelial cell function. *Atherosclerosis,* 215**,** 339-47.

IM, G. I., SHIN, Y. W. & LEE, K. B. 2005. Do adipose tissue-derived mesenchymal stem cells have the same osteogenic and chondrogenic potential as bone marrow-derived cells? *Osteoarthritis and cartilage / OARS, Osteoarthritis Research Society,* 13**,** 845-53.

IMAIZUMI, T., ITAYA, H., NASU, S., YOSHIDA, H., MATSUBARA, Y., FUJIMOTO, K., MATSUMIYA, T., KIMURA, H. & SATOH, K. 2000. Expression of vascular endothelial growth factor in human umbilical vein endothelial cells stimulated with interleukin-1alpha -- and autocrine regulation of angiogenesis and inflammatory reactions. *Thrombosis and Haemostasis,* 83**,** 949-55.

INTRONA, M., LUCCHINI, G., DANDER, E., GALIMBERTI, S., ROVELLI, A., BALDUZZI, A., LONGONI, D., PAVAN, F., MASCIOCCHI, F., ALGAROTTI, A., MICO, C., GRASSI, A., DEOLA, S., CAVATTONI, I., GAIPA, G., BELOTTI, D., PERSEGHIN, P., PARMA, M., POGLIANI, E., GOLAY, J., PEDRINI, O., CAPELLI, C., CORTELAZZO, S., D'AMICO, G., BIONDI, A., RAMBALDI, A. & BIAGI, E. 2014. Treatment of graft versus host disease with mesenchymal stromal cells: a phase I study on 40 adult and pediatric patients. *Biol Blood Marrow Transplant,* 20**,** 375-81.

ITO, T., SAWADA, R., FUJIWARA, Y. & TSUCHIYA, T. 2008. FGF-2 increases osteogenic and chondrogenic differentiation potentials of human mesenchymal stem cells by inactivation of TGF-beta signaling. *Cytotechnology,* 56**,** 1-7.

IVASCU, A. & KUBBIES, M. 2006. Rapid generation of single-tumor spheroids for high-throughput cell function and toxicity analysis. *J Biomol Screen,* 11**,** 922-32.

IVERS, L. P., CUMMINGS, B., OWOLABI, F., WELZEL, K., KLINGER, R., SAITOH, S., O'CONNOR, D., FUJITA, Y., SCHOLZ, D. & ITASAKI, N.

2014. Dynamic and influential interaction of cancer cells with normal epithelial cells in 3D culture. *Cancer Cell Int,* 14**,** 014-0108.

IWANIEC, U. T., MOSEKILDE, L., MITOVA-CANEVA, N. G., THOMSEN, J. S. & WRONSKI, T. J. 2002. Sequential treatment with basic fibroblast growth factor and PTH is more efficacious than treatment with PTH alone for increasing vertebral bone mass and strength in osteopenic ovariectomized rats. *Endocrinology,* 143**,** 2515-26.

JAGER, W., HORIGUCHI, Y., SHAH, J., HAYASHI, T., AWREY, S., GUST, K. M., HADASCHIK, B. A., MATSUI, Y., ANDERSON, S., BELL, R. H., ETTINGER, S., SO, A. I., GLEAVE, M. E., LEE, I. L., DINNEY, C. P., TACHIBANA, M., MCCONKEY, D. J. & BLACK, P. C. 2013. Hiding in plain view: genetic profiling reveals decades old cross contamination of bladder cancer cell line KU7 with HeLa. *J Urol,* 190**,** 1404-9.

JANICKI, P., KASTEN, P., KLEINSCHMIDT, K., LUGINBUEHL, R. & RICHTER, W. 2010. Chondrogenic pre-induction of human mesenchymal stem cells on beta-TCP: enhanced bone quality by endochondral heterotopic bone formation. *Acta biomaterialia,* 6**,** 3292-301.

JAVERZAT, S., AUGUSTE, P. & BIKFALVI, A. 2002. The role of fibroblast growth factors in vascular development. *Trends in Molecular Medicine,* 8**,** 483-489.

JI, J., SUN, W., WANG, W., MUNYOMBWE, T. & YANG, X. B. 2014. The effect of mechanical loading on osteogenesis of human dental pulp stromal cells in a novel in vitro model. *Cell Tissue Res,* 358**,** 123-33.

JOHNSON, D. E. & WILLIAMS, L. T. 1993. Structural and functional diversity in the FGF receptor multigene family. *Adv Cancer Res,* 60**,** 1-41.

JONES, E. A., KINSEY, S. E., ENGLISH, A., JONES, R. A., STRASZYNSKI, L., MEREDITH, D. M., MARKHAM, A. F., JACK, A., EMERY, P. & MCGONAGLE, D. 2002. Isolation and characterization of bone marrow multipotential mesenchymal progenitor cells. *Arthritis & Rheumatism,* 46**,** 3349-3360.

JONES, E. Y. 2000. *Understanding cell signalling systems: paving the way for new therapies*, Philos Trans A Math Phys Eng Sci. 2015 Mar 6;373(2036). pii: 20130155.

JØRGENSEN, N. R., HENRIKSEN, Z., SØRENSEN, O. H. & CIVITELLI, R. 2004. Dexamethasone, BMP-2, and 1,25-dihydroxyvitamin D enhance a more differentiated osteoblast phenotype: validation of an in vitro model for human bone marrow-derived primary osteoblasts. *Steroids,* 69**,** 219-226.

JUHASOVA, J., JUHAS, S., KLIMA, J., STRNADEL, J., HOLUBOVA, M. & MOTLIK, J. 2011. Osteogenic differeniation of miniature pig mesenchymal stem cells in 2D and 3D environment. *Physiological research,* 60**,** 559-71.

KALRA, J., DRAGOWSKA, W. H. & BALLY, M. B. 2015. Using Pharmacokinetic Profiles and Digital Quantification of Stained Tissue Microarrays as a Medium-Throughput, Quantitative Method for Measuring the Kinetics of Early Signaling Changes Following Integrin-Linked Kinase Inhibition in an In Vivo Model of Cancer. *J Histochem Cytochem,* 63**,** 691-709.

KANG, N. H., HWANG, K. A., KIM, S. U., KIM, Y. B., HYUN, S. H., JEUNG, E. B. & CHOI, K. C. 2012. Potential antitumor therapeutic strategies of human amniotic membrane and amniotic fluid-derived stem cells. *Cancer Gene Ther,* 19**,** 517-22.

KARP, J. M. & LENG TEO, G. S. 2009. Mesenchymal Stem Cell Homing: The Devil Is in the Details. *Cell Stem Cell,* 4**,** 206-216.

KATOH, M. 2002. WNT and FGF gene clusters (review). *Int J Oncol,* 21**,** 1269-73.

KEATING, A. 2012. Mesenchymal stromal cells: new directions. *Cell Stem Cell,* 10**,** 709-16.

KERR, C. L., SHAMBLOTT, M. J. & GEARHART, J. D. 2006. Pluripotent Stem Cells from Germ Cells. *Methods in Enzymology,* 419**,** 400-426.

KERR, G., SHELDON, H., CHAIKUAD, A., ALFANO, I., VON DELFT, F., BULLOCK, A. N. & HARRIS, A. L. 2015. A small molecule targeting ALK1 prevents Notch cooperativity and inhibits functional angiogenesis. *Angiogenesis,* 18**,** 209-17.

KEUNG, A. J., HEALY, K. E., KUMAR, S. & SCHAFFER, D. V. 2010. Biophysics and dynamics of natural and engineered stem cell microenvironments. *Wiley Interdisciplinary Reviews: Systems Biology and Medicine,* 2**,** 49-64.

KIM, H., HUANG, L., CRITSER, P. J., YANG, Z., CHAN, R. J., WANG, L., CARLESSO, N., VOYTIK-HARBIN, S. L., BERNSTEIN, I. D. & YODER, M. C. 2015. Notch ligand Delta-like 1 promotes in vivo vasculogenesis in human cord blood-derived endothelial colony forming cells. *Cytotherapy,* 17**,** 579-92.

KIM, J. M., SHIN, H. I., CHA, S. S., LEE, C. S., HONG, B. S., LIM, S., JANG, H. J., KIM, J., YANG, Y. R., KIM, Y. H., YUN, S., RIJAL, G., LEE-KWON, W., SEO, J. K., GHO, Y. S., RYU, S. H., HUR, E. M. & SUH, P. G. 2012. DJ-1 promotes angiogenesis and osteogenesis by activating FGF receptor-1 signaling. *Nat Commun,* 3**,** 1296.

KLIMANSKAYA, I. 2013. Embryonic stem cells from blastomeres maintaining embryo viability. *Semin Reprod Med,* 31**,** 49-55.

KNIGHTON, D., AUSPRUNK, D., TAPPER, D. & FOLKMAN, J. 1977. Avascular and vascular phases of tumour growth in the chick embryo. *British Journal of Cnacner,* 35.

KNISS, D. A. & SUMMERFIELD, T. L. 2014. Discovery of HeLa Cell Contamination in HES Cells: Call for Cell Line Authentication in Reproductive Biology Research. *Reprod Sci,* 21**,** 1015-1019.

KOGA, T., NIIKURA, T., LEE, S. Y., DOGAKI, Y., OKUMACHI, E., NISHIDA, K., KURODA, R. & KUROSAKA, M. 2013. In vitro hypertrophy and calcification of human fracture haematoma-derived cells in chondrogenic differentiation. *International orthopaedics,* 37**,** 961-7.

KOLLAR, K., SEIFRIED, E. & HENSCHLER, R. 2011. Therapeutic potential of intravenously administered human mesenchymal stromal cells. *Hamostaseologie,* 31**,** 269-74.

KOOB, S., TORIO-PADRON, N., STARK, G. B., HANNIG, C., STANKOVIC, Z. & FINKENZELLER, G. 2011. Bone formation and neovascularization

mediated by mesenchymal stem cells and endothelial cells in critical-sized calvarial defects. *Tissue engineering. Part A,* 17**,** 311-21.

KOPP, H. G. & RAFII, S. 2007. Thrombopoietic cells and the bone marrow vascular niche. *Annals of the New York Academy of Sciences,* 1106**,** 175-9.

KRAMPERA, M., MARCONI, S., PASINI, A., GALIÈ, M., RIGOTTI, G., MOSNA, F., TINELLI, M., LOVATO, L., ANGHILERI, E., ANDREINI, A., PIZZOLO, G., SBARBATI, A. & BONETTI, B. 2007. Induction of neural-like differentiation in human mesenchymal stem cells derived from bone marrow, fat, spleen and thymus. *Bone,* 40**,** 382-390.

KRONENBERG, H. M. 2003. Developmental regulation of the growth plate. *Nature,* 15**,** 332-7.

KUHN, L. T., OU, G., CHARLES, L., HURLEY, M. M., RODNER, C. M. & GRONOWICZ, G. 2013. Fibroblast growth factor-2 and bone morphogenetic protein-2 have a synergistic stimulatory effect on bone formation in cell cultures from elderly mouse and human bone. *J Gerontol A Biol Sci Med Sci,* 68**,** 1170-80.

KULAR, J., TICKNER, J., CHIM, S. M. & XU, J. 2012. An overview of the regulation of bone remodelling at the cellular level. *Clin Biochem,* 45**,** 863-73.

KUME, T. 2009. Novel insights into the differential functions of Notch ligands in vascular formation. *J Angiogenes Res,* 1**,** 2040-2384.

KUSUMBE, A. P., RAMASAMY, S. K. & ADAMS, R. H. 2014. Coupling of angiogenesis and osteogenesis by a specific vessel subtype in bone. *Nature,* 507**,** 323-328.

LAJTHA, L. G. 1967. Stem cells and their properties. *Proc Can Cancer Conf,* 7**,** 31-9.

LANCASTER, M. A. & KNOBLICH, J. A. 2014. Organogenesis in a dish: modeling development and disease using organoid technologies. *Science,* 345**,** 17.

LAURENT, J., FRONGIA, C., CAZALES, M., MONDESERT, O., DUCOMMUN, B. & LOBJOIS, V. 2013. Multicellular tumor spheroid models to explore cell cycle checkpoints in 3D. *BMC cancer,* 13**,** 73.

LEE, S. L., HSU, E. C., CHOU, C. C., CHUANG, H. C., BAI, L. Y., KULP, S. K. & CHEN, C. S. 2011. Identification and characterization of a novel integrin-linked kinase inhibitor. *J Med Chem,* 54**,** 6364-74.

LEVORSON, E. J., MOUNTZIARIS, P. M., HU, O., KASPER, F. K. & MIKOS, A. G. 2013. Cell Derived Polymer/Extracellular Matrix Composite Scaffolds for Cartilage Regeneration, Part 1: Investigation of Co-cultures and Seeding Densities for Improved Extracellular Matrix Deposition. *Tissue engineering. Part C, Methods.*

LEWUS, K. E. & NAUMAN, E. A. 2005. In vitro characterization of a bone marroe stem cell-seeded collagen gel composite for soft tissue grafts: effects of fiber number and serum concentration. *Tissue Engineering,* 11**,** 1015-25.

LI, J., MAREDDY, S., TAN, D. W., CRAWFORD, R., LONG, X., MIAO, X. & XIAO, Y. 2009. A minimal common osteochondrocytic differentiation

medium for the osteogenic and chondrogenic differentiation of bone marrow stromal cells in the construction of ostechondral grafts. *Tissue Engineering Part A,* 15**,** 2481-2490.

LI, J., WONG, W. H., CHAN, S., CHIM, J. C., CHEUNG, K. M., LEE, T. L., AU, W. Y., HA, S. Y., LIE, A. K., LAU, Y. L., LIANG, R. H. & CHAN, G. C. 2011. Factors affecting mesenchymal stromal cells yield from bone marrow aspiration. *Chin J Cancer Res,* 23**,** 43-8.

LI, L., ZHOU, Q., VOSS, T. C., QUICK, K. L. & LABARBERA, D. V. 2015. High-throughput imaging: Focusing in on drug discovery in 3D. *Methods,* 20**,** 30154-7.

LIAO, F. L., CHEN, R. L., JIANG, S. & TIAN, C. 2014. [Effect of notch signaling pathway on VEGF promoting rat mesenchymal stem cell proliferation]. *Zhongguo Shi Yan Xue Ye Xue Za Zhi,* 22**,** 1068-71.

LIU, H., KEMENY, D. M., HENG, B. C., OUYANG, H. W., MELENDEZ, A. J. & CAO, T. 2006. The immunogenicity and immunomodulatory function of osteogenic cells differentiated from mesenchymal stem cells. *J Immunol,* 176**,** 2864-71.

LIU, L. Y., HOU, Y. S., CHAI, J. K., HU, Q., DUAN, H. J., YU, Y. H., YIN, H. N., HAO, D. F., FENG, G., LI, T. & DU, J. D. 2013. Basic fibroblast growth factor/vascular endothelial growth factor in the serum from severe burn patients stimulates the proliferation of cultured human umbilical cord mesenchymal stem cells via activation of Notch signaling pathways. *J Trauma Acute Care Surg,* 75**,** 789-97.

LIU, Z., FAN, F., WANG, A., ZHENG, S. & LU, Y. 2014. Dll4-Notch signaling in regulation of tumor angiogenesis. *J Cancer Res Clin Oncol,* 140**,** 525-36.

LLOYD, M. M., GRIMA, M. A., RAYNER, B. S., HADFIELD, K. A., DAVIES, M. J. & HAWKINS, C. L. 2013. Comparative reactivity of the myeloperoxidase-derived oxidants hypochlorous acid and hypothiocyanous acid with human coronary artery endothelial cells. *Free Radic Biol Med,* 65**,** 1352-62.

LONG, T., YANG, J., SHI, S. S., GUO, Y. P., KE, Q. F. & ZHU, Z. A. 2014. Fabrication of three-dimensional porous scaffold based on collagen fiber and bioglass for bone tissue engineering. *J Biomed Mater Res B Appl Biomater,* 27**,** 33328.

LU, J., TANG, Y., FARSHIDPOUR, M., CHENG, Y., ZHANG, G., JAFARNEJAD, S. M., YIP, A., MARTINKA, M., DONG, Z., ZHOU, J., XU, J. & LI, G. 2013. JWA inhibits melanoma angiogenesis by suppressing ILK signaling and is an independent prognostic biomarker for melanoma. *Carcinogenesis,* 34**,** 2778-88.

LU, W., JI, K., KIRKHAM, J., YAN, Y., BOCCACCINI, A. R., KELLETT, M., JIN, Y. & YANG, X. B. 2014. Bone tissue engineering by using a combination of polymer/Bioglass composites with human adipose-derived stem cells. *Cell Tissue Res,* 356**,** 97-107.

LUGINBUEHL, V., MEINEL, L., MERKLE, H. P. & GANDER, B. 2004. Localized delivery of growth factors for bone repair. *European Journal of Pharmaceutics and Biopharmaceutics,* 58**,** 197-208.

LUH, B. S. 1995. Industrial production of soy sauce. *Journal of Industrial Microbiology,* 14**,** 467-471.

MA, J., YANG, F., BOTH, S. K., PRINS, H. J., HELDER, M. N., PAN, J., CUI, F. Z., JANSEN, J. A. & VAN DEN BEUCKEN, J. J. 2014. In vitro and in vivo angiogenic capacity of BM-MSCs/HUVECs and AT-MSCs/HUVECs cocultures. *Biofabrication,* 6**,** 015005.

MAEHARA, H., SOTOME, S., YOSHII, T., TORIGOE, I., KAWASAKI, Y., SUGATA, Y., YUASA, M., HIRANO, M., MOCHIZUKI, N., KIKUCHI, M., SHINOMIYA, K. & OKAWA, A. 2010. Repair of large osteochondral defects in rabbits using porous hydroxyapatite/collagen (HAp/Col) and fibroblast growth factor-2 (FGF-2). *Journal of orthopaedic research : official publication of the Orthopaedic Research Society,* 28**,** 677-86.

MAES, C., CARMELIET, P., MOERMANS, K., STOCKMANS, I., SMETS, N., COLLEN, D., BOUILLON, R. & CARMELIET, G. 2002. Impared angiogenesis and endochondral bone formation in mice lacking the vascular endothalial growth factor isoforms VEGF164 and BEGF188. *Mechanims of Development,* 111**,** 61-73.

MAHAY, D., TERENGHI, G. & SHAWCROSS, S. G. 2008. Schwann cell mediated trophic effects by differentiated mesenchymal stem cells. *Experimental Cell Research,* 314**,** 2692-2701.

MALLADI, P., XU, Y., CHIOU, M., GIACCIA, A. J. & LONGAKER, M. T. 2005. Effect of reduced oxygen tension on chondrogenesis and osteogenesis in adipose-derived mesenchymal cells. *American Journal of Physiology and Cell Physiology,* 290**,** 1339-1146.

MANNA, P. & JAIN, S. K. 2014. Effect of PIP3 on adhesion molecules and adhesion of THP-1 monocytes to HUVEC treated with high glucose. *Cell Physiol Biochem,* 33**,** 1197-204.

MAO, Q., LIN, C., GAO, J., LIANG, X., GAO, W., SHEN, L., KANG, L. & XU, B. 2014. Mesenchymal stem cells overexpressing integrin-linked kinase attenuate left ventricular remodeling and improve cardiac function after myocardial infarction. *Mol Cell Biochem,* 397**,** 203-14.

MARETZKY, T., EVERS, A., ZHOU, W., SWENDEMAN, S. L., WONG, P. M., RAFII, S., REISS, K. & BLOBEL, C. P. 2011. Migration of growth factor-stimulated epithelial and endothelial cells depends on EGFR transactivation by ADAM17. *Nat Commun,* 2.

MARIANO, E. D., TEIXEIRA, M. J., MARIE, S. K. & LEPSKI, G. 2015. Adult stem cells in neural repair: Current options, limitations and perspectives. *World J Stem Cells,* 7**,** 477-82.

MARQUASS, B., SOMERSON, J. S., HEPP, P., AIGNER, T., SCHWAN, S., BADER, A., JOSTEN, C., ZSCHARNACK, M. & SCHULZ, R. M. 2010. A novel MSC-seeded triphasic construct for the repair of osteochondral defects. *Journal of orthopaedic research : official publication of the Orthopaedic Research Society,* 28**,** 1586-99.

MARTELLO, G. & SMITH, A. 2014. The nature of embryonic stem cells. *Annu Rev Cell Dev Biol,* 30**,** 647-75.

MATHE, G. 1964. [Treatment of Leukemia with Allogenic Bone Marrow Transplantation]. *Brux Med,* 44**,** 559-62.

MATSUMOTO, T., TURESSON, I., BOOK, M., GERWINS, P. & CLAESSON-WELSH, L. 2002. p38 MAP kinase negatively regulates endothelial cell survival, proliferation, and differentiation in FGF-2-stimulated angiogenesis. *J Cell Biol,* 156**,** 149-60.

MATTHEWS, B. G., GRCEVIC, D., WANG, L., HAGIWARA, Y., ROGULJIC, H., JOSHI, P., SHIN, D. G., ADAMS, D. J. & KALAJZIC, I. 2014. Analysis of alphaSMA-labeled progenitor cell commitment identifies notch signaling as an important pathway in fracture healing. *J Bone Miner Res,* 29**,** 1283-94.

MCBEATH, R., PIRONE, D. M., NELSON, C. M., BHADRIRAJU, K. & CHEN, C. S. 2004. Cell shape, cytoskeletal tension, and RhoA regulate stem cell lineage commitment. *Dev Cell,* 6**,** 483-95.

MEIJER, G. J., DE BRUIJN, J. D., KOOLE, R. & VAN BLITTERSWIJK, C. A. 2007. Cell-based Bone Tissue Engineering. *PLoS Medicine,* 4**,** 260-264.

MENDICINO, M., BAILEY, A. M., WONNACOTT, K., PURI, R. K. & BAUER, S. R. 2014. MSC-based product characterization for clinical trials: an FDA perspective. *Cell Stem Cell,* 14**,** 141-5.

MEZENTSEV, A., MERKS, R. M., O'RIORDAN, E., CHEN, J., MENDELEV, N., GOLIGORSKY, M. S. & BRODSKY, S. V. 2005. Endothelial microparticles affect angiogenesis in vitro: role of oxidative stress. *Am J Physiol Heart Circ Physiol,* 289**,** 6.

MIKI, Y., SUZUKI, T., TAZAWA, C., YAMAGUCHI, Y., KITADA, K., HONMA, S., MORIYA, T., HIRAKAWA, H., EVANS, D. B., HAYASHI, S., OHUCHI, N. & SASANO, H. 2007. Aromatase localization in human breast cancer tissues: possible interactions between intratumoral stromal and parenchymal cells. *Cancer Res,* 67**,** 3945-54.

MILLER, J. R. & MOON, R. T. 1996. Signal transducti through B-catenin and specification of cell fate during embryogenesis *Genes & Development,* 10**,** 2527-2539.

MINARDI, S., CORRADETTI, B., TARABALLI, F., SANDRI, M., VAN EPS, J., CABRERA, F. J., WEINER, B. K., TAMPIERI, A. & TASCIOTTI, E. 2015. Evaluation of the osteoinductive potential of a bio-inspired scaffold mimicking the osteogenic niche for bone augmentation. *Biomaterials,* 62**,** 128-37.

MIRAOUI, H., OUDINA, K., PETITE, H., TANIMOTO, Y., MORIYAMA, K. & MARIE, P. J. 2009. Fibroblast growth factor receptor 2 promotes osteogenic differentiation in mesenchymal cells via ERK1/2 and protein kinase C signaling. *J Biol Chem,* 284**,** 4897-904.

MOCHIZUKI, H., CHOONG, C.-J. & YASUDA, T. 2014. The promises of stem cells: stem cell therapy for movement disorders. *Parkinsonism & Related Disorders,* 20**,** S128-S131.

MOENS, S., GOVEIA, J., STAPOR, P. C., CANTELMO, A. R. & CARMELIET, P. 2014. The multifaceted activity of VEGF in angiogenesis - Implications for therapy responses. *Cytokine Growth Factor Rev,* 25**,** 473-82.

MOHAMMADI, Z., AFSHARI, J. T., KERAMATI, M. R., ALAMDARI, D. H., GANJIBAKHSH, M., ZARMEHRI, A. M., JANGJOO, A., SADEGHIAN, M. H., AMERI, M. A. & MOINZADEH, L. 2015. Differentiation of adipocytes

and osteocytes from human adipose and placental mesenchymal stem cells. *Iran J Basic Med Sci,* 18**,** 259-66.

MOLONEY, D. J., PANIN, V. M., JOHNSTON, S. H., CHEN, J., SHAO, L., WILSON, R., WANG, Y., STANLEY, P., IRVINE, K. D., HALTIWANGER, R. S. & VOGT, T. F. 2000. Fringe is a glycosyltransferase that modifies Notch. *Nature,* 406**,** 369-375.

MOORE, K. A. & LEMISCHKA, I. R. 2006. Stem cells and their niches. *Science,* 311**,** 1880-5.

MOREAU, J. L. & XU, H. H. 2009. Mesenchymal stem cell proliferation and differentiation on an injectable calcium phosphate-chitosan composite scaffold. *Biomaterials,* 30**,** 2675-82.

MORGAN, T. H. 1917. The theory of the gene. *The American Naturalist,* 51**,** 513-544.

MUELLER, M. B., FISCHER, M., ZELLNER, J., BERNER, A., DIENSTKNECHT, T., PRANTL, L., KUJAT, R., NERLICH, M., TUAN, R. S. & ANGELE, P. 2010. Hypertrophy in mesenchymal stem cell chondrogenesis: effect of TGF-beta isoforms and chondrogenic conditioning. *Cells Tissues Organs,* 192**,** 158-66.

MURPHY, M., FINK, D., HUNZIKER, E. & BARRY, F. 2003. Stem Cell Therapy in a Caprine Model of Osteoarthritis. *Arthritis & Rheumatism,* 48**,** 3464-3474.

MURPHY, M. K., MASTERS, T. E., HU, J. C. & ATHANASIOU, K. A. 2015. Engineering a fibrocartilage spectrum through modulation of aggregate redifferentiation. *Cell Transplant,* 24**,** 235-45.

NAKANO, N., NISHIYAMA, C., YAGITA, H., HARA, M., MOTOMURA, Y., KUBO, M., OKUMURA, K. & OGAWA, H. 2015. Notch signaling enhances FcepsilonRI-mediated cytokine production by mast cells through direct and indirect mechanisms. *J Immunol,* 194, 4535-44.

NAM, M. H., LEE, H. S., SEOMUN, Y., LEE, Y. & LEE, K. W. 2011. Monocyte-endothelium-smooth muscle cell interaction in co-culture: proliferation and cytokine productions in response to advanced glycation end products. *Biochim Biophys Acta,* 9**,** 907-12.

NEWMAN, S. A. 1996. Sticky fingers: Hox genes and cell adhesion in vertebrate limb development. *BioEssays,* 18**,** 171-174.

NG, F., BOUCHER, S., KOH, S., SASTRY, K. S., CHASE, L., LAKSHMIPATHY, U., CHOONG, C., YANG, Z., VEMURI, M. C., RAO, M. S. & TANAVDE, V. 2008. PDGF, TGF-beta, and FGF signaling is important for differentiation and growth of mesenchymal stem cells (MSCs): transcriptional profiling can identify markers and signaling pathways important in differentiation of MSCs into adipogenic, chondrogenic, and osteogenic lineages. *Blood,* 112**,** 295-307.

NOAD, J., GONZALEZ-LARA, L. E., BROUGHTON, H. C., MCFADDEN, C., CHEN, Y., HESS, D. A. & FOSTER, P. J. 2012. MRI tracking of transplanted iron-labeled mesenchymal stromal cells in an immune-compromised mouse model of critical limb ischemia. *NMR in biomedicine.*

NOMBELA-ARRIETA, C., RITZ, J. & SILBERSTEIN, L. E. 2011. The elusive nature and function of mesenchymal stem cells. *Nature reviews. Molecular cell biology,* 12**,** 126-31.

NOVAK, A., HSU, S. C., LEUNG-HAGESTEUN, C., RADEVA, G., PAPKOFF, J., GROSSCHEDL, R. & DEDHAR, S. 1998. Cell adhesion and the integrin-linked kinase regulate the LEF-1 and b-catenin signaling pathways. *Proceedings of the National Academy of Sciences of the United States of America,* 95**,** 4374-4379.

NOVOSEL, E. C., KLEINHANS, C. & KLUGER, P. J. 2011. Vascularization is the key challenge in tissue engineering. *Adv Drug Deliv Rev,* 63**,** 300-311.

O'DEA, R. D. & KING, J. R. 2013. The isolation of spatial patterning modes in a mathematical model of juxtacrine cell signalling. *Math Med Biol,* 30**,** 95-113.

OE, K., MIWA, M., SAKAI, Y., LEE, S. Y., KURODA, R. & KUROSAKA, M. 2007. An in vitro study demonstrating that haematomas found at the site of human fractures contain progenitor cells with multilineage capacity. *The Journal of Bone and Joint Surgery,* 89-B**,** 133-38.

OH, J. Y., LEE, R. H., YU, J. M., KO, J. H., LEE, H. J., KO, A. Y., RODDY, G. W. & PROCKOP, D. J. 2012. Intravenous Mesenchymal Stem Cells Prevented Rejection of Allogeneic Corneal Transplants by Aborting the Early Inflammatory Response. *Molecular therapy : the journal of the American Society of Gene Therapy,* 20**,** 2143-2152.

ONISHI, K. & ZANDSTRA, P. W. 2015. LIF signaling in stem cells and development. *Development,* 142**,** 2230-6.

ORNITZ, D. M. & ITOH, N. 2001. Fibroblast growth factors. *Genome Biol,* 2**,** 9.

PANDULA, P. K., SAMARANAYAKE, L. P., JIN, L. J. & ZHANG, C. F. 2014. Human umbilical vein endothelial cells synergize osteo/odontogenic differentiation of periodontal ligament stem cells in 3D cell sheets. *J Periodontal Res,* 49**,** 299-306.

PARK, H. J., ZHANG, Y., GEORGESCU, S. P., JOHNSON, K. L., KONG, D. & GALPER, J. B. 2006. Human umbilical vein endothelial cells and human dermal microvascular endothelial cells offer new insights into the relationship between lipid metabolism and angiogenesis. *Stem Cell Rev,* 2**,** 93-102.

PARK, J. G., LEE, D. H., MOON, Y. S. & KIM, K. H. 2014. Reversine increases the plasticity of lineage-committed preadipocytes to osteogenesis by inhibiting adipogenesis through induction of TGF-beta pathway in vitro. *Biochemical and biophysical research communications,* 446**,** 30-6.

PARK, K. E. & TELUGU, B. P. 2013. Role of stem cells in large animal genetic engineering in the TALENs-CRISPR era. *Reprod Fertil Dev,* 26**,** 65-73.

PATI, S., KHAKOO, A. Y., ZHAO, J., JIMENEZ, F., GERBER, M. H., HARTING, M., REDELL, J. B., GRILL, R., MATSUO, Y., GUHA, S., COX, C. S., REITZ, M. S., HOLCOMB, J. B. & DASH, P. K. 2011. Human mesenchymal stem cells inhibit vascular permeability by modulating vascular endothelial cadherin/beta-catenin signaling. *Stem cells and development,* 20**,** 89-101.

PAUL, H., REGINATO, A. J. & SCHUMACHER, H. R. 1983. Alizarin red S staining as a screening test to detect calcium compounds in synovial fluid. *Arthritis and rheumatism,* 26**,** 191-200.

PAZZAGLIA, U. E., CONGIU, T., SIBILIA, V. & QUACCI, D. 2014. Osteoblast-osteocyte transformation. A SEM densitometric analysis of endosteal apposition in rabbit femur. *J Anat,* 224**,** 132-41.

PHINNEY, D. G., KOPEN, G., RIGHTER, W., WEBSTER, S., TREMAIN, N. & PROCKOP, D. J. 1999. Donor variation in the growth properties and osteogenic potential of human marrow stromal cells. *Journal of Cellular Biochemistry,* 75**,** 424-436.

PITTENGER, M. F. 1999. Multilineage Potential of Adult Human Mesenchymal Stem Cells. *Science,* 284**,** 143-147.

PLOTNIKOV, A. N., SCHLESSINGER, J., HUBBARD, S. R. & MOHAMMADI, M. 1999. Structural basis for FGF receptor dimerization and activation. *Cell,* 98**,** 641-50.

PONTE, A. L., MARAIS, E., GALLAY, N., LANGONNE, A., DELORME, B., HERAULT, O., CHARBORD, P. & DOMENECH, J. 2007. The in vitro migration capacity of human bone marrow mesenchymal stem cells: comparison of chemokine and growth factor chemotactic activities. *Stem cells,* 25**,** 1737-45.

POPOVA, S. N., RODRIGUEZ-SÁNCHEZ, B., LIDÉN, Å., BETSHOLTZ, C., VAN DEN BOS, T. & GULLBERG, D. 2004. The mesenchymal α11β1 integrin attenuates PDGF-BB-stimulated chemotaxis of embryonic fibroblasts on collagens. *Developmental Biology,* 270**,** 427-442.

POTIER, E., FERREIRA, E., DENNLER, S., MAUVIEL, A., OUDINA, K., LOGEART-AVRAMOGLOU, D. & PETITE, H. 2008. Desferrioxamine-driven upregulation of angiogenic factor expression by human bone marrow stromal cells. *J Tissue Eng Regen Med,* 2**,** 272-8.

PRASAD, M., RERIANI, M., KHOSLA, S., GOSSL, M., LENNON, R., GULATI, R., PRASAD, A., LERMAN, L. O. & LERMAN, A. 2014. Coronary microvascular endothelial dysfunction is an independent predictor of development of osteoporosis in postmenopausal women. *Vasc Health Risk Manag,* 10**,** 533-8.

RAHMAN, M. S., AKHTAR, N., JAMIL, H. M., BANIK, R. S. & ASADUZZAMAN, S. M. 2015. TGF-beta/BMP signaling and other molecular events: regulation of osteoblastogenesis and bone formation. *Bone Res,* 3.

RAMASAMY, S. K., KUSUMBE, A. P., WANG, L. & ADAMS, R. H. 2014. Endothelial Notch activity promotes angiogenesis and osteogenesis in bone. *Nature,* 507**,** 376-380.

RAUH, J., MILAN, F., GUNTHER, K. P. & STIEHLER, M. 2011. Bioreactor Systems for Bone Tissue Engineering. *Tissue Engineering Part B-Reviews,* 17**,** 263-280.

RAVI, M., PARAMESH, V., KAVIYA, S. R., ANURADHA, E. & SOLOMON, F. D. 2015. 3D cell culture systems: advantages and applications. *J Cell Physiol,* 230**,** 16-26.

REHMAN, J., LI, J., ORSCHELL, C. M. & MARCH, K. L. 2003. Peripheral blood "endothelial progenitor cells" are derived from monocyte/macrophages and secrete angiogenic growth factors. *Circulation,* 107**,** 1164-9.

RINGDEN, O., UZUNEL, M., RASMUSSON, I., REMBERGER, M., SUNDBERG, B., LONNIES, H., MARSCHALL, H. U., DLUGOSZ, A., SZAKOS, A., HASSAN, Z., OMAZIC, B., ASCHAN, J., BARKHOLT, L. & LE BLANC, K. 2006. Mesenchymal stem cells for treatment of therapy-resistant graft-versus-host disease. *Transplantation,* 81**,** 1390-1397.

RINKER, T. E., HAMMOUDI, T. M., KEMP, M. L., LU, H. & TEMENOFF, J. S. 2014. Interactions between mesenchymal stem cells, adipocytes, and osteoblasts in a 3D tri-culture model of hyperglycemic conditions in the bone marrow microenvironment. *Integr Biol (Camb),* 6**,** 324-37.

RIVRON, N. C., RAISS, C. C., LIU, J., NANDAKUMAR, A., STICHT, C., GRETZ, N., TRUCKENMULLER, R., ROUWKEMA, J. & VAN BLITTERSWIJK, C. A. 2012. Sonic Hedgehog-activated engineered blood vessels enhance bone tissue formation. *Proceedings of the National Academy of Sciences of the United States of America,* 109**,** 4413-8.

ROBERTS, J. L., MAILLARD, J. Y., WADDINGTON, R. J., DENYER, S. P., LYNCH, C. D. & SLOAN, A. J. 2013. Development of an ex vivo coculture system to model pulpal infection by Streptococcus anginosus group bacteria. *J Endod,* 39**,** 49-56.

ROBINSON, S. P., LUDWIG, C., PAULSSON, J. & OSTMAN, A. 2008. The effects of tumor-derived platelet-derived growth factor on vascular morphology and function in vivo revealed by susceptibility MRI. *Int J Cancer,* 122**,** 1548-56.

RODRIGUES, M. T., LEE, S. J., GOMES, M. E., REIS, R. L., ATALA, A. & YOO, J. J. 2012. Bilayered constructs aimed at osteochondral strategies: the influence of medium supplements in the osteogenic and chondrogenic differentiation of amniotic fluid-derived stem cells. *Acta biomaterialia,* 8**,** 2795-806.

ROMIEU-MOUREZ, R., FRANCOIS, M., BOIVIN, M. N., STAGG, J. & GALIPEAU, J. 2007. Regulation of MHC class II expression and antigen processing in murine and human mesenchymal stromal cells by IFN-gamma, TGF-beta, and cell density. *J Immunol,* 179**,** 1549-58.

ROSKOSKI, R., JR. 2007. Sunitinib: a VEGF and PDGF receptor protein kinase and angiogenesis inhibitor. *Biochem Biophys Res Commun,* 356**,** 323-8.

SAKAGUCHI, Y., SEKIYA, I., YAGISHITA, K. & MUNETA, T. 2005. Comparison of Human Stem Cells Derived From Various Mesenchymal Tissues. *Arthritis & Rheumatism,* 52**,** 2521-2529.

SAKAI, T., LI, S., DOCHEVA, D., GRASHOFF, C., SAKAI, K., KOSTKA, G., BRAUN, A., PFEIFER, A., YURCHENCO, P. D. & FASSLER, R. 2003. Integrin-linked kinase (ILK) is required for polarizing the epiblast, cell adhesion, and controlling actin accumulation. *Genes Dev,* 17**,** 926-40.

SALEH, F. A., FRITH, J. E., LEE, J. A. & GENEVER, P. G. 2012. Three-dimensional in vitro culture techniques for mesenchymal stem cells. *Methods Mol Biol,* 916**,** 31-45.

SALEH, F. A., WHYTE, M., ASHTON, P. & GENEVER, P. G. 2011a. Regulation of Mesenchymal Stem Cell Activity by Endothelial Cells. *Stem cells and development,* 20**,** 391-403.

SALEH, F. A., WHYTE, M. & GENEVER, P. G. 2011b. Effects of endothelial cells on human mesenchymal stem cell activity in a three-dimensional in invitro model. *European Cells and Materials,* 22**,** 242-57.

SANDERSON, J. T., LETCHER, R. J., HENEWEER, M., GIESY, J. P. & VAN DEN BERG, M. 2001. Effects of chloro-s-triazine herbicides and metabolites on aromatase activity in various human cell lines and on vitellogenin production in male carp hepatocytes. *Environ Health Perspect,* 109**,** 1027-31.

SASAKI, J., HASHIMOTO, M., YAMAGUCHI, S., ITOH, Y., YOSHIMOTO, I., MATSUMOTO, T. & IMAZATO, S. 2015. Fabrication of Biomimetic Bone Tissue Using Mesenchymal Stem Cell-Derived Three-Dimensional Constructs Incorporating Endothelial Cells. *PLoS One,* 10.

SASANO, H. & HARADA, N. 1998. Intratumoral aromatase in human breast, endometrial, and ovarian malignancies. *Endocr Rev,* 19**,** 593-607.

SCHNERCH, A., CERDAN, C. & BHATIA, M. 2010. Distinguishing between mouse and human pluripotent stem cell regulation: the best laid plans of mice and men. *Stem cells,* 28**,** 419-30.

SCHOFIELD, R. 1978. RELATIONSHIP BETWEEN SPLEEN COLONY-FORMING CELL AND HEMATOPOIETIC STEM-CELL - HYPOTHESIS. *Blood Cells,* 4**,** 7-25.

SCOTTI, C., PICCININI, E., TAKIZAWA, H., TODOROV, A., BOURGINE, P., PAPADIMITROPOULOS, A., BARBERO, A., MANZ, M. G. & MARTIN, I. 2013. Engineering of a functional bone organ through endochondral ossification. *Proceedings of the National Academy of Sciences of the United States of America,* 110**,** 3997-4002.

SCOTTI, C., TONNARELLI, B., PAPADIMITROPOULOS, A., SCHERBERICH, A., SCHAEREN, S., SCHAUERTE, A., LOPEZ-RIOS, J., ZELLER, R., BARBERO, A. & MARTIN, I. 2010. Recapitulation of endochondral bone formation using human adult mesenchymal stem cells as a paradigm for developmental engineering. *Proceedings of the National Academy of Sciences of the United States of America,* 107**,** 7251-6.

SENSEBE, L., KRAMPERA, M., SCHREZENMEIER, H., BOURIN, P. & GIORDANO, R. 2010. Mesenchymal stem cells for clinical application. *Vox sanguinis,* 98**,** 93-107.

SHI, S. & GRONTHOS, S. 2003. Perivascular niche of postnatal mesenchymal stem cells in human bone marrow and dental pulp. *J Bone Miner Res,* 18**,** 696-704.

SHIMAZUI, T., SCHALKEN, J. A., KAWAI, K., KAWAMOTO, R., VAN BOCKHOVEN, A., OOSTERWIJK, E. & AKAZA, H. 2004. Role of complex cadherins in cell-cell adhesion evaluated by spheroid formation in renal cell carcinoma cell lines. *Oncol Rep,* 11**,** 357-60.

SHIODA, N., MORIGUCHI, S., YAMAMOTO, Y., MATSUSHIMA, T., SASAHARA, M. & FUKUNAGA, K. 2009. Changes in hippocampal spine morphology and synaptic plasticity induced by conditional loss of

PDGFR-β are associated with memory impairment in mutant mice. *Neuroscience Research,* 65, Supplement 1**,** S67.

SHUI, C. & SCUTT, A. 2001. Mild heat shock induces proliferation, alkaline phosphatase activity and mineralization in human bone marrow stromal cells and Mg-63 cells in vitro. *Journal of Bone and Mineral Research* 16**,** 731-742.

SIDDAPPA, R., LICHT, R., VAN BLITTERSWIJK, C. & DE BOER, J. 2007. Donor variation and loss of multipotency during in vitro expansion of human mesenchymal stem cells for bone tissue engineering. *Journal of orthopaedic research : official publication of the Orthopaedic Research Society,* 25**,** 1029-41.

SIMON, P. 2003. Early failure of the tissue engineered porcine heart valve SYNERGRAFT™ in pediatric patients. *European Journal of Cardio-Thoracic Surgery,* 23**,** 1002-1006.

SIMON, R., APARICIO, R., HOUSDEN, B. E., BRAY, S. & BUSTURIA, A. 2014. Drosophila p53 controls Notch expression and balances apoptosis and proliferation. *Apoptosis,* 19**,** 1430-43.

SIMS, D., DUCHEK, P. & BAUM, B. 2009. PDGF/VEGF signaling controls cell size in Drosophila. *Genome Biol,* 10**,** R20.

SISASK, G., MARSELL, R., SUNDGREN-ANDERSSON, A., LARSSON, S., NILSSON, O., LJUNGGREN, O. & JONSSON, K. B. 2013. Rats treated with AZD2858, a GSK3 inhibitor, heal fractures rapidly without endochondral bone formation. *Bone,* 54**,** 126-32.

SMITH, C. L. & MANSOUR, J. M. 2000. Indentation of an osteochondral repair: sensitivity to experimental variables and boundary conditions. *J Biomech,* 33**,** 1507-11.

SONG, S. W., CHANG, W., SONG, B. W., SONG, H., LIM, S., KIM, H. J., CHA, M. J., CHOI, E., IM, S. H., CHANG, B. C., CHUNG, N., JANG, Y. & HWANG, K. C. 2009. Integrin-linked kinase is required in hypoxic mesenchymal stem cells for strengthening cell adhesion to ischemic myocardium. *Stem cells,* 27**,** 1358-65.

SORRELL, J. M., BABER, M. A. & CAPLAN, A. I. 2007. A self-assembled fibroblast-endothelial cell co-culture system that supports in vitro vasculogenesis by both human umbilical vein endothelial cells and human dermal microvascular endothelial cells. *Cells Tissues Organs,* 186**,** 157-68.

SPENCER, J. A., FERRARO, F., ROUSSAKIS, E., KLEIN, A., WU, J., RUNNELS, J. M., ZAHER, W., MORTENSEN, L. J., ALT, C., TURCOTTE, R., YUSUF, R., COTE, D., VINOGRADOV, S. A., SCADDEN, D. T. & LIN, C. P. 2014. Direct measurement of local oxygen concentration in the bone marrow of live animals. *Nature,* 508**,** 269-73.

STAHL, A., WENGER, A., WEBER, H., STARK, G. B., AUGUSTIN, H. G. & FINKENZELLER, G. 2004. Bi-directional cell contact-dependent regulation of gene expression between endothelial cells and osteoblasts in a three-dimensional spheroidal coculture model. *Biochemical and biophysical research communications,* 322**,** 684-92.

STEGEN, S., VAN GASTEL, N. & CARMELIET, G. 2015. Bringing new life to damaged bone: The importance of angiogenesis in bone repair and regeneration. *Bone,* 70**,** 19-27.

STEINBERG, M. S. 1975. Adhesion-guided multicellular assembly: a commentary upon the postulates, real and imagined, of the differential adhesion hypothesis, with special attention to computer simulations of cell sorting. *J Theor Biol,* 55**,** 431-43.

STREET, J., BAO, M., DEGUZMAN, L., BUNTING, S., PEALE, F. V., FERRARA, N., STEINMETZ, H., HOEFFEL, J., CLELAND, J. L., DAUGHERTY, A., VAN BRUGGEN, N., REDMOND, H. P., CARANO, R. A. D. & FILVAROFF, E. H. 2002. Vascular endothelial growth factor stimulates bone repair by promoting angiogenesis and bone turnover. *Proceedings of the National Academy of Sciences,* 99**,** 9656-9661.

SUMPIO, B. E., TIMOTHY RILEY, J. & DARDIK, A. 2002. Cells in focus: endothelial cell. *The International Journal of Biochemistry & Cell Biology,* 34**,** 1508-1512.

SUN, X., MEYERS, E. N., LEWANDOSKI, M. & MARTIN, G. R. 1999. Targeted disruption of Fgf8 causes failure of cell migration in the gastrulating mouse embryo. *Genes Dev,* 13**,** 1834-46.

SUN, X. Z., ZHOU, D. & CHEN, S. 1997. Autocrine and paracrine actions of breast tumor aromatase. A three-dimensional cell culture study involving aromatase transfected MCF-7 and T-47D cells. *J Steroid Biochem Mol Biol,* 63**,** 29-36.

SURANI, M. A., DURCOVA-HILLS, G., HAJKOVA, P., HAYASHI, K. & TEE, W. W. 2008. Germ line, stem cells, and epigenetic reprogramming. *Cold Spring Harb Symp Quant Biol,* 73**,** 9-15.

SUTHERLAND, R. M. 1988. Cell and Environment Interactions in tumour microregions: the multicell spheroid model. *Science,* 240**,** 178-184.

TAKAGI, S., TAKEMOTO, A., TAKAMI, M., OH-HARA, T. & FUJITA, N. 2014. Platelets promote osteosarcoma cell growth through activation of the platelet-derived growth factor receptor-Akt signaling axis. *Cancer science,* 105**,** 983-8.

TAKAHASHI, K. & YAMANAKA, S. 2006. Induction of pluripotent stem cells from mouse embryonic and adult fibroblast cultures by defined factors. *Cell,* 126**,** 663-76.

TAKEBE, T., SEKINE, K., ENOMURA, M., KOIKE, H., KIMURA, M., OGAERI, T., ZHANG, R. R., UENO, Y., ZHENG, Y. W., KOIKE, N., AOYAMA, S., ADACHI, Y. & TANIGUCHI, H. 2013. Vascularized and functional human liver from an iPSC-derived organ bud transplant. *Nature,* 499**,** 481-4.

TAMAMA, K., KAWASAKI, H. & WELLS, A. 2010. Epidermal growth factor (EGF) treatment on multipotential stromal cells (MSCs). Possible enhancement of therapeutic potential of MSC. *J Biomed Biotechnol,* 2010**,** 795385.

TAN, C., CRUET-HENNEQUART, S., TROUSSARD, A., FAZIL, L., COSTELLO, P., SUTTON, K., WHEELER, J., GLEAVES, M., SANGHERA, J. & DEDHAR, S. 2004. Regulation of tumor angiogenesis by integrin-linked kinase (ILK). *Cancer Cell,* 5**,** 79-91.

TANNOUS, O., STALL, A. C., GRIFFITH, C., DONALDSON, C. T., CASTELLANI, R. J., JR. & PELLEGRINI, V. D., JR. 2013. Heterotopic bone formation about the hip undergoes endochondral ossification: a rabbit model. *Clinical orthopaedics and related research,* 471**,** 1584-92.

TANOUE, A., NASA, Y., KOSHIMIZU, T., SHINOURA, H., OSHIKAWA, S., KAWAI, T., SUNADA, S., TAKEO, S. & TSUJIMOTO, G. 2002. The α1D-adrenergic receptor directly regulates arterial blood pressure via vasoconstriction. *Journal of Clinical Investigation,* 109**,** 765-775.

THOMA, C. R., ZIMMERMANN, M., AGARKOVA, I., KELM, J. M. & KREK, W. 2014. 3D cell culture systems modeling tumor growth determinants in cancer target discovery. *Adv Drug Deliv Rev,* 69-70**,** 29-41.

THOMAS, J. L., BAKER, K., HAN, J., CALVO, C., NURMI, H., EICHMANN, A. C. & ALITALO, K. 2013. Interactions between VEGFR and Notch signaling pathways in endothelial and neural cells. *Cell Mol Life Sci,* 70**,** 1779-92.

THOMPSON, R. N., YATES, C. A. & BAKER, R. E. 2012. Modelling cell migration and adhesion during development. *Bulletin of mathematical biology,* 74**,** 2793-809.

TIMMERS, L., LIM, S. K., HOEFER, I. E., ARSLAN, F., LAI, R. C., VAN OORSCHOT, A. A., GOUMANS, M. J., STRIJDER, C., SZE, S. K., CHOO, A., PIEK, J. J., DOEVENDANS, P. A., PASTERKAMP, G. & DE KLEIJN, D. P. 2011. Human mesenchymal stem cell-conditioned medium improves cardiac function following myocardial infarction. *Stem Cell Res,* 6**,** 206-14.

TONDREAU, T., MEULEMAN, N., DELFORGE, A., DEJENEFFE, M., LEROY, R., MASSY, M., MORTIER, C., BRON, D. & LAGNEAUX, L. 2005. Mesenchymal stem cells derived from CD133-positive cells in mobilized peripheral blood and cord blood: proliferation, Oct4 expression, and plasticity. *Stem cells,* 23**,** 1105-12.

TRAPHAGEN, S. B., TITUSHKIN, I., SUN, S., WARY, K. K. & CHO, M. 2013. Endothelial invasive response in a co-culture model with physically-induced osteodifferentiation. *J Tissue Eng Regen Med,* 7**,** 621-30.

URICH, E., PATSCH, C., AIGNER, S., GRAF, M., IACONE, R. & FRESKGARD, P. O. 2013. Multicellular self-assembled spheroidal model of the blood brain barrier. *Scientific reports,* 3**,** 1500.

VAES, B., WALBERS, S., GIJBELS, K., CRAEYE, D., DEANS, R., PINXTEREN, J. & VAN'T HOF, W. 2015. Culturing protocols for human multipotent adult stem cells. *Methods Mol Biol***,** 1785-3_5.

VAN WIERINGEN, T., KIMANI, S. G., HULTGÅRD-EKWALL, A.-K., FORSBERG, J., REYHANI, V., ENGSTRÖM, Å. & RUBIN, K. 2009. Opposite effects of PDGF-BB and prostaglandin E1 on cell-motility related processes are paralleled by modifications of distinct actin-binding proteins. *Experimental Cell Research,* 315**,** 1745-1758.

VAN ZANT, G. & LIANG, Y. 2012. Concise review: hematopoietic stem cell aging, life span, and transplantation. *Stem cells translational medicine,* 1**,** 651-7.

VATER, C., KASTEN, P. & STIEHLER, M. 2011. Culture media for the differentiation of mesenchymal stromal cells. *Acta biomaterialia,* 7**,** 463-77.

VIALE-BOURONCLE, S., GOSAU, M. & MORSCZECK, C. 2014. NOTCH1 signaling regulates the BMP2/DLX-3 directed osteogenic differentiation of dental follicle cells. *Biochemical and biophysical research communications,* 443**,** 500-4.

VIDAL, M. A., WALKER, N. J., NAPOLI, E. & BORJESSON, D. L. 2012. Evaluation of senescence in mesenchymal stem cells isolated from equine bone marrow, adipose tissue, and umbilical cord tissue. *Stem cells and development,* 21**,** 273-83.

VINCI, M., GOWAN, S., BOXALL, F., PATTERSON, L., ZIMMERMANN, M., COURT, W., LOMAS, C., MENDIOLA, M., HARDISSON, D. & ECCLES, S. A. 2012. Advances in establishment and analysis of three-dimensional tumor spheroid-based functional assays for target validation and drug evaluation. *BMC biology,* 10**,** 29.

VOLAREVIC, V., ARSENIJEVIC, N., LUKIC, M. L. & STOJKOVIC, M. 2011. Concise review: Mesenchymal stem cell treatment of the complications of diabetes mellitus. *Stem cells,* 29**,** 5-10.

WALSH, D. A., MCWILLIAMS, D. F., TURLEY, M. J., DIXON, M. R., FRANSES, R. E., MAPP, P. I. & WILSON, D. 2010. Angiogenesis and nerve growth factor at the osteochondral junction in rheumatoid arthritis and osteoarthritis. *Rheumatology,* 49**,** 1852-61.

WANG, H., PANG, B., LI, Y., ZHU, D., PANG, T. & LIU, Y. 2012. Dexamethasone has variable effects on mesenchymal stromal cells. *Cytotherapy,* 14**,** 423-30.

WANG, H., ZANG, C., LIU, X. S. & ASTER, J. C. 2015. The role of Notch receptors in transcriptional regulation. *J Cell Physiol,* 230**,** 982-8.

WANG, L., RUDERT, W. A., LOUTAEV, I., ROGINSKAYA, V. & COREY, S. J. 2002. Repression of c-Cbl leads to enhanced G-CSF Jak-STAT signaling without increased cell proliferation. *Oncogene,* 21**,** 5346-55.

WANG, W., LIU, Q., ZHANG, Y. & ZHAO, L. 2014. Involvement of ILK/ERK1/2 and ILK/p38 pathways in mediating the enhanced osteoblast differentiation by micro/nanotopography. *Acta biomaterialia,* 10**,** 3705-15.

WEARING, H. J., OWEN, M. R. & SHERRATT, J. A. 2000. Mathematical modelling of juxtacrine patterning. *Bulletin of mathematical biology,* 62**,** 293-320.

WELF, E. S. & HAUGH, J. M. 2011. Signaling pathways that control cell migration: models and analysis. *Wiley Interdiscip Rev Syst Biol Med,* 3**,** 231-40.

WEN, L., WANG, Y., WANG, H., KONG, L., ZHANG, L., CHEN, X. & DING, Y. 2012. L-type calcium channels play a crucial role in the proliferation and osteogenic differentiation of bone marrow mesenchymal stem cells. *Biochemical and biophysical research communications,* 424**,** 439-45.

WEN, Z., LIAO, Q., HU, Y., YOU, L., ZHOU, L. & ZHAO, Y. 2013. A spheroid-based 3-D culture model for pancreatic cancer drug testing, using the acid phosphatase assay. *Braz J Med Biol Res,* 46**,** 634-42.

WHYTE, J. L., BALL, S. G., SHUTTLEWORTH, C. A., BRENNAN, K. & KIELTY, C. M. 2011. Density of human bone marrow stromal cells regulates commitment to vascular lineages. *Stem Cell Research,* 6**,** 238-250.

WILSON, H. V. 1907. A new method by which sponges may be artifically reared. *Science,* 7**,** 912-915.

WOODRING, P. J., HUNTER, T. & WANG, J. Y. 2003. Regulation of F-actin-dependent processes by the Abl family of tyrosine kinases. *J Cell Sci,* 116**,** 2613-26.

WU, X., HOU, T., LUO, F., XING, J., HE, Q., JIN, H., XIE, Z. & XU, J. 2013. Vascular endothelial growth factor and physiological compressive loading synergistically promote bone formation of tissue-engineered bone. *Tissue engineering. Part A,* 19**,** 2486-94.

WYLER VON BALLMOOS, M., YANG, Z., VOLZMANN, J., BAUMGARTNER, I., KALKA, C. & DI SANTO, S. 2010. Endothelial progenitor cells induce a phenotype shift in differentiated endothelial cells towards PDGF/PDGFRbeta axis-mediated angiogenesis. *PLoS One,* 5**,** e14107.

XIAO, X., WANG, W., LIU, D., ZHANG, H., GAO, P., GENG, L., YUAN, Y., LU, J. & WANG, Z. 2015. The promotion of angiogenesis induced by three-dimensional porous beta-tricalcium phosphate scaffold with different interconnection sizes via activation of PI3K/Akt pathways. *Scientific reports,* 5**,** 9409.

XIE, J., WANG, W., SI, J. W., MIAO, X. Y., LI, J. C., WANG, Y. C., WANG, Z. R., MA, J., ZHAO, X. C., LI, Z., YI, H. & HAN, H. 2013. Notch signaling regulates CXCR4 expression and the migration of mesenchymal stem cells. *Cell Immunol,* 281**,** 68-75.

XIONG, J., YANG, Q., LI, J. & ZHOU, S. 2014. Effects of MDM2 inhibitors on vascular endothelial growth factor-mediated tumor angiogenesis in human breast cancer. *Angiogenesis,* 17**,** 37-50.

YAMAGUCHI, Y., OHNO, J., SATO, A., KIDO, H. & FUKUSHIMA, T. 2014. Mesenchymal stem cell spheroids exhibit enhanced in-vitro and in-vivo osteoregenerative potential. *BMC Biotechnol,* 14**,** 014-0105.

YAO, Q., RENAULT, M.-A., CHAPOULY, C., VANDIERDONCK, S., BELLOC, I., JASPARD-VINASSA, B. E., DANIEL-LAMAZI `ERE, J.-M., LAFFARGUE, M., MERCHED, A., DESGRANGES, C. & GADEAU, A.-P. 2014. Sonic hedgehog mediates a novel pathway of PDGF-BB–dependent vessel maturation. *Blood,* 123, 2429-37.

YAYON, A., KLAGSBRUN, M., ESKO, J. D., LEDER, P. & ORNITZ, D. M. 1991. Cell surface, heparin-like molecules are required for binding of basic fibroblast growth factor to its high affinity receptor. *Cell,* 64**,** 841-8.

YI, F., LIU, G. H. & BELMONTE, J. C. I. 2012. Rejuvenating liver and pancreas through cell transdifferentiation. *Cell Research,* 22**,** 616-619.

YOON, S. H., RAMALINGAM, M. & KIM, S. J. 2015. Insulin stimulates integrin-linked kinase in UMR-106 cells: potential role of heparan sulfate on syndecan-1. *J Recept Signal Transduct Res,* 8**,** 1-5.

YOUNGER, A., WING, K., PENNER, M. & CRESSWELL, M. 2015. A study to evaluate the safety of platelet-derived growth factor for treatment of

osteochondral defects of the talus. *Knee Surg Sports Traumatol Arthrosc,* 22**,** 22.

ZANETTA, M., QUIRICI, N., DEMAROSI, F., TANZI, M. C., RIMONDINI, L. & FARE, S. 2009. Ability of polyurethane foams to support cell proliferation and the differentiation of MSCs into osteoblasts. *Acta biomaterialia,* 5**,** 1126-36.

ZENG, Y., ZHU, L., HAN, Q., LIU, W., MAO, X., LI, Y., YU, N., FENG, S., FU, Q., WANG, X., DU, Y. & ZHAO, R. C. 2015. Preformed Gelatin Microcryogels as Injectable Cell Carriers for Enhanced Skin Wound Healing. *Acta biomaterialia,* 30**,** 30040-4.

ZHANG, H., HILTON, M. J., ANOLIK, J. H., WELLE, S. L., ZHAO, C., YAO, Z., LI, X., WANG, Z., BOYCE, B. F. & XING, L. 2014. NOTCH inhibits osteoblast formation in inflammatory arthritis via noncanonical NF-kappaB. *J Clin Invest,* 124**,** 3200-14.

ZHAO, L., LIU, L., WU, Z., ZHANG, Y. & CHU, P. K. 2012. Effects of micropitted/nanotubular titania topographies on bone mesenchymal stem cell osteogenic differentiation. *Biomaterials,* 33**,** 2629-41.

ZHAO, Y. & ADJEI, A. A. 2015. Targeting Angiogenesis in Cancer Therapy: Moving Beyond Vascular Endothelial Growth Factor. *Oncologist,* 20**,** 660-73.

ZHENG, K., WANG, G., LI, C., SHAN, X. & LIU, H. 2015. Knockdown of ILK inhibits glioma development via upregulation of E-cadherin and downregulation of cyclin D1. *Oncol Rep,* 34**,** 272-8.

ZIPFEL, W. R., WILLIAMS, R. M., CHRISTIE, R., NIKITIN, A. Y., HYMAN, B. T. & WEBB, W. W. 2003. Live tissue intrinsic emission microscopy using multiphoton-excited native fluorescence and second harmonic generation. *Proceedings of the National Academy of Sciences of the United States of America,* 100**,** 7075-80.

ZULLO, J. A., NADEL, E. P., RABADI, M. M., BASKIND, M. J., RAJDEV, M. A., DEMAREE, C. M., VASKO, R., CHUGH, S. S., LAMBA, R., GOLIGORSKY, M. S. & RATLIFF, B. B. 2015. The Secretome of Hydrogel-Coembedded Endothelial Progenitor Cells and Mesenchymal Stem Cells Instructs Macrophage Polarization in Endotoxemia. *Stem cells translational medicine.*